Risk to Water Security on Small Islands: A Numerical Modeling Approach

by

Shannon Tyler Holding

B.Sc.(Hons. Hydrogeology), University of Waterloo, 2006

Thesis in Partial Fulfillment of the
Requirements for the Degree of
Doctor of Philosophy

in the
Department of Earth Sciences
Faculty of Science

SIMON FRASER UNIVERSITY

Fall 2014

Approval

Name: **Shannon Tyler Holding**

Degree: **Doctor of Philosophy**

Title: ***Risk to Water Security on Small Islands: A Numerical Modeling Approach***

Examining Committee:

Chair: Dr. Dan Gibson
Associate Professor

Dr. Diana Allen
Senior Supervisor
Professor

Dr. Dirk Kirste
Supervisor
Associate Professor

Dr. Kirsten Zickfeld
Internal Examiner
Assistant Professor
Geography

Dr. Holly Michael
External Examiner
Associate Professor
Geological Sciences
University of Delaware

Date Defended/Approved: December 8th, 2014

Partial Copyright Licence

Abstract

The aim of this research is to characterise risk to water security for small islands. This is achieved by modeling the spatial and temporal impact from major stressors affecting water resources on small islands, and then evaluating the risk to water security through an integrated assessment framework. Numerical density-dependent flow and transport modeling is used to evaluate the response of the freshwater lens on Andros Island in The Bahamas to various climate change and human stressors including: sea level rise, changes in recharge, and increased pumping. SEAWAT models showed a reduction of freshwater lens volume by up to 24% under projected sea level rise and reduced recharge. The response time of the freshwater lens increased with stressor magnitude, resulting in a longer lens adjustment period. In addition, greater upconing was observed for pumping scenarios simulated under projected climate change conditions than under current conditions. The impact of a 2004 storm overwash event on Andros Island was simulated using HydroGeosphere. Results show that potable water is restored one month sooner when timely remedial actions are implemented; however, if delayed by four days or more, there is no improvement in recovery time. To extend the research more broadly, simulations of overwash for various island types observed worldwide were conducted. Dominant factors affecting freshwater lens response include vadose zone thickness and geologic heterogeneity, such as low or high permeability zones, whereas the dominant factor affecting freshwater lens recovery is recharge rate. A framework to characterise risk to water security was developed specific to an island hydrogeological setting. A freshwater lens susceptibility map was generated using the results of the numerical modeling. Hazard threats from climate change and human stressors (derived from numerical modeling and a land-use survey) were overlaid on the susceptibility map to represent vulnerability. Combining vulnerability with loss (or consequence) yielded a risk to water security map. High risk areas are largely concentrated within the developed areas near high chemical hazard activities, as well as along portions of the coastline. These maps were provided to local partners to inform water management policies and raise awareness about factors impacting water security.

Keywords: Small islands; Freshwater Lens; Numerical Modeling, Water Security; Risk Assessment; Response to Stressors

God, this is your PhD. I could not have done this without you and I look forward to what you'll do with it in the future.

Acknowledgements

First and foremost, I'd like to acknowledge and thank my senior supervisor, Dr. Diana Allen, for her support and direction. I especially appreciated the opportunity to attend and present at conferences which provided motivation and helpful input for much of my research. I also thank Dr. Dirk Kirste for his input as my committee member, Dr. Kirsten Zickfeld for being an examiner at both my comprehensive exam and my defence, and Dr. Holly Michael for her helpful comments and critique as my external examiner. This research has greatly benefitted from the reviews of these individuals, and many others.

The research was carried out with financial support from the Natural Sciences and Engineering Research Council of Canada (NSERC) through a Discovery Grant to Diana Allen, a grant from The Nature Conservancy Caribbean and The Bahamas National Trust (under the Royal Bank of Canada's Blue Water Project), and the Simon Fraser University Community Trust Endowment Fund.

John Bowleg and Richard Cant, from The Bahamas Water and Sewerage Corporation, provided a wealth of background information and assistance coordinating field visits. In addition, Agnessa Lundy and Shenique Albury, with The Nature Conservancy Caribbean, oversaw the survey and assisted in orienting me to issues on Andros Island. I'm especially thankful for Agnessa's interest in our work at the early stages, which led to the expansion of the scope to form the basis of my doctoral research. More generally, I'd like to thank the people of Andros Island for their openness and concern for water security, and for the beauty of the island itself, which brightened up my work days.

Table of Contents

List of Tables

List of Figures

Chapter 1.

Background

The goal of this research is to evaluate small island water security. This is achieved by characterising the spatial and temporal impact from major stressors affecting water resources on small islands. Risk to water security is then characterised through an integrated assessment framework. The following chapter provides background context to the research and an outline of the research objectives.

1.1. Introduction

Water security describes the quantity and quality of water available for human use, environmental demand, and economic interests (Global Water Partnership, 2000; Grey and Sadoff, 2007). It encompasses the different aspects of a water system and describes the ability of that system to support various uses. Traditionally, water security assessments have integrated the different stressors and their effects on the water system to provide a snapshot of the current condition (Falkenmark, 1999; Sullivan et al., 2003). However, recent work suggests that in order to effectively manage future changes to the water system, it is important to also evaluate the risk to water security (Dunn et al., 2012). Few water security assessments incorporate a component of risk. Those that do, such as source water protection assessments, primarily focus on the vulnerability of the aquifer and are limited in scope. Numerical models provide a tool to refine the characterisation of risk to water security by evaluating the response of the water system to various stressors. The integration of numerical modeling into water security risk assessments has previously focussed on well capture zone analysis in the context of contaminant transport (e.g. Simpson et al., 2013). Such approaches consider travel times from surface sources to the well within the modeled capture zone. However, this approach is not suitable for island settings where the water system is vulnerable to a

wider range of hazards impacting both the quantity and quality of available fresh water (e.g. seawater encroachment, inundation from storm surge, and surface contaminants). In addition, pathways for contamination are not strictly vertical (saltwater intrusion occurs laterally and vertically) and the response time of the aquifer to these hazards is not solely dependent on the vertical percolation rate, which traditional aquifer susceptibility mapping focuses on. Water security assessments for islands must consider processes affecting both quality and quantity and how they vary at different spatial and temporal scales.

The goal of this research is to assess the risk to water security for islands from major stressors. Freshwater resources on small islands are particularly vulnerable as they are limited in size and are easily compromised. Climate change stressors impacting water security for islands include sea level rise (SLR) and coastal inundation, changes to average climate conditions which might impact recharge, and the occurrence of extreme weather events such as storm surge. Human-induced stressors include over-extraction of groundwater and land-use activities that may potentially lead to contamination of water sources. The water system responds to these stressors at different spatial and temporal scales, which is evaluated through the use of numerical groundwater modeling. Risk to water security is then characterised through the development of a risk assessment framework that represents the impact of major stressors for current and future scenarios.

The research was conducted in partnership with The Nature Conservancy Northern Caribbean Office as well as the local water management body, the Bahamas Water and Sewerage Corporation. The findings will contribute to the characterisation of risk to water security on small islands, and will also form a case study for the UNESCO GRAPHIC (Groundwater Resources Assessment under the Pressures of Humanity and Climate Change) Programme. GRAPHIC uses regional case studies to build understanding of how the groundwater system interacts with the global water cycle and responds to climate change and human-induced pressures. This knowledge supports the advancement of sustainable groundwater management practices that mitigate projected future impacts and protect freshwater availability (UNESCO GRAPHIC, 2008). Because groundwater is a major source of fresh water, it plays a significant role in

sustaining human life and ecosystems. Therefore, it is critical to understand the groundwater system in order to protect the current resources and be able to adapt to future changes (Green et al., 2011).

The following sections summarise relevant previous studies which provide context for the unique contributions of this research.

1.2. Island Freshwater Resources

Most fresh water on small islands is present as groundwater/freshwater lenses which float on top of the surrounding salt water due to the lower density of fresh water (Falkland, 1991). Freshwater lenses (FWL) develop due to infiltrating precipitation, which is held in the subsurface (aquifer) above the salt water (Falkland, 1991). The interface between the salt water and fresh water is described by Kohout (1960) as hydro-dynamically stable, whereby the fresh water is continually discharging to the ocean, pushing back the salt water, and forms a saltwater wedge along the coastline (Figure 1.1). The extent of the FWL is maintained by the hydraulic gradient of the lens which determines the amount of fresh water discharging along the coastline and counteracting the surrounding salt water (Falkland, 1991). Underlying the FWL is a mixing zone of brackish water, which can vary in thickness from less than a metre to tens of metres (Falkland, 1991).

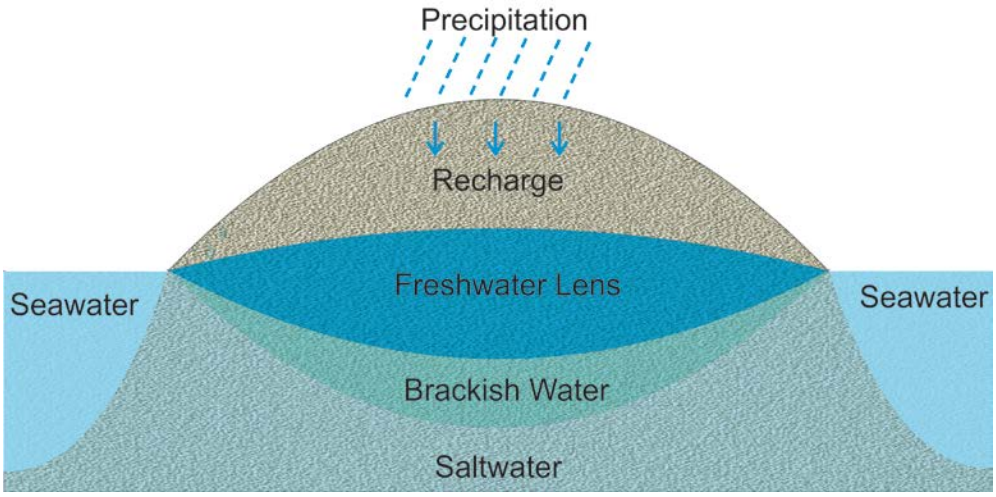

Figure 1.1. Freshwater lens of a small island

There are several factors affecting the FWL morphology (i.e. thickness and extent). Groundwater recharge is the primary source of fresh water to the lens; therefore, recharge is critical for maintaining the lens extent. Consequently, factors affecting the amount of recharge to the system have a significant impact on the development and morphology of the FWL (Ayers and Vacher, 1986). These factors include precipitation, evapotranspiration (which is related to temperature, windspeed, relative humidity and other climate variables, as well as vegetative and ground cover), runoff and interception (which is related to vegetative cover, ground cover, soil thickness, and topography), and other site-specific factors (Scanlon et al., 2002). The catchment or recharge area is also an important factor in determining the amount of recharge. Islands of small catchment size receive limited volumes of recharge and consequently have small FWLs. The shape of low-lying islands has an impact on the sustainability of the freshwater resource due to the ratio of coastline length to aquifer area where spherical islands are able to develop larger lenses than very narrow islands (White and Falkland, 2010). Islands of high relief may also have larger FWLs than low-lying islands, as the high relief allows for higher hydraulic gradients to develop and thus thicker lenses (Falkland, 1991; Robins and Lawrence, 2000). The configuration of geologic units and associated hydraulic conductivities also affect FWL development. Islands with geologic layers having high hydraulic conductivity or interbedded impermeable layers may result in a thinner FWL (Vacher, 1988; White and Falkland, 2010).

The FWL is vulnerable to degradation from the surrounding salt water through several mechanisms, as shown in Figure 1.2. Saltwater contamination can occur laterally along the coastlines due to the effects of SLR (Bobba, 2002). It may also occur downward from the surface following storm surge overwash and inundation (Anderson, 2002; Terry and Chui, 2012). Storm surges generally occur during hurricanes and other storms, where large waves form above high tide levels and may cause inland flooding and inundation (National Oceanic and Atmospheric Agency (NOAA), 2014). Saltwater intrusion may also occur from below the lens as upconing due to over-pumping of the lens (Falkland, 1991; Werner et al., 2009). In addition, a reduction in recharge can compromise the FWL, leading to salt contamination or loss of lens volume (Falkand, 1991; Oude Essink, 2001). The FWL is also vulnerable to chemical and/or pathogen contamination from human activities. Due to limited space within the island footprint,

potentially harmful activities (such as waste disposal) can be in close proximity to watershed catchments, which may lead to chemical and/or pathogen contamination of groundwater. Thus, the water system on an island is susceptible to multiple stressors that impact water quantity and quality from all directions. This presents a unique challenge to FWL vulnerability.

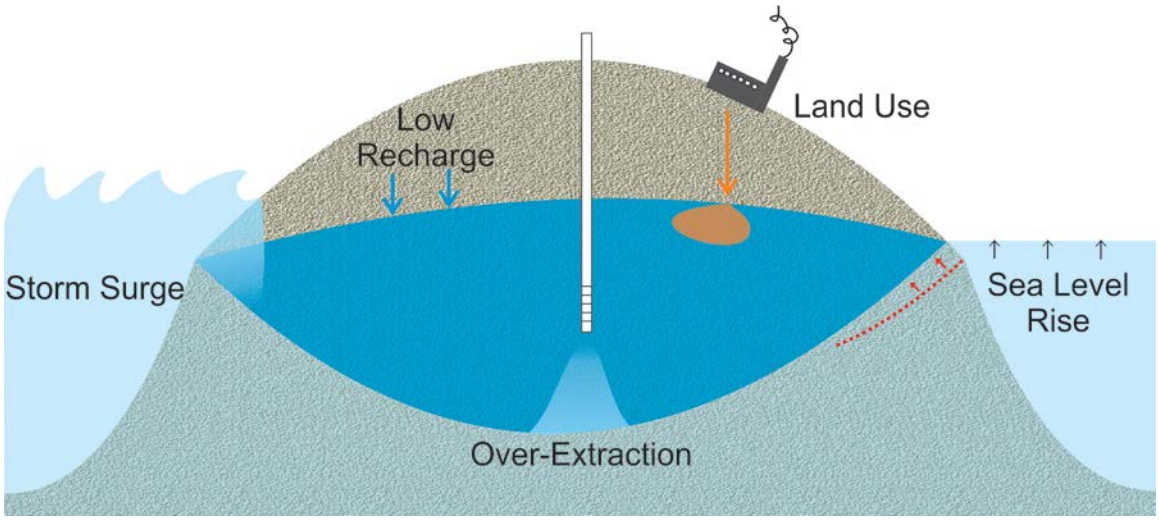

Figure 1.2. Common climate change and human stressors impacting the FWL

The many factors controlling FWL development and morphology demonstrate that the freshwater resources of small islands rely on a delicately balanced hydrogeological system. Because the island hydrogeological system is self-contained and the FWLs are limited in size (due to the nature of small islands), there is a low capacity to buffer stresses when imbalances in the system occur. The impact of stressors on the FWL is also exacerbated by socio-economic factors (Holman, 2006). For instance, on many small islands infrastructure development and settlement are shifting away from traditional inland locations towards the coastlines, where the FWL is more vulnerable, (Ranjan et al., 2009; Cashman et al., 2010). In general, low-lying islands are particularly susceptible to disturbances in the hydrogeological system as a consequence of the low hydraulic gradient within the lens and limited thickness of the lens (Falkland, 1991). Due to topography, they are also more susceptible to saltwater

inundation from SLR[1] and from storm surge overwash. Therefore, the freshwater resources of small low-lying islands may be particularly vulnerable to stressors from climate change and human activities.

1.3. Climate Change

Observations and predictions of climate change have been studied for many decades and have gained increasing attention in the last 30 years. In 1988, the United Nations Environment Programme and the World Meteorological Organisation formed a scientific body called the Inter-Governmental Panel on Climate Change (IPCC). The purpose of the IPCC is to provide an objective source of research findings on climate change. Five assessment reports (ARs) have been prepared every 5-6 years since 1990 (IPCC, 1990; IPCC, 1995; IPCC, 2001; IPCC, 2007). The most recent Fifth Assessment Report (AR5) was released in stages, beginning in late 2013 (IPCC, 2013; IPCC, 2014). The assessment reports are structured into three working group sub-reports: "The Physical Science Basis", "Impacts, Adaptation, and Vulnerability", and "Mitigation of Climate Change". Each working group summarises the current research on climate change as it pertains to the focus of the group. Throughout the IPCC assessment reports, it is clear that global mean annual temperatures have been rising in the last century due to anthropogenic driven climate change. Global climate models (GCMs) have been developed to provide sophisticated projections of mean global temperatures based on future scenarios of greenhouse gas emissions. Four main scenario families are defined in the Special Report on Emissions Scenarios (SRES; Nakicenovic and Swart, 2000). These scenarios provide different hypothetical emission rates for the

[1] With respect to SLR, island hydrogeological systems can be classified as either topographically or flux controlled, as described by Werner and Simmons (2009). When sea level rises, the FWL also rises in the subsurface because it floats on the underlying salt water. In topographically controlled systems, the FWL is near to the ground surface and is not able to rise without outcropping at the ground surface. As SLR occurs, the FWL is reduced in extent. The FWL in flux controlled (or flux limited) systems is able to rise in the subsurface as SLR occurs; however, the lens is limited by the amount of freshwater flux (i.e. recharge) it receives. With low recharge, the FWL is not able to maintain the hydraulic gradient between the fresh and salt water along the coast, and therefore, cannot maintain the FWL extent (Michael et al., 2013). In general, flux controlled systems are less vulnerable to SLR; however, as the magnitude of SLR increases, the system will become topographically limited, and therefore, more vulnerable.

future. The scenario that represents the “worst-case” (i.e. the greatest anticipated change) is the A2 scenario. This study relies largely on the results of the AR4 and subsequent research based on AR4 generation models. However, the recently released AR5 Working Group I report provides climate change projections based on Representative Concentration Pathways (RCPs). The RCPs use recent greenhouse gas emissions (radiative forcing) data and will replace the former SRES emissions scenarios from AR4 moving forward. However, after accounting for the scenario specifications, the projected climate change based on the RCPs is comparable in pattern and magnitude to that determined for the SRES scenarios in AR4 (IPCC, 2013).

As mentioned above, the freshwater resources of small islands are identified as being particularly vulnerable to climate change impacts because they have limited capacity to buffer stresses to the hydrogeological system (Bricker, 2007; Bates et al., 2008; IPCC, 2013). Global climate projections for small islands generally indicate an increase in air temperature by 2100, which may lead to increased evaporation losses (IPCC, 2013). Where precipitation is also projected to decrease, this may lead to an overall decrease in groundwater recharge and an increase in water deficits, especially during the dry season (Singh, 1997). Conditions of reduced groundwater recharge disturb the balance of freshwater outflow necessary to maintain the extent of the FWL, and may lead to loss of freshwater resources due to saltwater intrusion (Ranjan et al., 2009; White and Falkland, 2010; Mollema and Antonellini, 2013).

Global SLR is also projected under global warming; however, the rate and amount of rise is spatially variable depending on several factors, such as the shape of the coastline as well as the geographical location (White et al., 2005). Global projections of SLR by 2100 range from 0.26-0.98 m, depending on the emissions scenario (IPCC, 2013). However, there is great uncertainty as to the rate at which sea level will rise, and the impact that SLR will have on small islands because significant geographic variability has been observed (White et al., 2005; Meyssignac et al., 2012).

There is also uncertainty as to whether the occurrence of tropical cyclones and hurricanes will increase, as factors that have a strong influence on their occurrence, such as the El Nino Southern Oscillation, are not well captured in GCMs (Lugo, 2000; IPCC, 2007; IPCC, 2014). Recent GCMs suggest that although the frequency of

hurricanes may decrease globally, it is likely that they will become more intense (Angeles et al., 2007; Biasutti et al., 2012). In general, it is the more intense hurricanes that create events, such as storm surge and coastal inundation, which can result in damage to freshwater resources (Biasutti et al., 2012). In addition, rising sea level is likely to increase the occurrence of storm surge and other extreme tidal events (IPCC, 2014).

1.4. Water Security

The term 'water security' has grown in popularity over the past decade and is used by a wide range of disciplines to describe and characterise the water system (Bakker, 2012). Water security describes the quantity and quality of water available for human use, environmental demand, and economic interests (Global Water Partnership, 2000; Grey and Sadoff; 2007). There are varying definitions of water security across different disciplines, but essentially they represent "access to sufficient quantity of water of acceptable quality to support human, environmental and economic needs" (Cook and Bakker, 2012). The United Nations' working definition of water security also includes aspects of political stability and prevention of water-related disasters (UNESCO-IHP, 2012).

Several water security assessment tools are available, most of which are based on the classification of a set of indicators. Examples of indicators include: water stress as a measure of water usage versus availability (Falkenmark et al., 2007); water efficiency in food production (Rockström et al., 2007); water availability for basic human needs or environmental needs (Lautze and Manthrithilake, 2012); water quality indicators measuring ecosystem health or human health (Dunn and Bakker, 2011); and the capacity for water governance (van Leeuwen et al., 2012). The assessment tools are designed for different spatial scales from municipal to regional to national; however, the indicators are generally measured at a specific point in time. Therefore these assessments do not asses the risk from potential consequences in the future. In order to effectively inform water governance, assessments of water security should aim to describe the current situation alongside the risk of undesirable change (Dunn et al., 2012).

1.5. Risk Assessment

Risk assessments are used in a wide variety of disciplines, from natural hazard management and engineering to actuarial finance and public health. Common to all risk assessments is the evaluation of the likelihood of adverse consequences occurring (Zwahlen, 2004). There is a multitude of different risk assessment approaches and frameworks to address different purposes and objectives (e.g., Adger, 2006; Birkmann, 2006; IPCC, 2012). However, there have been few studies applying risk assessment principles to water security. A risk assessment approach allows the evaluation of multiple stressors that contribute to water insecurity.

Risk describes the vulnerability to a hazard and the loss (sometimes also referred to as exposure or consequence) experienced if that hazard were to occur. Vulnerability is characterised by the predisposition (or susceptibility) to a hazard and the characteristics of the hazard itself. Different risk assessments identify the principal components of risk using different terminology or meanings, which can lead to confusion. For the purpose of this study, previous work is presented using a consistent terminology based on the following definitions:

$$\text{Risk} = \text{Vulnerability to hazards} \times \text{Loss due to hazard occurrence} \quad (1.1)$$

where

$$\text{Vulnerability} = \text{Susceptibility} \times \text{Hazard characteristics and presence} \quad (1.2)$$

Few water security assessments, particularly groundwater assessments, have characterised risk; most assessments have focused on characterising the susceptibility (commonly referred to as the intrinsic vulnerability) of the aquifer. Rarely are specific hazards included except in the context that such hazards exist and can be expected to enter into the aquifer system and move through the system in a particular way. The term specific vulnerability has been used to assess the behaviour of a specific contaminant along its flow path. Moreover, few approaches consider the loss component. Notable examples of water security assessments that evaluate risk include those developed under the European Commission COST Action 620, such as COPK, LEA, VULK, and

time-input (Zwahlen, 2004), as well as a groundwater quality risk assessment framework developed to support source-water protection strategies (Simpson et al., 2013). There are several popular methods that characterise “aquifer vulnerability”, such as DRASTIC (Aller et al., 1987), GOD (Foster and Hirata, 1988), AVI (Van Stempvoort et al., 1992), SINTACS (Civita and De Maio, 1997) and EPIK (Doerfliger and Zwahlen, 1997) (noting that vulnerability is intrinsic and thus is termed susceptibility in this study). Other assessments of aquifer susceptibility generally rely on the principles developed in the preceding examples, whereby a series of indicators are assigned weighted values and are combined to produce an overall index of aquifer susceptibility. Modifications may be made to represent unique aspects of a particular system, such as karst; however, the overarching principles remain the same. Groundwater susceptibility assessments are usually based on a scenario of chemical (or biological) contamination derived from land use activities, whereby hazards are introduced at the land surface and travel vertically down to the water table. However, such assessments are not fully suitable for an island context where the pathways for contamination are not exclusively vertical, as previously discussed.

In addition, the components that determine risk vary in time and space so it is important to include temporal and spatial dynamics in risk assessment (IPCC, 2012). Therefore, water security risk assessments may benefit from integration with numerical modeling, which is able to characterise the spatial and temporal response of the hydrogeological system to various stressors. Models provide information related to the nature, timing and duration of potential impacts that can be used to define the hazards, likelihood of occurrence, aquifer susceptibility, and loss due to hazard occurrence. This results in assessments that reflect the hydrogeological behaviour of the specific study location and provide better defined areas of risk to water security.

1.6. Modeling

Numerical hydrologic models provide a key tool to understand the groundwater system and enable prediction of the hydrological response to various future stresses (Green et al., 2011). Numerous models of climate change impacts on groundwater resources have been developed, from local to global scales (Scibek and Allen, 2006;

Angeles et al., 2007; Döll, 2009; Goderniaux et al., 2011). These models generally rely on the outputs of global or regional climate models to define future climate projections, which are then coupled with the hydrogeological system through either empirical or physically based relationships (Holman et al., 2012). The direct impacts of climate change on groundwater resources, such as changes in precipitation or SLR, are more commonly modeled than the indirect impacts, such as changes in vegetation, land use or irrigation demand. The climate data used in hydrogeological models range from global averages, to regional approximations and local downscaled datasets, all of which bring a high level of uncertainty into the models (Taylor et al., 2013). However, numerical models provide insight on how different hydrogeological environments may respond to predicted climate shifts.

Modeling the impacts of climate change on small islands (and indeed coastal aquifers more generally) adds a level of complexity due to the dynamics of fresh water and salt water mixing processes along the coastline and underlying the FWL. For these types of coastal problems, a density-dependent flow and solute transport model is needed to account for the density differences and concentration gradients between fresh water and salt water. Density-dependent flow and solute transport modeling is inherently complex because the model must solve both the flow and solute transport equations iteratively. This results in greater accumulated numerical error (Konikow, 2011). The computational demand can also become significant for models that integrate additional factors, such as the influence of tidal fluctuation on FWL dynamics (Ghassemi et al., 1999). Therefore, these models are usually used to provide reasonable representations of the FWL, rather than simulating the exact morphology observed in the field. In general, density-dependent flow and solute transport modeling provides an effective tool to evaluate specific processes impacting FWL dynamics.

Previous modeling studies of FWLs and coastal aquifers have investigated the impact of SLR (Masterson and Garabedian, 2007; Werner and Simmons, 2009; Terry and Chui, 2012; Ataie-Ashtiani et al., 2013; Langevin and Zygnerski, 2013; Rasmussen et al., 2013), storm surge and wave wash-over events (Anderson, 2002; Anderson and Lauer, 2008; Chui and Terry, 2012; Chui and Terry, 2013; Yang et al., 2013), increases in pumping (Singh and Gupta, 1999; Banerjee and Singh, 2011; Jakovovic et al., 2011),

as well as other processes impacting FWL dynamics, such as changes in recharge (Schneider and Kruse, 2005; Sulzbacher et al., 2012).

Although many aspects of climate change and human impacts on groundwater resources have been modeled previously, few studies have investigated both the spatial and temporal response of the FWL to the simulated stressors, or the cumulative impact of multiple stressors. Simulating all of the different components impacting water security in a single model would be a complex and very challenging task. Therefore, hydrologic models alone are generally not capable of characterising water security, but are nonetheless powerful tools when integrated into water security assessment frameworks.

1.7. Research Objectives

The freshwater resources on small islands are impacted by many different stressors related to climate change and human activities. However, there are no risk assessment methodologies that address the unique water security issues encountered on small islands, where the freshwater resources are susceptible to hazards from numerous directions. In addition, the spatial and temporal response of the FWL on small islands to stressors is not fully characterised. The IPCC AR5 (IPCC, 2014) also identified data gaps in current research regarding island water security. For instance, there is a lack of studies that focus at the small, island specific scale. Most studies are at a regional scale. In addition, studies often do not incorporate concerns from the local context, especially those related to the outer (non-primary) islands within a given country (Barnett et al., 2008; IPCC, 2014). This results in a lack of awareness at the local level about the specific threats posed, which can discourage actions that reduce vulnerability (Nunn, 2009; IPCC, 2012). Communication of risk to inform policy-makers and engage local populations is likely to increase resilience to impacts and is critical for effective adaptation (Dunn et al., 2012; IPCC, 2012; IPCC, 2013). Therefore, identifying risk to water security allows policy-makers to make informed plans for the future and mitigate potential impacts.

The specific objectives of this study are as follows:

1. To characterise the spatial and temporal impacts of major stressors on the FWL of small islands;
2. To develop a risk assessment methodology tailored to evaluate risk to water security on small islands; and,
3. To present risk in an accessible format for use by policy-makers and local stakeholders.

1.8. Scope of Work

The following work was undertaken to achieve the research objectives:

- Recharge modeling to estimate both current and future recharge amounts.
- Numerical density-dependent flow and transport modeling (using SEAWAT) at an island-scale to evaluate the impact of long-acting stressors, including SLR and changes to recharge. These models were also used to evaluate the FWL response to land-use activities, such as pumping.
- Coupled surface-subsurface numerical modeling (using HydroGeoSphere with density-dependent flow and solute transport) at a small-scale to evaluate the impact of short-acting stressors, in particular, storm surge overwash.
- Evaluating the factors affecting FWL recovery from overwash events using examples of other island types.
- Developing a risk assessment framework that uses the results of the modeling.
- Implementing the risk assessment and preparing map-based results for use by policy-makers.

1.9. Organization of Thesis

The thesis is comprised of six chapters.

Chapter 1 provides an introduction to the main concepts and outlines the objectives and scope of the research. Chapter 2 presents the relevant background data for the field site. Chapter 3 details the methodology employed in the research, with a particular focus on the development of the numerical models.

Chapter 4, 5, and 6 were prepared primarily as papers and have been submitted for publication, as described below. The chapters present the papers as submitted/published, with minor formatting changes. All papers were co-authored with my senior supervisor, Dr. Diana Allen; however, I completed the research and prepared the paper, with Dr. Allen providing technical input, guidance, and editing.

Chapter 4 – From days to decades: numerical modeling of freshwater lens response to climate change stressors on small islands. This paper was submitted for publication to Hydrology and Earth System Sciences, authored by S.T. Holding and D.M. Allen. The paper has been accepted for publication as a Discussion paper, within the review and open discussion process of Hydrology and Earth System Sciences journal. The paper presents the results of the numerical modeling for long-acting and short-acting stressors, with a focus on the spatial and temporal response of the FWL.

Chapter 5 – Impact of wave overwash on small islands. This paper is prepared as a manuscript that presents the results of a generalised assessment of wave overwash impact on small island freshwater resources based on numerical modeling.

Chapter 6 – Risk to water security for small islands: an assessment framework and application. This paper was submitted for publication to Regional Environmental Change, authored by S.T. Holding and D.M. Allen. The paper presents the risk assessment of water security for Andros Island.

Chapter 2.

Study Area

The research presented in this thesis focuses on Andros Island, The Bahamas, as a proto-type for the assessment, although the outcomes of the research will be applicable to other islands and coastal areas. Andros Island, The Bahamas, was chosen as a representative island due to the availability of baseline hydrogeological data, monitoring records for historical storm surge occurrence, and relatively low development allowing for representative baseline modeling of the hydrogeological system.

2.1. Physical Setting

Andros Island is the largest island in The Bahamas, located in the Caribbean approximately 200 km southeast of Florida and 40 km west of the capital city Nassau, on New Providence Island (Figure 2.1 inset location map). It covers approximately 14,000 km^2 in area and is comprised of several smaller islands and cays divided into four districts: North Andros, Central Andros, Mangrove Cay, and South Andros (Figure 2.1). The island is generally low-lying; the highest elevations of approximately 20 metres above sea level (masl) correspond to a ridge that parallels the east coast, while the lowest elevations (<1 masl) are along the west coast. The eastern coastline borders the Tongue of the Ocean canyon and slopes steeply from the landmass. The western coastline is along the Great Bahama Bank with shallow offshore bathymetry for over 100 km from the coastline. The west coast contains many wetlands and saltwater marshes, while the rest of the island is largely covered by forest. There are no large surface water bodies on Andros Island; however, there are many ponds, which represent outcroppings of the water table and pooling of precipitation (Little et al., 1973). The population of Andros Island is approximately 7,500 residents (2010 census) with the majority of

settlements located along the east coast. There is a single major highway that extends the length of the island connecting the settlements.

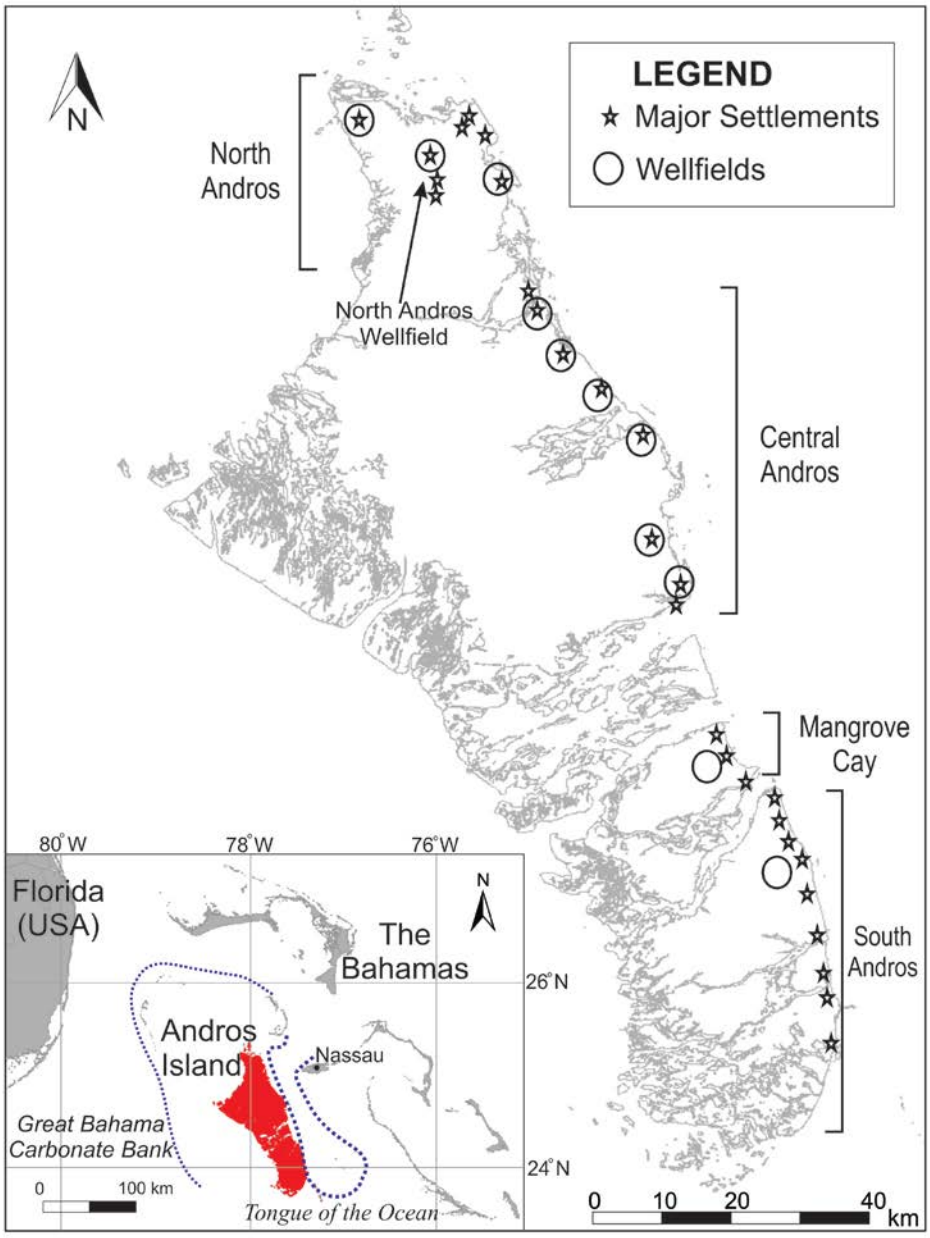

Figure 2.1. Location map of Andros Island, The Bahamas showing the location of major settlements and wellfields

2.2. Geology

The geology of Andros Island is predominantly Pleistocene Lucayan Limestone Formation composed of eolian dune deposits (Little et al., 1973). The Lucayan Limestone is 40 m thick (Beach and Ginsburg, 1980) with a porosity between 10-20% (Boardman and Carney, 1997). Discontinuity surfaces (unconformities) within the limestone are present as layers of paleosols recurring in the upper stratigraphy (Beach and Ginsburg, 1980). These layers represent previous episodes of sub-aerial exposure and are largely concentrated within the top 20 m, although they have been observed at different depths and frequency of occurrence in different boreholes across The Bahamas (Beach and Ginsburg, 1980; Boardman and Carney, 1997). Underlying the Lucayan Limestone is a porous, highly karstic, and relatively more permeable stratigraphic unit termed the Pre-Lucayan, which is present from 43 m below ground surface (mbgs) (Boardman and Carney, 1997) to at least 75 mbgs. The geology below 75 mbgs has not been observed as most studies have focused on the shallow, freshwater-bearing units (Boardman and Carney, 1997); however, deposits of carbonates on the Great Bahama Bank are estimated to be up to 7 km thick (Cant and Weech, 1986). The soil zone is often absent, or present only as a very thin layer, across Andros Island (Tarbox, 1986). The soils that are present are highly porous, with low organic content, and are generally derived from weathered limestone, ooid deposits, and limited loess (Little et al., 1973).

2.3. Hydrogeology

2.3.1. Freshwater Lens Extent and Morphology

The principal freshwater aquifer on Andros Island is the Lucayan Limestone. No fresh water has been observed within the Pre-Lucayan Limestone and the average depth of the base of the freshwater lenses (FWL) is above the contact between Lucayan and Pre-Lucayan formations. The water table is generally shallow, within approximately 1-2 m of ground surface. Figure 2.2 shows a simplified stratigraphic column showing the location of the key hydrogeological features.

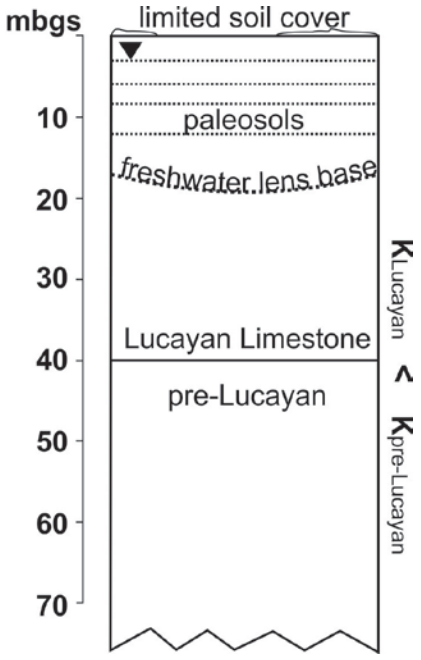

Figure 2.2. Simplified stratigraphic column. The base of the freshwater lens lies within the Lucayan Formation. The hydraulic conductivity (K) of the Lucayan is thought to be less than the hydraulic conductivity of the pre-Lucayan.

An important source of hydrogeological data is a land survey conducted in the 1970s, which summarised the results of multiple hydrogeological investigations on Andros Island (Little et al., 1973). These data provide a baseline estimate of the FWL morphology at specific locations and are provided in Appendix A (Table A1). Salinity profiles were conducted for 130 boreholes installed open to bedrock and located throughout the island. In addition to measuring the depth to the water table in these boreholes, the concentration of salinity was measured at 1.5 m depth intervals during drilling, immediately after borehole completion, and several weeks later to determine the depth to the base of the FWL. The data show that salinity concentrations often increased after borehole completion and, over time, resulted in a shallower depth to the base of the FWL than observed during drilling (Figure 2.3 shows data from Borehole 75). The precise mechanism causing this apparent thinning of the FWL in the borehole following drilling is unclear. Possible explanations are that once the borehole extends to a lower depth (often penetrating the base of the lens), the natural freshwater-saltwater interface

is disturbed and salt water rises within the open borehole[2]. The transition between fresh and salt water is not abrupt as shown on Figure 2.3. Using electrical resistivity surveying, Wolfe et al. (2001) showed that the zone of brackish water between the fresh and salt water isohalines is approximately 10 m thick.

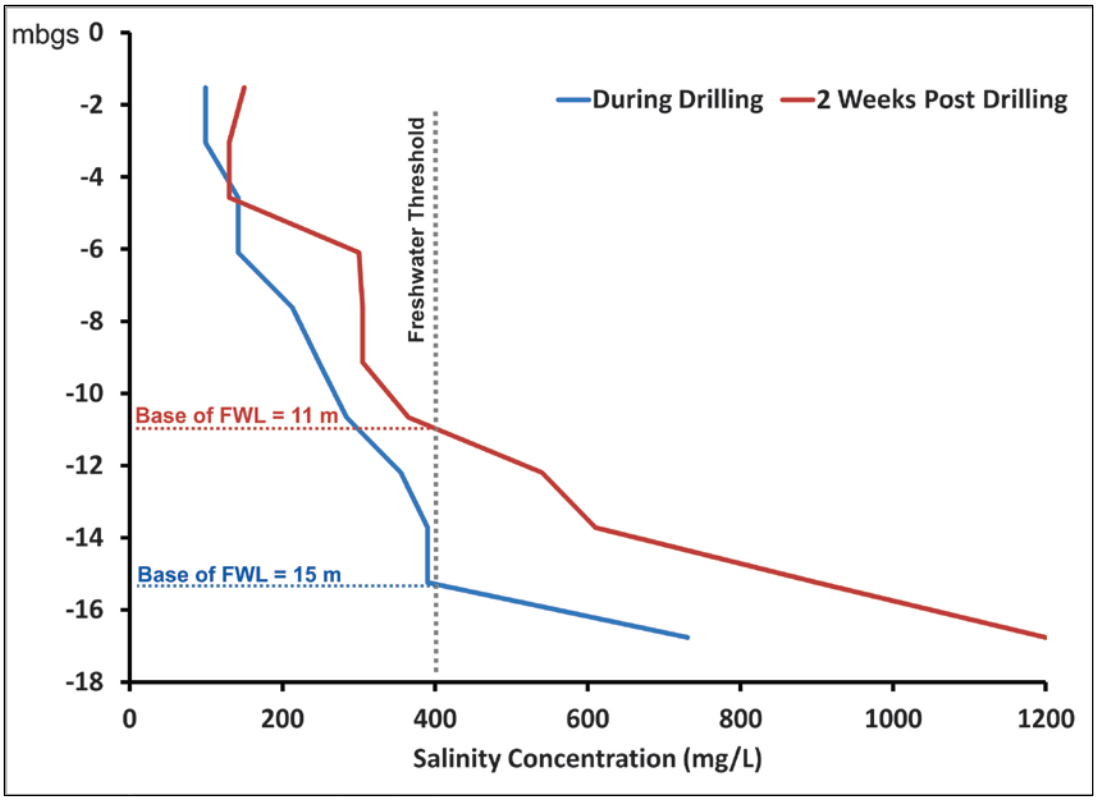

Figure 2.3. Salinity profile from Borehole 75 (data from Little et al., 1973); Salinity concentrations with depth are shown during drilling and 2 weeks post drilling. Data are provided in Appendix A, Table A.1.

Given the observed transition in salinity from fresh to salty water, the FWL is defined in this study by a threshold concentration of 0.4 grams per litre (g/L) or less of salt, which effectively corresponds to total dissolved solids (TDS). Figure 2.3 shows this

[2] This may occur because the hydrostatic pressure of the accumulating freshwater in the lens effectively depresses the underlying salt water (Ritzi et al., 2001). An open borehole has a lower hydrostatic pressure as it is exposed to atmospheric pressure from the surface. The salt water is at higher pressure at depth and therefore displaces the freshwater upward, making it appear as though the FWL is thinner. In addition, the permeability of the aquifer generally increases with depth so that deeper boreholes extend into higher permeability rocks, which increases mixing along the fresh/saltwater interface (pers. comm., Vincent Post, August 11, 2014).

threshold. This threshold concentration is based on the water quality guidelines for salinity in the municipal supply on Andros Island. It also falls within common definitions of fresh water containing less than 1 g/L of TDS (Freeze and Cherry 1977; Barlow 2003). The World Health Organisation (WHO) drinking water guidelines do not stipulate a maximum threshold for chloride in water, except as it relates to unacceptable taste. The WHO recognizes that water that tastes fresh often has a salt concentration (such as that of sodium chloride) less than 0.25 g/L; however, in regions where there is naturally more salt in the water there may be a higher taste threshold (WHO, 2011).

The locations of historic boreholes in North Andros were mapped at the time (Little et al., 1973) and are shown on Figure 2.4; however, maps indicating the locations of historic boreholes in the other districts are not available. In addition, the majority of these boreholes have been lost since the 1970s and, due to the limited road network on the island, access to the inland and western coast is restricted so few new boreholes have been drilled. Overall, there are few current data regarding the extent and morphology of the FWL on Andros.

Previous studies have shown that there are multiple FWLs distributed across the smaller islands and cays that comprise Andros Island. In general, the term FWL used in this thesis refers to the three predominant lenses in North/Central Andros, Mangrove Cay and South Andros, the largest of which is located in North/Central Andros. The maximum observed depth of the FWL was 39 mbgs. This depth was confirmed in several boreholes where multiple chloride measurements were made over time, indicating a stable depth of FWL measurement. The average depth of the FWL from all 130 boreholes was 16.0 ± 7.5 mbgs. Average depth to water is 1.0 ±0.8 mbgs, with maximum depth up to 5 mbgs underneath the high topography ridge. The elevations relative to mean sea level for top and base of the FWL are generally not known because ground surface elevations were not measured for the boreholes and their locations are inaccurate. However, the maximum elevation of the FWL in North Andros has been estimated to be around 2 masl (Ritzi et al., 2001). A geophysical study using more than 50 electrical resistivity surveys across North Andros indicated that the thickness of the lens in this region of the island ranged from 3 to 20 m (Wolfe et al., 2001). The lens is generally shallower in the southern regions of Andros Island (e.g. Mangrove Cay and

South Andros) compared to the northern regions (e.g. North and Central Andros) with a measured thickness of at least 15 m (pers. comm., municipal water supply manager, Bahamas Water and Sewerage Corporation). The historical extent of the lenses was mapped based on wellfield data, anecdotal observations and inferences about the vegetation patterns and topography (pers. comm., municipal water supply manager, Bahamas Water and Sewerage Corporation). The historical estimated extent of the FWL is shown on Figure 2.4.

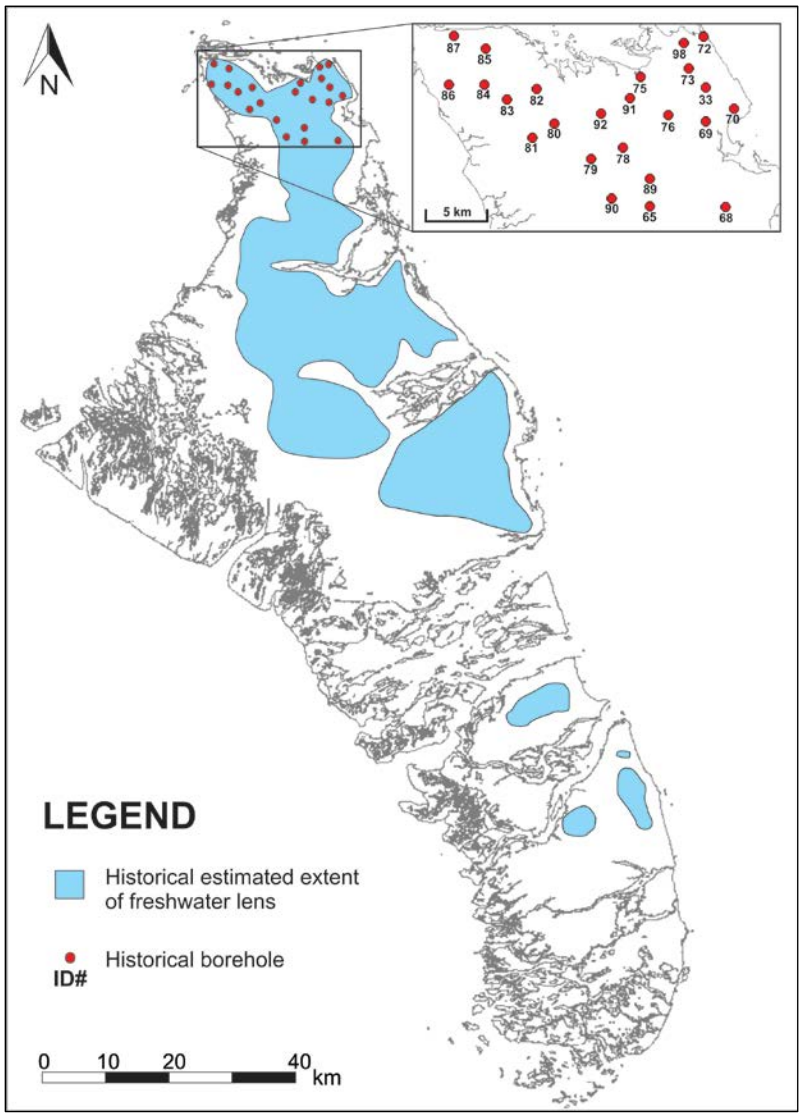

Figure 2.4. Historical estimate of FWL extent. Borehole identification numbers correspond to Appendix A, Table A1 (data from Bahamas Water and Sewerage Corporation and Little et al., 1973)

The thickness of the FWL on Andros Island is significantly less than the theoretical lens calculated using the Badon Ghyben-Herzberg approximation (Cant and Weech, 1986), which predicts lens thickness to be 40 times the head above sea level. The Badon Ghyben-Herzberg approximation assumes a sharp interface between salt water and fresh water (i.e. no transition zone), static salt water, and only horizontal flow in the lens. It is therefore not always valid for small island aquifers where geological features developed as secondary porosity may result in high conductivity layers that affect the lens morphology, or where the vertical flow component is significant and thick mixing zones develop (Falkland, 1991; Robins and Lawrence, 2000). On Andros Island, the FWL thickness is closer to 10-15 times the average head above sea level (Ritzi et al., 2001). Previous studies have hypothesized that the shallowness of the lens on Andros Island is due in part to the presence of the paleosol layers which reduce the hydrostatic pressure of the FWL, causing a raised saltwater interface (Ritzi et al., 2001). The effect of the paleosols on the FWL is investigated using numerical modeling in Chapter 3.

2.3.2. Aquifer Hydraulic Properties

Few data are available on the hydraulic properties of the aquifer (Lucayan Limestone). An estimate of hydraulic conductivity was derived from the analysis of historical pumping test data for Andros Island, resulting in a geometric mean of 5.4×10^{-3} ± 1.7×10^{-3} m/s and ranging from 1.5×10^{-4} to 3.8×10^{-2} m/s (Whitaker and Smart, 1997). The historical data included 38 specific capacity single-well pumping test results. The tests were limited in duration (30-60 minutes) to minimize the occurrence of upconing. Transmissivity estimates were calculated from the pumping test data using the Theis method, and hydraulic conductivity values were derived assuming that the saturated depth of the well represented the aquifer thickness (Whitaker and Smart, 1997). Specific capacity was observed to be highly variable depending on the location of tested wells. In some areas, the specific capacity was very low, on the order of 2.2 litres per minute, while nearby boreholes had much higher specific capacity requiring high pumping rates (500 litres per minute) to achieve measurable drawdown (Little et al., 1973; Whitaker and Smart, 1997). Tidal response tests were also conducted in boreholes and indicated a limited tidal effect within the FWL, although a larger tidal response was observed in

deep boreholes that penetrated the base of the lens (Little et al., 1973). Therefore, these tests were not suitable for determining the hydraulic properties of the fresh aquifer, but confirmed the high permeability at depth (Little et al., 1973). Storativity was estimated at $1x10^{-5}$ and porosity estimated at 10-20% (Little et al., 1973; Boardman and Carney, 1997).

2.3.3. Recharge

Precipitation is lost primarily through evapotranspiration (Little et al., 1973); very little precipitation forms overland runoff or soil moisture storage due to the thin or absent soil zone, the high permeability of the limestone, and minimal paved areas (Tarbox, 1986). The remaining water constitutes the sole recharge to the aquifer. Previous studies estimated recharge in Mangrove Cay and South Andros at approximately 300 mm/year (Little et al., 1973). No recharge estimates are available for North and Central Andros. Recharge is expected to occur throughout the year; however, increases in recharge rates are expected during the summer rainy season, when the majority of precipitation occurs (see section 2.4).

2.3.4. Conceptual Model

In summary, the overall conceptual understanding of the hydrogeology of Andros Island based on the literature review is as follows:

- Fresh water on Andros Island is contained in several FWLs distributed across the smaller islands and cays that comprise Andros Island.
- The lenses form primarily through recharging precipitation as there are no significant surface water bodies. There is little soil development and paved areas, therefore runoff of precipitation and soil moisture storage are minimal.
- The morphology (depth, extent and thickness) of the FWL is estimated from historical data. The maximum observed thickness of the lens is 39 m, with an average thickness of 16 m.
- The FWL is contained entirely within the Lucayan limestone and does not intersect the underlying higher permeability limestone which is present below a depth of 43 mbgs.
- Several paleosol layers representing previous sub-aerial exposure are present in the upper 20 m of the aquifer. These layers are present on other islands in

The Bahamas and may affect the morphology of the lens, causing it to be thinner than if the aquifer geology were homogenous (the role of paleosols is explored in more detail in Chapter 3).

2.3.5. Water Supply

The majority of potable water for The Bahamas is groundwater, the largest supply of which is found on Andros Island (Tarbox, 1986; Bowleg and Allen, 2011). Chlorinated water[3] is supplied via underground pipes to the majority of settlements on Andros Island by the Bahamas Water and Sewerage Company (BWSC). The BWSC also provides water to settlements in South Andros via tanker trucks that refill reservoir tanks. All water provided by the BWSC is extracted from the FWL via eleven wellfields distributed throughout the island (shown on Figure 2.1). The largest extraction of groundwater occurs in North Andros from the North Andros Wellfield. Small, privately operated, reverse osmosis saltwater treatment systems are used on Andros Island to support some tourism and industrial facilities; however, these are few in number due to high operational costs. Private wells are also operated; however, the Bahamian Government encourages residents of the island to use the BWSC supplied water for the protection of their health from potentially contaminated shallow groundwater. There are no sewerage or wastewater treatment facilities on Andros Island, so all properties rely on private septic systems for wastewater disposal. Private wells are used largely for irrigation and/or industrial operations.

Water quality within the FWL is relatively steady throughout the year with little seasonal change in salt concentration between the wet and dry seasons. However, as is common for most FWL aquifers, there is potential for upconing of the underlying salt water leading to salt contamination of the FWL. Large diameter trench wells pumped at low rates are much less likely to cause upconing compared to small diameter, deep boreholes (Tarbox, 1986; Bear at al., 1999). Therefore, at the North Andros Wellfield, a series of interconnected trenches is used to skim water from the top of the FWL. The wellfield consists of 300 m-long trenches that are approximately 1 m wide and 2 m deep

[3] The water is naturally of good quality, safe for consumption and is only chlorinated as a precautionary measure.

(Wolfe et al., 2001; Bowleg and Allen, 2011). Each trench radiates from a central cruciform (central node connecting two or more trenches), which has a minimum of two and maximum of four trenches that drain towards the center (Figure 2.5). The cruciforms situated at the northern end of the wellfield are spaced several hundreds of metres apart and are connected by culverts, whereas all limbs within the southern cruciforms are interconnected. There are a total of 35 cruciforms and approximately 40 km of trenches. All cruciforms in the North Andros Wellfield are shown in Figure 2.7. Water within each cruciform flows by gravity to a central sump where it is pumped into reservoir tanks for treatment and distribution into the BWSC water lines (Bowleg and Allen, 2011). Shallow boreholes are utilised in some of the BWSC wellfields on Andros Island; however, the volume of water extracted is significantly less than that extracted at the North Andros Wellfield.

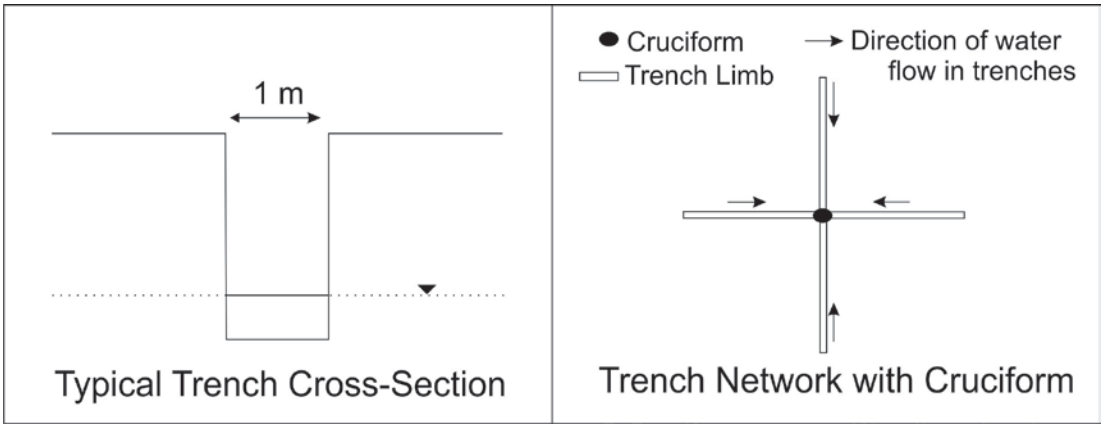

Figure 2.5. Wellfield trench illustration

The North Andros Wellfield was developed to meet the demands of a growing population and tourism industry on the neighbouring island of New Providence. Pumping of the North Andros Wellfield began in 1977 and increased over the years to a daily rate of approximately 4.8 million Igpd, or 18,170 m^3/day (Wolfe et al., 2001; Bowleg and Allen, 2011). The estimated available freshwater supply from the North Andros wellfield is approximately 6 million Igpd (Bowleg and Allen, 2011). In late 2011, pumping from the wellfield was reduced when export of water off-island ceased due to the installation of additional reverse osmosis (RO) systems by the BWSC in New Providence. The use of RO systems, instead of groundwater, was partly due to a perception that water from the FWL on North Andros is less reliable (i.e. prone to contamination from storm surge

overwash). Although the current needs of North and Central Andros are met by extractions in the North Andros Wellfield, there is demand for water in Mangrove Cay and South Andros as the lenses there are much smaller (see Figure 2.4). Transportation of water from North Andros to the southern districts remains a challenge because there are no pipelines (or road networks) connecting the separate sections of the island.

2.4. Climate

2.4.1. Historical Climate Data

Rainfall patterns in the Bahamas are spatially variable, generally occurring as heavy events over a short period of time (Gamble and Jordan, 2006). The majority of precipitation occurs during the rainy (wet) season from May to October (Little et al., 1973; Cant and Weech, 1986; Bukowski et al., 1999; Bowleg and Allen, 2011). The Bahamas is situated within the Atlantic Hurricane Belt, an area that is prone to hurricanes, which occur predominantly between June 1st and November 30th (National Hurricane Center, National Oceanic and Atmospheric Administration (NOAA), 2014a). The Bahamas is regularly affected by hurricanes that pass nearby or make landfall on the islands; at least 50 hurricanes passed within 200 km of Nassau between 1886 and 1999 (Bowleg and Allen, 2011).

Climate data (daily precipitation and mean daily temperature) for Andros Island were provided by the Bahamas Department of Meteorology. The nearest operational weather station is Nassau Airport (located 40 km east of Andros Island; Figure 2.1) with daily temperature and precipitation records from 1979 to 2008. Daily precipitation records were also available from 1971 to 2000 for a weather station located on South Andros, which is no longer operational; however, no temperature records were available for this station. The southern region of Andros is known to receive less rainfall than the northern region; therefore, separate monthly averages for precipitation and temperature were calculated for the northern regions (North and Central Andros) and the southern regions (Mangrove Cay and South Andros) for the period 1979-2000. The averages for the northern part of Andros were based on the temperature and precipitation records from the Nassau weather station, whereas the averages for the southern portion of

Andros were based on temperature records from Nassau and precipitation records from the South Andros weather station. The resulting monthly averages for 1979-2000 are presented in Table 2.1. The current climate averages are shown alongside climate change projections in Figure 2.6.

Table 2.1. Monthly climate averages (1979-2000)

Parameter	D	J	F	M	A	M	J	J	A	S	O	N
Monthly Mean Temperature (°C) *North/South*	22.4	21.5	21.8	22.3	23.8	25.5	27.2	28.1	28.1	27.7	29.5	24.5
Monthly Mean Precipitation (mm) *North*	47.3	50.3	51.6	65	84.3	108.1	212.7	161.5	234.1	177.5	163.6	85.7
Monthly Mean Precipitation (mm) *South*	53.0	35.5	38.9	42.4	45.4	106.5	105.2	63.6	80.9	100.0	125.9	91.4

2.4.2. Climate Change Projections

Climate change projections are presented in regular reports prepared by the Inter-governmental Panel on Climate Change (IPCC). This research relies on climate change projections from the IPCC 4th Assessment Report (AR4) (IPCC, 2007) as well as subsequent studies utilising the AR4 generation of climate models. The recently released 5th Assessment Report (AR5) provides climate change projections based on Representative Concentration Pathways (RCPs), which use recent greenhouse gas emissions data and which replace the former SRES emissions scenarios used in AR4 (IPCC, 2007). There is general agreement between the projections for the Caribbean region based on the AR4 emissions scenarios and the new RCP scenarios (IPCC, 2013).

The Caribbean region is expected to see a mean increase of more than 2°C warming by 2100 for all seasons relative to the baseline used in AR4 (Biasutti et al., 2012). The warming is expected to manifest as increases in record high temperatures, the occurrence of warmer nights, and longer duration of heat waves (defined as periods with greater than 5°C increases from average temperatures). Other projected changes

include a 30% decrease in summer (rainy season) precipitation, reduced length of the rainy season, more frequent or more severe droughts, and increased length of the dry season (Biasutti et al., 2012). These projected changes for the Caribbean are likely to lead to an overall decrease in groundwater recharge and an increase in water deficits, especially during the dry season (Singh, 1997; Cashman et al., 2010).

Determining climate change projections from global climate models (GCMs) poses a challenge for small islands as the spatial scale (grid size) of GCMs is much larger (i.e. typically 200-600 km^2) compared to the land area of most small islands (IPCC, 2014). GCM data require some form of downscaling for application to small islands; however downscaled data are not often available at the island scale (United Nations Development Programme (UNDP), 2010). The UNDP prepared country-specific projections of climate change for 52 developing countries, including The Bahamas, to provide accessible data at a smaller scale (McSweeney et al., 2010). The projections are based on the results of 15 GCMs for three different AR4 emissions scenarios (A2, A1B, and B1). The GCM results for the A2 scenario (likely to result in the greatest change in climate) are re-gridded on a 2.5° x 2.5° grid across The Bahamas. As downscaling of the data to the local scale was not performed, the projections are based on a coarse spatial resolution of the GCM and may not represent local-scale variability. Although this is a limitation of the climate change projections, in the absence of downscaled data, the projections were considered appropriate for this study. Summaries of observed trends and projected changes in temperature and precipitation were compiled as shifts for seasonal three-month groupings (McSweeney et al., 2010). For each grouping, a range in values (minimum, median, and maximum) determined from the 15 models is provided based on the different emissions scenarios for the 2030s, 2060s and 2090s. The median shift for the A2 scenario, projected for the 2090s, within the grid cell containing Andros Island was selected for each seasonal grouping of temperature and precipitation. The shifts were then applied to the climate averages for the northern and southern regions of Andros Island, as summarised in Table 2.2.

Table 2.2. Projected climate shifts and monthly averages (2100)

Parameter	D	J	F	M	A	M	J	J	A	S	O	N
Temperature Shift (°C)		+2.8			+3.0			+3.2			+3.2	
Projected Monthly Mean Temperature (°C) *North/South*	25.2	24.3	24.6	25.3	26.8	28.5	30.4	31.3	31.3	30.9	32.7	27.7
Precipitation Shift (mm)		-2			-18			-24			+12	
Projected Monthly Mean Precipitation (mm) *North*	45.3	48.3	49.6	47	66.3	90.1	188.7	137.5	210.1	189.5	175.6	97.7
Projected Monthly Mean Precipitation (mm) *South*	51.0	33.5	36.9	24.4	27.4	88.5	81.2	39.6	56.9	112.0	137.9	103.4

The projected climate averages indicate that the average daily temperature will increase during all seasons (between 2.8-3.2°C) by the 2090s. The majority of the change to precipitation is projected to occur during the summer; precipitation is projected to decrease significantly (up to 42% reduction relative to current conditions) with some increases in the early winter. The projected monthly temperature and precipitation data are shown alongside the current temperature and precipitation data in Figure 2.6.

The median of the A2 scenario was selected to represent the potential future climate conditions for the scenario expected to result in the greatest change. However, it may under or over-estimate the changes to climate that will be realised over that time period. Overall, the projected climate shifts represent conditions with less precipitation and higher temperatures - a drier and hotter climate state. However, there is significant uncertainty related to climate modeling, such that within a single scenario (A2) the range in temperature increase is 2.1° to 4.7°C and the range in precipitation shift is from -80 to +62 mm depending on GCM. Therefore, future climate conditions may vary significantly from the projections provided in Table 2.2 (i.e. the climate state may actually be wetter than current conditions, with smaller increases in temperature).

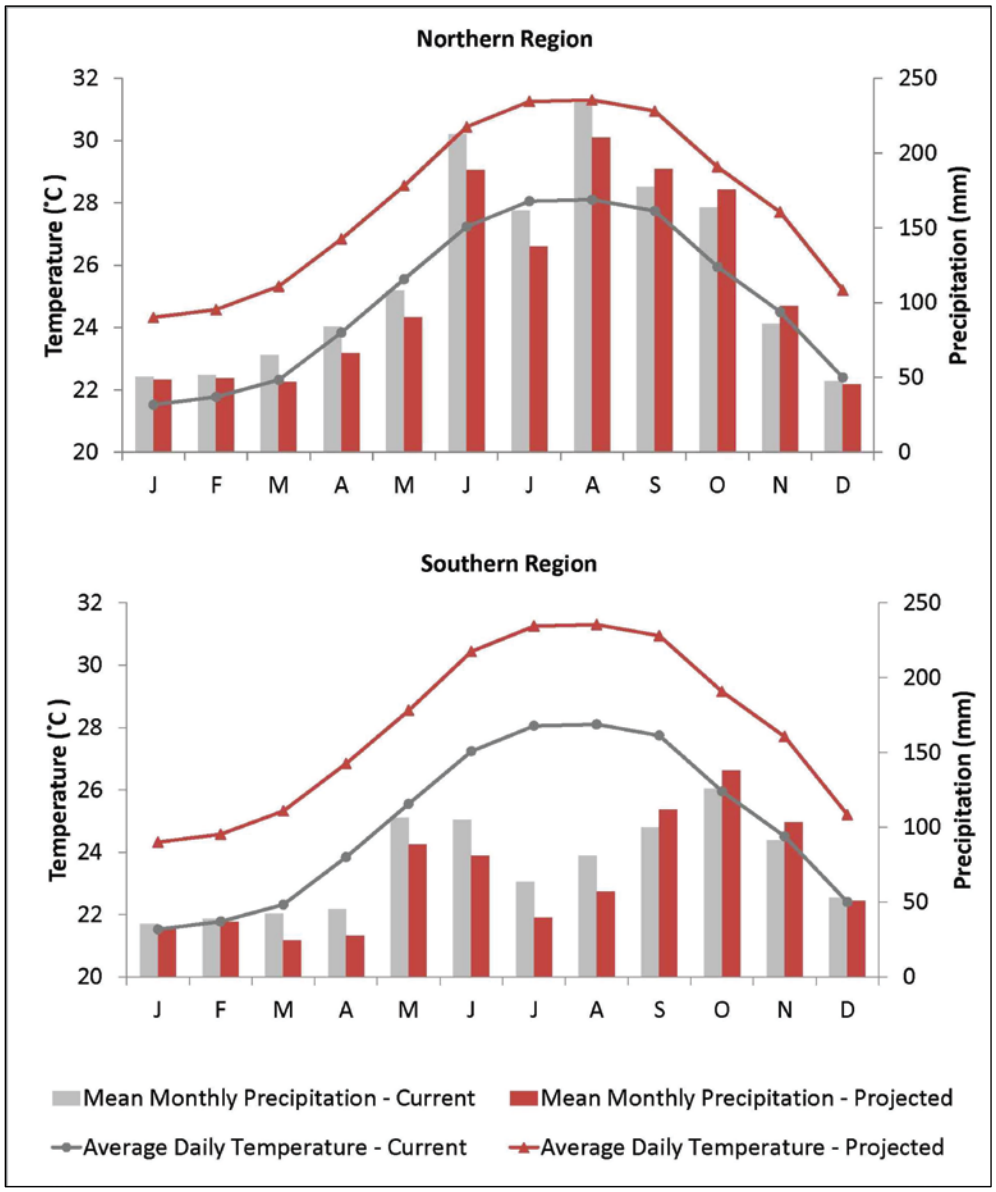

Figure 2.6. **Current and projected temperature and precipitation averages for the northern region (North and Central Andros) and the southern region (Mangrove Cay and South Andros).**

2.5. Coastal Processes

The coastal boundaries are important in a small island setting where the FWL is surrounded by seawater. Low-lying islands, such as Andros Island, are also particularly vulnerable to impacts along the coast such as sea level rise and storm surge.

2.5.1. Sea Level Rise

Global sea level rise (SLR) is projected under global warming; however, the rate and amount of rise is spatially variable depending on several factors, such as the proximity to and shape of the coastline as well as the geographical location (White et al., 2005). Global projections of SLR by 2100 range from 0.26-0.98 m (depending on the RCP scenario), with the medium RCP4.5 scenario predicting SLR ranging from 0.5-0.6 m by 2100 for the Caribbean relative to 1986-2005 baseline (IPCC, 2013). In comparison, AR4 predictions ranged from 0.2-0.6 m by 2100 relative to the same baseline (IPCC, 2007). Over the past 60 years, the rate of SLR in the Caribbean has been close to the global average of 1.8 mm/year (Palanisamy et al., 2012). Regional probabilistic predictions for the Caribbean project a mean SLR in 2100 ranging from 0.3-2.6 m relative to 1980 (Obeysekera et al., 2013). However, there is great uncertainty as to the rate at which sea level will rise and the impact that SLR will have on small islands as significant geographic variability has been observed (White et al., 2005; Meyssignac et al., 2012).

2.5.2. Wave Overwash

Wave overwash often occurs as storm surge during tropical cyclones or hurricanes when high winds cause large waves that break above the high tide levels, potentially causing inundation inland (NOAA, 2014b). There is uncertainty as to whether the occurrence of tropical cyclones and hurricanes will increase in the Caribbean, as factors which have a strong influence on their occurrence, such as the El Nino Southern Oscillation (ENSO), are not well captured in GCMs (Lugo, 2000; Christensen et al., 2007; IPCC, 2014). Recent GCMs suggest that although the frequency of hurricanes may decrease globally, it is likely that they will become more intense (Angeles et al.,

2007; Biasutti et al., 2012). In general, it is the more intense storms that create events resulting in damage to freshwater resources such as storm surge and coastal inundation (Biasutti et al., 2012). In addition, rising sea level is likely to increase the occurrence of storm surge overwash and other extreme tidal events.

Storm surge wave height depends on several factors, including distance from the storm center, direction of storm travel, storm intensity, and the bathymetry of the coastline (Irish et al., 2008). Storm surge modeling was previously conducted for The Bahamas to determine typical wave heights projected to occur due to various hurricane strengths and direction of storm travel (Rolle, 1990). The SLOSH modeling code (Jelesnianski et al., 1984) was used to couple a hurricane model with a storm surge model (Rolle, 1990). An ensemble of 13 storm directions, each with up to 20 different possible travel paths, was compiled based on historical hurricane records. The SLOSH model was run for each storm ensemble with a Category 1 to 5 intensity rating on the Saffir Simpson Hurricane Scale. The resulting storm surge wave heights were then mapped out for Nassau and other nearby islands. Although Andros Island was not specifically mapped, it was assumed that the results of nearby islands were applicable to Andros Island based on similar bathymetry and location. Typical wave heights occurring at coastlines bordering the Great Bahama Bank are 6 masl, whereas typical wave heights occurring along the Tongue of the Ocean are 3 masl (Rolle, 1990).

2.5.3. Historic Storm Surge

In September 2004, Hurricane Frances caused a storm surge on the west coast of Andros Island that resulted in extensive salinization of the North Andros Wellfield. The hurricane ranged from a Category 4 to Category 2 on the Saffir Simpson Hurricane Scale while it travelled across The Bahamas from the southeast to northwest (Franklin et al., 2006). The exact time of occurrence and the nature of the storm surge are unknown because the western coast of Andros Island is largely unpopulated. The surge occurred between September 3rd- 4th 2004, while Hurricane Frances passed near Andros Island. After the hurricane had passed, evidence of the storm surge was observed, such as flooded ground and the presence of marine fish at inland locations (Bowleg and Allen, 2011). The likely extent of the storm surge was based on observations of damage and

evidence of flooding, which was observed to be up to 1 m deep. The area affected by the storm surge included parts of the North Andros Wellfield (Figure 2.7).

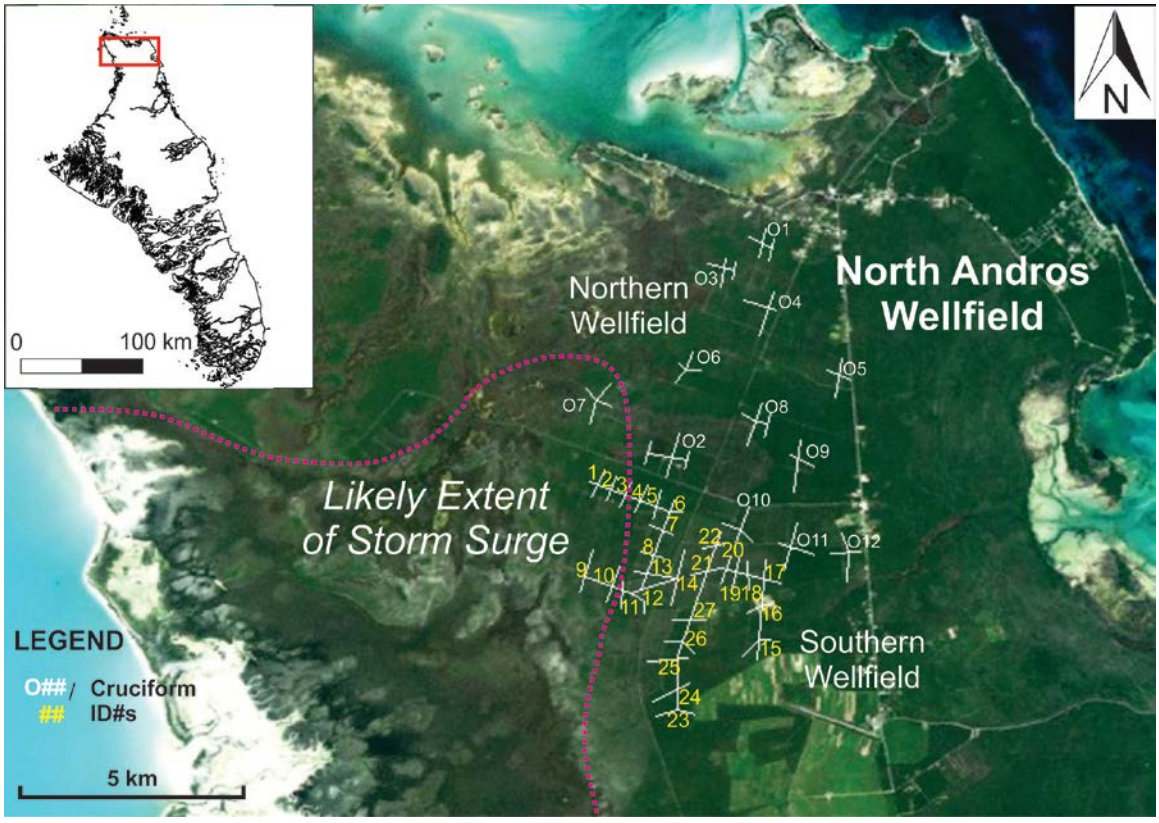

Figure 2.7. North Andros Wellfield and extent of storm surge

Hurricane Frances made landfall in southern Florida, where storm surges of up to 1.8 m were recorded, and caused heavy storms as far north as Ontario, Canada (Franklin et al., 2005). The hurricane is estimated to have caused $8.9 billion of damage within the USA (with extensive property damage in The Bahamas not included) and a total of 8 deaths from the USA and The Bahamas (Franklin et al., 2005). It was retired from the official rotation of storm names due to the damage sustained throughout the Caribbean and the USA.

Regular monitoring of electrical conductivity (EC) in the trenches of the North Andros Wellfield is conducted by the BWSC. Monitoring generally occurs once per month in all of the trenches, although for unknown reasons, this is not always completed. Monitoring records were provided by the BWSC for this study from 2004-2011, only for the southern cruciforms, because the northern cruciforms (identification numbers

preceded by an O in Figure 2.7) were mostly unaffected by the storm surge. EC was measured in the trenches and chloride concentrations were calculated by the BWSC based on the EC measurements. Water samples were occasionally collected and submitted to a laboratory for chemical analysis to determine the actual chloride concentrations. Chloride concentration data are available for May 2004 (pre-storm), September 7th (immediately post-storm surge), September 15th (following remedial action) and July/August 2005 (approximately one year post-storm surge) (Table 2.3). Additional data are available as monthly values for 2006, 2007 and 2009-2011, which include measurements and observations of color, turbidity, pH, temperature, and EC (not shown).

Unfortunately, chloride concentration values are not included in data from 2006 to 2011. Therefore, for this study, chloride concentrations were estimated from the ratio of EC to chloride using 2004-2005 data[4]. Calculated chloride values for 2004, 2005, 2006, and 2009 are presented in Table 2.3. Data from 2007 are not presented because they are incomplete and the EC measurements were taken from different locations than those used in the other datasets (i.e. not at the central node of the cruciform). No data were provided for 2008.

[4] Thus, the same conversion factor from EC to Cl concentration was used. It assumes that the EC to Cl concentration conversion used by BWSC is correct.

Table 2.3. Wellfield chloride concentrations (pre- and post-storm surge)

Cruciform	Chloride Concentration (mg/L)					
	May 12th, 2004	Sep. 7th, 2004	Sep. 15th, 2004[1]	Jul./Aug. 2005	Sep. 2006[2]	Sep. 2009[2]
1	217	12954	11406	878	464	145
2	268	13023	9997	899	395	158
3	266	12609	7662	1027	256	220
4	282	12524	7520	926	534	238
5	303	10625	6334	832	641	204
6	297	13165	7215	927	333	241
7	291	11493	5303	873	501	281
8	270	10747	5102	868	400	295
9	229	11864	7593	1522	444	-[3]
10	283	11923	5812	1542	493	-[3]
11	264	11923	5073	1499	405	-[3]
12	254	11992	4363	1224	605	-[3]
13	265	-	3765	883	-	-[3]
14	234	-	1234	844	-	222
15	188	3740	1459	372	321	90
16	222	4377	944	408	314	106
17	223	6233	1320	385	313	118
18	216	7465	986	435	268	122
19	228	7475	1129	507	263	109
20	269	7018	998	577	241	89
21	250	10021	956	520	250	114
22	165	5872	900	543	266	103
23	359	4233	3131	483	311	126
24	283	4768	3177	651	342	134
25	311	5438	3309	618	-	229
26	272	7511	3654	806	419	188
27	265	7055	3775	398	301	133

Note: 1) Sep. 15th Cl concentrations were measured following corrective action. 2) Measured Cl concentrations were not provided in original dataset; values shown are based on the ratio of EC to Cl from 2004/2005 data. 3) No measurements were made in these trenches throughout 2009-2011.

The pre-surge chloride concentration data indicate that there is little seasonal trend in conductivity throughout the year (i.e. no discernible trend in concentration between wet and dry seasons). Values range from 188 to 359 mg/L Cl^-, with spatially variable distribution (i.e. no area where the higher concentrations are more likely to occur). Based on monitoring data, seawater is known to have contaminated some of the western trenches in the network, particularly Cruciforms 1 to 12 and 21 (Figure 2.7). Monitoring data are not available for Cruciform O7, although BWSC staff indicated that it was flooded by the storm surge. Salinity (as chloride concentration) rose from less than 400 mg/l in all trenches prior to Hurricane Frances to around 13,000 mg/L following the storm surge in several of the most westward trenches (namely Cruciforms 1, 2 and 6). Overall there was an average of a 3000% percent increase in Cl^- concentrations.

The monitoring data also confirm the recovery of fresh water in the North Andros Wellfield trenches. The contaminated trenches were pumped, beginning on September 8th, as a form of remedial action to remove the salt water. Salinity in the affected trenches improved, as shown by the chloride concentration reducing by up to 88% on September 15th, relative to the maximum recorded concentrations in each trench. However, remedial pumping of the trenches was not completed because fresh water was required to support post-hurricane relief efforts on other islands. Therefore, the contaminated trenches were closed off from the wellfield system to allow for extraction of fresh water from the unaffected parts of the FWL (pers. comm., BWSC manager). Several of these contaminated trenches remained closed for two years due to poor water quality (including Cruciforms 9, 10 and 11). The wellfield eventually recovered to normal salinity concentrations over several years (Bowleg and Allen, 2011) with all trenches recovered by 2009.

2.6. Land-Use and Water Management Initiatives

Andros Island is less developed than many other Bahamian islands, especially given its large land area, and efforts are in place to protect the natural environment from commercial development (The Nature Conservancy (TNC), 2011). There are five national parks on Andros Island, covering more than 236,000 acres, focussed on protecting various aspects of the ecological system such as land-crab habitat, sections

of the barrier reef, pine forests, mangroves and wetlands (TNC, 2011). In 2010, a Global Environmental Fund (GEF)-funded “Integrated Water Conservation and Management (IWCAM)” project was conducted on Andros Island. The project compiled an overview of major land-use activities, identified potential areas of concern for contamination, and provided valuation of the resources on the island (IWCAM, 2011; TNC, 2011). The IWCAM project also included the preparation of a water conservation strategy, which recommended that a geospatial database be prepared to identify all potential threats to the freshwater resources of Andros Island (Environ, 2010).

There are few industries on Andros Island, except for a textile dying factory, a water bottling plant, and several farms. Commercial businesses include four airports, approximately 34 hotels and 18 fuel stations (TNC, 2011). In addition, the United States Navy operates an underwater weapons testing facility called AUTEC (Atlantic Undersea Test and Evaluation Center) on the east coast of Central Andros. Most residents are employed in one of two industries: resource-based industries such as fishing, and tourism-related service provision (IWCAM, 2011). Historically, forestry was also a significant economic activity on Andros Island, as well as farming in North and Central Andros (Little et al., 1973). However, the farming industry currently comprises only 1% of the island’s economic activity (IWCAM, 2011). Due to the lack of a significant soil zone on Andros Island, most farms rely on crushing the upper bedrock to form a soil-like medium for planting (Little et al., 1973).

The RBC Blue Water Project™ was initiated in 2012 to foster watershed conservation in The Bahamas. The project is focussed on Andros Island and is implemented in partnership with the Bahamas National Trust and TNC. TNC is responsible for project components related to a survey of hazards and sanitation practices, the compilation of a geospatial database of potential threats to the FWL, the development of a water management plan, and the provision of technical seminars to promote water-saving technologies. The results of the survey are presented in Section 2.8, below.

The water management plan was prepared in April 2013 with the objective of quantifying the freshwater resources of Andros Island, evaluating future demand, and

identifying threats to the resource. However, due to project timing, this plan was prepared before the hazard survey was completed and without input from the research presented in this thesis, although efforts were made to collaborate. Therefore, the contents of the plan largely reflect historical information already presented in the preceding sections, particularly the land survey conducted in the 1970s (Little et al., 1973). The plan identified water conservation as a key action point and emphasized the need for water-saving technologies (Environ, 2013). However, this is in contradiction to the results of the survey (discussed below), which show that contamination poses a significant threat to the FWL. Moreover, the BWSC water use data indicate that the volume of the fresh water available on Andros Island is sufficient to meet the needs of the population, if managed correctly. Other recommendations include converting vertical borehole wellfields to horizontal trenches to prevent upconing, berms to protect trenches from storm surge, and the proper installation and maintenance of septic fields (Environ, 2013).

In meeting with local residents, community representatives, and the BWSC staff during field visits conducted as part of this research, a key water management issue on Andros Island was raised in relation to the perception that the FWL was not a reliable source of water. This perception may be a consequence of 1) the poor water quality that resulted from the impact of the storm surge in 2004, 2) concern about the proximity of wellfields to settlements, 3) potential chemical and pathogen contamination, and 4) distrust in the BWSC due to political issues. As a result, many residents rely solely on bottled water for drinking water and support investments into RO systems. RO systems are promoted as an alternate source of fresh water (which supplies a large proportion of water on New Providence); however, there are high operational costs involved which are susceptible to fluctuations in the cost of energy (White and Falkland, 2010). Since export of water to New Providence has stopped, there is a surplus of fresh water available in North Andros, and conservationists are concerned that the FWL on North Andros will be threatened by increases in potentially hazardous activities such as mining and farming (pers. comm., Andros Conservancy and Trust and BWSC representatives). Proposals for mining projects include the quarrying of bedrock within the FWL; limestone located within fresh water is desirable because it does not require additional washing to remove salt water before use in construction. Due to the greater thickness of the lens in the

northern part of Andros and the accessible road network in this area, these mining projects often target areas very near to the North Andros Wellfield (pers. comm., BWSC manager). These activities may disrupt the lens causing major upconing in these areas. Because the FWL is currently underutilised and public perception has discredited the quality of naturally occurring fresh water to some degree, there is concern that there will be little opposition to activities which have the potential to significantly damage the lens. Potential consequences include loss of the FWL in a country with limited freshwater resources and a reduced resilience of Andros Island to adapt to changes in climate and economic conditions. Future policy decisions regarding the protection and use of the FWL on Andros Island may have significant implications for the long-term sustainability of the lens.

2.6.1. Hazard Survey

A door to door survey was conducted as part of The RBC Blue Water Project™. The survey was designed through consultation with SFU (this research) to gather information related to water supply, wastewater treatment and sanitation facilities, solid waste disposal, and chemical use and disposal. The survey was implemented by a local consulting firm, MCK Environmental, from April to May 2013. A follow-up survey was conducted in January 2014 to evaluate the impact of the technical seminars hosted by TNC. The survey results are summarised in Table A3 and Figure A1, Appendix A.

Surveyed properties included all commercial businesses and industrial operations as well as a sample of residences from each settlement in the four districts of Andros Island. The surveyed residences were selected to represent the variety of building type in each settlement (i.e. apartments, single-family dwellings, mixed residential/commercial properties, etc.). The survey was conducted through in-person interviews with residents, business owners, or a staff member knowledgeable about activities on the property. The content of the survey was divided into four sections: Water Supply; Wastewater Disposal; Solid Waste Disposal; and Chemical Storage and Disposal. Additional questions were included for properties conducting activities with specific concerns (e.g. farms). The survey form is provided on Table A2 in Appendix A.

The survey was completed at the majority of the targeted properties; a total of 273 properties were surveyed. Properties that declined to participate in the survey or were reluctant to provide information included AUTEC, several community clinics, and the water bottling plant. For these properties, assumptions were made regarding the potential hazards present based on the results from similar properties and anecdotal information. The survey results were compiled into a database and each property was assigned an identification number. Most respondents were willing to provide the information requested and cooperated with the surveyor by providing a high level of detail regarding the activities on their properties. One topic that respondents were less certain of was private well construction. In many cases, the respondents did not know the exact depth of the well or the method of construction. Therefore, there is a lower confidence in the results regarding well construction. Other challenges with the survey implementation included a lack of knowledgeable respondents available for each property and reluctance in completing the survey due to distrust of how the results would be used. Some local residents indicated that they were unhappy about the creation of national parks and protected areas on Andros Island because they felt that the parks restrict their access for fishing and other activities. In addition, they felt that the benefits, in terms of increased tourism related to the ecological reserves, are reaped by large companies and the government, rather than the local residents. Details of the survey implementation and challenges encountered are documented in the MCK Environmental report, “Blue Water Project Community Surveys”, which is available through the TNC.

The results indicate that 25% of properties surveyed have a private well, with the majority of the remaining properties relying on water supply provided by BWSC. Responses were varied in terms of well maintenance and protection (i.e. covers on the well) for properties with private wells. Some respondents use chlorine tablets regularly in the wells and keep the wellhead secured and clean, whereas others do not cover the well or perform well maintenance. The majority of respondents (regardless of water supply) indicated that their water is fresh throughout the year. A few private wells in South Andros reported pumping brackish water all the time, and several respondents in North Andros reported that the BWSC water supply is slightly salty during the dry season. Additionally, respondents in Cargill Creek expressed concern regarding contamination of the water supply due to the close proximity of the community clinic to

the wellfield. In general, respondents were satisfied with the quality of fresh water on the island.

The majority of properties on the island rely on septic tanks to manage wastewater. Regular maintenance of the systems is not performed by most respondents, except for properties in Love Hill where regular septic tank pumping is common practice. The location where the pumped contents are disposed of was not provided, although the Department of Environmental Health indicated that there is a designated location away from the settlement. Other minor maintenance performed by respondents includes repairing cracks in the cover of the tank and occasionally adding enzyme and bacterial cultures to assist in the microbiological activity of the system. In some cases, respondents reported adding chlorine tablets to the system as part of regular maintenance. This is harmful to the bacterial populations that are required for the septic system to operate properly and may result in improper waste treatment and release of pathogens to the aquifer.

Disposal of solid waste and household garbage was reported to occur at the designated landfills for each settlement. Scheduled waste collection services are provided in several settlements, whereas other settlements and most businesses are responsible for transporting waste to the landfills themselves. Informal landfills are present throughout Andros Island, often within an old quarry or a roadside clearing. Indiscriminate dumping of waste was also observed along the roadside during site visits. Waste is generally unsorted, with household waste alongside appliances and used vehicles/machinery (an exception being the San Andros Landfill where materials are sorted). Some scrap metal is recycled as well as bottles and cans, which are sent to New Providence. None of the landfills (formal and informal) have liners, covers or containment facilities to manage waste.

Chemical use and storage includes household cleaners such as bleach, engine oil, automotive fluids, fuel, paint, paint thinners and drain cleaners. Quantities present at each property were reported within a range of values (i.e. 5-20 gallons, 20-50 gallons, etc.). Disposal of used chemicals generally occurs by pouring the material on the ground or in a pit, or pouring it into the septic system. This practice likely leads to contamination of the FWL by direct infiltration through the shallow unsaturated zone, or through

leaching from the septic system. In addition, disposal of chemicals into septic systems may harm the bacterial populations and render the system dysfunctional, thus releasing not only the chemicals themselves but untreated sewage into the aquifer. Chemical waste that is not disposed of on the property is brought to the landfills where it is disposed of on the ground surface or left in containers that eventually deteriorate. One exception is used engine oil which is reported to be recycled for use in road building, construction and wood treatment.

Agricultural areas are concentrated around the settlements of San Andros and Bahamas Agricultural Research Community (BARC). The majority of farms use irrigation from private wells on site. A wide range of pesticides and fertilizers are used, with the frequency and type of product applied recorded in the survey. Several farms also raise livestock (e.g. cows, pigs, sheep, chickens) and the number of animals was also recorded in the survey.

Community clinics dispose of cleaning products and expired medicine in septic systems. Biomedical waste, gauze, and dressings are incinerated in drums on site. Sharps and other materials are sent to the landfill. Embalming occurs at the clinics and fluids are stored on site. Information related to the location and size of cemeteries on the island was not provided by the Bahamas Department of Health. However, in general, cemeteries tend to be located beside churches, clinics or along the coastline and are small (i.e. 10-20 graves).

2.7. Potential Impacts of Climate Change and Human Stressors on the FWL

The primary source of fresh water on Andros Island is groundwater, which is recharged solely through precipitation. Therefore, changes to the rate of precipitation or other climatic factors affecting recharge (e.g. an increase in evapotranspiration (ET)) are likely to have a significant impact on the FWL. The projected climate changes for the Caribbean suggest that recharge for Andros Island will be lower in the future, based on warmer temperatures increasing ET losses as well as reduced precipitation, particularly during the summer season when a significant proportion of annual recharge would

normally occur. Under conditions of reduced recharge, the FWL would in principle not sustain the same discharge along the lens periphery and would likely shrink in size as salt water encroaches inland. This effect has been observed in field studies in The Bahamas, whereby the lens was shown to contract during periods of reduced rainfall (Greaver and Sternberg, 2010).

In contrast, the effect of SLR alone is not likely to be significant on the FWL because as the sea level rises, the lens also rises in the aquifer (is buoyed up) and there is little loss of fresh water (White and Falkland, 2010). However, this rise in the FWL would only occur if the unsaturated zone of the aquifer is thick enough to accommodate a rise in the water table (Werner and Simmons, 2009). For Andros Island, SLR alone may not pose a significant threat to the FWL; however SLR is likely to increase the occurrence of storm surge and wave overwash events which cause inland seawater inundation. The resulting salinization of the aquifer from overwash could compromise the availability of freshwater resources.

Human factors, such as over-pumping and chemical/pathogen contamination are also likely to have significant impacts on the freshwater quantity and quality. The cumulative impact of multiple climate related changes as well as human factors is not well known; numerical modeling presented in this research aims to investigate these impacts.

Chapter 3.

Modeling Methodology

This chapter details the numerical modeling conducted during this research. It highlights aspects of the modeling that were not included in Chapters 4, 5 and 6 given that these were written for publication in scientific journals and necessarily only provided brief overviews of the modeling approach and results.

The numerical models were developed using two different density-dependent modeling codes: SEAWAT (Langevin et al., 2007) and HydroGeoSphere (HGS) (Therrien et al., 2010). The models were developed to simulate the FWL according to observed conditions. The term “calibration” is used loosely herein to refer to a comparison of the simulated versus observed features of the FWL (e.g. spatial distribution, thickness), rather than a quantitative evaluation of the model against hydraulic heads or concentrations which would require a comprehensive dataset.

3.1. SEAWAT Modeling

SEAWAT was used to develop island-scale models for Andros Island with long simulation timescales. This code was selected as it is capable of simulating density-dependent flow and solute transport, which is required in order to model the saltwater/freshwater interactions and development of the freshwater lens (FWL). SEAWAT does not model the surface domain or variably saturated subsurface domains; however, simulation within these domains was not necessary, as the focus of the modeling exercise is the development of the FWL in the subsurface and its response to stressors.

SEAWAT solves the groundwater flow equation based on Darcy's law, assuming the subsurface is fully saturated, and solute transport based on the advection-dispersion equation. Density-dependence is incorporated by expressing the groundwater flow equation in terms of equivalent freshwater heads and including changes to fluid density related to the transport of dissolved constituents. Equivalent freshwater heads describe the hydraulic head observed for a fluid with higher density, relative to the equivalent head that would be observed if the fluid were pure water. The solution for the groundwater flow equation determines the hydraulic head distribution within the model. However, the hydraulic head distribution also affects the solute concentration distribution, as solute moves within the model domain partly based on advection of groundwater. The solution of the advection dispersion equation determines the distribution of solute, which then also impacts the density, and thus the equivalent hydraulic head distribution. The flow equation affects the distribution of solute, so that the advection dispersion equation is then solved based on the results of the flow equation. Therefore, both the groundwater flow and solute transport solutions must be solved for each time step, which may be achieved implicitly or explicitly within SEAWAT. This refers to whether the flow equation is solved separately to the solute transport equation for each time step, or whether it is solved simultaneously. In this study an explicit coupling approach was used (as is discussed in Section 3.1.5) so that the flow equation is solved for each time step before the solute transport solution is performed.

3.1.1. Model Domain

Initially, a series of quasi two-dimensional (2-D) cross-sectional models were constructed to test the conceptual model (see Section 2.3.4) and constrain model parameters such that a representative FWL morphology on Andros Island could be simulated. Using cross-sectional models allowed for a wide range of model configurations to be tested within a reasonable computational time. The results of the cross-sectional models were then applied to the final three-dimensional (3-D) baseline model of the FWL on Andros Island. Both the cross-sectional and 3-D models were calibrated to observations of the FWL thickness on Andros Island (see Chapter 2).

The cross-sectional models were based on a simple rectangular box model representing a west-east cross-section through the northern tip of Andros Island (indicated on Figure 3.1).

Figure 3.1. Andros Island map with location of the two-dimensional cross-section used to test the conceptual model

The baseline dimensions of the models were 20 km wide, 200 m deep (vertical thickness into the subsurface) and a single unit thickness (Figure 3.2). The model included 44 layers, with individual layer thicknesses of 1 m in the upper 20 m of the model domain, which transitioned to 2.5, 5 and then 10 m thickness from a depth of 60 m to the base of the domain. The top surface of the model was flat - no site-specific ground elevation was included. A surface elevation of 0 masl was assigned. In reality, the FWL will be domed above sea level in order to generate a freshwater flow system; however, this aspect of the FWL morphology was not considered at this stage of the modeling process, as the hydraulic head simulated in the FWL is of greater significance and represents any changes in FWL morphology between model results.

The shape of the peripheral boundaries of the model domain was evaluated by defining them as either straight vertical or sloping (to make a trapezoid, thereby representing the natural sloping shoreline of Andros Island). The depth to the base of the FWL was the same regardless of which peripheral boundary shape was used, and the

shape of the lens was similar in relation to the position of the boundaries (Figure 3.3), although the lens for the sloped scenario is slightly smaller in extent due to the smaller domain size. Therefore, vertical peripheral boundaries, or rectangular box models (as shown on Figure 3.2) were used in this study, as the shape of the boundary, at this grid size, appears not to influence the FWL morphology. However, for smaller models, the shape of the boundary may be important to consider.

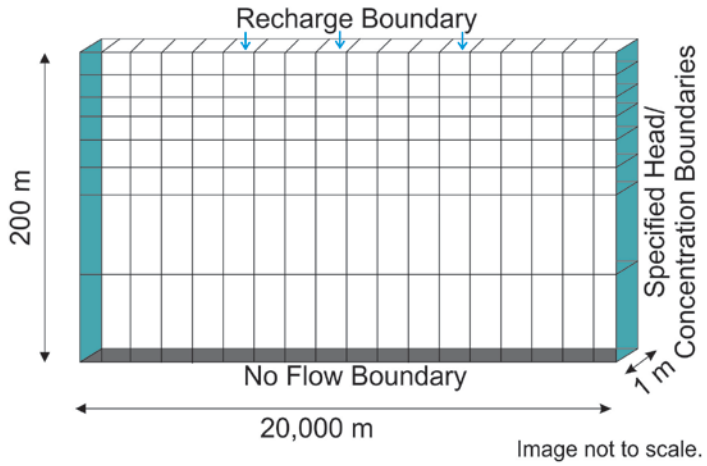

Figure 3.2. Cross-sectional model domain (all layers are not shown)

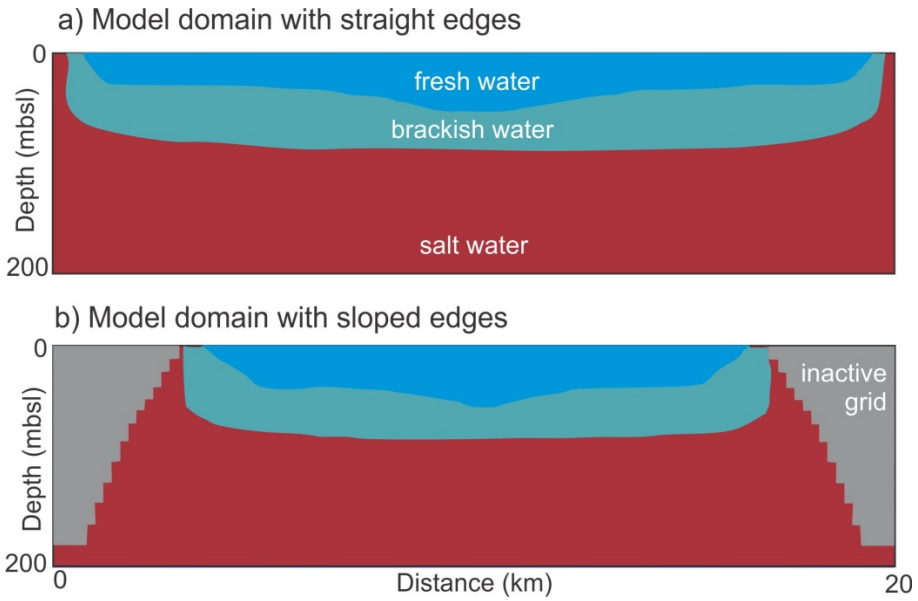

Figure 3.3. Comparison of model results for a) domain with vertical boundaries; and b) domain with sloped boundaries

3.1.2. Boundary Conditions

Specified head boundaries were assigned along both vertical sides of the domain from the base of the model (i.e. 200 mbgs) to the same elevation as the top surface of the model (i.e. 0 masl) (Figure 3.2). Density was specified at 1025 kg/L to simulate seawater. A specified concentration of 35 g/L salt was assigned to each of specified head cells as point source boundaries. Point source boundaries in SEAWAT are used to assign a concentration to any water that enters the domain from the specified head (or flux) boundary. This configuration corresponds to the conceptual model, whereby the salt water enters the domain along the sea boundary. No flow boundaries were assigned (by default) along the base of the model domain. Recharge is the only input of fresh water to the hydrogeological system and, therefore, is the main mechanism by which the simulated FWL develops in the model. Recharge was applied to the top layer of the model with concentration of 0 g/L to simulate the average annual recharge to the aquifer. Details concerning recharge estimation are provided below.

The initial concentration of all cells in the model domain was assigned at 35 g/L (i.e. salty). Therefore, the simulations represent freshening of the system. Note: equally an initial concentration of 0 g/L salt could have been assigned. FWL development achieved steady-state morphology within 100 years of simulation time for all model simulations.

Recharge Modeling

The annual recharge amount for Andros Island was estimated using the United States Environmental Protection Agency's software HELP (Hydrologic Evaluation of Landfill Performance) (Schroeder et al., 1994). HELP utilises a storage routing technique based on hydrological water balance principles to determine how precipitation falling on the land surface is partitioned. The physical properties of the soil/aquifer material as well as the overlying vegetation and surface characteristics are defined. In determining the water balance, it accounts for interception, runoff along surface slope, infiltration, evapotranspiration, vegetative growth, soil moisture storage, lateral subsurface drainage (if desired), unsaturated vertical drainage, and percolation (leakage). Therefore, recharge is the portion of precipitation that is not lost to the other components of the

water balance and leaks out the base of the profile. HELP has been used to estimate recharge for a variety of climatic and physiographic settings in previous studies (Scibek and Allen, 2006; Jyrkama and Sykes, 2007; Toews and Allen, 2009; Allen et al., 2010).

Within HELP, a representative vertical percolation profile is defined for the area of interest. Previous studies (listed above) have run HELP for different combinations of profile depths, properties, etc. However, in this study, a single representative profile is used given the uniform geology of Andros Island. The depth of the profile represents the approximate thickness of the vadose zone; the top of the profile corresponds to the ground surface and the base of the profile corresponds to the approximate water table depth (Figure 3.4). Although the water table depth does vary according to saturation conditions, the profile is restricted to vertical percolation (with no lateral subsurface drainage), so all excess water exits the profile at the base.

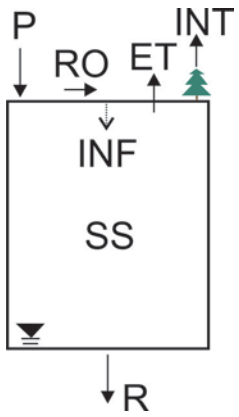

Figure 3.4. Sketch of HELP vertical percolation profile. P - precipitation; RO - runoff; ET – evapotranspiration; INT - interception; INF – infiltration; SS – soil moisture storage; R – recharge.

Average depth to water on Andros Island is 2 m (Section 2.3.1); although under the high elevation areas the depth to water may be 5-10 m. The depth of the vertical percolation profile was varied using different observations of depth to water on Andros Island: 1, 2, 5, and 10 mbgs. Results are presented in Table 3.1, and indicate that the average annual recharge varies by less than 1% between the different profile depths. This is likely the result of the relatively high hydraulic conductivity (K) of the geologic layer, which was based on field data and calibration of the cross-sectional models (see discussion below on K values). The depth of the vertical percolation profile was therefore set to 2 m, corresponding to the typical observed depth to water on Andros Island.

Table 3.1. Vertical percolation profile depth sensitivity analysis

Depth	Resulting Recharge Value (mm/year)
1	878
2	877
5	872
10	871

The parameters for the lithology profile are presented in Table 3.2. No soil zone was specified due to the generally thin/absent soils on Andros Island. The entire profile was defined as limestone (K=864 m/day). Vegetation cover was assigned to the highest class in the software (a leaf area index of 5) based on the large proportion of pine forests (Schroeder et al., 1994). As the majority of the island (and therefore, the recharge area) is covered in pine forests, spatial variability in recharge rates for areas that are not vegetated was not considered. The evaporative zone depth was assigned 1.02 m, based on the presence of deep root systems for the pine trees as similar values for the southeastern U.S. (Schroeder et al., 1994). The growing season was assumed to be 365 days based on the warm climate and absence of a drastic dry season. The surface was assigned zero slope based on topography of Andros Island and limited runoff anticipated (Tarbox, 1986). The average wind speed was determined from meteorological data for The Bahamas. Field capacity (0.10) and wilting point (0.05) were assigned values less than the estimated porosity (0.15) in the absence of measured values.

Table 3.2. Input parameters for HELP model

Parameter	Value
Depth of Profile [1]	2 m
Saturated Vertical Hydraulic Conductivity of limestone	864 m/day
Porosity	0.15
Field Capacity	0.10
Wilting Point	0.05
Vegetation	Excellent stand of grass [1]
Evaporative Zone Depth (m)	1.02 [3]
Growing Season (days)	365
Average Windspeed (km/hour)	14.8

Notes:
1. Excellent stand of grass corresponds to a Leaf Area Index of 5.
2. Maximum allowable value based on the presence of large trees where root zones are likely to develop deep into the subsurface.

100-year climate data series were generated using the stochastic weather generator (WGEN) included in HELP. WGEN was developed by the USDA Agricultural Research Service (Richardson and Wright, 1984) and yields daily values of precipitation, temperature and solar radiation. Two data series were generated: one for North Andros and one for South Andros because the historical climate differs between the two regions. WGEN produces stochastic daily weather series using historical climate parameters (e.g. mean monthly temperature, mean minimum temperatures on wet/dry days, mean solar radiation, etc.) from specific climate stations contained in the WGEN database for local probability processes that determine the climate patterns (monthly normals, statistical coefficients). These statistical coefficients include the mean maximum and minimum temperature on a wet or dry day, mean solar radiation on a wet or dry day, probability of precipitation on a wet day for each month, and the probability of precipitation on a dry day for each month. The coefficients constrain the patterns of the weather events produced by the stochastic weather generator according to the specified monthly normals. Daily precipitation is generated using a model that is based on the Markov Chain model, which provides randomisation of the amount of precipitation that occurs, and the Two-parameter Gamma distribution model, which governs the probability of a precipitation event occurring. The occurrence of rain on a given day has

a major influence on the values of temperature and solar radiation for the day. WGEN generates precipitation independently of the other variables and then generates temperature and solar radiation according to whether the day is wet or dry.

The average annual precipitation on North Andros is 1442 mm/yr, while on and South Andros it is 889 mm/yr. Temperature averages were not available for South Andros; therefore, the monthly averages for North Andros were applied to both models. Other climate parameters were identical for both models. These include average windspeed (14.8 km/hour) and relative humidity (77%) which were provided by The Bahamas Meteorological Office. The historical statistical coefficients were based on values for the nearest climate station (Miami, Florida, USA) in the WGEN database.

The HELP model begins as a dry lithology profile whereby several decades of climate data are required to "wet" the profile and establish stable recharge conditions (Liggett and Allen, 2010). Once stable conditions are reached (here occurring within 10 years simulation time), the daily leakage through the base of the lithology profile (recharge) was recorded. Annual recharge values were determined for each simulation year and averaged to produce the average annual recharge. Annual recharge values for North Andros ranged from 514 to 1,412 mm/year with an average annual recharge of 877±177 mm/year. Values for South Andros ranged from 204 to 794 mm/year with an average annual recharge of 426±104 mm/year. The average annual recharge values appear to be reasonable estimates based on the hydrogeological setting (i.e. high K and thin vadose zone); however, the actual recharge value is not known for Andros Island. The average annual recharge estimates were used as input for the northern and southern SEAWAT models, respectively.

3.1.3. Hydrostratigraphy

The three principal hydrostratigraphic units included in the SEAWAT model are the Lucayan Limestone from surface to 40 mbgs, the Pre-Lucayan Limestone from 40 mbgs to the bottom of the model domain, and paleosols which are generally around 1 m thick and present in the top 20 m of the subsurface (see conceptual model in Section 2.3.4).

Several models were developed to test the conceptual hydrostratigraphic setup and K values to simulate the FWL on Andros Island. Cross-sectional models were initially run using an isotropic K for the entire model domain, representing Lucayan Limestone. The K value was varied within a range based on previous studies (from $1x10^{-5}$ to 10 m/s). With K values higher than 0.1 m/s, the simulated lens is very small and limited in extent (Figure 3.5a). With lower K values ($1x10^{-3}$ m/s and lower), the lens becomes warped in shape; and at very low K values, it does not develop at all (Figure 3.5b). Through trial and error, it was determined that a FWL of reasonable morphology (i.e. developing in the subsurface across the whole of the model domain) was achieved when a K value of 0.01 m/s was assigned to the Lucayan Limestone. However, if the model consists of a single hydrostratigraphic unit, the resulting FWL extends deep within the model domain (to approximately 90 mbgs), which is not a realistic representation of the shallow FWL on Andros Island (Figure 3.5c). Therefore, heterogeneities were inserted into the model as discussed below.

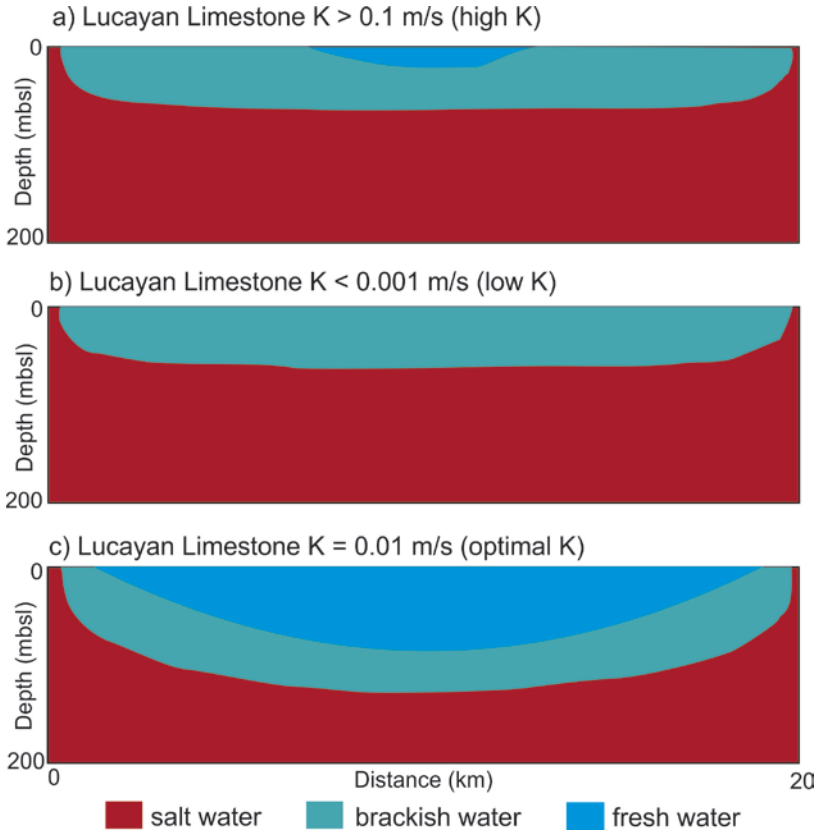

Figure 3.5. Comparison of hydraulic conductivity (K) values for Lucayan Limestone

A higher K pre-Lucayan basement and higher K paleosols were added to the model domain (as described below) to test whether these features would result in a thinner FWL. Adding the pre-Lucayan basement as a higher conductivity (1 m/s) unit below the Lucayan (from 40 mbgs to the base of the model domain) resulted in the FWL extending much shallower, to a depth of approximately 23 mbgs. Although this was an improvement from the previous model, the FWL was still too deep within the model domain relative to field observations. Therefore, paleosols were also added to the model. Previous studies have characterised the paleosols as low K layers (Ritzi et al., 2001); however, anecdotal evidence indicates that the layers are very weathered and may be highly conductive. In this study, the paleosols were represented by relatively high K layers (interbeds) within lower K Lucayan limestone. Assigning a low K to the paleosols (i.e. < 0.01 m/s) resulted in the lens being perched, which is not observed in the field (Figure 3.6a). Whereas, representing the paleosols as high K layers within lower K limestone (i.e. > 0.01 m/s) resulted in thin lenses being developed similar to field observations (Figure 3.6b). This approach is consistent with other studies based in The Bahamas, which have suggested that layers of high K in the subsurface are responsible for development of thin FWLs (Wallis et al., 1991). When two paleosols of 1 m each were assigned at different depths (9 and 14 mbgs or 5 and 10 mbgs), the resulting base of the FWL was the same at 17 mbgs (Figure 3.6b). This indicates that the model is not sensitive to the specific positioning of the paleosols, but rather the presence of paleosols in the upper layers of the model domain. Therefore, the use of two, high K, 1 m thick paleosols located at approximately 9 and 14 mbgs was determined to be suitable for the model simulations.

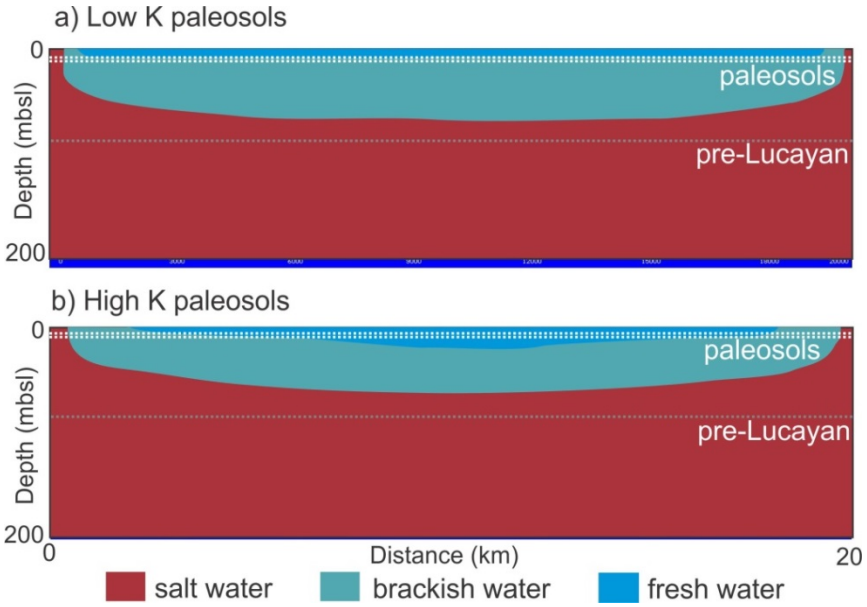

Figure 3.6. Comparison of paleosols relative hydraulic conductivity: a) lower than the Lucayan Limestone K; and b) higher than the Lucayan Limestone K

3.1.4. Additional Aquifer Parameters

Anisotropy was introduced to the Lucayan and paleosol units where the K in the horizontal direction was altered in successive simulations to be both higher and lower by one order of magnitude than that in the vertical direction. No change in FWL morphology was observed for these scenarios. This may be because the anisotropy/geological heterogeneity introduced by the paleosols within the Lucayan Limestone has a larger impact on the FWL morphology than anisotropy within each respective geological unit. Based on these results, and lack of field data regarding anisotropy within the principal aquifer geology, it was determined that anisotropy was not an important factor to include in simulating the FWL on Andros Island.

In order to identify a suitable dispersivity value, a range of values for longitudinal, horizontal transverse and vertical transverse dispersivity (α_L, α_{TH} and α_{TV}, respectively) were tested in the model. α_L controls the dispersion of salt along the main flow direction, α_{TH} controls dispersion horizontally and α_{TV} vertically (perpendicular to the flow direction). α_L was assigned as 1 , 10, or 100 m, with ratios of α_{TH} : α_{TH} and α_{TV} : α_L varying (e.g. 0.1, 0.01, or 0.001). When α_L was 100 m, regardless of the α_{TH} and α_{TV}

values, the lens did not develop. The lowest salt concentration was 5 g/L and the morphology of the brackish zone appears to be related to numerical dispersion deriving from too large a dispersivity value (Figure 3.7a). Through trial and error, a reasonable range for dispersivity in the model was determined to be α_L: 1 m; α_{TH}: 0.1 m; and α_{TV}: 0.1 or 0.01 m (both values produce the same results), as shown on Figure 3.7b.

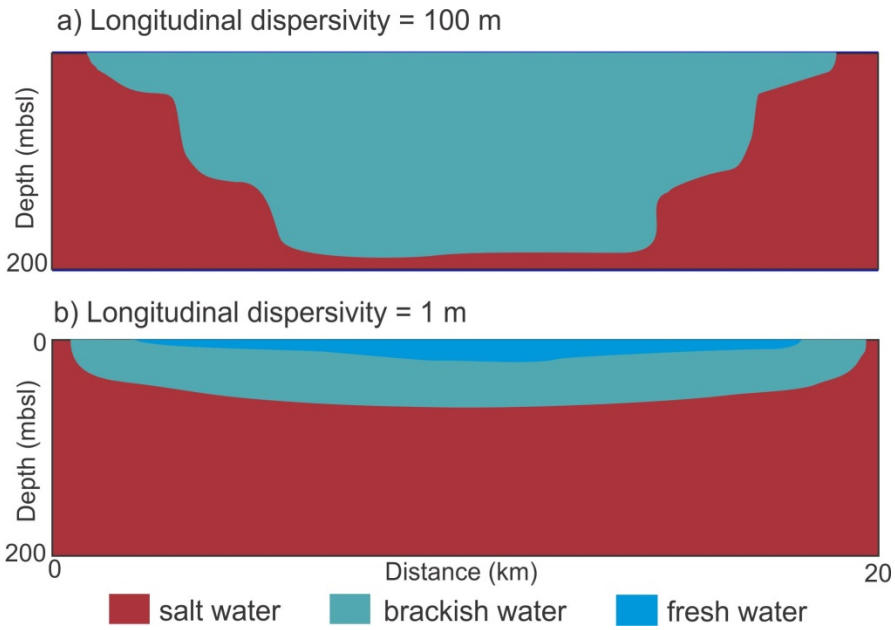

Figure 3.7. Comparison of results for two values of longitudinal dispersivity

Other parameters specified in the model include effective porosity (0.15), which was based on field data (see Chapter 2), and specific storage ($1.0x10^{-5}$), which was based on literature estimates for weathered bedrock (Younger, 1993). The diffusion coefficient was assigned the default value of 0 m^2/day (i.e. neglecting molecular diffusion), as the hydrogeological system was assumed to be a dispersion dominated system due to the high K values. These parameters were not adjusted for the models.

3.1.5. Model Run Settings

SEAWAT model run settings were determined through optimisation. In the Variable Density Flow settings, density was derived based on salt concentration alone, and inter-nodal density was computed using the central-in-space algorithm. The water table correction (which accounts for the small difference in water table determination related to density-differences) was not applied as model convergence could not be

achieved when this was included. In the Viscosity settings, viscosity was calculated from salt, and no temperature dependency was introduced.

The Waterloo Hydrogeologic Solver (WHS) was used for solving the flow equation; this solver is packaged in the Visual MODFLOW graphic-user interface software. Solver settings were adjusted to allow the model to converge. The maximum outer and inner iterations were set to 75 and 50, respectively, and the head change criterion was set to $1x10^{-4}$ m, the residual criterion to 10, the damping factor to 1, and the relative residual criterion to 0. Simulations with lower values for the convergence criteria did not result in model convergence, regardless of the solver used. The maximum outer and inner iterations refer to the maximum number of attempts the model can make at a partial solution (in principal, increasing with accuracy for every iteration), before reaching model convergence. The head change criterion determines when model convergence is reached and affects the accuracy of the solution as it determines when the solution for any given time step is acceptable (i.e. when the change in head between the previous and current iteration is acceptable). Because larger values result in potentially greater numerical error, the smallest head change criterion that allowed for model convergence was applied. Initial time steps were 14 minutes with a maximum time step of one day.

Solute transport was determined using the implicit generalised conjugate gradient (GCG) solver, with upstream finite difference for advection. This solver often results in shorter computing times and allows for varying transport time steps to be used during the model run. When solving a transient problem (such as solute transport), additional numerical error may be introduced resulting from grid or time discretization that is too coarse. The Peclet number describes the ratio between the model grid dimension or nodal spacing (Δl) and the dispersivity (α), whereas the Courant number describes the model grid dimensions (Δl) and time step size (Δt) in relation to the velocity of water movement (v). To minimise the numerical error of the solution, model setup generally targets Peclet and Courant numbers less than one (Anderson and Woessner, 1992).

$$\text{Peclet} = \frac{\Delta l}{\alpha_L}; \quad \text{Courant} = v\frac{\Delta t}{\Delta l} \tag{3.1}$$

The transport time steps are calculated automatically to meet the convergence criterion and satisfy the stability criteria. Based on the model setup, the Courant stability criteria indicate that transport time step lengths should be less than 0.6 days, whereas the actual transport time step lengths ranged from 7.9×10^{-8} to 6.3×10^{-7} seconds. For the dominant flow direction within the model domain (i.e. α_L), the Peclet number is 1.

Coupling of the flow and solute transport solutions was performed explicitly, whereby the flow equation is solved first and the results are then used for the solution of the solute transport equation (one time step lag). An implicit solution is likely to result in a more realistic solution (Aquanty, 2013) when the model is stressed with step-wise changes (as will be presented in the following sections). However, model convergence was not achieved regardless of coupling settings with an implicitly coupled approach and, following the advice of a SEAWAT developer, this approach was abandoned and the explicitly coupled solution was considered a reasonable result (pers. comm., Christian Langevin, July 6, 2014). The model run settings are summarised in Table 3.3.

Table 3.3. SEAWAT model run settings

Setting	Value
Flow solver	Waterloo Hydrogeologic Solver (WHS)
Maximum outer iterations	75
Maximum inner iterations	50
Head change criterion	1.0×10^{-4} m
Residual criterion	10
Damping factor	1
Relative residual criterion	0
Model time steps	Initial: 14 minutes; Maximum: 1 day
Transport solver	Implicit Generalised Conjugate Gradient (GCG)
Transport time step length	7.9×10^{-8} to 6.3×10^{-7} seconds
Flow and transport coupling	Explicit

3.1.6. Three-dimensional Models

The 3-D model simulated the entire Andros Island. The island was split into two separate models to allow for greater grid cell resolution within the maximum allowable grid dimensions of 500 x 500 x 200 cells. North and Central Andros are included in the northern model and Mangrove Cay and South Andros are included in the southern model. All input parameters are the same for the northern and southern models, except for the recharge boundary condition, which was assigned according to the recharge estimates for the north and the south as discussed above. Areas where the FWL is not likely to develop were designated as inactive cells, and thus not included in the model domain. These areas include the saltwater marshes on the western coast of the island, the majority of the small islands within the bights and southern tip of the island, and areas where the landmass is heavily intersected by saltwater “creeks” (Figure 3.8). It is highly unlikely these areas are able to sustain a FWL capable of water supply (i.e. having a thickness > 2 m). Therefore, these areas were not included, as the focus of this study is on areas of the FWL that represent potential water supply.

Figure 3.8. Three-dimensional model domain for Andros Island

The 3-D model was developed using the representative hydraulic parameters identified through the cross-sectional modeling (Table 3.4). The hydraulic parameters were determined as those that resulted in a FWL thickness that corresponds to the available field data for North Andros, as discussed in previous sections. Limited data are available for other areas of Andros Island; therefore, the overall conceptualization of the hydrostratigraphy and the hydraulic parameters determined for North Andros were assumed to apply across the rest of Andros Island. This assumption of horizontal continuity of the hydrostratigraphy and uniform parameters introduces uncertainty to the modeling results. It is likely that the 3D models do not capture spatial heterogeneity adequately, and consequently, spatial variations in the FWL morphology that might result from heterogeneity. Lack of data for model validation is a limitation of this study, although it is a common challenge encountered in studies of small island hydrogeology (Robins, 2013). Therefore, the 3-D models provide an estimate of the current freshwater

resources on Andros Island, based on a common conceptualization of the hydrostratigraphy and common hydraulic parameters.

The 3-D models formed the baseline FWL models, which were run for 50 years simulation time to allow the FWL to develop.

Table 3.4. Three-dimensional SEAWAT model parameters

Parameter	Value
Model Domain	200 m model domain; 40 m Lucayan Limestone; 160 m pre-Lucayan Limestone
Paleosol Depths	9-10 mbgs and 14-15 mbgs
Hydraulic Conductivity	Lucayan: 864 m/day – paleosols: 8640 m/day – Pre-Lucayan: 86400 m/day
Effective Porosity	0.15
Specific Storage	$1x10^{-5}$ m^{-1}
Dispersivity	Longitudinal 1.0 m; Transverse (vertical & horizontal) 0.1 m
Diffusion Coefficient	0 m^2/day
Specified Head Boundary	0 masl along model domain periphery; specified density 1.025 kg/L
Concentration at Specified Head Boundary	35 g/L along model domain periphery
Initial Concentration	35 g/L throughout model domain
Recharge	877 mm/year (north) and 426 mm/year (south); concentration 0 g/L

3.1.7. Modeling Stressors

In order to evaluate the impact of potential stressors on the FWL, a series of 3-D models was developed to simulate stressors related to climate change and human activities. These models were based on the baseline FWL model described in the previous section. Below is an overview of the changes made to the SEAWAT model. The results of the climate change stressors are discussed in Chapter 4. Results for the human impact stressors were incorporated into the risk assessment in Chapter 6; however, detailed presentation and discussion of the results are presented below.

Climate Change Simulations

Climate change stressors simulated in this study include altered groundwater recharge and sea level rise. Changes to groundwater recharge were determined by re-modeling recharge in HELP using the projected 2090s climate based on the median of 15 global climate models of the A2 emissions scenario (Section 2.4.2). As in the baseline recharge modeling, recharge estimates were produced for North and South Andros, and these values were applied to the SEAWAT models for each region, respectively.

Sea level rise was simulated by increasing the elevation of the specified head boundaries in the model domain according to the projected mean sea level increase of 0.6 m by the 2090s (relative to 1980). Loss of land surface due to inundation associated with sea level rise was not simulated, as the areas anticipated to be inundated are located within a single grid cell such that the position of the ocean boundary would not change within the model (see Section 6.3, Figure 6.5c).

To evaluate the impact on the FWL, observation wells were placed in the models to capture a discrete record of simulated concentration for every time step. Details concerning the placement of these wells are given in Chapter 4.

Human Impact Simulations

The current pumping regime for groundwater extraction on Andros Island was not simulated in the baseline model in order to represent natural historical conditions for the FWL; however, the current pumping regime was simulated alongside scenarios of increased pumping from the wellfields to evaluate the response of the FWL to pumping stressors. The results of these simulations were used to assess the hazard threat from pumping activities in the risk assessment framework, presented in Chapter 6. As the results are not explicitly discussed in Chapter 6, they are presented below.

The historical pumping rates for each wellfield were based on the 2011 average daily pumping rates, provided by the Bahamas Water and Sewerage Corporation (Table 3.5). For this study, the wellfields are numbered one to eleven, from north to south on Andros Island (see Chapter 2, Figure 2.1).

Table 3.5. Historical pumping rates for wellfields on Andros Island

Wellfield #	Initial Pumping Rate (m^3/day)
1	45
2	605
3	355
4	36
5	50
6	32
7	295
8	23
9	100
10	205
11	173

An initial simulation was conducted using the historical pumping rates. Scenarios of increased pumping were then simulated by creating several stress periods throughout the model runs, whereby the wells were pumped at progressively higher rates: 2, 4, 6, 8, and 10 times the current average daily pumping rates. Each pumping rate was sustained for 20 years to allow the FWL to respond and reach a new steady-state condition. After the highest pumping rate was simulated, all pumping was stopped and the recovery of the FWL was observed for the remaining 10 years of the simulation. These scenarios were simulated in the baseline FWL model as well as in the climate change model to observe potential differences in response to pumping under climate change conditions.

Simulations of the historical pumping rates resulted in no upconing, suggesting that the FWL is able to sustain current pumping rates. For simulations of increased pumping rates, upconing of salt water was observed at all wellfield locations (although at different pumping rates) in both the baseline and climate change models. At some locations, the upconing occurred at the base of the FWL and did not affect the quality of the water in the well; however, at other locations the upconing saltwater reached the top surface of the FWL, resulting in the well pumping salty water. The results of the simulations conducted using the baseline FWL model (Figure 3.9a) are presented

alongside those from the simulations conducted using the climate change model (Figure 3.9b). Results are presented in terms of the upconing (upward movement of the base of the FWL relative to the historical pumping rate model) observed at each well.

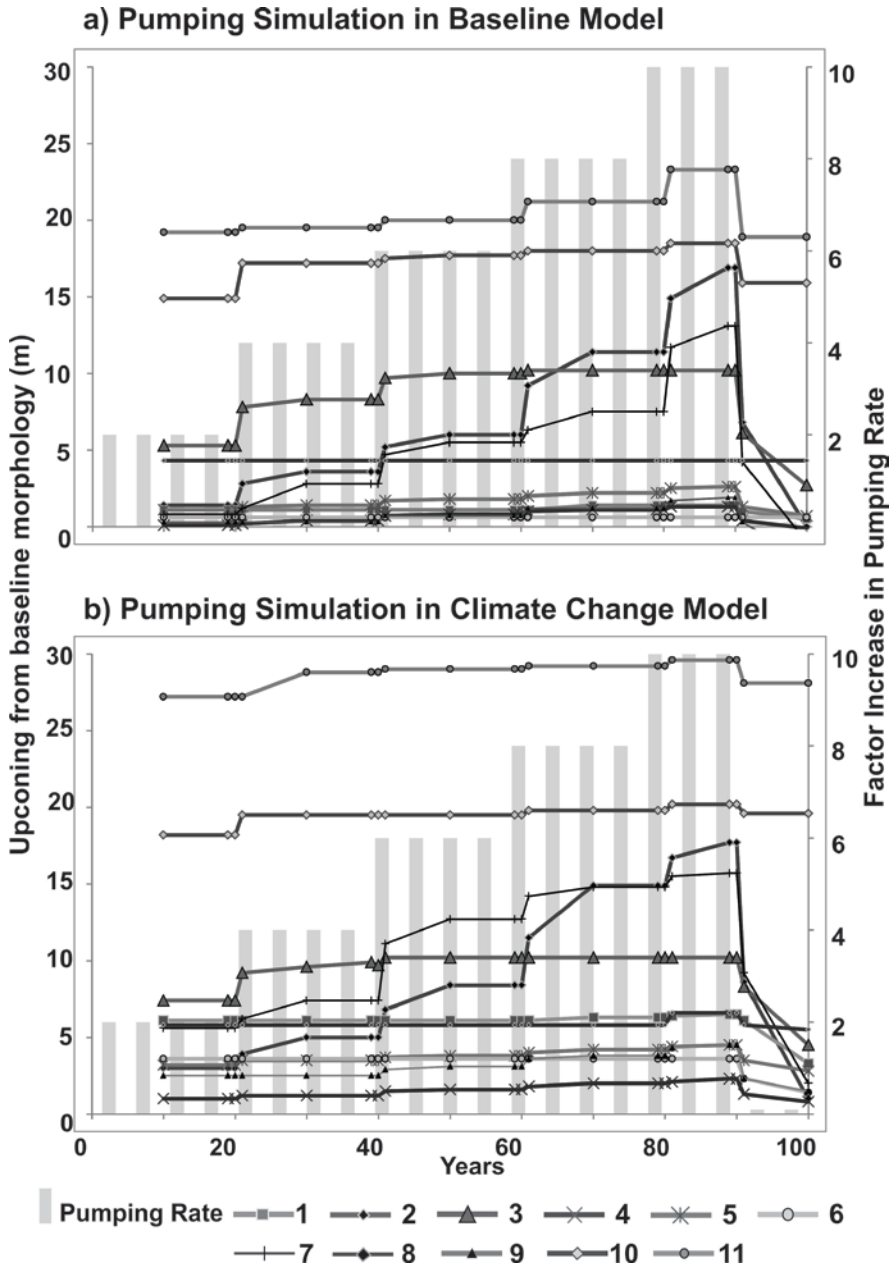

Figure 3.9. Upconing observed in wellfields modeled under a) current and b) future climate change conditions. Well numbers (indicated in the legend across the bottom of the figure) correspond to wellfields on Andros Island. The solid bars represent pumping rates (no scale) that are gradually increased by 2, 4, 6, 8 and 10 times the current pumping rate.

When the pumping scenarios were simulated within the climate change model, the magnitude of upconing increased for all wells. Well 11, which was fresh throughout the pumping scenarios in the baseline model, became salty in the climate change model, and Well 7 became salty at a lower pumping rate (Figure 3.9).

After pumping was stopped, a significant proportion of the upconing was reversed within 1 year, and within 10 years, the FWL approached the baseline morphology with limited residual upconing present. However, when pumping was simulated within the climate change models, there was larger residual upconing for all wells. This is related to the lower recharge applied in the climate change models that slows down the recovery of the FWL following stresses, such as over-pumping. The results of the pumping simulations were incorporated into the risk assessment framework (see Chapter 6).

3.1.8. Evaluating Model Output

In order to evaluate the current FWL morphology and to compare it to how it might change in response to climate change, the SEAWAT model island-scale results were quantitatively evaluated using a geographic information system (GIS). The steps followed are illustrated as a flowchart in Figure 3.10. The volume and area of the lens were calculated based on the threshold salt concentration (0.4 g/L; see Section 2.3.1). This approach allowed for quantitative comparison of the changes in FWL morphology between different stressors applied in the island-scale model.

For each simulation, the groundwater concentrations for each grid cell were exported to the ESRI ArcGIS software program as a series of point shapefiles (one file for each layer of the model). The point shapefiles were merged into a single file and edited to only include the deepest points that had concentrations of 0.4 mg/L or less of salt (i.e. the base of the FWL). This file was then interpolated to a raster using the Natural Neighbour deterministic interpolation method based on the elevation field (z). The cell size of the interpolation was set to 50 in order to obtain a smooth interpolated raster surface. The area and volume of the viable FWL was determined using the analysis function Surface Volume. The resulting calculations may not represent the

actual volume and area of the FWL because the base of the FWL was interpolated in GIS and the modeling contains inherent uncertainty related to the uncertainty of the input hydraulic parameters and assumptions made in the model setup of a uniform hydrostratigraphy (as discussed in preceding sections). However, these estimates allow for quantitative comparison of the model results so that the impact of different stressors applied in the model simulations may be evaluated.

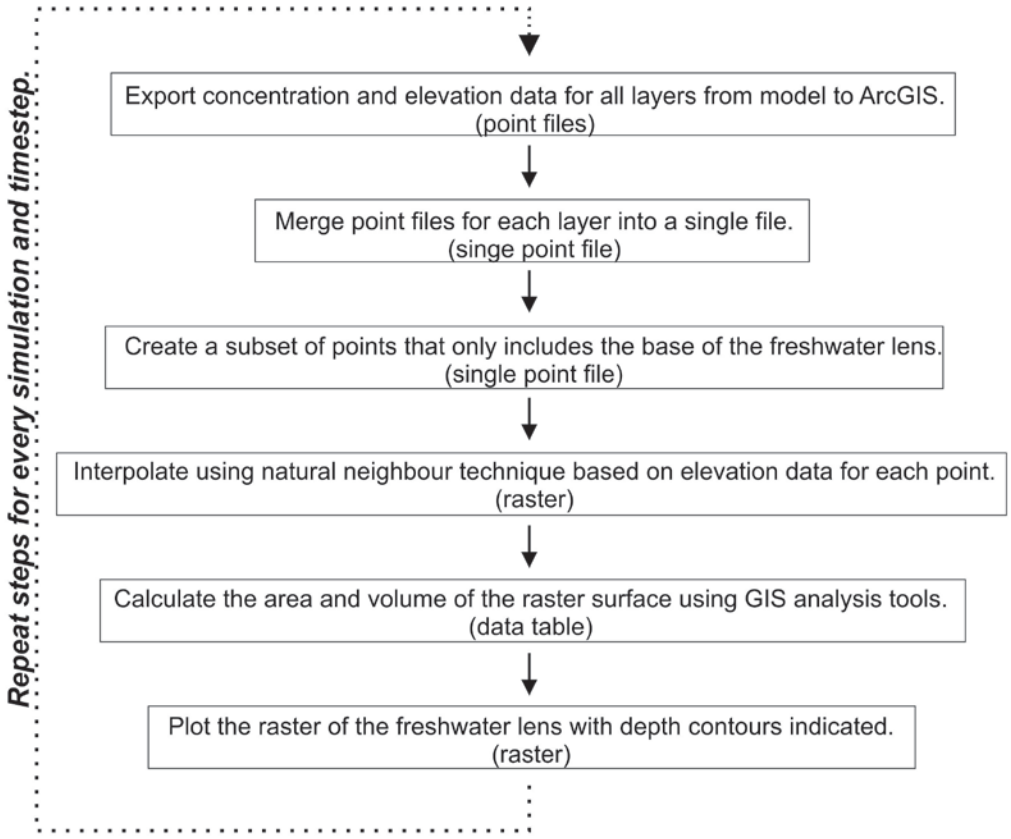

Figure 3.10. SEAWAT output data processing flowchart for estimating changes in area and volume of the FWL

3.2. HydroGeoSphere (HGS) Modeling

HGS was used to develop local-scale models that simulate storm surge overwash events. Modeling storm surge requires a code that can simulate density-dependent flow and solute transport across three hydrologic domains: the surface, the unsaturated subsurface, and the saturated subsurface. Few studies include a dynamic

surface domain, although it is an important component representing the introduction of salt water into the system during a storm surge overwash event. HGS couples the three hydrologic domains within a fully integrated approach, whereby it performs the simultaneous solution of the surface and variably saturated subsurface for each time step. This approach provides more realistic representations of the major processes than simpler or independently coupled models (Goderniaux et al., 2009). HGS uses the control volume finite element approach to solve Richards' equation and Darcy's law for the variably-saturated subsurface (in 3D) coupled with the diffusive-wave approximation of the St Venant equation for the surface domain (in 2D) (Therrien et al., 2010). Details of the numerical theory and implementation can be found in the user manual (Aquanty, 2013). HGS is written in FORTRAN 95 and relies on a pre-processor called "grok". The user specifies commands collected in grok input files (unformatted text files) which form the main user interface of the model. Once the model has run, output files are produced which can be evaluated in a number of visual post-processing software, including Tecplot 360 (which was used for this study). HGS is built as a flexible tool whereby the user may choose to specify parameters that are available, or otherwise rely on default values.

3.2.1. North Andros Wellfield

HGS models were developed to characterise FWL contamination and subsequent recovery of an aquifer following a storm surge overwash event. The models were developed to evaluate the impact of storm surge specifically in the context of a trench-based wellfield on Andros Island. As such, the model represents a highly discretized, 2-D cross-section of one of the trenches in the North Andros Wellfield (Figure 3.11).

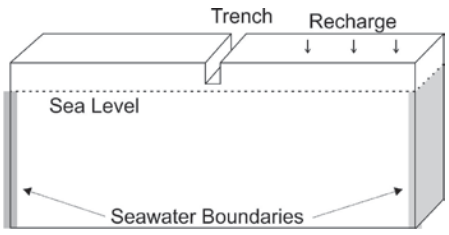

Figure 3.11. Basic model setup in HydroGeoShere

The models were calibrated based on critical factors that are expected to affect FWL contamination and recovery. These critical factors include: recharge, thickness of the vadose zone, aquifer hydraulic conductivity, geological heterogeneity (e.g. paleosols), water table gradient, and thickness of the FWL. Field data for North Andros Island (as presented earlier) comprise the calibration criteria, summarised in Table 3.6.

Table 3.6. Calibration criteria for North Andros Island

Parameter	Value
Vadose Zone Thickness	1.5-2 m
Water Table Elevation	2 masl
Hydraulic Conductivity	86 – 8,640 m/day
Hydraulic Gradient	0.0005 – 0.001
Porosity	0.15

Note: See Chapter 2 for data sources.

Model Domain

The physically-based seawater boundaries are important components in simulating flow within a FWL. In reality, these boundaries are located along the coastline; however, the coastline is far from the North Andros Wellfield. Therefore, local-scale models were developed using boundary conditions assigned in such a way as to simulate a realistic flow field surrounding the trench. To limit computational time, the model setup that satisfied the calibration criteria (Table 3.6) with the smallest domain width was selected as the baseline model for this study (Figure 3.12). Determination of an appropriate model domain width is discussed in further detail in the following sections.

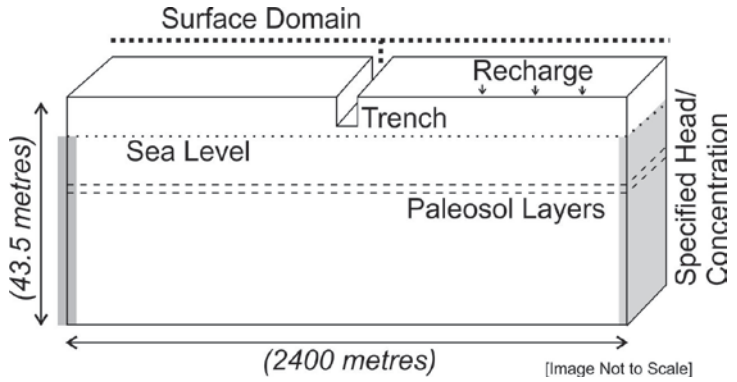

Figure 3.12. HydroGeoSphere model domain and setup

The model domain covers a horizontal extent of 2400 m and a vertical extent of 43.5 m, with sea level at 3.5 mbgs, based on ground surface estimates for North Andros Island and model optimisation to result in the representative vadose zone thickness. The vertical extent of the domain was based on the observed thickness of the principal aquifer material, Lucayan Limestone. The model domain was 1 unit thickness, with a uniform horizontal grid spacing of 1 m. Paleosols were simulated in the subsurface as 1 m thick zones at 9 and 14 mbgs (corresponding to field observations). The trench is 1 m wide, positioned within the centre of the model domain, extending 2 mbgs to intersect with the top of the water table. No surface slope was included in the model based on the topography of Andros Island and limited runoff anticipated (Tarbox, 1986). Vertical grid refinement varied from 1 m thick in the lower 20 m, to 0.5 m thick in the overlying 20 m, and 0.35 m thick in the uppermost 3.5 m. The grid was refined in order to optimise simulation of flow and transport across the three hydrologic domains and to allow for the evaluation of small-scale changes in response to overwash impacts. The surface domain was defined across the top of the model domain as a single layer of model nodes, draped over the topography of the model domain “ground surface” (Figure 3.12).

Boundary Conditions

Recharge was applied to the surface domain as an annual average quantity based on the HELP recharge modeling, presented earlier (Section 3.1.2). Although HGS is capable of partitioning rainfall into the different components of the water balance (i.e. streamflow, runoff, soil storage, evapotranspiration and recharge), this feature was not utilised due to the absence of measured values or detailed data regarding the unsaturated zone parameters and surface features. To evaluate the model sensitivity to the recharge values, simulations were run with lower recharge values set to 50% lower than the recharge estimates obtained from HELP. The results of the HELP recharge modeling may be slightly over-estimated for use at the small temporal scale of the HGS models because the intensity of precipitation events is not accounted for in HELP. Daily precipitation is applied to the lithology profile evenly over a 24 hour period, when in reality, precipitation events occur within shorter time intervals (hourly) and often lead to some pooled water on the ground surface. The results of the lower recharge simulations indicated that there was no change to the steady-state morphology of the FWL within the focus area surrounding the trench; however, it took 2 months longer for the FWL to

recover from the simulated storm surge overwash event (see Chapter 4 for further details). As there are no field data for the actual evapotranspiration and recharge rates, and the FWL morphology was unaffected, the original HELP recharge modeling results were considered suitable for this study.

To represent flooding of the surface with seawater, specified head and specified concentration boundaries were also assigned to the surface domain during the simulated inundation period.

Specified head and specified concentration boundaries were assigned to both sides of the model domain to represent seawater. Although specified concentration boundaries may not represent the seawater circulation along the coastlines as accurately as third-type Cauchy boundary conditions (which simulate the transport of salt water into the system based on the flux of water along the boundary calculated from the head distribution), these more complex boundaries were not considered necessary for the objectives of the modeling. Instead, the simpler specified concentration boundaries were applied because they provide a reasonable approximation of the seawater boundary in terms of the effect on FWL development near the trenches, whereas the model results that are most likely to be affected by the boundary conditions (i.e. near the coastal freshwater/saltwater mixing zone) are not the focus of the models.

The hydraulic head within the FWL was not specified in the model but allowed to develop under the influence of recharge, coastal boundary conditions, and the hydraulic properties of the aquifer. The hydraulic head is an important calibration parameter as it affects the amount of mounding of the top surface of the lens, and thus the elevation of the top of the lens and thickness of the vadose zone.

No flow boundaries were assigned by default along the base of the model domain which represents the base of the primary aquifer material, the Lucayan Limestone. The pre-Lucayan Limestone was neglected in these models given the small spatial scale focussed around the trenches and because the FWL was able to develop to the calibration depth within the Lucayan Limestone without the more permeable basement layer present.

Model Parameters

Surface domain properties were assigned using default parameters within the code, as well as under advice of HGS model developers (pers. comm. Young-Jin Park, Aquanty, March 7, 2014). Surface domain parameters (listed in Table 3.8) generally define flow of runoff across the surface domain and include the Manning friction coefficients (in the x and y directions), the obstruction height, and rill storage height. Manning friction coefficients describe the friction of water flow across the surface domain. The obstruction and rill storage heights define the minimum water depth required for flow and represent the retention of water in micro-topography depressions and vegetation along the ground surface. However, in this study, there is no horizontal flow of water across the surface domain as there is no surface slope. Flow only occurs in the vertical direction, towards the subsurface. In addition, lateral flow within the trench in the surface domain was neglected as it was assumed to have a negligible impact on the storm surge impact and recovery of the aquifer. This is because most trench-based wellfields rely on gravity flow, and therefore, water tends to move very slowly within the trenches and is observed to be almost stagnant unless it is actively being drained. Therefore, the friction coefficients do not impact the simulation results and were left at the default values (0.5). Although, the obstruction and rill storage heights are not necessary in relation to lateral flow within the surface domain, they do affect flow in the vertical direction, as discussed below.

Water exits the surface domain by infiltrating vertically into the subsurface domain. HGS couples the surface domain to the subsurface by calculating the fluid exchange due to the hydraulic gradient (and the subsequent solute exchange due to the concentration gradient) between the domains. Fluid exchange is governed by the vertical saturated hydraulic conductivity of the subsurface and a relative permeability term determined by the ratio of the water depth in the surface and the obstruction height and rill storage height. In general, the relative permeability term enables water to flow from the surface domain to the subsurface domain under the saturated vertical hydraulic conductivity when the water depth in the surface reaches above the obstruction and rill storage height. In this study, these heights were set very low (0.001m) in the absence of measured/estimated values for the ground surface, and to maximise fluid exchange,

which occurs essentially whenever there is water depth in the surface domain greater than the subsurface hydraulic head.

Coupling between the surface and subsurface domain occurs using a dual node approach, whereby each node in the surface domain has a corresponding node in the subsurface domain, separated by a small distance defined as the coupling length. Solute exchange occurs from the surface to subsurface domain according to advection-dispersion and Fickian diffusion processes along the coupling length. A coupling dispersivity is specified which determines the dispersivity to be applied during solute exchange. The coupling length is determined to balance computational time with accuracy of the results, whereby the smaller the length, the more accurate the solution of surface-subsurface coupling. Previous studies have found that the model results are generally insensitive to this parameter as long as it is less than 0.01 m, or the cumulative obstruction and rill storage height (Goderniaux et al., 2009; Liggett et al., 2012). Simulations were run where the coupling length parameter was reduced to 1.0×10^{-4} m, and, as expected, no changes in FWL morphology were observed.

Density-dependent flow was applied whenever the model domain was fully-saturated based on several fluid parameters. These include the concentration and density of the solute which were assigned to represent seawater. Fluid viscosity was set as constant (rather than dynamic) to simplify computational demand. Density-dependence is solved in HGS using the Newton-Raphson linearization and the Picard methods. Further details of HGS model parameters and numerical approach can be found in the user's manual (Aquanty, 2013).

The properties of the unsaturated zone (presented in Table 3.8) were assigned based on van Genuchten functions describing the saturation-pressure relationship:

$$Sw = Swr + (1 - Swr)\left[1 + \left|\alpha \Psi\right|^{\beta}\right]^{-v} \qquad (3.2)$$

(van Genuchten, 1980; Aquanty, 2013)

where, Sw (water saturation); Swr (residual water saturation); α (inverse air entry suction); Ψ (pressure head); β (pore size distribution) and *v* (coefficient equal to 1-1/β).

Pressure-saturation and saturation-permeability tables are generated within HGS based on the van Genuchten parameters specified; an example of these tables is shown in Figure 3.13. The van Genuchten parameters were based on the defaults for HGS, except for alpha. Alpha is inversely related to air entry suction and is normally fitted to experimental results; however, studies have developed estimates for the parameter based on common subsurface materials (Schaap et al., 2001). Generally, van Genuchten parameters relate to unconsolidated soils within the unsaturated zone and are not widely used in bedrock studies. The HGS default parameter for alpha is 3.52, representing sand (Schaap et al., 2001; Aquanty, 2013); however, other studies have determined that the potential range of appropriate alpha values for different types of bedrock is between 0.03-0.6 m^{-1} (Contractor and Jenson, 2000). Therefore, values for alpha were adjusted within this range during calibration and the final value of 0.3 was selected as the best value to simulate the observed FWL morphologies for each island.

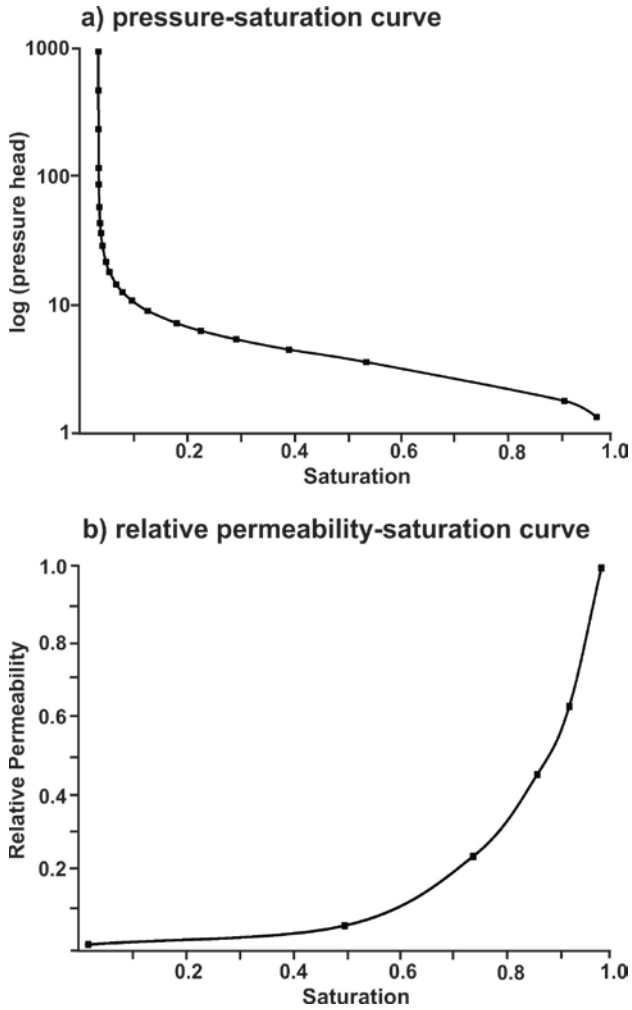

Figure 3.13. HGS-generated pressure-saturation and relative permeability-saturation data (alpha = 0.3)

Fluid flow and solute transport within the saturated subsurface occurs under the hydraulic, concentration and density gradients, as influenced by the hydraulic properties of the subsurface (presented in Table 3.8). The hydraulic conductivities of the principal aquifer (Lucayan Limestone) and the interbedded paleosols were determined by calibration within the range of values from field data (Chapter 2). As mentioned previously, the model domain was assigned, for computational reasons, as the smallest width possible while still meeting the calibration criteria. Therefore, several different model configurations were tested by varying the model domain width and the hydraulic conductivity (within the observed range for Lucayan limestone and paleosols) to identify the combination of parameters with the smallest domain width that best approximates observed conditions. With increasing model domain width, the elevation of the water

table and hydraulic gradient increase, whereas the thickness of the lens decreases. The opposite response was observed with increasing K values. An example of the relationship between K and the model domain width is provided in Table 3.7 for a variety of widths and K values that were tested.

Table 3.7. Comparison of results for varying model domain width and hydraulic conductivity (K) of the principal aquifer

		Model Domain Width (m)		
Aquifer K (m/day)		50	200	300
1	Elevation water table (masl)	1.2	1.6	-
1	Hydraulic gradient	0.006	0.007	-
1	FWL thickness (m)	35	21	-
10	Elevation water table (masl)	-	1.3	1.4
10	Hydraulic gradient	-	0.002	0.0022
10	FWL thickness (m)	-	33	29

Following the conceptual model and results of the SEAWAT modeling, paleosols were assigned K values one order of magnitude higher than the Lucayan Limestone. Simulations were run with vertical anisotropy within the Lucayan Limestone assigned one order of magnitude higher and lower, which resulted in no change to the FWL morphology. This corresponds with results from the SEAWAT models, and therefore, the K values for all aquifer materials were assigned as isotropic. Effective porosity was assigned based on the range in field data. Dispersivities were assigned based on the suitable range determined during SEAWAT modeling, which also corresponds to the dimensions of the elements within the model domain (i.e. element size). In the absence of measured values, other parameters, such as specific storage (1.0×10^{-5}), were based on default values in the model code (Aquanty, 2013).

The full list of parameters applied in the HGS model are presented in Table 3.8.

Table 3.8. HydroGeoSphere model parameters

Parameter	Value
Surface Properties:	
x and y-friction	0.5
rill storage height	0.001 m
obstruction storage height	0.001 m
coupling length	1.00e-2 m
coupling dispersivity	0.1
longitudinal dispersivity	1.0
transverse dispersivity	0.1
Unsaturated Properties:	
residual water saturation	0.05
van Genuchten alpha α	0.3 / 3.52 m^{-1}
van Genuchten betar β	3.2
Aquifer Properties:	
recharge	877 mm/year
aquifer K	86.4 m/day
paleosol K	864 m/day
paleosol positioning	9 and 14 mbgs
effective porosity	0.15
specific storage	1.0e-5
longitudinal dispersivity	1.0
transverse horizontal dispersivity	0.1
transverse vertical dispersivity	0.01
Fluid Properties	
maximum density	1025 kg/m^3
salt concentration	35.0 g/L
fresh concentration	0.0 g/L
fluid viscosity	constant

Model Run Settings

HGS solver settings were based on the default settings described in the user's manual (Aquanty, 2013). Deviations from the default parameters include the initial time step size, which was set to $1.0x10^{-5}$ days to allow for model convergence during

inundation when large changes occur over a short period of time. Another deviation was the maximum time step (one day) and maximum time step multiplier (1.2), which were reduced from the default values to optimise simulation accuracy. Other model run settings were based on advice of HGS model developers to troubleshoot model run issues (pers. comm. Young-Jin Park, Aquanty, March 7, 2014).

The modeling approach involves three separate modeling phases: 1) development of the FWL to steady state conditions; 2) short temporal-scale modeling of the rise in salt water height accompanying the overwash; and 3) recovery of the FWL. The three phases are required to accommodate the different temporal scales (i.e. decades for FWL development and hours for storm surge occurrence) as well as to assign the time-varying boundary conditions. The heads and concentrations at the end of each phase are used as initial conditions for the subsequent phases; however, the boundary conditions are changed to reflect the different scenarios. The boundary conditions for Phase 1 (FWL development) are as described in the preceding sections. For Phase 2 (inundation), a specified head and specified concentration boundary are assigned to the surface domain, which are then removed for Phase 3 (FWL recovery). The specific model simulations are described in detail in Chapter 4. Example grok input files for each of the phases are provided in Appendix B.

3.2.2. Global Island Type Assessment

HGS models were also developed to characterise the FWL response to storm surge, or overwash more generally, for a variety of island hydrogeological settings. The aim of the modeling was to provide approximations of each island hydrogeological setting that allowed for comparison between island types based on a consistent, simple modeling approach.

Models were developed for six island types based on an example island representing the typical hydrogeological setting for each type. The model setups, parameters, and run settings were based on a similar approach as described in the previous section, with some adjustments as described below. Details of the model

domains and simulations are provided in Chapter 5. An example model domain is shown for island Type I in Figure 3.14.

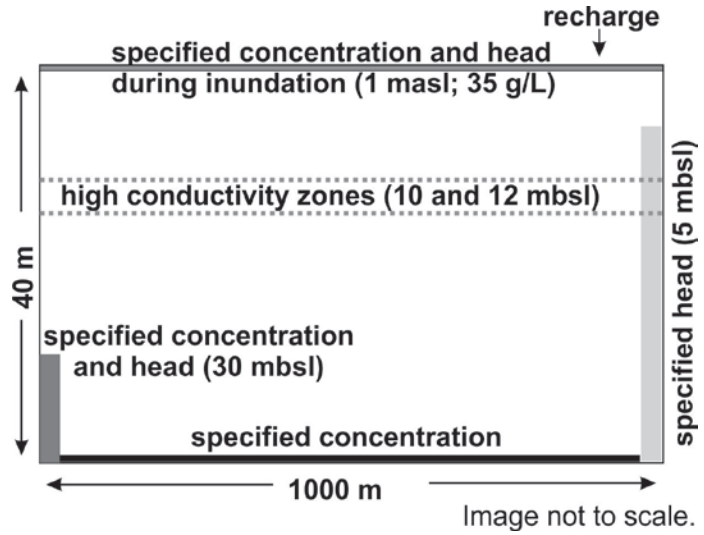

Figure 3.14. HGS model setup (example shown for island Type I – Mauritius)

For these simulations, the model domains do not represent a full cross-section of the island, but rather the near-coast zone, where a storm surge overwash is expected to occur. Accordingly, the left side of the domain is assigned a specified head and concentration boundary representing the ocean, and the right side of the model domain is assigned a specified head boundary representing water table according to the inland hydrogeological setting (based on observations for each island). Other studies evaluating overwash events employ similar boundary conditions whereby the gradient is fixed from inland to the coast (Sivakumar and Elango, 2010; Chui and Terry, 2012; Yang et al., 2013).

Given the small domain size, it was necessary to constrain the FWL depth. In order to develop a full representation of the FWL and underlying salt water, it would have been necessary to develop full scale island models, which would require more detailed data for each island. Therefore, a specified concentration boundary condition was applied to the base of the model domain to truncate the bottom of the FWL. The specified concentration boundaries were applied in order to fix the FWL thickness to that observed in the field to ensure that the saltwater plume from the overwash moves within the flow field of the lens, and does not exit the base of the lens. When models were run without this boundary, the FWL extended at least to the base of the model domain

(example shown for island Type III on Figure 3.15a). This is due to the relationship between FWL thickness (and depth) and model domain width, presented in the preceding section (see Table 3.7), whereby the smaller the model domain width, the thicker the FWL.

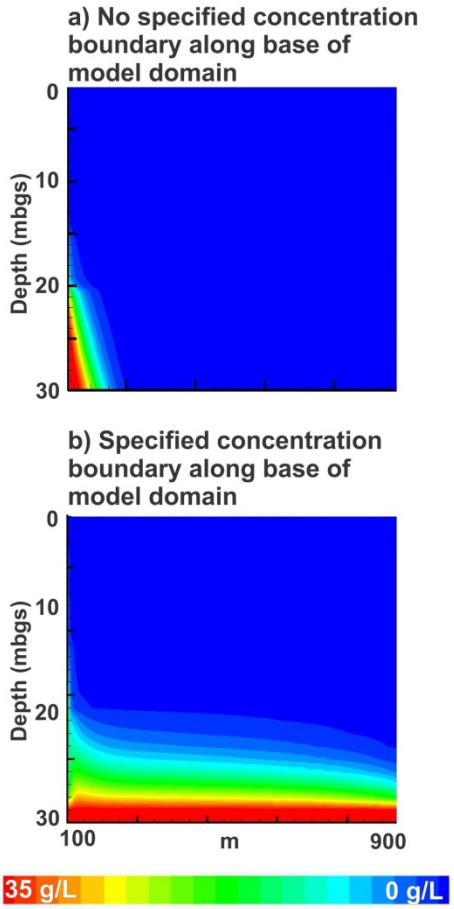

Figure 3.15. Results of specified concentration boundary along model domain base; results shown for island Type III – Andros

This approach is considered to be reasonable for the purposes of this study for a number of reasons. First, the specified concentration boundaries do not affect the FWL response or the recovery results. Separate models were run without the specified concentration boundaries (i.e. zero flux) and the results for lens response and recovery were unchanged (although the simulated FWL was thicker without the boundaries). This is because the models generate a representative volumetric flux through the lens regardless of the boundary conditions along the base of the model. The focus of the

models is on shallow processes within the upper portion of the FWL, and therefore, the boundary type along the base does not influence the model results. Additionally, previous simulations using HGS (described in Chapter 3.2.1) indicated that the FWL does not shift (upward or downward) within the subsurface during inundation and recovery, such that the base of the lens remains at a relatively constant elevation. The base of the lens is not depressed during inundation, and although the concentrations in the lens change significantly as the saltwater plume moves through the lens, the approximate base of the lens does not shift. Previous studies also observe that the saltwater plume does not exit the FWL by sinking through the base of the lens, but instead is discharged towards the coast, along the flow field within the lens (Illangasekare et al., 2006; Terry and Chui, 2012). Therefore, the purpose of applying the specified concentration boundaries is to simulate the base of the FWL within the model domain, at the observed depth, to ensure that the saltwater plume does not migrate through the base of the lens, but rather along the flow field within the lens. Therefore, although the boundaries along the base of the models are forced, they provide a realistic representation of the flow field through the lens so that FWL response and recovery may be simulated (Figure 3.15b).

Chapter 4.

Response of the Freshwater Lens

This chapter was submitted as a paper entitled, “From days to decades: numerical modeling of freshwater lens response to climate change stressors on small islands”, to Hydrology and Earth System Sciences.

4.1. Introduction

Small islands are particularly vulnerable to stressors associated with climate change. The freshwater lens (FWL) is generally sensitive to hydrological disturbances, as a consequence of the low hydraulic gradient and limited thickness of the lens (Vacher, 1988; Falkland, 1991; Robins and Lawrence, 2000; White and Falkland, 2010). As groundwater recharge is the primary source of fresh water to a FWL, an adequate amount of recharge is critical for maintaining the lens morphology (Falkland, 1991). Changes in groundwater recharge due to climate change are likely to result from increases in temperature and changes in the spatial distribution, frequency and magnitude of precipitation (Green et al., 2011). Conditions of reduced recharge disturb the balance of freshwater outflow necessary to maintain the extent of the FWL, and may lead to loss of freshwater volume due to saltwater intrusion (Oude Essink, 2001; Ranjan et al., 2009).

Sea level rise (SLR) may result in inundation and a landward shift of the saltwater interface, particularly on low-lying islands (Bear et al., 1999). This would result in a loss of FWL volume, either by a reduction in areal extent and/or a thinning of the lens (Oude Essink, 2001). Projected changes in the frequency of hurricanes and tropical storms are uncertain (Intergovernmental Panel on Climate Change (IPCC), 2014); however, there is evidence to suggest that storms may become more intense, increasing

the likelihood of storm surge occurrence (Biasutti et al., 2012). Storm surge overwash can lead to salt contamination of the FWL and a temporary loss of fresh water (Anderson, 2002; Illangasekare et al., 2006; Terry and Falkland, 2010). Due to topography, low-lying islands are more susceptible to saltwater inundation from SLR and storm surge overwash.

Previous modeling studies have investigated aspects of climate change impacts on the FWLs of islands or coastal aquifers. Simulations of decreased recharge resulted in more saltwater intrusion and impact to water supply infrastructure than simulations of SLR alone (Rasmussen et al., 2013). However, for regions with future projected increases in recharge, the impact of SLR and other stresses (i.e. increases in pumping) may be counteracted by increased recharge (Sulzbacher et al., 2012). Analytical and numerical models of SLR indicate that the degree of saltwater intrusion (or loss of FWL volume) resulting from SLR depends on many factors. Whether the hydrogeological system is recharge-limited or topography-limited (Michael et al., 2013) influences whether or not the water table rise that accompanies SLR can be accommodated by the system. Werner and Simmons (2009) showed that less saltwater intrusion is expected when the system is recharge-limited (flux-controlled). Unsurprisingly, the degree of land surface inundation was found to control the amount of saltwater intrusion (Ataie Ashtiani et al., 2013), and the impact of SLR on saltwater intrusion is enhanced by groundwater extraction from coastal wellfields (Bobba, 2002; Langevin and Zygnerski, 2013).

Models of storm surge overwash events have been developed to evaluate their impact on the FWL. Most of these models used codes that ignore the surface domain. However, Yang et al. (2013) used a fully-coupled subsurface and surface approach that simulated tidal activity, coastal flow dynamics, and a hypothetical storm surge on a coastal aquifer. All models indicate initial salt contamination of the FWL, which recovers to fresh concentrations over time due to fresh water recharging at surface and density-driven downward migration of salt water (Terry and Falkland, 2010). The occurrence of multiple storm surges (Anderson, 2002) and accumulations of salt water at the surface in low depressions (Chui and Terry, 2012) may increase the time for recovery of the lens. Where the vadose zone becomes thinner under conditions of SLR (because the FWL has risen in the subsurface), the impact of storm surge alongside SLR may result in less

salt contamination of the FWL (Chui and Terry, 2013). However, the salt contamination that does occur under SLR conditions remains close to the surface of the lens (Terry and Chui, 2012). Wider islands generally result in less FWL contamination than narrow islands, as a result of their thicker FWL morphology (Chui and Terry, 2013).

Although many aspects of climate change impacts on FWL have been modeled previously, few studies have investigated both the spatial and temporal response of the FWL to the stressors. Climate change related stressors operate at various spatial and temporal scales: island-wide impacts due to SLR and changes in recharge occur over long time periods, on the order of decades, whereas local-scale impacts due to storm surge overwash occur over short time periods, on the order of days. This study evaluates the spatial and temporal response of an island FWL to various climate change stressors using a numerical modeling approach. To account for the varying temporal and spatial scales of the stressors, two different density-dependent flow and transport modeling codes are used. SEAWAT (Langevin et al., 2007) models were developed at an island scale to simulate long-acting stressors, including SLR and change in recharge. HydroGeoSphere (HGS; Therrien et al., 2010) models were developed at a local scale to simulate storm surge which is a short-acting stressor. The study aims to identify critical factors and stressors that may affect freshwater resources of small, low-lying islands using Andros Island in The Bahamas as a representative island. The results of the study are intended to be applicable to other islands with similar hydrogeological settings.

4.2. Site Description

The study site is Andros Island in The Bahamas. Andros Island has undergone limited development and groundwater exploitation; therefore, the hydrogeological data collected in the 1970s (Little et al., 1973) are considered generally representative of current conditions and can be used for baseline model calibration. Andros Island is representative of other low-lying carbonate islands with thin FWLs commonly found throughout the Caribbean and Pacific regions (Falkland, 1991; Vacher and Quinn, 1997).

Andros Island is the largest island in The Bahamas, and is located 200 km southeast of Florida (Figure 4.1). It is 14,000 km^2 in area and is comprised of several

smaller islands and cays. The highest elevation on the island is 20 metres above sea level (masl) along a ridge that parallels the east coast, whereas lower elevations (< 1 masl) are common towards the west. The western coastline is largely composed of wetlands and saltwater marshes, and therefore, most settlements are along the east coast of the island (Figure 4.1). The remainder of the island is largely covered in pine forest. There are no permanent surface water bodies on the island.

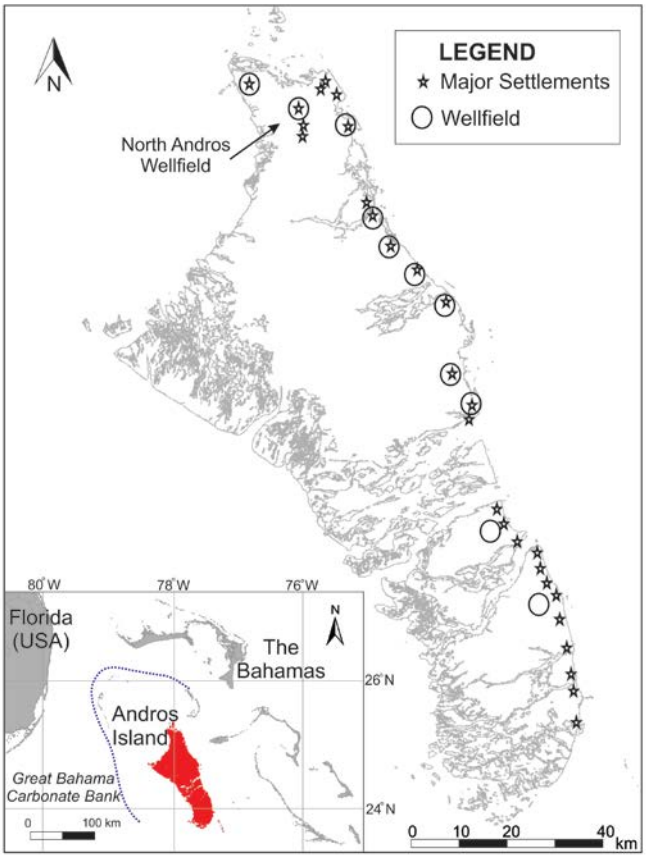

Figure 4.1. Andros Island indicating the location of settlements and wellfields

Andros Island is located on the Great Bahama carbonate bank (Figure 4.1). The geology of the island is predominantly Pleistocene Lucayan Limestone Formation, which is approximately 40 m thick (Beach and Ginsburg, 1980). Discontinuity surfaces (unconformities) within the limestone are present as layers of paleosols recurring in the upper stratigraphy (Beach and Ginsburg, 1980). These layers represent episodes of sub-aerial exposure and are largely concentrated within the top 20 m of the Lucayan (Beach and Ginsburg, 1980; Boardman and Carney, 1997). Underlying the Lucayan is a

cavernous, highly karstic, and relatively more permeable unit termed the pre-Lucayan, which is present from 43 m below ground surface (mbgs) to at least 75 mbgs (Boardman and Carney, 1997). The geology below this depth has not been observed as most studies focus on the shallow, freshwater-bearing units; however, deposits of carbonates on the Great Bahama bank are estimated to be up to 7 km thick (Cant and Weech, 1986).

Due to its large size, the FWL on Andros Island represents the principal source of natural fresh water for The Bahamas. Most local residents rely on the municipal potable water supply, which extracts groundwater from the lens via 11 wellfields distributed across the island (Figure 4.1). The local drinking water guidelines define potable water as having a salt concentration of less than 0.4 g/L. The largest of these wellfields is the North Andros Wellfield. As is common with many FWLs, there is potential for upconing of the underlying salt water and degradation of the lens if wells are deep and the lens thin (Werner et al., 2009; White and Falkland, 2010). Therefore, the wellfields on Andros employ horizontal trench-based groundwater extraction or a series of interconnected shallow boreholes pumped at low rates. Typical depth of the wellfields is between 1 and 5 mbgs; however, some private wells are installed deeper. Water flows within the trench-based wellfields under a very low gradient, towards a central low sump where water is pumped to storage reservoirs.

The hydrogeology of Andros Island is based on previous studies, most of which were conducted around the wellfields and other developed areas. The principal aquifer is the unconfined Lucayan Limestone as the older (deeper) geological units are too permeable and thus are not able to prevent fresh water from mixing with the surrounding salt water (Cant and Weech, 1986; Schneider and Kruse, 2003). Soil zones are sparse, and minimal runoff occurs during precipitation events (Little et al., 1973; Tarbox, 1987). The FWL is recharged solely through infiltrating precipitation, which generally occurs during the wet season from May to October (Bukowski et al., 1999). Average annual precipitation in the south is 39% less than average annual precipitation in the north of Andros Island (Cant and Weech, 1986; Bahamas Department of Meteorology, Climate Averages 1979-2000). Based on resistivity surveys conducted in the north of the island, the thickness of the FWL ranges from 3 to 20 m (Wolfe et al., 2001); however, previous

studies cite the maximum thickness as 34 m (Cant and Weech, 1986) and borehole salinity profiles indicate the maximum thickness of the lens is up to 39 m (Little et al., 1973). The lens is generally shallower in the southern regions of Andros Island compared to the northern regions, with a measured thickness of at least 15 mbgs (pers. comm., municipal water supply managers, Bahamas Water and Sewerage Corporation). The elevation of the lens inland is approximately 2 masl (Ritzi et al., 2001) with typical depth to water of 1-2 mbgs, although it is deeper (up to 5 mbgs) under the high topography ridge along the east coast (Little et al., 1973; Boardman and Carney, 1997). The hydraulic conductivity of the principal aquifer (Lucayan Limestone) is estimated to range from 86 to 8,640 m/day based on short duration, single-well specific capacity pumping tests conducted in the 1970s (Whitaker and Smart, 1997). The hydraulic gradient (ranging from 0.0005 to 0.001) was determined from historic field observations and estimates of the FWL morphology (Little et al., 1973). Porosity ranges from 10-20% (Bukowski et al., 1999). Sparse hydrogeological field data are available for the majority of the island; therefore, in the past, the morphology of the FWL was largely inferred based on vegetation patterns, geological setting and anecdotal observations. Because Andros Island is composed of several small islands and cays, the FWL is also composed of multiple lenses present on the different land masses. Lenses are anticipated to be present across most of the island, except in areas that are heavily intersected by saltwater marshes and wetlands.

In September 2004, Hurricane Frances caused a storm surge on the west coast of Andros Island, which resulted in extensive salinization of the North Andros Wellfield (Figure 4.2). The hurricane ranged from a Category 4 to Category 2 on the Saffir Simpson Hurricane Scale while it travelled across The Bahamas from the southeast to northwest (Franklin et al., 2006). The surge occurred September 3-4, 2004, while Hurricane Frances passed near Andros Island. The exact time of occurrence of the storm surge and the actual extent of the overwash are unknown because the western coast of Andros Island is largely unpopulated. However, after the hurricane had passed, evidence of the overwash was observed, such as flooded ground and the presence of marine fish at inland locations (Bowleg and Allen, 2011). The likely extent of the overwash is thus based on observations of damage following the surge (e.g. water

marks on trees, presence of seaweed and marine organisms, etc.) and is shown on Figure 4.2.

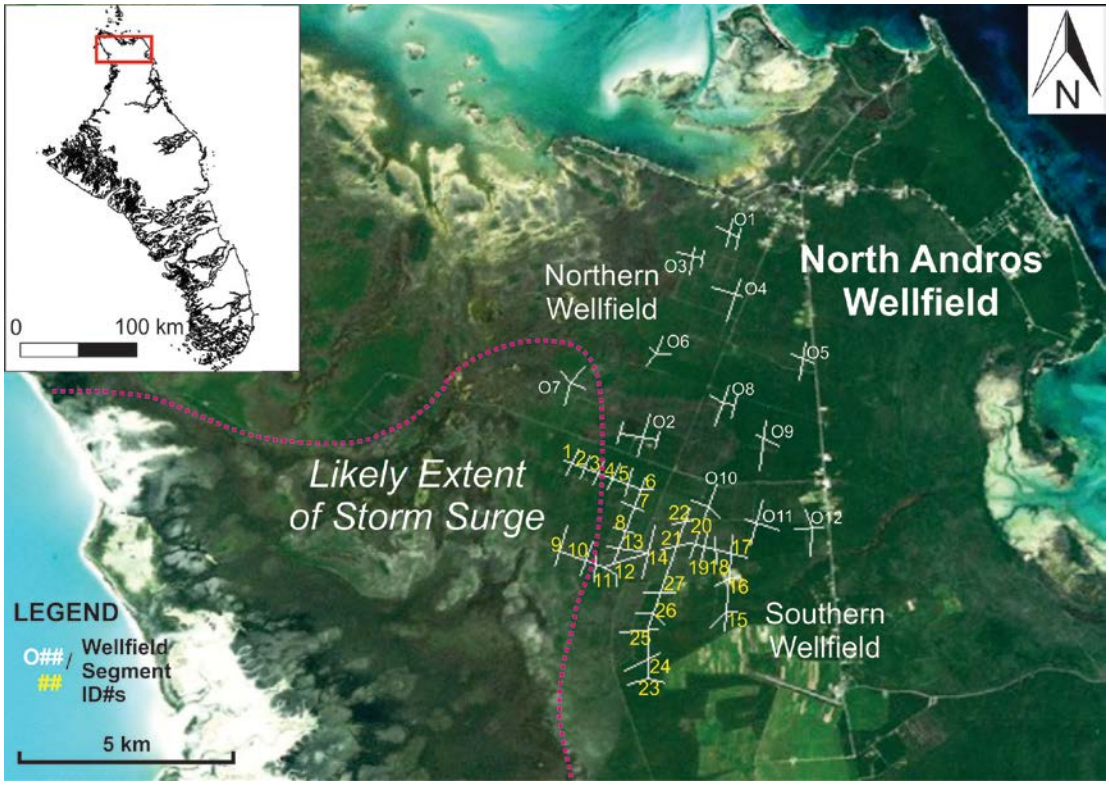

Figure 4.2. Layout of the North Andros Wellfield indicating the likely extent of the 2004 Hurricane Frances storm surge overwash

Salinity concentration data from the southern wellfield (Figure 4.2) were provided from the water managers for the dates: May 2004 (pre-storm), September 7th (immediately post-storm surge), September 15th (following remedial action) and July/August 2005 (approximately one year post-storm surge). These data are presented on Figure 4.3, which illustrates the abrupt increase in salinity within the trenches following the storm surge and the eventual recovery to pre-storm concentrations. As a form of remedial action, the contaminated trenches were pumped to remove the ponded seawater beginning on September 8th (approximately 4 days following the storm surge). Salinity in the affected trenches improved, reducing by up to 88% on September 15th, relative to the maximum recorded concentrations in each trench. However, remedial pumping of the trenches was not completed because fresh water was required to support post-hurricane relief efforts on other islands. Therefore, some of the contaminated trenches were closed off from the wellfield system to allow for extraction of

fresh water from the unaffected parts of the FWL and were not drained. Several of these contaminated trenches remained closed for two years due to poor water quality. Trenches that were drained are distinguished from those that were not in Figure 4.3. The wellfield eventually recovered to normal salinity concentrations between one and two years post-storm, with all trenches recovered by 2009.

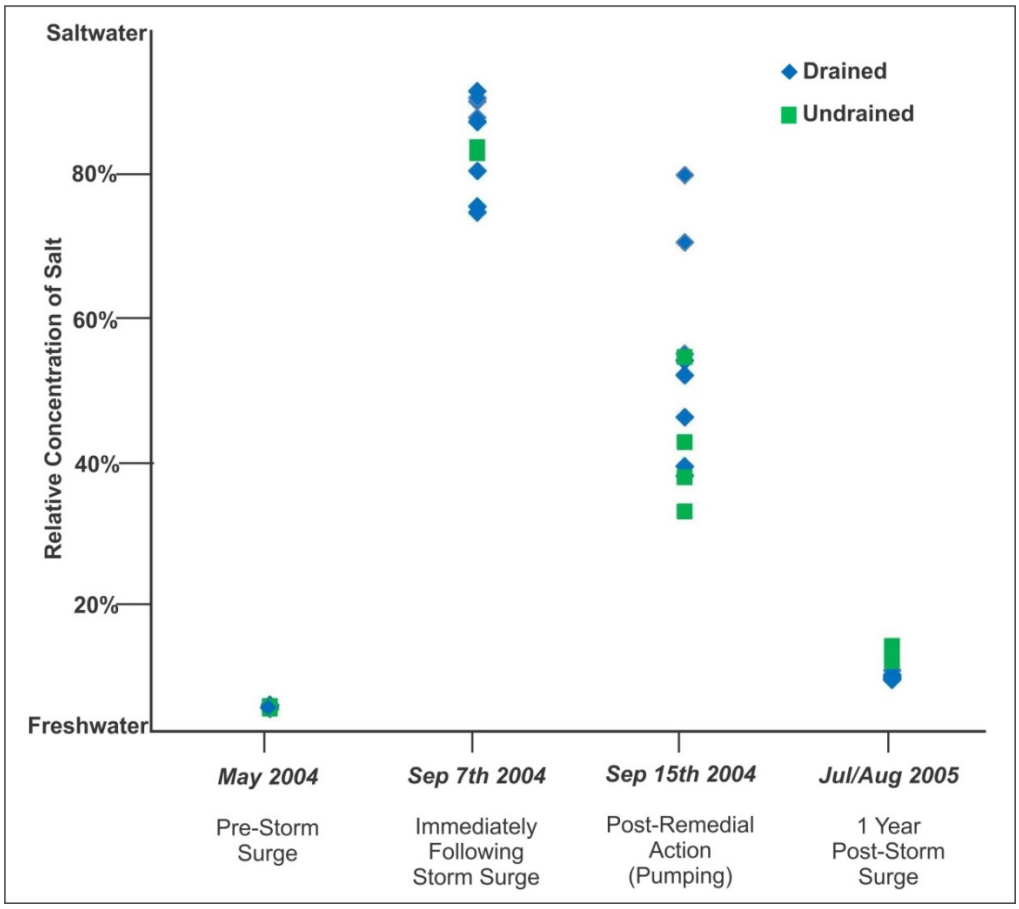

Figure 4.3. Salinity monitoring data before and after the 2004 Hurricane Frances storm surge. Data are shown for the southern trench segments of the North Andros Wellfield only. See Figure 4.2 for the location of the trench segments.

4.3. Methodology

4.3.1. SEAWAT Model: Long-Acting Stressors

Baseline Model Setup

A three-dimensional numerical density-dependent groundwater flow and solute transport model was developed using SEAWAT. The island was simulated using two separate models, a northern and southern model, to allow for refined grid resolution and a reasonable run time for each simulation. Each model was run for 100 years during which time the FWLs developed; both models reached steady state (i.e. no further change in lens morphology) within 20-25 years. Specified head boundaries were defined along the perimeter of the domain to simulate sea level, with density specified at 1.025 kg/L, representative of typical seawater composition. Specified concentration boundaries were assigned to the same grid cells as the specified head boundaries with concentrations of 35 g/L salt. The initial concentration of the entire model domain was specified at 35 g/L salt. The ground surface for the model was based on a digital elevation model (DEM) for Andros Island (90 m resolution). The model grid was uniform in plan-view covering all of Andros Island with each grid cell 500 m by 500 m. In the vertical dimension, the model included 44 layers, with individual layer thicknesses of 1 m in the upper 20 m of the model domains, which transitioned to 2.5, 5 and then 10 m thickness at depths of (20, 40 and 60 mbgs, respectively) to the base of the domain (200 mbgs).

Hydraulic conductivity of the principal aquifer was based on field data (Little et al., 1973), and a sensitivity analysis was conducted to identify a representative configuration and associated hydraulic properties of the layers to simulate the observed FWL thickness on Andros Island. Previous studies had characterised the paleosols as low hydraulic conductivity layers (Ritzi et al., 2001); however, anecdotal evidence indicates that the layers are very weathered and may be highly conductive. In this study, the paleosols are represented by relatively high hydraulic conductivity layers (interbeds) within lower permeability limestone. This layer configuration with the assigned layer hydraulic properties is supported by model calibration. Assigning a low conductivity to the paleosols resulted in the lens being perched, which is not observed in the field.

Whereas, representing the paleosols as high conductivity layers within lower conductivity limestone resulted in thin lenses being developed, similar to field observations. This approach is consistent with other studies based in The Bahamas, which have suggested that layers of high hydraulic conductivity in the subsurface are responsible for thin FWLs (Wallis et al., 1991). The best configuration of aquifer layers and hydraulic conductivities are provided in Table 4.1.

Recharge was applied to the top layer of the model with concentration of 0 g/L salt to simulate the average annual recharge to the aquifer. Recharge is the only input of fresh water to the hydrogeological system and, therefore, is the main mechanism by which the simulated FWL develops in the model. The annual recharge amount for Andros Island was estimated using the United States Environmental Protection Agency's software HELP (Hydrologic Evaluation of Landfill Performance) (Schroeder et al., 1994). HELP utilises a storage routing technique based on hydrological water balance principles. It accounts for soil moisture storage, runoff, interception, and evapotranspiration. HELP has been used to estimate recharge for a variety of climatic and physiographic settings (Scibek and Allen, 2006; Jyrkama and Sykes, 2007; Toews and Allen, 2009; Allen et al., 2010).

Within HELP, a representative vertical percolation profile was defined for the unsaturated zone. The depth of the profile was 2 m, based on a sensitivity analysis using the minimum and maximum observed depths to the water table on Andros Island. No soil zone was specified due to the generally thin/absent soils on Andros Island (Little et al., 1973). The lithology was homogeneous (representing limestone), with a saturated hydraulic conductivity (864 m/day) based on the mean value from field studies (Little et al., 1973) and the calibrated value from the baseline SEAWAT model. Vegetation cover was assigned to the highest class in the software (a leaf area index of 5) based on the large proportion of pine forests. The surface was assigned zero slope given that minimal runoff is observed. The wilting point was assigned 0.05 and field capacity 0.1 in the absence of measured values.

Two 100-year climate data series were generated using the embedded stochastic weather generator; one for North Andros and one for South Andros because

the historical climate differs between the two regions. The average annual precipitation on North Andros is 1442 mm/yr, while on and South Andros it is 889 mm/yr. Temperature averages were not available for South Andros, therefore the monthly averages for North Andros were applied to both models. Other climate parameters (e.g. windspeed and relative humidity) were identical for both models. The historical statistical parameters for climate were based on values for the nearest climate station (Miami, Florida, USA) in the weather generator database.

The average annual recharge for the north was estimated at 877 mm/year, with a minimum monthly average of 24 mm in December and a maximum monthly average of 163 mm in August. The average annual recharge for the south was estimated at 426 mm/year, with a minimum monthly average of 17 mm in February and a maximum monthly average of 70 mm in October. These values were used as input for the northern and southern SEAWAT models, respectively.

The hydrogeological parameters assigned to the SEAWAT model, based on field data and sensitivity analyses, are summarised in Table 4.1. Storage parameters were based on common values for the aquifer lithology (Younger, 1993). The wellfields were not simulated in the baseline model in order to represent natural historical conditions. Given their small size, the wellfields are not anticipated to affect the freshwater lens response. If the system were head-controlled, however, at a local scale a rise in water table could result in more loss of freshwater from the top of the lens.

Table 4.1. SEAWAT model parameters

Parameter	Value
Model Domain	200 m deep; lateral extent same as island extent
Lucayan/ Pre-Lucayan interface	40 mbgs
Paleosol Depths	9-10 mbgs and 14-15 mbgs
Hydraulic Conductivity	Lucayan: 864 m/day – paleosols: 8640 m/day – Pre-Lucayan: 86400 m/day
Specific Storage / Specific Yield	$1x10^{-5}$ m^{-1} / 0.2
Effective Porosity	0.15
Dispersivity	Longitudinal 1.0 m; Transverse (Vertical & Horizontal) 0.1 m
Specified Head Boundary	0 masl along model domain periphery; specified density 1.025 kg/L
Concentration at Specified Head Boundary	35 g/L along model domain periphery
Initial Concentration	35 g/L throughout model domain
Recharge	877 mm/year (north) and 426 mm/year (south); concentration 0 g/L
Time Steps	Initial: 14 minutes; Maximum: 1 day

Climate Change Simulations

Future climate for this study was based on published climate change projections for The Bahamas (United Nations Development Programme (UNDP), 2010). The projections were derived from 15 global climate models (GCMs) simulating three emissions scenarios (SRES A2, A1B, and B1). Summaries of projected changes were compiled as seasonal shifts for three-month groupings (McSweeney et al., 2010). For each grouping, a range in values (minimum, median, and maximum) for each emissions scenario was provided for the 2030s, 2060s and 2090s. The median seasonal shift in temperature and precipitation projected for the 2090s for the A2 scenario (expected to result in the greatest change) was selected for Andros Island, as summarised in Table 4.2. Average daily temperature for the 2090s is projected to increase during all seasons

(between 2.8-3.2°C). Changes to precipitation are projected to occur primarily during the summer (up to 42% reduction relative to current conditions). Overall, the projected climate shifts represent conditions with less precipitation and higher temperatures - a drier and hotter climate state. However, using the median shifts for a single emissions scenario does not account for the significant uncertainty related to climate models. For the A2 scenario, temperature increases from 2.1° to 4.7°C, and the range in shifts in precipitation is from -80 to +62 mm depending on GCM.

Table 4.2. Projected climate shifts for the 2090s, and the resulting projected values for seasonal temperature and monthly mean precipitation for North and South Andros

Parameter	D	J	F	M	A	M	J	J	A	S	O	N
Temperature Shift (°C)	+2.8			+3.0			+3.2			+3.2		
Projected Monthly Mean Temperature (°C) *North/South*	25.2	24.3	24.6	25.3	26.8	28.5	30.4	31.3	31.3	30.9	32.7	27.7
Precipitation Shift (mm)	-2			-18			-24			+12		
Projected Monthly Mean Precipitation (mm) *North*	45.3	48.3	49.6	47.0	66.3	90.1	188.7	137.5	210.1	189.5	175.6	97.7
Projected Monthly Mean Precipitation (mm) *South*	51.0	33.5	36.9	24.4	27.4	88.5	81.2	39.6	56.9	112.0	137.9	103.4

Changes to groundwater recharge were determined by re-modeling recharge in HELP using the projected 2090s climate. The seasonal climate shifts (applied evenly to each month according to season) were applied to the monthly normals for temperature and precipitation in the weather generator, and a new stochastic weather series was generated to represent the projected future climate. This approach is consistent with that used in other studies (e.g. Scibek and Allen, 2006). The adjusted climate data series was then used as input to the vertical percolation profile to determine the annual average groundwater recharge expected under projected climate change.

As in the baseline recharge modeling, recharge estimates were produced for North and South Andros, and these values were applied to the SEAWAT models for each region, respectively. The predicted average annual recharge under future projected climate change for the north is 777 mm/year (11% decrease), with a minimum monthly average of 18 mm in March and a maximum monthly average of 130 mm in August. The predicted average annual recharge for the south is 360 mm/year (15% decrease), with a minimum monthly average of 4 mm in July and a maximum monthly average of 82 mm in November.

In order to quantify the uncertainty related to the potential range in climate shifts, additional HELP models were run with the worst-case scenario (maximum temperature increases and precipitation losses) and with the best-case scenario (minimum temperature increases and precipitation losses) for the A2 scenario. The resulting recharge estimates range from 395 to 1124 mm/year (-55% to +28% relative to baseline) for the north and 117 to 662 mm/year (-73% to +55% relative to baseline) for the south. This represents a significant potential range in changes to recharge on Andros Island and a large component of uncertainty. A 55 to 73% decrease in recharge would have very serious implications for freshwater resources on Andros Island. Based on the impact of an 11 to 15% decrease in recharge on the FWL morphology, as presented in the following sections, this would result in a very small and thin lens. In contrast, the potential increases in recharge, from 28% to 55%, may result in a thicker, larger lens that may be more robust to other stressors. However, these ranges of potential recharge were not carried through the SEAWAT models because the focus of the study was on response time rather than sensitivity of the FWL to various climate change projections.

SLR was simulated by increasing the elevation of the specified head boundaries in the model domain. Loss of land surface due to inundation associated with SLR was not simulated, as the grid resolution of the model is larger than the inundation anticipated based on ground surface elevation. Therefore, the boundaries at the edge of the model domain are anticipated to remain at the same model grid cell, only representing a higher specified head value. Although SLR has been already observed over the last several decades (White et al., 2005), there is uncertainty as to the rate that it will occur in the future (Rahmstorf, 2007). Geographic variability in the rates of SLR is

also expected (White et al., 2005). Therefore, a predicted mean sea level increase of 0.6 m by the 2090s (relative to 1980) was selected as an average estimate based on global and regional projections of SLR (IPCC, 2007; Rahmstorf, 2007; Obeysekera, 2013). The hydrogeological system of Andros Island is considered recharge-limited rather than topography-limited, because there is some capacity for the FWL to rise in the unsaturated zone without leading to surface flooding (Werner and Simmons, 2009).

Both the reduction in recharge and SLR were simulated in the models as incremental instantaneous shifts. Three models were run: one for recharge reduction alone, one for SLR alone, and one including both stressors. The baseline model was run for 50 years to allow the FWL to develop. The recharge and specified head boundary values were then adjusted every 10 years until reaching the projected values for the 2090s. This assumes uniform rates of change throughout the 100 year simulation.

Observation wells were defined in the models to capture a discrete record of simulated concentration for every time step. The observation wells were located within the center of the FWL and at the edge of the FWL to represent areas that are anticipated to be, respectively, most resilient and most vulnerable to stressors. The northern model consists of one landmass and, therefore, one principal FWL, whereas the southern model consists of multiple landmasses. As discussed below, two principal lenses form in the southern model. Therefore, two observation wells were assigned in the northern model and four observation wells were assigned in the southern model, representing central and peripheral wells for each anticipated FWL. The wells are identified as A and B to distinguish between the two principal lenses in the southern model. Each well was assigned from the ground surface to 5 mbgs (as an open borehole), corresponding to the maximum depth of most wells/wellfields on Andros Island.

In order to evaluate changes to the FWL morphology in response to climate change, the SEAWAT model island-scale results were quantitatively evaluated using a geographic information system (GIS). The volume and area of the lens were calculated based on a threshold salt concentration (0.4 g/L or less) and porosity. Although there are inaccuracies inherent in this approach, it provides an estimate of the lens morphology that allows for quantitative comparison of the changes in FWL morphology between

different stressors applied in the island-scale model. This threshold concentration is based on the water quality guidelines for salinity in the municipal supply on Andros Island. It also falls within common definitions of fresh water containing less than 1.0 g/L of TDS (Freeze and Cherry, 1977; Barlow, 2003). The World Health Organisation (WHO) drinking-water guidelines do not stipulate a maximum threshold for salt in water, except as it relates to unacceptable taste. The WHO recognises that water that tastes fresh often has a salt concentration of less than 0.25 g/L; however, in regions where there is naturally more salt in the water there may be a higher taste threshold (WHO, 2011).

4.3.2. HydroGeoSphere Model: Short-Acting Stressor

Modeling the impact of storm surge overwash on a hydrogeological system involves simulating density-dependent flow and solute transport across the surface, the vadose zone and the saturated domain. HydroGeoSphere (HGS) was identified as the most suitable tool to simulate these coupled processes because it is a fully integrated surface and variably saturated subsurface model that is capable of simulating these processes across all domains. By solving the surface and subsurface flow equations simultaneously, HGS provides more realistic representations of the major processes than simpler or independently coupled models (Goderniaux et al., 2009).

One of the mechanisms of aquifer contamination following storm surge is from open wells or trenches that provide direct access to the water table and collect the salt water during inundation (Terry and Falkland, 2010). In addition, salt water trapped within a borehole, or other direct pathway into the aquifer, may lead to prolonged release of salt water into the surrounding aquifer (Illangesekare et al., 2006). These features may delay recovery of the aquifer and, therefore, are an important component to include in modeling studies of storm surge impacts (Chui and Terry, 2013). Major consequences to water supply are likely to result when storm surge waves strike trench-based wellfields or open boreholes, as occurred on Andros Island in 2004. Notwithstanding this risk, trench-based wellfields are commonly used on low-lying islands to limit upconing. The models developed for this study aim to characterise aquifer damage and recovery from a storm surge overwash, specifically in the context of a trench-based wellfield and the impact on water supply.

The model domain represents a highly discretized, two-dimensional cross-section of one of the trenches in the North Andros Wellfield (Figure 4.4). The models were not developed in 3-D as groundwater flow (and thus, the FWL response and recovery to an overwash event) occurs perpendicular to the coast as observed in the island-scale SEAWAT models. Therefore, 3D flow is not anticipated to impact the results. The width of the model domain was made as small as possible for computational reasons. Therefore, several different model configurations were tested by varying the model domain width and the hydraulic conductivity distribution (limestone and paleosols) to identify the combination of parameters that best approximates observed conditions. The physically-based seawater boundaries are important components in simulating flow within a FWL. In reality, these boundaries are located along the coastline; however, the coastline is far from the North Andros Wellfield. Therefore, local-scale models were developed using boundary conditions assigned in such a way as to simulate a realistic flow field surrounding the trench. The local-scale models were calibrated based on critical factors that are expected to affect FWL contamination and recovery. These critical factors include: recharge, thickness of the vadose zone, aquifer hydraulic conductivity, geological heterogeneity (e.g. paleosols), water table gradient, and thickness of the FWL. Field data for each of these factors (as presented earlier) comprise the calibration criteria as summarised in Table 4.3.

Table 4.3. Observed conditions from North Andros used for calibrating the HGS model

Parameter	Value
Vadose Zone Thickness	1.5-2 m
Water Table Elevation	2 masl
Gradient	0.0005 – 0.001
Average Velocity	0.3 m/day
Thickness of Lens	15-20 m

With increasing model domain width, the elevation of the water table and gradient both increase, whereas the thickness of the lens decreases. The opposite response was observed when hydraulic conductivity was increased. The model setup that satisfied the calibration criteria with the smallest domain width was selected as the baseline model for this study.

The model uses a finite element approach with block elements that range from 0.35-1.0 m. Grid refinement was done in order to optimise simulation of flow and transport across the three hydrologic domains and to allow for the evaluation of small-scale changes in response to overwash. The model domain covers a horizontal extent of 2400 m and a vertical extent of 43.5 m, with sea level assumed to be 3.5 mbgs. The vertical extent of the domain was determined to represent the Lucayan Limestone. The model domain was 1 unit thickness, with a uniform horizontal grid spacing of 1 m. Vertical grid refinement varied from 1 m thick in the lower 20 m, to 0.5 m thick in the overlying 20 m, and 0.35 m thick in the uppermost 3.5 m. Paleosols were simulated in the subsurface as 1 m thick zones at 9 and 14 mbgs (corresponding to field observations). The hydraulic conductivity was defined as isotropic at 86.5 m/day for the portion of the domain (representing the Lucayan Limestone) and 865 m/day for the paleosols. The hydraulic conductivities are lower than that used in the SEAWAT model in order to calibrate the FWL morphology at the local-scale surrounding the trench; however, the hydraulic conductivity values applied to this model lie within the observed range based on field data (Table 4.3). The underlying high conductivity pre-Lucayan limestone was not included in the model as it was observed to not have a significant impact on the FWL morphology at the scale of the model.

The trench itself extends 2 mbgs, intersecting the top of the water table. Most trench-based wellfields rely on gravity flow; therefore, water tends to move very slowly within the trenches and is observed to be almost stagnant unless the trench is actively being drained. Therefore, lateral flow within the trench was assumed to have a negligible impact on the storm surge impact and recovery of the aquifer. The model provides a snapshot of the impact of trench-based wellfields in terms of salt water capture and transport into the aquifer, which may be scaled up to represent the whole wellfield.

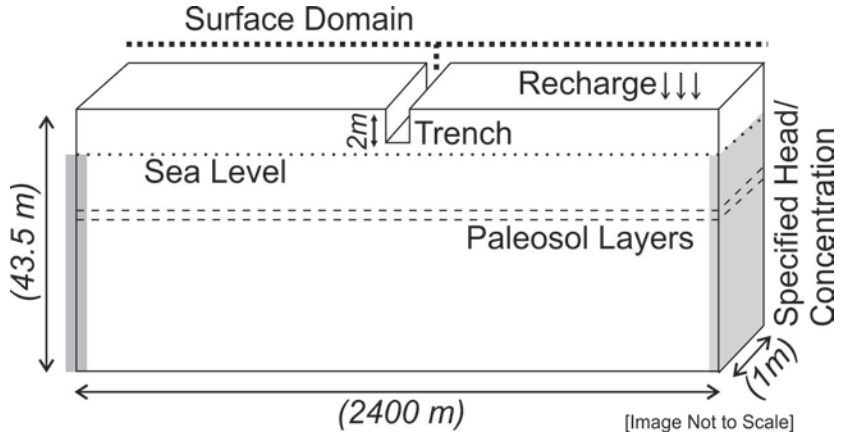

Figure 4.4. HydroGeoSphere model domain and boundary conditions

Specified head with associated concentration boundaries were assigned to both sides of the model to represent the surrounding seawater (Figure 4.4). Recharge was applied to the surface domain as an annual average quantity based on the HELP recharge modeling, presented earlier. Recharge provides the only input of fresh water that enables the FWL to develop. The boundary conditions and hydrogeological parameters assigned to the HGS model are summarised in Table 4.4.

Table 4.4. HGS model parameters

Parameter	Value
Model Domain	2,400 m model domain width; 43.5 m domain depth (representing Lucayan Limestone)
Paleosol Depths	9-10 mbgs and 14-15 mbgs
Trench Dimensions	1 m wide, 2 m deep.
Hydraulic Conductivity	Lucayan limestone: 86.4 m/day; paleosols: 864 m/day
Effective Porosity	0.15
Specific Storage	$1x10^{-5}$ m^{-1}
Dispersivity	Longitudinal 1.0 m; Transverse Horizontal 0.1 m; Transverse Vertical 0.01 m
Specified Head Boundary	0 masl along model domain periphery; specified density 1.025 kg/L
Concentration at Specified Head Boundary	35 g/L along model domain periphery
Initial Concentration	35 g/L throughout model domain
Recharge	877 mm/year; concentration 0 g/L
Time Steps	Initial time step: 0.8 seconds Maximum time step: 1 day

The simulation of storm surge overwash required three separate modeling phases: 1) development of the FWL to steady state conditions; 2) short temporal-scale modeling of the rise in salt water height accompanying the overwash; and 3) recovery of the FWL. The heads and concentrations at the end of each phase are used as initial conditions for the subsequent phases; however, the boundary conditions are changed to reflect the different scenarios. The three phases are required to accommodate the different temporal scales (i.e. decades for FWL development and minutes for storm surge occurrence) as well as to assign the time-varying boundary conditions. All model simulations used the same initial steady state FWL (Phase 1) and simulation of the storm surge overwash (Phase 2). Different scenarios of remedial action were simulated for Phase 3 and compared to the baseline recovery scenario.

Phase 1: FWL Development

Phase 1 is model spin-up period during which the FWL develops. The initial concentration in the baseline model domain was salty (35 g/L), with the only source of fresh water being recharge. The model was run for 50 years to reach steady state.

Phase 2: Storm Surge Inundation

Phase 2 simulates the occurrence of a storm surge overwash event. The surface domain was inundated with up to 1 m of water, based on observations following the 2004 storm surge on Andros Island. Flooding was simulated at a gradual rate of 0.1 m per 10 minute stress period to satisfy model convergence criteria. Once full inundation was reached (1.5 hours after start of flooding), the maximum flood level was held constant for 2 hours. The actual period of inundation is not known, so this period was estimated to allow for sufficient salt water to enter the system. The salt concentration of the flood water was assigned as 35 g/L to represent seawater.

Phase 3: Recovery of the FWL

Phase 3 involved simulating the recovery of the FWL. Several different scenarios were tested to enable comparison of recovery times when different factors are varied. All scenarios are based on the output from Phase 2, with the head and concentration boundaries of the surface domain unconstrained to allow release of the salty flood water. All other boundaries remained the same as the initial Phase 1 model.

A baseline recovery scenario was simulated for 10 years following the storm surge to allow the salt water to be flushed out of the system under the influence of recharge. In the baseline recovery model, the FWL returns naturally to its original morphology.

Several other scenarios were simulated to represent different remedial actions. Following a storm surge event when the trenches are filled with salt water, a common remedial action is to drain out the trenches to remove the captured salt water (Illangasekare, 2006; Terry and Falkand, 2010; Chui and Terry, 2012). Draining, or pumping out the trenches, is meant to improve the recovery time and assist with removal

of the salt water from the system. However, draining may often be delayed due to access constraints or due to lack of coordination and emergency response following the storm surge. Therefore, models were developed where the trenches are drained at different times and for different durations to evaluate the impact of draining protocol on recovery times of the FWL and impact to water supply. Scenarios were modeled whereby draining was delayed by one, two, three, or four days after the storm surge (to reflect a delay in action). Other scenarios modeled draining initiated one day after the storm surge, whereby the duration of draining was one, two, or three days (to investigate the effect of sustained periods of draining).

For all recovery simulations, observation points were assigned within and immediately below the trench to monitor salt concentrations during recovery. This allowed for the comparison of recovery times between different scenarios, specifically the number of days for potable water to return to the trench and aquifer.

4.4. Results

4.4.1. Long-Acting Stressors

Baseline Model

The simulated FWL in the baseline model provides a snapshot of the average annual FWL morphology. The model results indicate that a FWL is present throughout most of the model domain (not shown); however, this study focuses on areas considered viable to provide a sustainable water supply, which are defined as having a lens thickness of greater than 2 m and concentration less than 0.4 g/L (Figure 4.5). The shape of the lens is relatively symmetrical in cross-section with an average hydraulic head of 1.8 masl, which corresponds to typical elevations observed of 2 masl. The estimated total area of the viable FWL on Andros Island is approximately 2,000 km^2 with a fresh water volume of $5.9x10^9$ m^3.

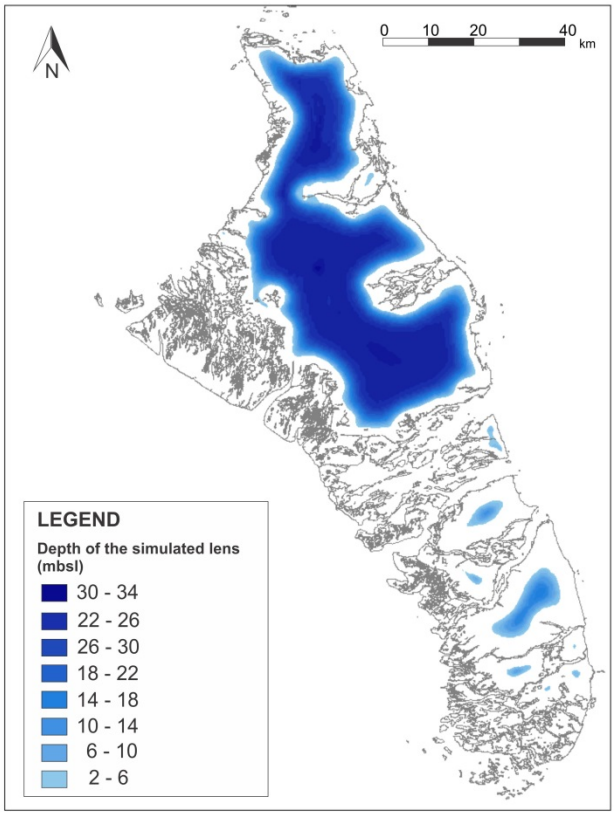

Figure 4.5. Baseline freshwater lens representing current conditions

The baseline model was calibrated to observations, where available, although these were sparse and based on varying time periods (from the 1970s to early 2000s). The term “calibration” is used here to refer to a comparison of the simulated versus observed features of the FWL, not a quantitative evaluation of model calibration. The extent of the lens generally corresponds to observations of freshwater occurrence (i.e. the presence of wells and wellfields) and the results of previous studies (Little et al., 1973; Cant and Weech, 1986; Wolfe et al., 2001). The FWL in the northern model is composed of a single lens that is much larger than the smaller, separate lenses in the southern model. Along the coastlines, particularly in the southern regions of the island, the simulated FWL tends to be situated further inland than is observed; however, the depth of the simulated lens in the south is consistent with field observations. The depth of the simulated lens in the northern regions of Andros Island falls within the range of maximum observed lens depth (up to 39 mbgs), although it is slightly deeper than typical observations of around 15 to 20 mbgs. Because most of the model parameters are based on field data and sensitivity analyses, the deeper simulated lens is likely the result

of slight over-estimation of recharge in the HELP model. HELP applies daily precipitation to the lithology profile evenly over a 24 hour period, when in reality, precipitation events occur within shorter time intervals (hourly) and leads to some pooled water on the ground surface. Given that the intensity of the precipitation events is not accounted for in HELP, the resulting recharge estimates may be slightly over-estimated. However, there is no clear basis upon which the recharge estimates can be adjusted to achieve better model calibration due to the lack of field data for actual evapotranspiration and recharge.

Some local-scale variations are neglected in the model due to the limitations of the large grid cell size required to cover the area of the island, which resulted in a low resolution of the ground surface elevation. In addition, the model was developed to represent the average annual FWL morphology and, therefore, does not include seasonal variation. Although the worst case scenario (e.g. lowest recharge during the dry season) is not accounted for in this study, other studies have shown that there is little seasonal variation in groundwater levels for islands of similar hydrogeological setting (Momi et al., 2005). Overall, the simulated lens is within the range of observed depths, although it represents a slight over-estimation of the freshwater resources in the northern region of Andros Island. The model provides a generalised estimate of the FWL morphology and serves as a reasonable baseline for investigating the impacts due to climate change stressors.

Climate Change Models

As noted above, the HELP model utilises site-specific climate averages so that predictions can be made regarding the impact of future climate conditions on recharge. Recharge is projected to decrease by 11% in the northern model and decrease by 15% in the southern model by the 2090s relative to baseline (current) recharge. This is due largely to decreases in average annual precipitation, and slight increases in evapotranspiration rates. Minimal changes in soil storage were simulated in the HELP model.

The results of the climate change modeling, including a reduction in recharge and a rise in sea level, indicate that the FWL will reduce in areal extent and volume under future climate change conditions. The percent change in FWL area and volume

relative to the baseline values are presented in Table 4.5. The change in area and volume of the lens indicate that the lens shrinks and thins in response to the stressors. For both the northern and southern models, simulations of reduced recharge alone result in the majority of FWL reduction, with SLR contributing a smaller proportion of FWL reduction. The FWL in the southern model is predicted to incur a greater percentage of loss of FWL compared to the northern model under climate change conditions. In the southern model, the results indicate a 19% volume loss due to reduced recharge compared to 5% volume loss due to SLR relative to baseline morphology. Whereas, in the northern model, 5% of volume loss is due to reduced recharge with 0.9% volume loss due to sea level rise. The simulated lens at the end of the 100 year simulation is presented, illustrating areal loss of lens relative to the baseline model (Figure 4.6).

Table 4.5. Percent change in freshwater lens morphology relative to the baseline model for the combined effect of reduced recharge and SLR

Modeled Region	% Change Area	% Change Volume
Northern	-4.1	-5.9
Southern	-16.8	-24.2

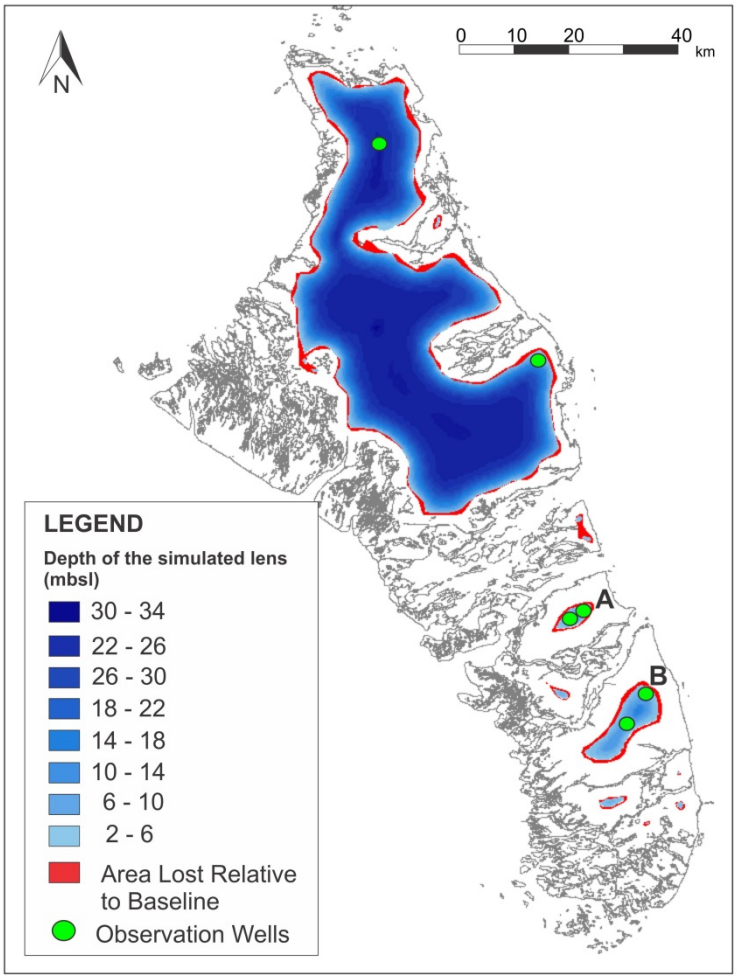

Figure 4.6. Model result for climate change simulations for the combined effect of reduced recharge and SLR, indicating area lost relative to baseline conditions

The simulated time-varying dissolved salt concentrations in the observation wells are shown in Figure 4.7. The simulated concentrations at most observation wells indicate that salinity in the lens progressively increases in response to the climate change shifts applied every 10 years starting at 50 years. Prior to 50 years, the model is spinning up from a fully salty state. Dissolved salt concentrations in all of the observation wells reach near steady state between stress periods (only very small changes continue to occur on the order of 10^{-10} g/L per day). The time to reach steady concentrations is relatively similar in all wells, ranging from 0.5 to 3 years and increasing as the simulation progresses. This indicates that even though the climate change shifts in each stress

period are the same magnitude, the FWL takes longer to adjust to the shifts as the cumulative magnitude of climate change increases.

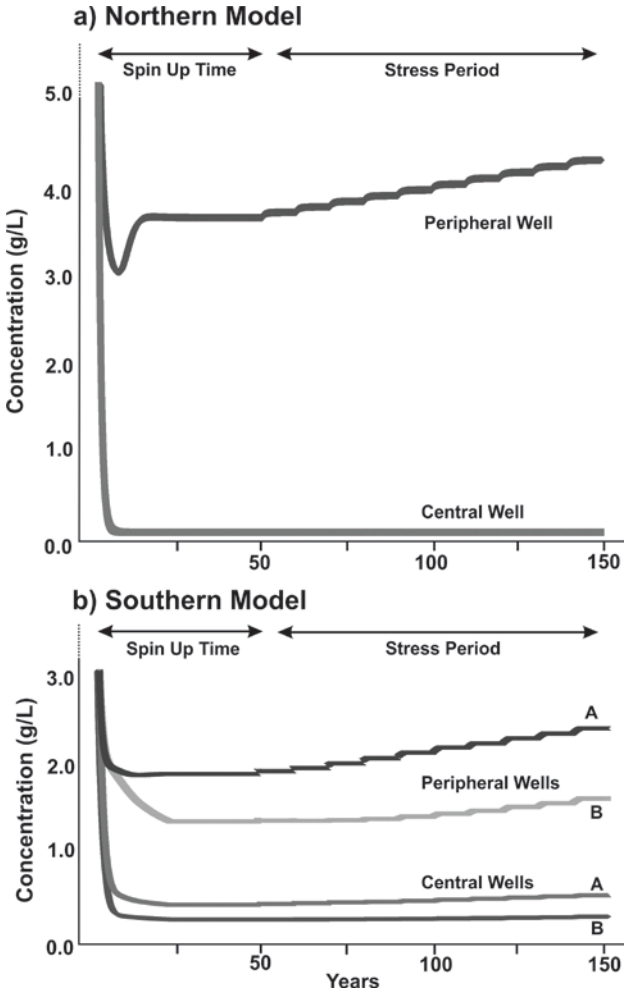

Figure 4.7. Simulated dissolved salt concentrations over time at the observation wells for climate change models: a) northern model b) southern model with two observation wells for each landmass shown.

The central wells were placed in areas that were anticipated to be more resilient to stressors, and the peripheral wells in areas that were anticipated to be more vulnerable to stressors (thereby showing a more immediate lens thinning). The simulation results are consistent with the anticipated behaviour. The peripheral observation wells have higher dissolved salt concentrations than the central wells because they are situated in the thinner part of the FWL, and therefore, are more likely to intersect the base of the lens. The highest dissolved salt concentrations are in the

peripheral well in the northern model, which is closer to the coast than the peripheral wells in the southern model. This is because the edge of the northern FWL extends further coastward than the southern FWL. Greater changes in dissolved salt concentration are also observed in the peripheral wells compared to the central wells, as would be expected.

4.4.2. Short-Acting Stressor

FWL Development and Storm Surge Inundation

The morphology of the FWL reaches steady state within 25 years at a maximum depth of 23 m below sea level (mbsl) (Phase 1; Figure 4.8a). The model is calibrated to observed conditions outlined in Table 4.3. The maximum elevation of the FWL is observed in the trench at 1.8 masl. The vadose zone surrounding the trench is approximately 1.7 m thick. The gradient across the model domain is 0.0015, with an average horizontal groundwater velocity of 0.87 m/day. The inflections on the sides of the lens at 9 and 14 mbgs reflect the high hydraulic conductivity paleosol layers.

Simulation of storm surge inundation (Phase 2) resulted in high salt concentrations at the surface of the model up to 1 m above ground surface, as per the applied boundary conditions (Figure 4.8b). The results of the inundation model are shown for a focus area within 25 m of the trench (focus area indicated on Figure 4.8a). Within the 2 hour inundation period, the salt water had already been transported into the vadose zone due to the hydraulic gradient associated with the surface flood, and had also filled the trench with salt water (Figure 4.8b).

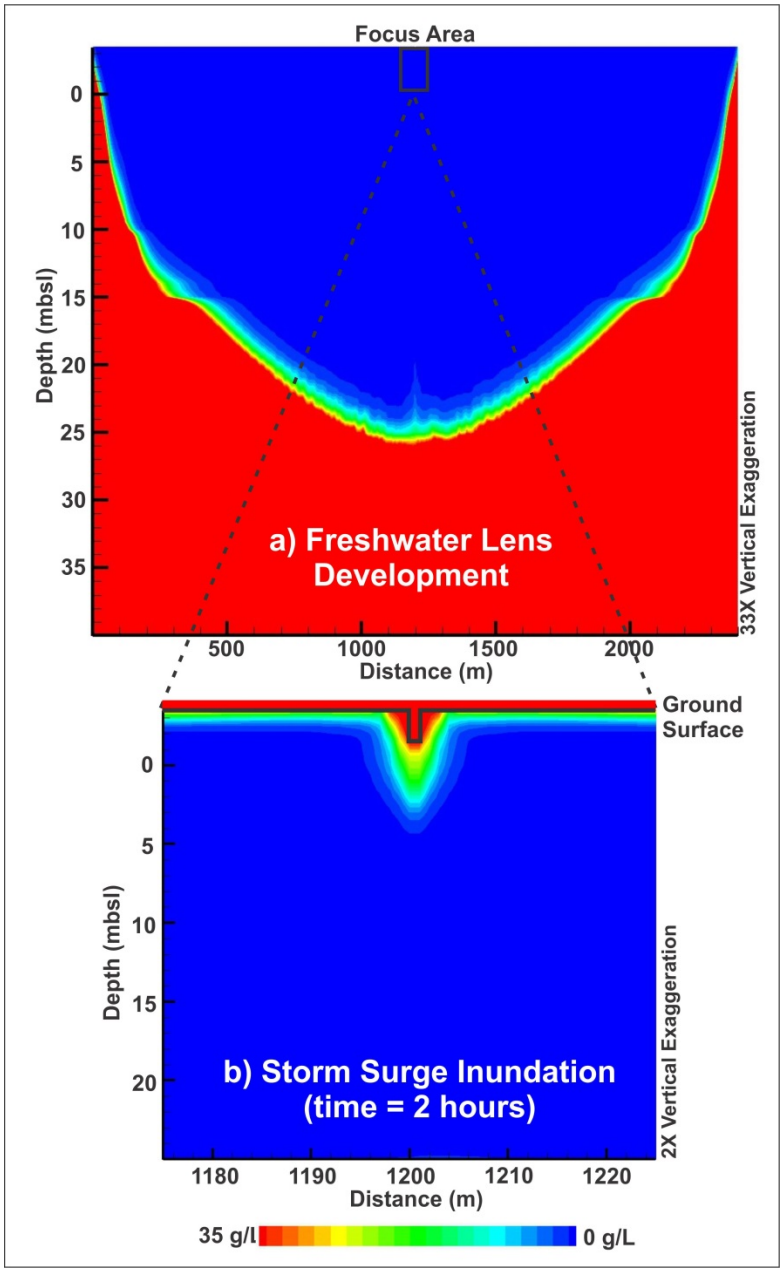

Figure 4.8. **a) FWL development after 50 years (Phase 1); b) Storm surge inundation in the focus area at 2 hours (Phase 2)**

Aquifer Recovery

The baseline recovery of the FWL (natural recovery) is shown for six times post storm surge (Figure 4.9): 12 hours, 1 day, 2 days, 1 month, 2 years, and 10 years. The baseline recovery scenario indicates that the FWL returns to its original morphology approximately 10 years post storm surge. The salt water is transported from the surface

domain into the aquifer system, where it forms a salt plume within the subsurface. This plume is flushed out over time due to the infiltrating freshwater recharge. Salt concentration within the trench returns to levels below the potable water threshold within 149 days following the storm surge for the baseline recovery scenario.

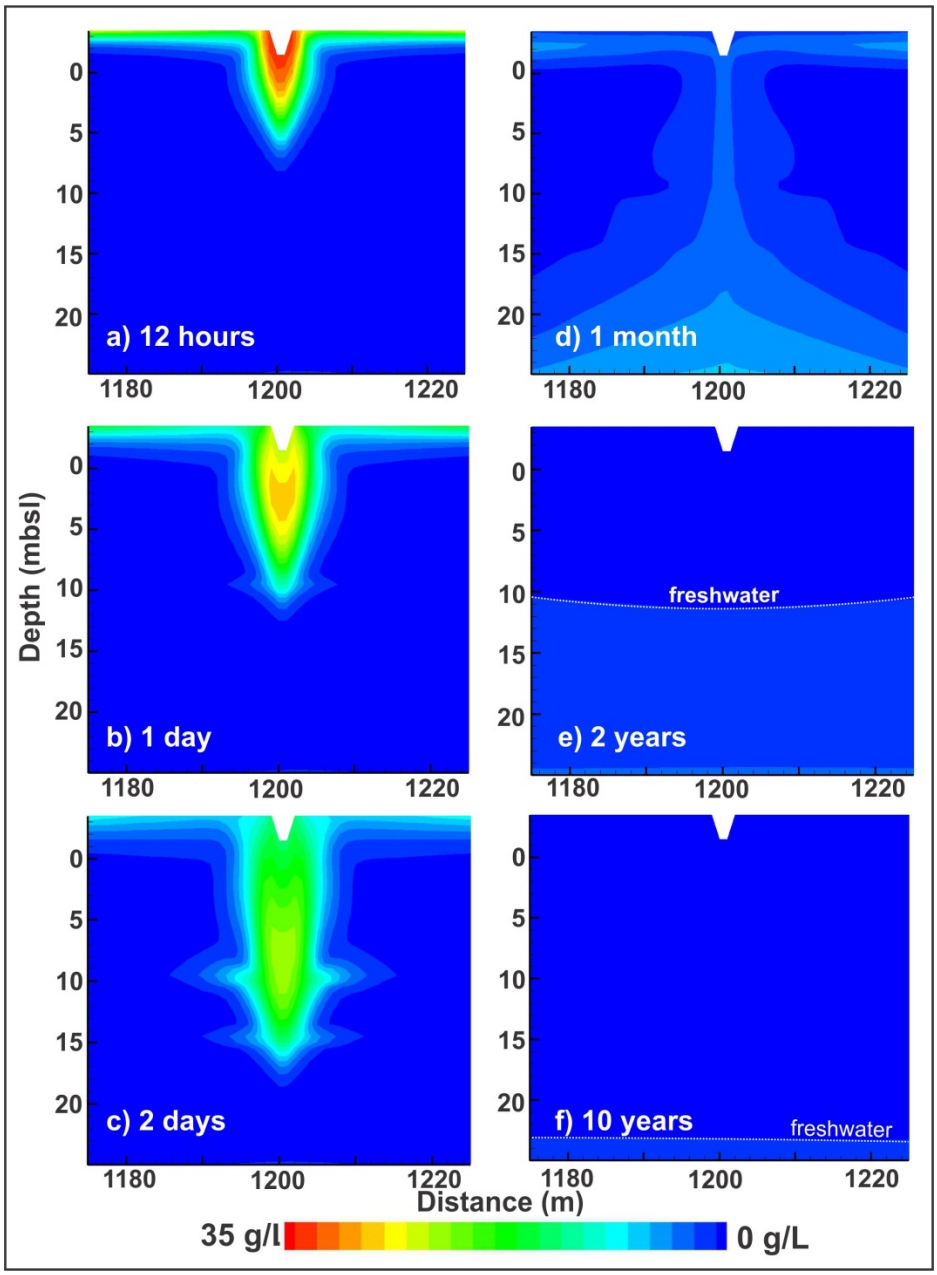

Figure 4.9. Baseline recovery of FWL post storm surge at a) 12 hours; b) 1 day; c)2 days; d) 1 month; e) 2 years and; f) 10 years

The results of the different draining scenarios are shown in Figure 4.10, alongside the baseline recovery scenario, as relative concentration data over time, where 1.0 represents salt water and 0.0 represents fresh water. The number of days to reach potable concentration in the trenches is indicated for each scenario. Observed concentration data for the North Andros Wellfield trenches are also presented in Figure 4.10. Trenches that were drained following the storm surge, and those that were isolated from the system and not drained, are distinguished by different symbols.

There is little difference in observed concentrations when comparing the trenches that were drained and those that were not. The observed concentrations are similar to the simulated concentrations immediately following the overwash event; however, at one year post-storm surge, the observed concentrations are slightly above the potable water threshold. By two years post-storm surge (not shown), the observed concentrations are similar to the simulated concentrations, and below the potable threshold.

Draining of the trenches generally results in a faster recovery. If draining occurs within one day of the storm surge, potable water returns to the trench by about 120 days (Figure 4.10), approximately one month sooner compared to the baseline recovery simulation (149 days). With every day that draining is delayed, it takes longer for potable water to return to the trench (corresponding to the small vertical lines on Figure 4.10 for each scenario). After a delay of three days, the recovery time for potable water to return is the same as the case when no remedial action is undertaken. Therefore, the improvements in recovery time are dependent on the timing of draining.

In contrast, the duration of draining (not shown) does not significantly improve recovery times. Draining that occurs for multiple days results in slightly longer times for potable water to return compared to short-duration draining (i.e. over a single day).

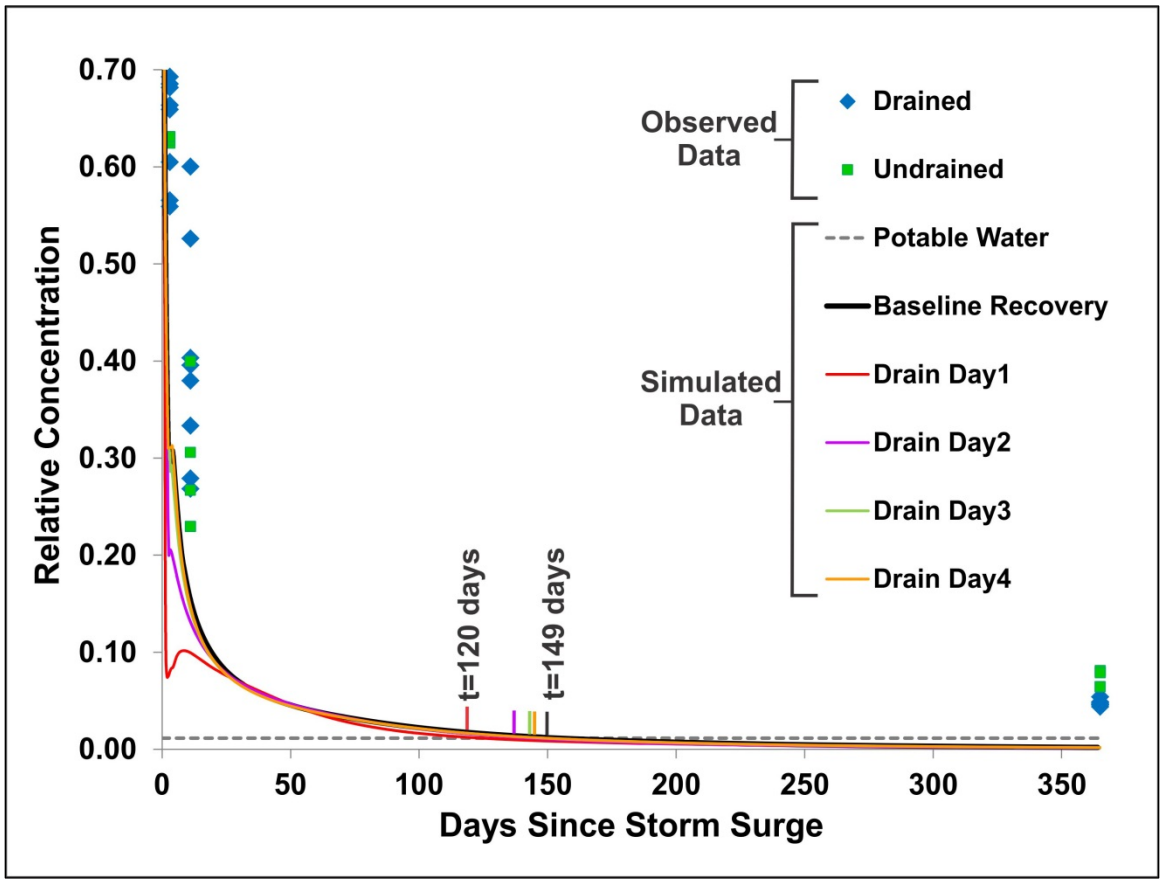

Figure 4.10. Observed and simulated concentrations within the trench. The times for concentrations to reach potable water threshold are indicated by the small vertical bars for the baseline recovery scenario (149 days) and the various scenarios of draining on different days following the surge (120 days for draining on day 1). The second, smaller increase in concentration observed for Scenario Drain Day 1 represents the end of the draining period, when high concentration water re-enters the trench from the surrounding aquifer and vadose zone.

As mentioned earlier, the observed data at one year post storm surge are higher than the model results, indicating that the trenches on Andros Island recovered slower than the model results. This is likely the result of several factors:

1. The amount of salt water entering the aquifer system largely depends on the time of inundation. As this was unknown, it was assumed as a two hour inundation. However, the inundation may have lasted much longer as no observations of the area were made until three days after the storm surge. To account for this uncertainty, a Phase 2 model was run with a longer inundation period of two days. The recovery from this storm surge scenario took at least two months longer, with higher

concentrations at one year post-storm surge. However, the FWL morphology recovered at the same time as the baseline scenario.

2. The amount of recharge that specifically occurred on Andros Island may have been different during 2004-2005. Alternate recovery simulations were run where recharge was applied as monthly averages based on the 2004 and 2005 rainfall data for Andros Island. These simulations resulted in longer recovery times, up to six weeks more than baseline recovery.
3. As previously discussed, the HELP recharge results may over-estimate actual recharge to the FWL. Therefore, additional models were run with recharge applied at half the baseline amount. These simulations indicated that recovery was delayed by two months.
4. Additional factors may impact the calibration to observed data. The models were developed based on field studies that were not all specific to the North Andros Wellfield area; therefore, hydrogeological conditions (such as porosity or hydraulic conductivity) at the wellfield may differ from those at the island scale.
5. The exact timing, duration and method of draining utilised on Andros Island are also unclear. While the best possible information was obtained from the Bahamas Water and Sewerage Corporation, it is likely that the details of operations were inexact.
6. Lastly, other hurricanes passed near to Andros Island in the weeks and months following Hurricane Frances; however, it is unknown whether any of these caused an additional storm surge event (National Hurricane Center, National Oceanic and Atmospheric Administration (NOAA), 2014). Regardless, the close passage of other storms would have attributed to atypical rainfall events. In addition, the concentration of recharging freshwater may be higher than 0 g/L during storms due to salt spray, thereby introducing higher salt concentrations at the surface and delaying recovery.

Although many factors contribute to the uncertainty in the calibration, the recovery models are likely reasonable representations that allow for comparison of the impact of remedial actions on recovery.

4.5. Discussion

4.5.1. Long-Acting Stressors

The volume and area of the freshwater lens are reduced under stressed conditions, indicating that the lens both shrinks and thins. A significant impact is

observed in areas where the lens shrinks (i.e. along the periphery), as most settlements and related infrastructure are typically near the coast on small islands (Ranjan et al., 2009; Cashman et al., 2010). As a result, any changes in the freshwater lens morphology within the coastal zone may affect access and availability of fresh water near the population centres.

The loss of FWL area and extent under climate change conditions is attributed more to the impact of changes to groundwater recharge than the impact of SLR. Although loss of land surface due to sea level rise was not simulated in the models, estimates based on ground surface elevation suggest loss of land surface (and resulting loss of freshwater lens volume) is limited. On islands with lower topography and/or smaller land area, inundation would have a greater effect on loss of freshwater lens volume. The model results for Andros Island are supported by other studies, which show that conditions of reduced groundwater recharge (or prolonged drought, which results in reduced recharge) disturb the balance of freshwater outflow necessary to maintain the extent and thickness of the FWL, thereby leading to loss of freshwater resources due to saltwater intrusion (Ranjan et al., 2009; White and Falkland, 2010; Mollema and Antonellini, 2013). In addition, the hydrogeological system on Andros Island is recharge-limited, meaning that the FWL is able to rise in the subsurface in response to SLR. Therefore, it is less vulnerable to SLR because the FWL is able to maintain a balance between the hydraulic gradient of the fresh and salt water (Michael et al., 2013). This assumption is only valid to a point; for higher magnitudes of SLR, the FWL would likely become topographically-limited and, therefore, have a larger response (i.e. loss of FWL) due to SLR. Although SLR appears not to be a significant factor for saltwater intrusion on Andros Island, it may increase the island's vulnerability to other events, such as extreme high tides and storm surge overwash. These events have the potential to result in significant impacts to the FWL, as is discussed below.

The northern regions of Andros Island appear to be more resilient to climate change stressors than the southern regions. Several factors contribute to the difference in response between the northern and the southern regions: 1) the south is composed of smaller landmasses, resulting in smaller areas for the FWLs to develop; 2) significantly less rainfall occurs in the south, meaning that there is less recharge to sustain the FWLs;

and 3) the topography of the south is generally lower than that in the north, resulting in a thinner lens and slightly lower hydraulic gradient of the FWLs. The combined impact of these factors is that the southern region of Andros Island has smaller FWLs that are more vulnerable to damage from stressors.

The simulated FWL on Andros takes longer to respond to climate change stressors as the magnitude of the cumulative stress increases (i.e. lower recharge and higher sea level). The implication is that as climate change progresses over time, the ability of the FWL to respond to these changes decreases. Because recharge is the main driver of lens formation and maintenance, when the rate of recharge is reduced, the response time of the hydrogeological system is also reduced. This has been observed in laboratory experiments (Stoeckl and Houben, 2012), whereby the lens takes longer to reach steady state when there is reduced input (i.e. specified flux or concentration boundaries) to the system. Therefore, areas where there is less recharge, such as the southern regions of Andros Island, are expected to take longer to react and adapt to stresses to the hydrogeological system.

4.5.2. Short-Acting Stressor

Trench-based wellfields result in large salt plumes that develop in the aquifer following a storm surge overwash. This is because the trench provides direct access for inundating salt water to travel into the aquifer. The salt plume remains larger surrounding the trench than in the rest of the aquifer throughout recovery, and takes 3 months longer to recover than the surrounding aquifer. This is supported by other studies where it was observed and modeled that areas where salt water pools or is collected during inundation (such as open boreholes or depressions) result in longer recovery times (Terry and Falkland, 2010, Chui and Terry, 2012).

The timing of remedial action (specifically draining of the trenches) is more critical than the duration of draining. It is critical to drain the trenches as soon as possible following a storm surge overwash in order to remove the initial salt load to the aquifer before it is transported deeper into the aquifer. After a certain period of delay, there is no improvement in recovery achieved by draining. This is illustrated in the simulation

results as well as the observation data, where there is little improvement in recovery for trenches on Andros Island that were drained after a 4 day delay. The time of this delay threshold, where there is still benefit to be gained in draining the trenches, will depend on many factors, such as the hydraulic conductivity, the groundwater velocity, and recharge rates. For most typical low-lying islands, the delay threshold is likely quite soon after storm surge due to the high hydraulic conductivity of geological materials normally found on low-lying islands (Ayers and Vacher, 1986). Coarser aquifer material may allow for faster salt transport into the aquifer (Chui and Terry, 2012). Although this effect may also speed up recovery, it means that there is a limited time in which to perform remedial action to remove the salt water. On Andros Island, the delay threshold is 3 days. The duration of draining should also be short, because longer durations of draining may result in slower recovery times. This is likely due to the fact that draining of the trenches removes the recharging fresh water, along with the salt water.

4.6. Conclusions

Stressors act over varying spatial and temporal scales to impact the FWL of low-lying islands. Both short and long-acting stressors may result in significant loss of freshwater resources. The model results are inherently uncertain due to uncertainty associated with the input data, model conceptualisation, and stressor scenarios. The greatest uncertainty lies in the simplification of the hydrogeology and the associated parameters. This is largely due to limited studies having been conducted on Andros. However, small islands often have limited capacity for hydrogeological investigations. Therefore, this study was not predictive, but rather aimed to identify the likely response based on the hydrogeological setting and the mean projected climate state derived from multiple climate change model scenarios. To rigorously address uncertainty, a series of models with a range of input parameters and climate scenarios would be required; however, this was beyond the scope of the current study. Within these limitations, the results of the study provide the following conclusions:

1. The impacts of stressors on the FWL are predicted to occur primarily in areas where the FWL is smaller or thinner, such as the periphery of the lens. As most settlements are concentrated within the coastal

zone, even small-scale changes to the FWL morphology in these areas may have significant implications for freshwater sustainability.

2. Change to groundwater recharge is identified as a key stressor to Andros Island, where greater impacts to the FWL are observed in areas with lower recharge.
3. The response time of the FWL (time to reach steady state) increases as the magnitude of the stressors increase. With increasing magnitude of change to the hydrogeological system, the FWL takes longer to adjust to the new state.
4. The FWL is generally able to recover from storm surge inundation over time as fresh recharge flushes the salt plume out of the aquifer. Eventually, the FWL returns to the original morphology.
5. Trench-based wellfields may increase the potential storm surge impacts on the FWL, depending on the hydraulic conductivity, the vadose zone thickness, and land cover. However, they also allow for remedial action (such as draining the trenches) to be undertaken which can improve recovery times. The sooner draining occurs, the more improvement in recovery, because, if draining is delayed by too long (in this case, 3 days or more), there is no improvement in recovery. The duration of draining has less effect on recovery and only needs to occur for a short period of time.

Chapter 5.

Assessment of Wave Overwash Impacts on Small Islands

This chapter is written as a paper entitled, “Impact of wave overwash on small islands: a generic assessment for multiple island settings”.

5.1. Introduction

Wave overwash events have significant impact on small island nations due to infrastructure damage and the economic costs of rehabilitation (Walsh et al., 2011). Overwash may also result in severe consequences to the freshwater resources of small islands as a result of salt contamination of the aquifer (Anderson, 2002). Wave overwash commonly occurs as a result of a storm surge during a hurricane, tropical cyclone or other high-intensity storm, whereby large waves break above normal high tide levels (Irish et al., 2008; National Oceanic and Atmospheric Agency (NOAA), 2014b). Overwash may also result from oceanic tsunamis (Illangasekare et al., 2006). The projected changes in cyclone and hurricane behaviour under future climate change are uncertain (Knutson et al., 2010); however, due to the potentially large impact of overwash, it has been recommended that research be carried out to characterise the susceptibility of small islands to these events (Walsh et al., 2011).

On islands, fresh water resides in a freshwater lens (FWL) that floats on top of the surrounding salt water within the aquifer (Falkland, 1991). Groundwater moves from areas of high to low hydraulic head within the FWL and discharges along the coastlines (Falkland, 1991). The main impact of overwash on an island FWL is that it causes temporary surface inundation of seawater resulting in saltwater contamination of the FWL (Anderson, 2002). There are three principal mechanisms of saltwater

contamination (Figure 5.1): 1) infiltration of salt water through the vadose zone during inundation; 2) ongoing infiltration of salt water from depressions that store ponded seawater; and 3) transport of salt water through open boreholes and/or trenches which provide direct access to the aquifer (Illangesekare, 2006; Terry and Falkland, 2010). The most rapid impact is through boreholes/trenches; however, the largest spatial impact is from infiltration through the vadose zone as contamination is able to occur over a wide extent (Illangesekare, 2006).

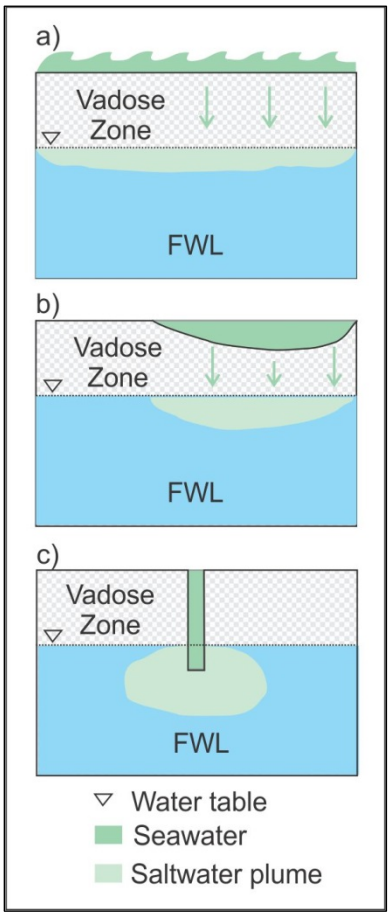

Figure 5.1. Mechanisms of saltwater contamination from overwash: a) infiltration through the vadose zone during inundation; b) infiltration from ponded seawater; c) direct transport to the saturated zone from open boreholes

During and following overwash inundation, a saltwater plume develops within the FWL, which moves downward through the lens due to two gradients: a density gradient between the fresh water in the lens and the infiltrating seawater; and the hydraulic gradient that drives groundwater flow within the FWL (Terry and Falkland, 2010).

Although the upper part of the lens becomes contaminated with salt, a pocket of fresh water trapped beneath the saltwater plume is often observed in field studies and modeling simulations (Terry and Falkland, 2010; Chui and Terry, 2012). However, effectively accessing this freshwater pocket for water supply poses an engineering challenge because drilling into the pocket is likely to lead to its contamination by the surrounding salt water. The water quality in the lens recovers over time as the saltwater plume discharges out of the lens (along the coast) and/or is diluted due to mixing with fresh water. Full recovery of the FWL is not always achieved as the occurrence of overwash may result in long-term changes to the FWL morphology, especially when multiple overwash events impact the same aquifer in close succession (Anderson and Lauer, 2008).

Previous studies have identified several factors that influence the FWL response and recovery from overwash events. These factors include the recharge rate, the vadose zone thickness, the hydraulic properties, and geologic heterogeneities.

Recharge is the main driver of FWL recovery following overwash as it delivers fresh water to the system that flushes out the salt water (Illangesekare, 2006; Sivakumar and Elango, 2009). Therefore, areas of low recharge experience less flushing, and thus the FWL recovers more slowly. In addition, low recharge rates typically lead to smaller FWLs, so that overwash may impact a larger proportion of the lens, thus having a greater overall impact on the island's freshwater supply.

The thickness of the vadose zone, or depth to the top of the lens, also influences how the overwash impacts the FWL (Illangesekare, 2006). During inundation, the vadose zone fills with seawater, which does not drain away when the overwash subsides. Therefore, the greater the thickness of the vadose zone, the greater the pulse of salt water reaching the aquifer (Chui and Terry, 2012). The vadose zone thickness varies seasonally in response to recharge variations. Over the longer term, the thickness of the vadose zone may also change in response to sea level rise, which is projected under future climate conditions. Particularly, in recharge-limited systems, the FWL will rise in accordance with the rise in sea level, thereby reducing the thickness of the vadose zone (Werner and Simmons, 2009). With higher sea level, the FWL may become

less contaminated during an overwash event because the vadose zone is thinner and the initial pulse of salt water that is captured in the vadose zone is reduced (Chui and Terry, 2012). However, a higher sea level may also lead to a lower hydraulic gradient within the lens such that flushing of the saltwater plume, and eventual recovery of the FWL, will take longer (Terry and Chui, 2012).

The hydraulic properties of the vadose zone and the saturated zone control the flow of water and the transport of salt within the lens. The hydraulic properties of the vadose zone determine the extent of saltwater contamination occurring during the initial inundation. If the vadose zone has relatively low hydraulic conductivity (K) (acting as a confining layer to the aquifer below), it may provide a protective layer above the aquifer and limit the amount of saltwater contamination reaching the lens. However, when the K of the vadose zone is high, it may lead to increased transport of salt water into the aquifer during inundation, resulting in a large saltwater plume. Aquifers with high saturated hydraulic conductivity (Ksat) may have high groundwater velocities, which can help the FWL to recover quickly due to increased advective movement of the saltwater plume out of the aquifer. Within relatively low K aquifers, the presence of geological heterogeneities with high K may have a significant influence on the impact of overwash events. For the case of continuous high K layers, the saltwater plume will migrate downward through the lens, but flow will be diverted along the high K layer and discharge along the periphery of the lens (Chui and Terry, 2012). In contrast, low K layers may delay flushing of the saltwater plume.

The results of previous studies have identified the various factors that affect the impact of overwash events on an island FWL. However, these factors are variably present depending on the hydrogeological setting of the island. The objective of this study is to evaluate the response and recovery of the FWL to overwash events on small islands from a global perspective. Evaluation of the impact of overwash events on all small islands would be challenging due to the lack of hydrogeological data available for many islands, as well as the large scope of such an undertaking. Instead, this study employs a generic classification of small islands based on geology, climate, FWL morphology, and water balance (Falkland, 1991; Robins and Lawrence, 2000) to characterise how the FWL might respond to overwash for different island types. This

enables a broad evaluation of the FWL response for any given island that can be associated with an island type.

Small islands can be classified into six categories: Type I – Young Volcanic; Type II – Old Volcanic; Type III – Low Coralline Limestone; Type IV – Recent Sedimentary; Type V – Upland Limestone; and Type VI – Near Continental Bedrock (Robins and Lawrence, 2000). The categories account for the typical hydrogeological setting (i.e. FWL morphology) of each island type; details of the classification are provided in previous studies (Falkand, 1991; Robins and Lawrence, 2000). In this study, the FWL response to overwash for each island type is characterised using a fully coupled surface-subsurface, density-dependent flow and solute transport modeling approach.

5.2. Methodology

Modeling the impact of overwash on a FWL involves simulating density-dependent flow and solute transport across the surface, the vadose zone, and the saturated domain. HydroGeoSphere (HGS; Therrien et al., 2010) was identified as the most suitable code to simulate the coupled processes because it is a fully integrated surface and variably saturated subsurface model capable of simulating density-dependent flow and solute transport. Popular modeling codes used in other overwash studies include SUTRA (Voss and Provost, 2008), SEAWAT (Langevin et al., 2007) and FEFLOW (DHI-WASY GmbH, 2010); however, none of these codes have the capability to simulate the surface domain where salt water is introduced to the hydrologic system. HGS has been successfully used to address various hydrological problems; however, as yet only one published study has applied HGS to specifically simulate coastal saltwater-freshwater interactions. Yang et al. (2013) used HGS to investigate coastal flow dynamics including the simulation of tidal fluctuations resulting in a hypothetical storm surge overwash. The modelling presented in this study does not require dynamic simulation of the surface domain (as lateral surface flow is not simulated) and technically could also be simulated using boundary conditions applied to the top of the unsaturated zone. However, this approach would neglect draining of the accumulated salt in the surface domain when the boundaries are removed. Although this is likely a small

proportion of the salt that would enter during the stressed time period, it would nonetheless be neglected if the surface domain is not included. By developing the models within HGS with the surface domain included, it also allows for potential future studies to integrate additional surface dynamics.

Each island type is characterised by an example island representing the typical hydrogeological setting. Simplified cross-sections of each example island are shown in Figure 5.2. Data for the example islands were collected from a survey and literature review of the hydrogeology of 43 small island developing states (Allen et al., 2014). The data provide representative parameters for each island model and include the following: aquifer geology and geologic heterogeneities, K values of the subsurface, porosity, recharge rate, thickness of the vadose zone, maximum hydraulic head near the coast, and FWL thickness (Table 5.1). These data are based on measurements and observations for the coastal zone (within 1 km from the coast) because this is where overwash is likely to occur. In addition, settlements and infrastructure are often concentrated along the coasts on small islands (Ranjan et al., 2009).

The hydrogeological settings of these island types are diverse. Aquifer materials range from unconsolidated sands to porous basalt and igneous bedrock (Table 5.1). In addition, geological heterogeneities contribute to a range of K values that may be higher or lower than the K of the principal aquifer material. The climatic settings also cover a wide range, whereby Type II (Santiago) and Type VI (Mahé) have lower recharge compared to the other islands (Table 5.1). The example island for Type II (Santiago) has a significantly lower recharge (60 mm/year) than the other islands and was selected to represent a low recharge environment so as to evaluate how low recharge may affect overwash recovery. Other Type II islands have higher recharge values (e.g., 1300 and 1900 mm/year for Tutuila and Tahiti, respectively; Allen et al., 2014). While the example islands were selected to represent a hydrogeological setting typical of each island type, there is variability and further sub-categories can be defined (e.g. high recharge or low recharge).

Table 5.1. Representative parameters within the coastal zone for each island type

Type	I	II	III	IV	V	VI
Description	Young Volcanic	Old Volcanic	Low Coral Limestone	Recent Sedimentary	Upland Limestone	Near Continental
Example Island	Mauritius	Santiago (Cape Verde)	Andros (The Bahamas)	Majuro (Marshall Islands)	Jamaica	Mahé (Seychelles)
Aquifer Geology (heterogeneities)	Basalt (high K lava tubes)	Basalt (vertical fractures and low K, tuff layers)	Porous Limestone (higher K paleosols)	Unconsolidated Alluvial Sand	Limestone (karstic features)	Weathered Granite (fractures)
Aquifer Ksat (heterogeneities Ksat) (m/day)	120 (8640)	100 (fractures: 1000; tuff: 0.1)	86 (864)	60	16 (8640)	0.0864 (8640)
Porosity	0.3	0.3	0.15	0.2	0.1	0.05
Recharge (mm/year)	969	60	877	953	909	539
Vadose Zone Thickness (m)	5	40	2	2	24	20*
Hydraulic Head (masl)	25	10	2	3	15	10*
FWL Thickness (m)	10-20	~10 (tuff causes perching of FWL)	20	12	~10 (karst known to cause thin FWL)	< 10*

Note: * values assumed based on typical fractured igneous rock as measured values are not available.

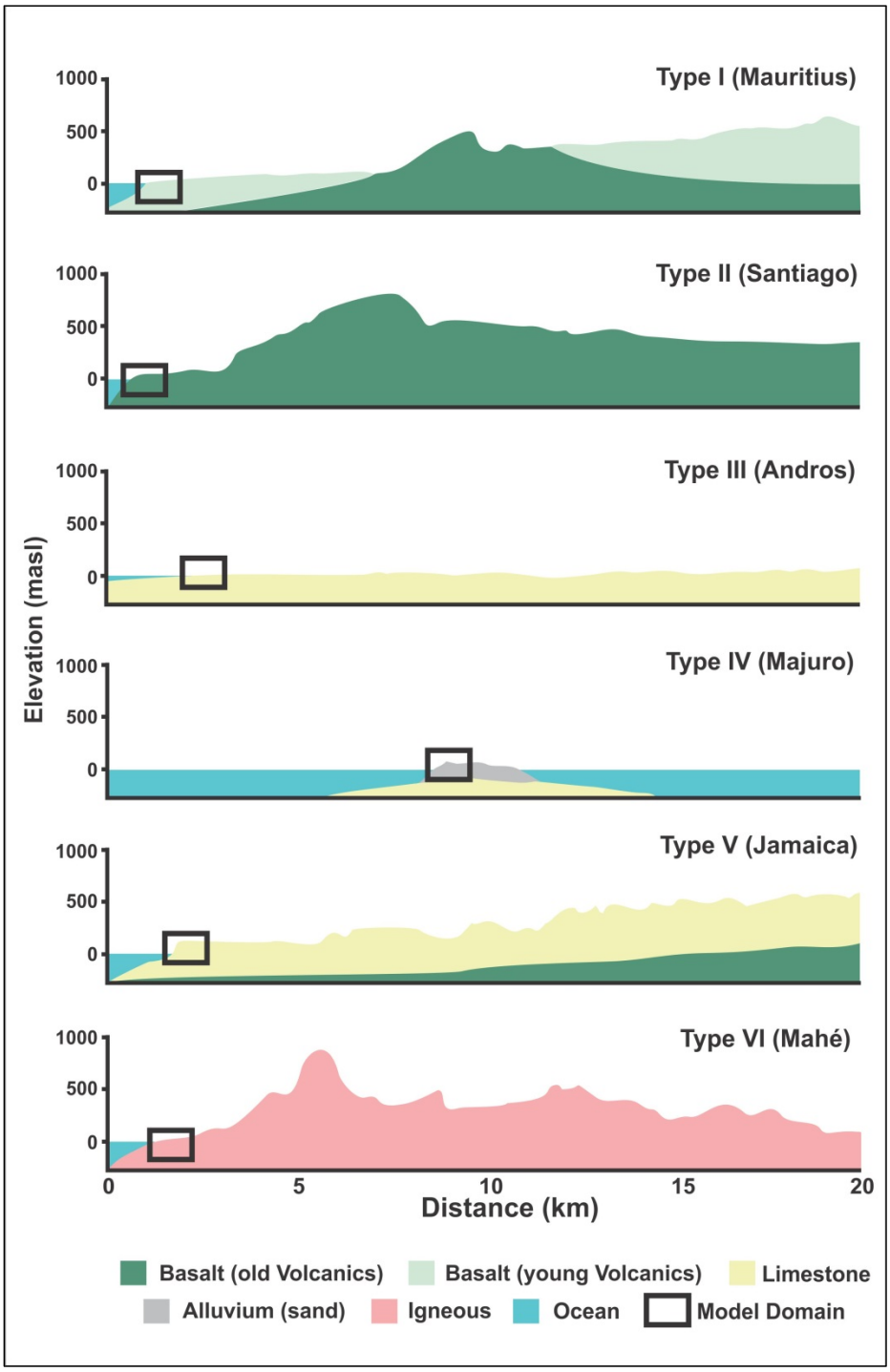

Figure 5.2. **Cross-sections for each island type indicating simplified topography, geology and the position of the model domains within the coastal zone**

5.2.1. Model Domains

The model domains for each island type were developed as cross-sections representing the near-coast hydrogeological setting (Figure 5.3). Cross-sectional models were used because groundwater flow (and thus, the FWL response and recovery to an overwash event) occurs perpendicular to the coast as observed in island-scale 3-D models (Chapter 4). Therefore, 3D flow is not anticipated to impact the results. In addition, the FWL generally extends significantly beyond the model domains so that it is reasonable to approximate the lens as an infinite strip island. Figure 5.2 shows the position of the model domain within the coastal zone. These small model domains were required for simulating the detailed responses at small scale. Thus, the models are not meant as detailed replications of the geometry of each island. Rather, the model boundary conditions were assigned in such a way as to generate the observed representative parameters and flow field in a local area near the coast (Table 5.1).

Each model domain is 1 km wide, with varying domain depths that aimed to generate the desired vadose zone thickness and FWL thickness (Table 5.1). As the models are cross-sectional, the domains are 1 m thick. Computational layers ranged from 0.25 m thick near the top of the model domain (i.e. the ground surface) to 1 m thick at the base of the domain to optimise simulation of flow and transport across the three hydrologic domains (surface, vadose zone, and saturated zone).

A flat surface was assumed for all models; no surface slope or topographic variations were included. Although runoff (occurring due to surface slope) would be expected to impact the degree of saltwater contamination resulting from an overwash event, it was assumed that regardless of surface slope, complete inundation of the surface domain occurs for a set period of time. Surface depressions may also affect the impact of overwash on the FWL; however, surface depressions are more likely to be present at a smaller scale than is meaningful for the broad scope of this study.

5.2.2. Model Setup

HGS simulates flow of water and transport of salt in a coupled fashion between the surface domain, the vadose zone, and the saturated zone, whereby it performs the

simultaneous solution of the three hydrologic domains for each time step. The surface domain in HGS is represented as 2D overland flow which is solved using the diffusive-wave approximation to the Saint Venant equations (Aquanty, 2013). The subsurface domain consists of 3D variably saturated flow which is solved using the control volume finite element method. In this study, lateral flow within the surface domain is neglected because there is no surface slope (as discussed previously), so the only movement of water in the surface domain is vertically downward, into the subsurface. HGS couples the surface domain to the subsurface domain by calculating the fluid and solute exchange according to the hydraulic and concentration gradients between the domains and a relative permeability term determined by the ratio of the water depth in the surface and the height of surface storage and micro-depressions (termed the rill storage and obstruction heights). In general, the relative permeability term enables water to flow from the surface domain to the subsurface domain under the saturated vertical hydraulic conductivity when the water depth in the surface reaches above the obstruction and rill storage heights. In this study, these heights were set very low (0.001m) in the absence of measured/estimated values for the ground surface, and to maximise fluid exchange, which occurs essentially whenever there is water depth in the surface domain greater than the subsurface hydraulic head. Coupling is performed using a dual node approach, whereby the corresponding nodes within the surface and subsurface domain are numerically separated by a very small distance, referred to as the coupling length. This value is determined during model development to minimise computational time (i.e. larger values) and to optimise the accuracy of the simulation (i.e. smaller values). Within the subsurface domain, water moves laterally and vertically through the vadose zone according to the 3D form of Richards' equation and van Genuchten functions (discussed below). In the saturated zone, water moves through the domain under the hydraulic and density gradients. Density-dependent flow is simulated under fully saturated conditions, based on the concentration-related density differences between fresh and salt water.

The simulation of the overwash event and subsequent movement of the saltwater plume required three separate modeling phases:

- Phase 1 - development of the FWL to steady state conditions;
- Phase 2 - short temporal-scale modeling of inundation; and
- Phase 3 - recovery of the FWL.

These three stages are required to accommodate the different temporal scales (i.e. decades for FWL development; minutes for overwash occurrence; and months to years for subsequent movement of the saltwater plume). The boundary conditions (discussed below) were adjusted at the beginning of each phase to simulate the respective process, and the heads and concentrations at the end of each phase were used as initial conditions for the subsequent phases.

All models were initiated with a salty (35 g/L) domain and spun-up until the FWL reached a steady-state (baseline) morphology (Phase 1 models). Phase 2 simulated the inundation event corresponding to a salt water source applied to the top surface of the model for a fixed period of time (details below). After inundation, the boundary conditions were reset to those used in the Phase 1 model to allow the salt water to be flushed out of the system (from natural recharge) and to allow the FWL to recover (Phase 3 models).

5.2.3. Boundary Conditions

The surface domain was defined across the top of the model domain. As surface slope is neglected in the models, there is no lateral flow across the surface domain; only vertical flow takes place. For Phase 1 and Phase 3 models, natural recharge was applied to the surface domain as an annual average quantity with a concentration of 0 g/L salt (Table 5.1). For Phase 2, a hypothetical overwash was simulated as a 1 m deep saltwater inundation within the surface domain (Phase 2 models). The inundation occurs gradually over a 1.5 hour period and is held constant for a further 2 hours. The duration of a given overwash event may vary from a few days to a few hours, so the inundation time period applied to the models was selected as an estimate to allow for sufficient salt water migration into the system. A specified concentration boundary of 35 g/L salt was applied to the surface domain during inundation to represent seawater.

For the Phase 1 simulations, the remaining boundary conditions were assigned specifically to generate the respective vadose zone thickness and the FWL thickness for each example island. The models were setup to produce realistic representations within the central part of the model domain. The flow boundary conditions control how water moves through the aquifer, and particularly the groundwater velocities across the model

domain. Where there is a large difference between the maximum hydraulic head and sea level, the hydraulic gradient is high, and the discharge rate is correspondingly high. Islands with steep topography near the coast can be expected to flush the salt water more quickly compared to islands with shallow topography (for the same K). Accordingly, the left side of the model domain (Figure 5.3) was assigned a specified head (corresponding to sea level) with a concentration of 35 g/L salt to represent the surrounding seawater. The right side of the domain was assigned a specified head boundary representing the observed hydraulic head in the FWL near the coast (within 1 km) according to island type (Table 5.1). The observed hydraulic head values are based on multiple measurements/observations collected across the coastal zone for each of the representative islands (Allen et al., 2014). Therefore, the inland specified head boundaries represent the topographic variations and width of each island in terms of their impact on the hydraulic gradient across the coastal zone. Other studies evaluating overwash events have employed similar boundary conditions, whereby a gradient is assigned from inland to the coast based on specified heads (Sivakumar and Elango, 2010; Chui and Terry, 2012; Yang et al., 2013).

Models run with the boundary conditions presented above generally simulated the FWL extending to the base of the model domains. However, the observed thicknesses of the FWLs are different for each island example and may be shallower than the model domain (Table 5.1). Therefore, in order to result in a FWL thickness that corresponds to field observations, specified concentration boundaries (35 g/L) were placed along the base of the domains to truncate the FWL and simulate the base of the lens. Previous studies observed that the saltwater plume does not exit the FWL by sinking through the base of the lens, but instead is discharged towards the coast, along the flow field within the lens (Illangasekare et al., 2006; Terry and Chui, 2012). Therefore, the purpose of applying the specified concentration boundaries is to simulate the base of the FWL at the observed depth. This is done to ensure that the saltwater plume does not migrate through the base of the lens, but rather remains within the lens. No specified concentration boundary was assigned on island Type II (Santiago) or island Type VI (Mahé). On island Type II, the low K tuff layers are known to cause perching of the FWL (Carreira et al., 2013) so that the tuff layer at the base of the model domain is considered to effectively simulate the base of the FWL. For island Type VI, the FWL

does not extend the full depth of the model domain due to the low K of the aquifer, and therefore, a specified concentration boundary was not necessary to simulate the observed FWL thickness.

To test whether or not the bottom specified concentration boundaries may affect the simulation of overwash impacts, these were removed and replaced only with zero flux boundaries (no salt source). The results of these models showed no change in the FWL response or recovery to overwash. This is because the models generate the same volumetric flux through the lens regardless of which boundary condition along the base of the model is used. Flux is determined by the hydraulic gradient, aquifer hydraulic properties (e.g. K), and the thickness of the lens, all of which are based on field observations. Therefore, although the boundaries along the base of the model domains are forced, they provide a realistic representation of the flow field through the lens so that FWL response and recovery may be simulated.

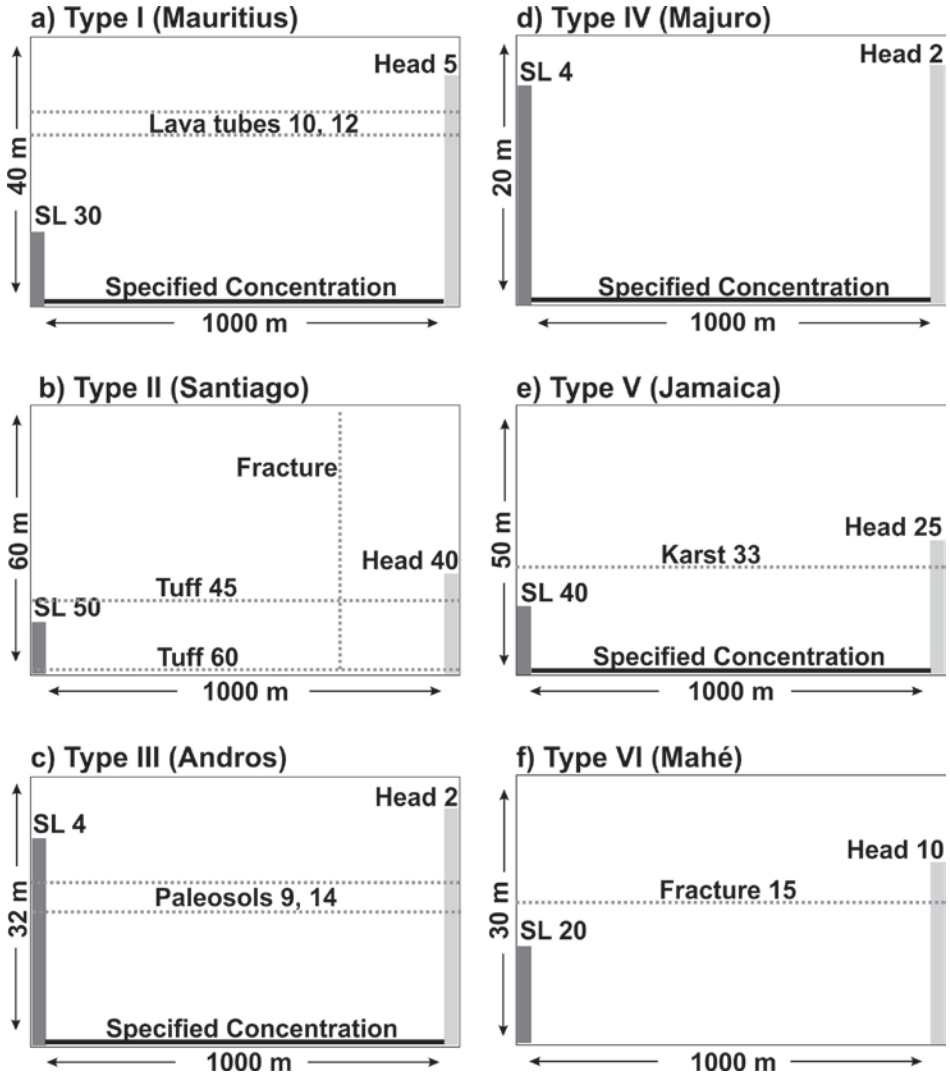

Figure 5.3. Model domains for each island type. Figures are not to scale. All values are in metres below ground surface (mbsl) and represent the respective depths of boundary conditions or features. SL = sea level boundaries; Head = inland specified head boundaries.

5.2.4. Model Properties

Because the surface domain did not include lateral flow, only a coupling length was specified. The coupling length was determined to be 0.01 m; there were no changes in model results when smaller coupling lengths were used.

The moisture-dependent K values for the vadose zone were determined from van Genuchten functions. Pressure-saturation and saturation-permeability tables are

generated within HGS based on the specified van Genuchten parameters: inverse of air entry pressure (α), pore-size distribution index (β), and residual water saturation. In the literature, van Genuchten parameters are available for a wide range of unconsolidated material types, but there are few studies that report values for bedrock. The van Genuchten parameters were assigned the default values (Table 5.2), except for α. An α of 0.3 was used to represent bedrock on all islands except for island Type IV (Majuro), where the aquifer is composed of unconsolidated sediments and the default for sand (α = 3.52) was used (Schaap et al., 2001). The α values for the geological heterogeneities (e.g. clay layers and paleosols) were not tailored to the materials as these layers are generally present below the vadose zone, and therefore, the van Genuchten functions are not applied.

The vadose zone and saturated zone share many of the same hydraulic properties such as Ksat, porosity and specific storage (Ss). Ksat and porosity values for the principal aquifer material were assigned according to the collected data for each island type (Table 5.1). Ss values were assigned the same value of $1x10^{-5}$ m^{-1} in the absence of more specific data, to represent a range of rock and sediment types (Younger, 1993).

Some models include geologic heterogeneities such as high K fracture zones, lava tubes, karstic features, or paleosols, as well as low K tuff layers (Figure 5.3). When present, these were introduced into the model domain in a representative fashion and assigned representative Ksat values based on the conceptual model for each island example (Table 5.1).

Dispersivity values were assigned in keeping with the scale of the model domain. A summary of the model parameters is presented in Table 5.2. Detailed discussion of the surface, vadose zone, and saturated zone properties can be found in Holding (2014).

Table 5.2. HydroGeoSphere parameters

Parameter	Value
coupling length	0.01 m
van Genuchten α	0.3 (bedrock) / 3.52 (sand) m^{-1}
van Genuchten β	3.18
residual water saturation	0.05
hydraulic conductivity	varied according to island type
porosity	varied according to island type
specific storage	1.0e-5 m^{-1}
longitudinal dispersivity	1.0
transverse horizontal dispersivity	0.1
transverse vertical dispersivity	0.01

5.2.5. Model Output

The model output was cropped for visualization purposes. Output within 100 m of the coast and at the inland edge of the model domain is strongly influenced by the boundary conditions. Therefore, the output near the boundary conditions is ignored. This approach is considered reasonable as the study aims to simulate the overall FWL response rather than the detailed near-coast processes.

Observation points were assigned to each model in the center of the domain (500 m from the left boundary) and at a depth approximately 2 m below the top of the simulated steady-state FWL. This depth was chosen to evaluate the impact and recovery of potable water supply following inundation at a depth from which most shallow wells and trench systems on small islands extract groundwater. For example, on island Type III (Andros Island), the trench system is approximately 2 m deep and functions to skim freshwater from the top of the FWL.

5.3. Results

5.3.1. Phase 1: FWL Development

The results of the Phase 1 models, showing the baseline FWL, are presented as spatial concentration distribution plots (Figure 5.4). The results are shown for the central part of the model domain only (the outer 100 m of each side of the model domain has been cropped), to neglect the area influenced by boundary effects as much as possible. Blue indicates fresh water and red represents salt water; the vadose zone is hatched. Time to reach a steady-state FWL morphology varies for each model (Table 5.3) and is indicated by "t_s". The top of the model domain represents ground surface; depth of the model domain is given as metres below ground surface (mbgs).

The resulting FWL morphology for each model is similar to observations for the example islands (Table 5.1). The FWL slopes downwards towards the coast, with a steeper slope on islands with a higher hydraulic gradient (as the top surface of the FWL represents the water table). The saltwater concentration boundaries along the base of the model domains (for island Types I, III, IV, and V) limit the FWL thickness so that it corresponds to observations for each island. Island Types II and VI did not include a specified concentration boundary along the base, as discussed previously. For island Type VI, there is a large area of salt water along the lower half of the model domain that forms due to the low K and low recharge rate for the island (Figure 5.4f). The formation of the salt area in this model is not related to the presence of the fracture zone, because the FWL develops to the same depth regardless of whether fractures are included or not. Although the results of this model are also cropped by 100 m on each side of the domain, the edges of the salt water in the results shown are domed due to boundary effects and are not realistic.

Most of the models show a transition zone from fresh water to salt water. The transition zone thickness varies depending on the depth of the seawater boundary on the left side of the model domain (see Figure 5.3). When the seawater boundary covers a large extent of the model depth, the transition zone is thicker, whereas, when the seawater boundary is present only near the base of the model domain, this zone is

thinner. The characteristics of the simulated transition zone do not impact the FWL response and recovery to overwash, and therefore, are not of relevance to this study.

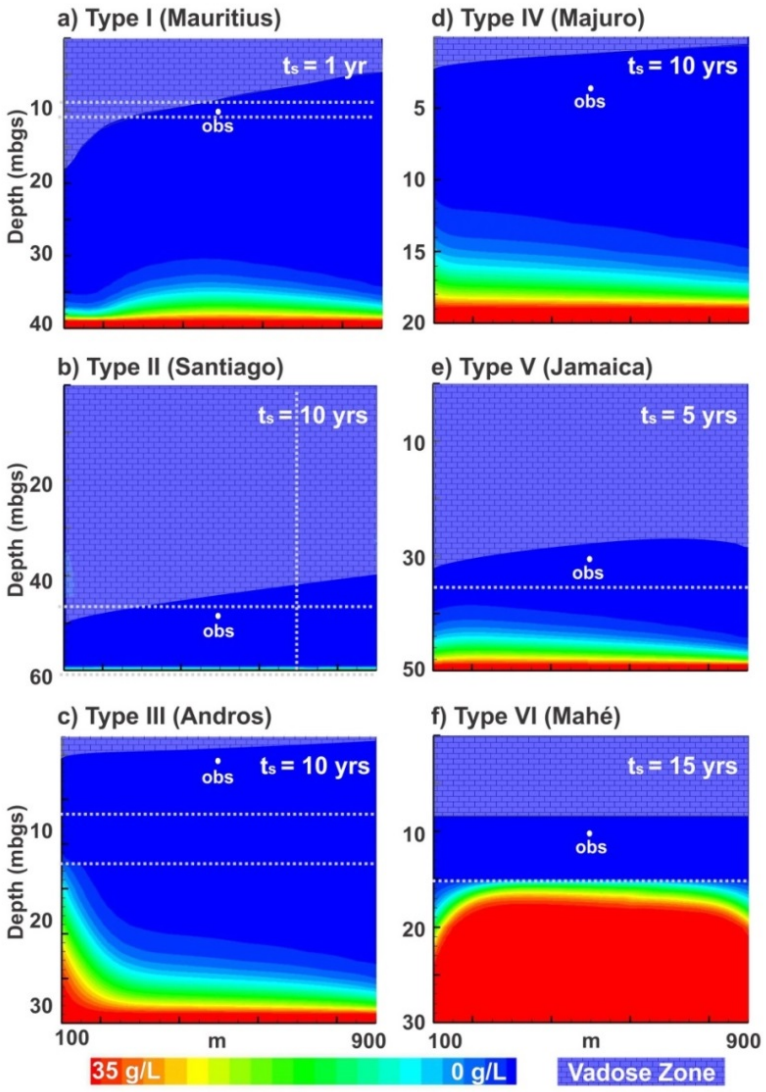

Figure 5.4. Concentration distribution for each island type. Time to reach the steady-state position of the FWL (in years) is indicated as" t_s"; depth of the model domain is given as mbgs; observation points are indicated by "obs"; geological heterogeneities (see Figure 5.3) are shown as dashed lines.

5.3.2. Phase 2: Inundation

The results of the Phase 2 models are shown at the end of the two-hour inundation period (Figure 5.5). As in Figure 5.4, the results are shown for the central part of the model domain; the outer 100 m of each side of the model domain is cropped. Salt water is transported through the unsaturated vadose zone during inundation. The solid black line in Figure 5.5 shows the initial (pre-Phase 2) position of the base of the vadose zone. For Type VI (Mahé), water does not infiltrate through the vadose zone during the inundation period. This results in an unsaturated zone that is sandwiched between two saturated zones. Over time, this residual unsaturated zone becomes saturated as the inundating water continues to infiltrate downwards to the FWL) (Figure 5.5f).

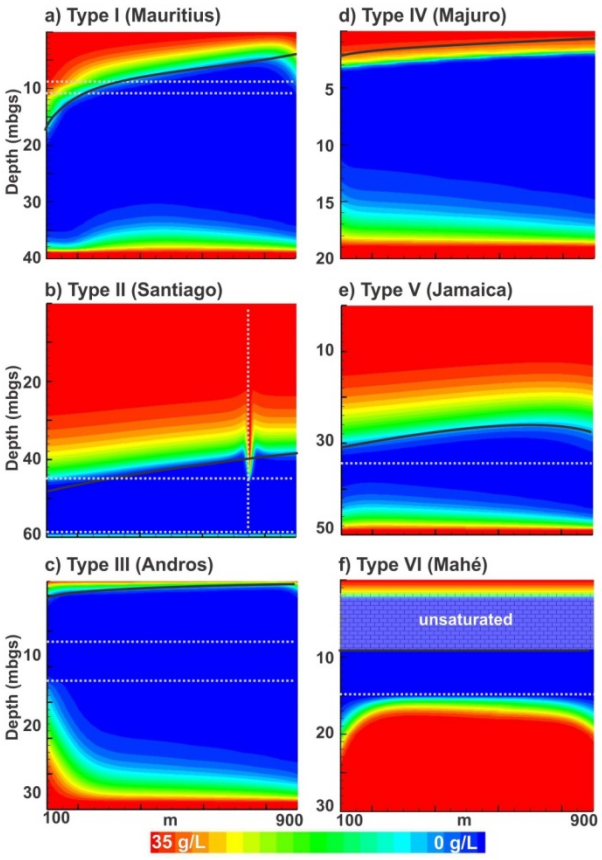

Figure 5.5. Concentration distribution after inundation period of 2 hours. The initial vadose zone depths are shown as solid lines; geological heterogeneities are shown as dashed lines.

5.3.3. Phase 3: FWL Recovery

Following inundation, a thin layer of fresh water forms at the top of the model domain from freshwater recharge. A pocket of trapped fresh water below the salt water is observed for all island types, with an example from island Type IV (Majuro) shown in Figure 5.6a. Depending on the island type, the freshwater pocket persists post-inundation for different durations ranging from 1 to 9 months, after which time it becomes salinized from the sinking saltwater plume (Figure 5.6b). Eventually the plume is flushed out towards the coast (Figure 5.6c). The jagged pattern of salinity migration in the subsurface shown in Figure 5.6b is due to the large vertical exaggeration required to include sufficient detail across the model domain, which also amplifies the density-driven convection cells that form. Sensitivity analyses were conducted to determine if the jagged salinity patterns were the result of numerical dispersion and model solution error. Simulations were run with grid discretization half the original values to check if the original grid was too large; separate simulations were run with dispersivity values one order of magnitude greater and one order of magnitude smaller to check if the original dispersivity was too high or too low. If significant changes were observed in the model results between these simulations and those run with the original values, it would suggest that the model solution was affected by numerical dispersion. However, the sensitivity analyses demonstrated no change in results for scenarios of smaller grid discretization or changed dispersivities, thus confirming that numerical instabilities in the model are likely not affecting the results.

The time until full recovery varies from 1 to 19 years, depending on the island type (Table 5.3). The longer recovery time of 19 years for island Type II (Santiago) is likely due to the low recharge rate (60 mm/year) and not necessarily the hydrogeological setting of the island type. In order to estimate what the recovery might be for a Type II island with a higher recharge rate, a series of models (Phase 1, 2, and 3) were run using recharge values one order of magnitude higher (600 mm/year). The resulting FWL recovered within 4 years, indicating that Type II islands with high recharge rates are likely to recover within a similar timeframe as the other island types.

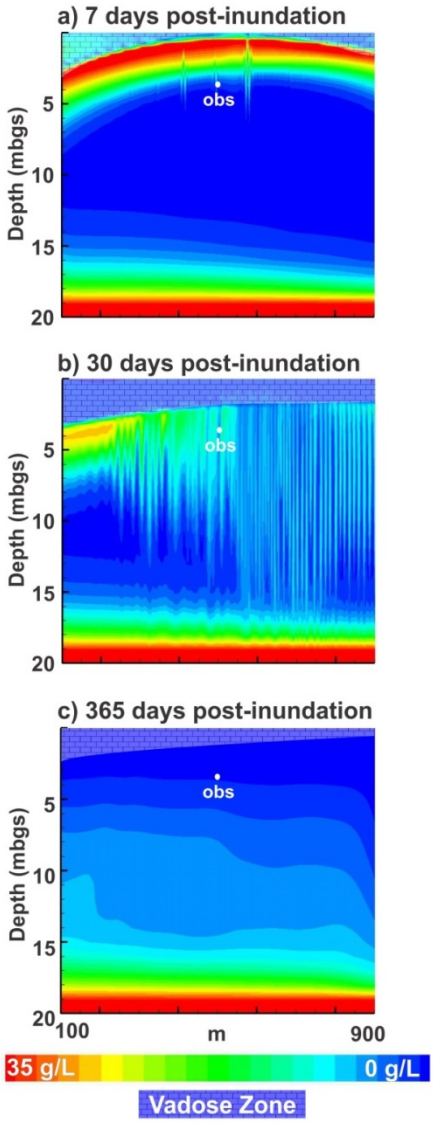

Figure 5.6. Recovery concentration distribution for Type IV (Majuro) at different times post-inundation: a) 7 days; b) 30 days; and c) 365 days

The presence of horizontally oriented, high K zones (such as paleosols, fractures and lava tubes) in island Types I, III, V, and VI limits the extent of saltwater migration through the FWL and prolongs the presence of freshwater pockets for these island types. Once the vertical infiltration of the saltwater plume reaches these features, the salt water discharges quickly out of the subsurface along the high K zone. For island Type V (Jamaica), saltwater plume migration only extends to the high K karstic features in the upper portion of the FWL. Therefore, the deeper FWL remains unaffected by the overwash event (Figure 5.7a). When high K zones (fractures) are oriented vertically

(Figure 5.7b), the inundating salt water migrates deeper into the FWL ahead of the main saltwater plume. However, in the case of island Type II (Santiago), the deeper saltwater contamination along the vertical fractures is limited due to the low K tuff zones that impede further vertical migration (Figure 5.7b). The presence of vertical low K zones (not shown) is likely to result in significant delays in FWL recovery due to the disruption in groundwater flow and flushing of the saltwater plume. Vertically oriented low K zones may occur on island Types I, II, and VI (Mauritius, Santiago, and Mahé) as dike swarms. Dikes can act as relatively impermeable barriers to horizontal flow within the FWL causing compartmentalised freshwater occurrences.

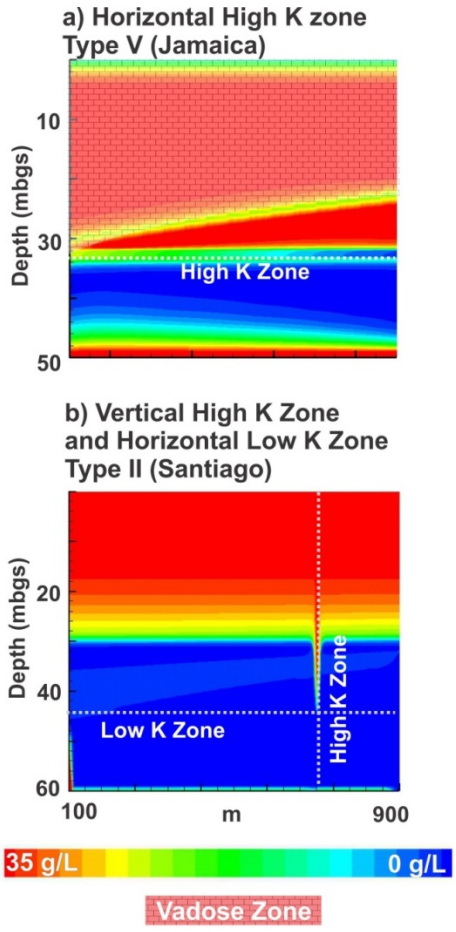

Figure 5.7. Influence of hydraulic conductivity (K) variability on FWL recovery. Horizontal high and low K zones prevent saltwater migration from penetrating deeper into the FWL; vertical high K zones result in deeper saltwater penetration.

Concentrations at the observation points were recorded throughout the simulations of FWL recovery (Figure 5.8). Maximum relative concentrations range from 0.07 to 0.86, with 1.0 representing seawater. Islands with the highest concentrations were Type II (Santiago) and Type V (Jamaica), both of which also have the thickest vadose zones allowing for a larger initial pulse of salt water to enter the system during inundation. Islands with thinner vadose zones (i.e. Types III and IV), have lower relative concentrations. Concentrations generally rise abruptly following the overwash event, and then decrease over time. Island Type VI (Mahé) has a delayed increase in concentration consistent with the slow infiltration of salt water (also seen in Figure 5.5). Concentrations oscillate for island Type II (Santiago) as salt water quickly migrates to the observation point through the high K fracture, but is then trapped along the low K tuff layers in density-driven convection cells. These oscillations are also observed in the other island types, although at a smaller scale, related to density-driven convection cells.

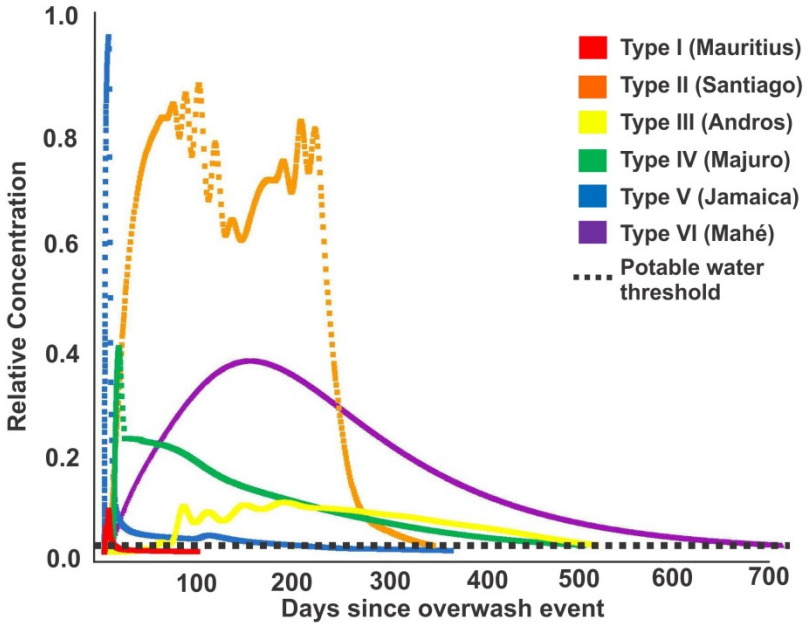

Figure 5.8. Relative concentration data at observation points following overwash event.

Table 5.3 shows the times to reach: 1) steady-state FWL; 2) FWL recovery to baseline morphology; and 3) recovery at the observation point. The time for recovery at the observation point is based on the time needed for water to return to a potable concentration. On each island, local water quality guidelines have different definitions of

potable water so a common value of 0.4 g/L or less (representative of guidelines used in The Bahamas - island Type III) was used.

The time it takes for a steady-state FWL to develop on each island ranges from 1 to 15 years, whereas the time for FWL recovery after inundation ranges from 1 to 6 years (with the case of the low-recharge Type II island taking up to 19 years). The time to reach recovery at the observation point following inundation (t_p) ranges from 10 to 716 days (Table 5.3). Recovery of potable water for island Type II (Santiago) under higher recharge conditions was the same as that for the original low recharge values.

Table 5.3. Temporal model results

Island Type	Time to reach steady-state FWL (t_s) (years)	Time to reach FWL recovery[1] (t_r) (years)	Time to reach recovery at obs points[2] (t_p) (days)
Type I - Mauritius	1	1	10
Type II - Santiago	10	19/4 [3]	346
Type III - Andros	10	2	522
Type IV - Majuro	10	6	505
Type V - Jamaica	5	2	368
Type VI - Mahé	15	3	716

Note: 1) Recovery of FWL is evaluated as return to baseline FWL morphology (i.e. thickness).
2) Recovery at observation points is evaluated as concentrations less than 0.4 g/L salt.
3) Longer recovery time for low (original) recharge; faster recovery time for high recharge.

5.4. Discussion

The dominant factor affecting the degree of saltwater contamination of the FWL resulting from inundation (i.e. FWL response) is the presence of geological heterogeneities with relatively higher or lower K than the principal aquifer materials. A pocket of fresh water persists for longer post-inundation when layers of high K are present near the top of the FWL. These layers flush out the salt water before it migrates deeper into the underlying freshwater pocket, as seen for island Type I, III, V, and VI. Another factor affecting FWL contamination is the thickness of the vadose zone, where thick vadose zones result in a large amount of salt water collected during inundation,

which must be flushed out of the subsurface (example Type II Santiago). However, when the vadose zone has a low K, the migration of salt into the subsurface is slow and may limit the amount of salt water entering the system from inundation (e.g. Type VI Mahé). Therefore, the response of the FWL to overwash depends largely on the geological heterogeneities, as well as a combination of the vadose zone thickness and K value.

The time until full recovery of the FWL depends on several factors including the degree of initial saltwater contamination, hydraulic properties, recharge rate and the presence of geological heterogeneities. Island Type II (Santiago) took the longest time to recover (19 years). The low recharge rate for the island was the primary reason for the slow recovery of the FWL. However, other factors also contributed to the slow recovery. The island has a thick vadose zone and relatively high aquifer K, which leads to a large saltwater plume developing in the subsurface. In addition, the vertically oriented high K fracture resulted in the salt water penetrating deep into the aquifer. The presence of horizontally-oriented low K tuff layers prevented the salt water from reaching deeper into the aquifer, but also delayed flushing of the salt water from this zone because flow rates were slow across the tuff layers. The range of recovery times for islands with varying hydraulic parameters but similar recharge rates is small (i.e. within 5 years of each other). The results of island Type II (tested for both low and high recharge) indicate FWL recovery is much longer for the observed low recharge on this particular island. However, under a scenario of higher recharge, the Type II model recovered within 4 years (i.e. similar rate to the other island types), suggesting that recharge rate is the dominant factor affecting FWL recovery.

Interestingly, the time until recovery of potable water at the observation points is not directly related to recovery of the FWL morphology to baseline conditions (Table 5.3). For instance, although Type II has the longest overall FWL recovery time, the observation point recovers much more quickly, at slightly less than 1 year (regardless of whether the original low recharge or a higher recharge value is used). The observation point recovery is also not related to the thickness of the vadose zone, as the islands with the thickest vadose zones (and highest saltwater concentrations recorded at the observation points) recover more quickly than those with thinner vadose zones and lower concentrations. The recovery of potable water is largely dependent on the specific

location of the observation point and the hydraulic properties of the subsurface. The observation points were assigned to represent a typical location of water supply infrastructure (shallow wells and trenches), near the surface of the FWL. The observation point for island Type I (Mauritius) is located within the high K zone (a likely target position for water supply wells), and therefore, recovers very quickly due to high K allowing quick flushing of the saltwater contamination. In contrast, for island Type III (Andros), the high K zones are deeper in the subsurface and so the top of the FWL takes longer to recover. The observation point for island Type II (Santiago) is located near a low K zone that collects the infiltrating salt water within the shallow part of the FWL. However, in this case, the top of the FWL is able to recover relatively quickly due to the vertical high K zone bringing in fresh recharge that flushes out the saltwater plume. Return of potable water concentrations at the observation points is significant as it represents the recovery of a potential water supply. Although the FWL may still be quite thin at this time, there may be recoverable quantities of fresh water available for consumption.

Some island types appear to have limited impact from overwash events due to a minimal FWL response (saltwater contamination) and/or fast FWL recovery, such as that observed for island Type I (Mauritius). However, the main water supply on many islands of Type I, II and VI, are not based in the predominant aquifers on the island, but rather on small, low-lying sedimentary aquifers present along the coastal areas (Allen et al., 2014). Therefore, the potential impact of overwash on the water supply for these islands may be greater, similar to island Type IV (Majuro). Any given island has specific circumstances that may affect the impact of overwash events on the FWL; however, the island is likely to reflect the general observations of FWL response and recovery for one of the island types.

The results presented in this study provide a comparison across island types that allows for general trends in FWL response and recovery to be observed. They are not meant for predictive purposes related to the specific time to reach FWL recovery or return of potable water on a given island due to limitations and simplifications applied in the study approach. For instance, soil zones and vegetation patterns were not included in the models. These would impact how quickly the salt water would migrate into the

subsurface during inundation. Surface slope and runoff were also not included, as well as surface depressions which may store salt water for prolonged inundation. In addition, the time of inundation may be significantly longer for a given overwash event. Omitting these features and details resulted in simplified models for each island type, rather than detailed correlation of the local, small-scale features and hydrogeology of each example island used in the study. This approach was adopted to allow for a comparative representation of the FWL response on different island types based on a consistent, theoretical overwash event.

This study has demonstrated the variety in FWL response to overwash events based on the hydrogeological settings of different island types. However, the occurrence of overwash events in the future is significantly affected by changes in climatic factors. Rising sea levels increase the likelihood of overwash by raising the baseline tide levels (Oude Essink, 2001; Walsh et al., 2011). Sea level rise is observed to be occurring at a global rate of approximately 1.8 mm/year (Church and White, 2011), which creates a higher baseline tide level so that extreme tide events may occur more frequently and result in overwash events. Changes to storm patterns may also affect the frequency or intensity of hurricanes and tropical storms which are common causes of storm surge overwash (Knutson et al., 2010). Understanding the physical variables and how they may impact the susceptibility of the FWL on a given island provides a useful tool to inform risk management when evaluated alongside the climatic variations for a given area.

5.5. Conclusions

Small islands may experience significant damage to the freshwater supply from overwash events. Many factors affect the FWL response and recovery following overwash events. These factors operate in combination, in a multitude of configurations depending on the unique hydrogeological setting of any given island. Recharge rate is the dominant factor, alongside the presence of geological heterogeneities. Islands with low recharge rates are likely to have long-lasting impacts to the FWL from overwash events. These islands are also likely to have thick vadose zones, which may result in a larger impact as the vadose zone stores a larger amount of the inundating seawater.

The presence of geological heterogeneities may promote or impede FWL recovery from an overwash event. Islands with vertically-oriented high K or horizontally-oriented low K features are likely to result in larger (or longer lasting) impacts to the FWL. In comparison, islands with horizontally-oriented high K features generally recover more quickly. In addition, a potable water supply may recover on the island before the FWL has fully recovered, particularly where the hydraulic parameters promote flushing of the saltwater plume (i.e. high K subsurface). Characterising the FWL response and recovery to overwash for a generalised classification of island types allows for the response of a given island to be anticipated based on its island type. This also allows for quick assessment of island susceptibility to overwash for any island that correlates to an island type. Future studies may incorporate these results with climatic trends related to the occurrence of overwash events for a given island to asses risk to overwash.

Chapter 6.

Island Water Security Risk Assessment

This chapter was submitted as a paper entitled, “Risk to water security for small islands: an assessment framework and application”, to Regional Environmental Change. The results presented in this chapter were also prepared as a report entitled “Freshwater Resource Risk Assessment for Andros Island”, in fulfillment of the grant provided by The Nature Conservancy to Dr. Diana Allen, Department of Earth Sciences at Simon Fraser University (SFU).This research formed a component of the Royal Bank of Canada Blue Water Project Leadership Grant, held in part by The Nature Conservancy, which is entitled: “Fostering Watershed Conservation in the Pine Islands of The Bahamas”.

6.1. Introduction

There is strong consensus that the impacts of climate change will have substantial consequences on small islands (Intergovernmental Panel on Climate Change (IPCC), 2014). In addition, small islands are susceptible to non-climate related impacts because the availability of fresh water depends on human (water use), hydrogeological and physiographic factors, such as island shape and topography (White and Falkland, 2010; IPCC, 2014). Despite the increasing number of assessments related to impacts of climate change on islands, there has been little research demonstrating how this information is used in policy-making and adaptation (IPCC, 2014). Communication of risk to inform policy-makers and engage local populations is likely to increase resilience to impacts and is critical for effective adaptation (Dunn et al., 2012; IPCC, 2012, 2013). In addition, climate impact research often does not incorporate concerns stemming from the local context (Barnett et al., 2008), especially those related to the outer (non-primary) islands within a given small island developing state (IPCC, 2014). Therefore, there is often a lack of awareness at the local level about the specific threats posed by climate

change (Nunn, 2009), which can discourage actions that reduce vulnerability (IPCC, 2012). For instance, previous studies in the Caribbean region have shown that increasing awareness about the risks related to tropical storms enhanced the effectiveness of adaptation and vulnerability reducing actions (Adger et al., 2011).

This study aims to assess risk to water security for a representative small island and present the risk information in an accessible format for policy-makers and local stakeholders. The work was undertaken in response to local policy-makers, conservationists, resource managers and the Government of The Bahamas identifying the need to characterise risk to freshwater resources. The risk assessment presented here was completed in partnership with The Nature Conservancy Northern Caribbean Office and forms part of a larger project addressing watershed protection on several Bahamian islands. Due to the availability of data, the focus of the study is Andros Island; however, the intention is to provide guidance and transfer key lessons learned to other similar islands within The Bahamas, and elsewhere. The components that determine risk vary in time and space so it is important to include temporal and spatial dynamics in risk assessment (IPCC, 2012). Thus, this work builds a risk assessment methodology that incorporates the temporal and spatial aspects of the major stressors impacting water security on Andros Island.

6.2. Water Security and Risk

Water security describes the quantity and quality of water available for human use, environmental demand, and economic interests (Global Water Partnership, 2000; Grey and Sadoff; 2007). There are varying definitions of water security across different disciplines, but essentially they represent “access to sufficient quantity of water of acceptable quality to support human, environmental and economic needs” (Cook and Bakker, 2012). The United Nations’ working definition of water security also includes aspects of political stability and prevention of water-related disasters (UNESCO-IHP, 2012). Water security within the small island context generally relates to groundwater, as most small islands do not have significant surface water bodies due to the high permeability of the subsurface geological materials (White and Falkland, 2010). Although some islands utilise springs and intermittent streams or rainwater harvesting as a water

supply source, groundwater tends to be the common source of sustainable water throughout the year.

Several water security assessment tools are available; most of which are based on the classification of a set of indicators that are measured at a specific point in time. Examples of indicators include: water stress as a measure of water usage versus availability (Falkenmark et al., 2007); water efficiency in food production (Rockström et al., 2007); water availability for basic human or environmental needs (Lautze and Manthrithilake, 2012); water quality indicators measuring ecosystem or human health (Dunn and Bakker, 2011); and the capacity for water governance (van Leeuwen et al., 2012). It can be argued that these indicator-based assessments do not assess "risk to water security" because the indicators are static in time and, as such, do not capture the potential consequences that may arise in an uncertain future (Dunn et al., 2012).

Risk describes the vulnerability to a hazard and the loss (sometimes also referred to as exposure or consequence) experienced if that hazard were to occur. Vulnerability is characterised by the predisposition (or susceptibility) to a hazard and the characteristics of the hazard itself. Different risk assessments identify the principal components of risk using different terminology or meanings, which can lead to confusion. For the purpose of this study, previous work is presented using a consistent terminology based on the following definitions:

$$\text{Risk} = \text{Vulnerability to hazards} \times \text{Loss due to hazard occurrence} \quad (6.1)$$

where

$$\text{Vulnerability} = \text{Susceptibility} \times \text{Hazard characteristics and presence} \quad (6.2)$$

Risk assessments are used in a wide variety of disciplines, from natural hazard management and engineering to actuarial finance and public health. Common to all risk assessments is the evaluation of the likelihood of adverse consequences occurring (Zwahlen, 2004). There is a multitude of different risk assessment approaches and frameworks to address different purposes and objectives (e.g., Adger, 2006; Birkmann, 2006; IPCC, 2012). Few water security assessments, particularly groundwater

assessments, have characterised risk; most assessments have focused on characterising the susceptibility (commonly referred to as the intrinsic vulnerability) of the aquifer. Rarely are specific hazards included except in the context that such hazards exist and can be expected to enter into the aquifer system and move through the system in a particular way. The term specific vulnerability has been used to assess the behaviour of a specific contaminant along its flow path. Moreover, few approaches consider the loss component. Notable examples of water security assessments that evaluate risk include those developed under the European Commission COST Action 620, such as COPK, LEA, VULK, and time-input (Zwahlen, 2004), as well as a groundwater quality risk assessment framework developed to support source-water protection strategies (Simpson et al., 2013).

There are several popular methods that characterise “aquifer vulnerability”, such as DRASTIC (Aller et al., 1987), GOD (Foster and Hirata, 1988), AVI (Van Stempvoort et al., 1992), SINTACS (Civita and De Maio, 1997) and EPIK (Doerfliger and Zwahlen, 1997) (noting that vulnerability is intrinsic and thus is termed susceptibility in this paper). Other assessments of aquifer susceptibility generally rely on the principles developed in the preceding examples, whereby a series of indicators are assigned weighted values and are combined to produce an overall index of aquifer susceptibility. Modifications may be made to represent unique aspects of a particular system, such as karst; however, the overarching principles remain the same.

Groundwater susceptibility assessments are usually based on a scenario of chemical (or biological) contamination derived from land use activities, whereby hazards are introduced at the land surface and travel vertically down to the water table. However, such assessments are not fully suitable for an island context where the pathways for contamination are not exclusively vertical (Chui and Terry, 2013). Fresh water on islands is contained within in a freshwater lens (FWL) that is replenished by fresh rainwater recharge (Figure 6.1a). The lens is susceptible to contamination introduced at ground surface, similar to other aquifers. However, the FWL is surrounded by salt water on the ocean boundary and is also underlain by salt water which may contaminate the aquifer. Storm surge may lead to wave overwash, thereby introducing salt water at surface (Anderson, 2002; Terry and Chui, 2012). Over-extraction of groundwater may cause

upconing of the salt water from below the lens or lateral saltwater intrusion from the coast (Falkland, 1991; Bobba, 2002). In addition, a reduction in recharge or a rise in sea level can also compromise the FWL, leading to salt contamination or loss of lens volume (Falkand, 1991; Oude Essink, 2001). Thus, the water system on an island is susceptible to a range of hazards from all directions that can impact water quantity and quality (Figure 6.1b).

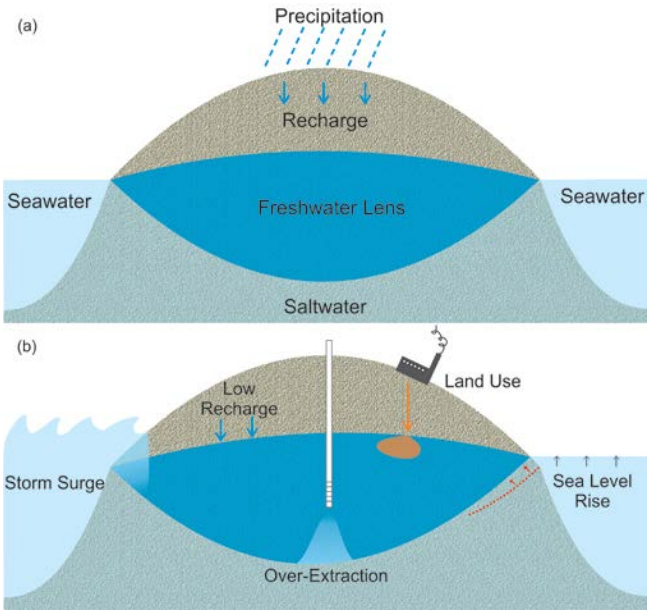

Figure 6.1. a) Freshwater lens; b) hazards to water security in an island setting

Climate change is expressed by multiple stressors acting on a variety of spatial and temporal scales (Adger, 2006). Increased temperatures and changes in the spatial distribution, frequency and magnitude of precipitation are expected to impact groundwater recharge (Green et al., 2011). Sea level rise will result in inundation and potentially a landward shift of the saltwater interface, particularly on low-lying islands. There is increasing research in risk assessment related to climate change impacts, particularly in support of adaptation and mitigation efforts (McCarthy et al., 2001). However, there are no risk assessment methodologies that address the unique scenarios encountered on small islands, where the freshwater resources are susceptible to hazards from numerous directions as described above. As such, a different approach for assessing vulnerability, and risk to water security, is needed for an island context. The specific objectives of this study are to: 1) develop a risk assessment methodology that is tailored to evaluate risk to water security for a small island that includes both the

temporal and spatial aspects of risk, and; 2) present risk in an accessible format for use in policy development by policy-makers and local stakeholders.

6.3. Methodology

The risk assessment was developed using Andros Island, The Bahamas as a case study area (Figure 6.2). The basic methodology, including the identification of components that represent the island context, are likely to be widely applicable to small islands, although the detailed framework presented in this study is influenced by the data that were available for Andros Island. Some components of the assessment are unique to Andros, such as the morphology of the freshwater lens (FWL), and these components would need to be tailored to local specifications if the methodology is applied elsewhere. Thus, the methodology described in this paper is intended to provide guidance for application to other similar islands.

The approach relied on a solid understanding of the hydrogeology of Andros Island, which was gained through numerical groundwater modeling. The models were developed using the density-dependent flow and transport code SEAWAT (Langevin et al., 2007), which is suitable for simulating groundwater conditions in coastal aquifers. Modeling was undertaken at an island-wide and small scale to: 1) simulate the current location and thickness of the FWL on Andros; and 2) assess the spatial and temporal response of the FWL to various human and climate stressors. An overview of the SEAWAT model setup for Andros is provided by Holding and Allen (2014). Figure 6.3 shows the model generated FWL, which is consistent with historical observations of lens location and thickness (Little et al., 1973). There are multiple FWLs on Andros Island; the thickest lens is situated in the northern region of Andros Island, and relatively thinner lenses are present in the southern regions.

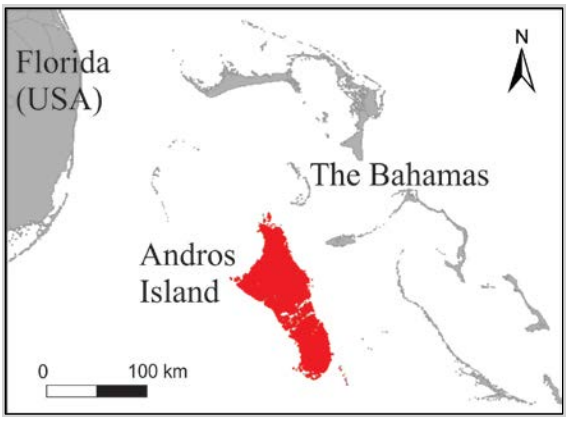

Figure 6.2. The location of Andros Island in The Bahamas

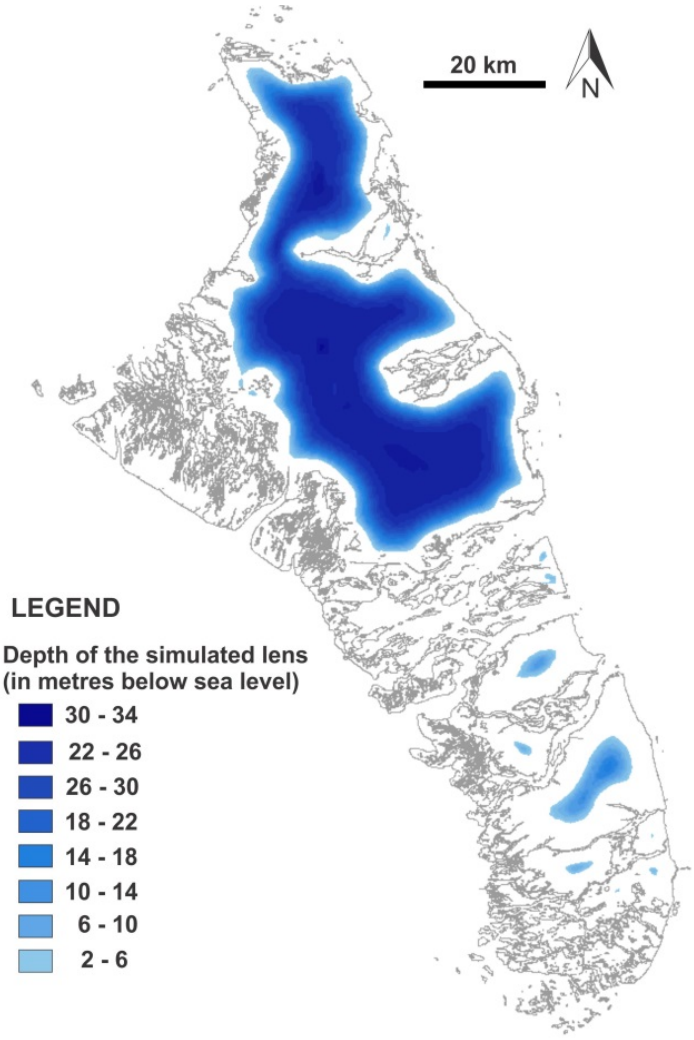

Figure 6.3. Simulated FWL on Andros Island

The risk assessment methodology is based on the basic risk equations (Equations 1 and 2) and illustrated in Figure 6.4. Indicators were developed using an assessment framework to assign scores to each of the components of risk and, ultimately, to derive a risk index. The assessment framework was built within a geographic information system (GIS) platform to represent spatial variability.

Temporal aspects of risk are reflected in the ranking of indicator scores that affect the overall risk index. Susceptibility is assessed to represent the current and potential future conditions of the lens, based on projections of climate change for the year 2100 (e.g. sea level rise, changes in recharge). In this way, the susceptibility indicator captures the potential temporal changes in susceptibility over this time period (i.e. present to 2100). Climate related hazards are also assessed based on projections for the year 2100, whereas, the assessment of human-related hazards incorporates the temporal aspects of hazard threat in terms of hazard duration or longevity. Therefore, the resulting risk indicators represent current conditions and the temporal variability of potential future conditions. Details concerning the approach used to assess each component of risk are described in the following sections.

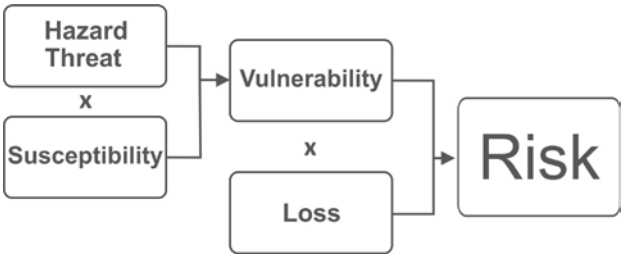

Figure 6.4. Risk tree used in this study

6.3.1. Susceptibility

Susceptibility refers to physical characteristics of the island that either promote or minimize damage from hazards; susceptibility is irrespective of whether hazards are present or not. In this study, susceptibility of the FWL was considered, rather than the entire island or aquifer. For continental settings, aquifer susceptibility is assessed based on the premise that the entire aquifer is of concern. However, on an island, fresh water resides in a FWL; therefore, the FWL will only be susceptible to hazards where it is present.

The susceptibility of the FWL to hazards was evaluated according to four categories: S_I: Intrinsic Susceptibility; S_{PP}: Preferential Pathways; S_{CT}: Coastal Topography; and S_{OT}: Overall Topography. Each category is described below. The scoring scheme is outlined in Table 6.1.

S_I - Intrinsic Susceptibility. The intrinsic susceptibility relates to the thickness of the FWL and the robustness of the lens to accommodate changes or buffer stressors, specifically the stressor of reduced recharge. Recharge modeling was undertaken using the HELP hydrologic model (Schroeder et al., 1994) for current and future climate conditions. Future climate projections for The Bahamas were based on results of an ensemble of global climate models (GCMs) (McSweeney et al., 2010) for the A2 emissions scenario, which is projected to result in the greatest impacts (IPCC, 2007). Numerical modeling of the FWL response to the scenario of reduced recharge was then carried out using SEAWAT. Susceptibility was ranked based on whether the FWL is thick (and therefore a potential water supply source) and whether the FWL is sensitive to reduced recharge based on the modeled response. Areas where loss of the FWL areal extent (i.e. shrinking of the lens) was modeled to occur under reduced recharge conditions were assigned a higher susceptibility score (10 for low robustness) compared to areas where the lens did not have as large a response (i.e. thinning of the FWL but no loss of areal extent) to changes in recharge (1 for high robustness). A moderate susceptibility score (5) was assigned when the FWL was too thin to be able to provide a large water supply. Zero susceptibility was assigned where the FWL was absent.

S_{PP} - Preferential Pathways: The susceptibility of the FWL may be enhanced due to preferential pathways. These pathways represent areas where the FWL may be exposed at surface (such as trench wellfields), potentially connected by vertical conduits such as open boreholes, or where the FWL has a strong hydraulic connection to the surface (for instance, underlying wetlands or seasonal ponds where water from the surface infiltrates to the water table). The FWL in these areas is therefore more susceptible to contamination either from chemicals or pathogens introduced at surface, or from overwash by seawater following a storm surge. A high susceptibility score was assigned to areas where a direct preferential pathway is present, for instance private wells, wellfields, or wet quarries (excavations extending below the water table). A

moderate score was assigned to areas where there was a potential for strong hydraulic connection with the surface, such as wetland areas or seasonal ponds. A low score was assigned where there was no preferential pathway present.

S_{CT} - Coastal Topography: The influence of coastal topography on susceptibility is represented by areas that are susceptible to saltwater inundation from sea level rise. Using the digital elevation model (DEM) for Andros Island, areas with ground elevation less than 2 metres above sea level (masl) were ranked with high susceptibility to inundation according to the 95th percentile mean sea level rise (1.78 masl) predicted by 2100 in the region (Obeysekera et al., 2013).

S_{OT} - Overall Topography: The influence of overall topography on susceptibility is represented by areas of the island that are susceptible to storm surge. Identification of these areas was based on a previous storm surge modeling study for The Bahamas, which indicated typical surge heights for different storm tracks and hurricane classifications (Rolle 1990). Although the modeling did not explicitly include Andros Island, the results for nearby islands were generalised for Andros Island based on bathymetry and the direction of the potential storm tracks, which traverse The Bahamas from all directions. Although bathymetry varies on the east and west coasts, the higher range of potential storm surge wave heights was assumed to occur on both coasts. The DEM was then used to identify low elevation areas adjacent to the coast (< 6 masl), which may offer pathways for storm waves to travel across the island, resulting in overwash of the FWL by seawater. The low elevation areas were assigned a high susceptibility score. Further predictive storm surge modeling could be undertaken to extend the simplified approach used in this study.

Separate susceptibility category maps were prepared in the GIS. The maps were then overlain, and the susceptibility scores summed to produce a total susceptibility value that varies spatially across the island. This value was normalised on a 1-10 scale, resulting in a **Total Susceptibility (S_{Total})** indicator map illustrating the range of susceptibilities from low (1) to high (10). Each category was mapped out as having either no susceptibility (0), or a ranking of low (1), moderate (5) or high (10) susceptibility. The scores were assigned to determine relative susceptibility within each

category. The resulting scores were then weighted equally among the different susceptibility categories in order to determine the final susceptibility indicator. Therefore, if an area ranked as having a moderate susceptibility for three categories (5+5+5=15), the resulting susceptibility indicator was higher than that of an area that was ranked as having high susceptibility for a single category and low in the other two (5+1+1=7). The equal weighting of each category, and standard application of low, moderate and high ranking ensures that the S_{Total} indicator equally represents the susceptibility from each category.

Table 6.1. Susceptibility scoring scheme

ID	Category	Score	Basis of Decision	Description
S_I	Intrinsic Susceptibility	10	Sensitive FWL of viable thickness (> 2 m thick)	FWL provides a large-scale water supply but is not sufficiently robust to accommodate potential future changes to recharge (i.e. loss of freshwater volume is modeled for changes in recharge).
		5	Thin FWL (< 2 m thick)	FWL not able to provide large-scale water supply, but may be used for limited domestic water supply. Not robust to changes in recharge.
		1	Robust FWL of viable thickness (> 2 m thick)	FWL provides a large-scale water supply and is sufficiently robust (i.e. no significant loss of freshwater volume modeled) to accommodate potential future changes to recharge.
		0	No FWL present	No FWL to be impacted.
S_{PP}	Preferential Pathways	10	Exposed FWL	Preferential pathways at quarries that extend below the water table; or at private wells or wellfields.
		5	Hydraulic connection to FWL	Moderate susceptibility where there is potential hydraulic connection to the FWL (e.g. where seasonal ponds and wetlands are present)
		0	FWL not exposed at surface	No preferential pathways.
S_{CT}	Coastal Topography	10	Low coastal elevation (< 2 m above sea level)	High susceptibility to inundation due to lower elevation.
		0	Higher coastal elevation (> 2 m above sea level)	Low susceptibility to inundation due to higher elevation.
S_{OT}	Overall Topography	10	Low topography and/or low elevation pathways (< 6 m above sea level)	Elevation less than typical storm wave height; low elevation pathway present from east to west coast.
		0	High topography (equal to or > 6 m above sea level)	Elevation higher than typical storm wave height.

6.3.2. Hazard Threat

Hazard threat was defined based on the major stressors impacting the freshwater resources on Andros Island. These include stressors related to human activities (contamination and pumping) as well as climate change (sea level rise and storm surge); note that the reduction in recharge was accommodated in the susceptibility modeling as described above. Hazards related to human activities were identified on Andros Island from the results of a door-to-door hazard survey conducted by a local Bahamian organisation (MCK Environmental) in partnership with The Nature Conservancy, a non-governmental conservation agency (MCK Environmental, 2013). The objective of the survey was to provide geospatial data for residents and businesses on Andros Island related to practices that have the potential to impact water security, such as chemical use, waste disposal, wastewater management and water supply. Hazards related to climate change were based on the modeled impact of sea level rise and storm surge on the FWL.

Human Activities

The hazard threat from human activities was determined based on the spatial data associated with each property identified in the door-to-door survey. Hazard threat indicators were assigned based on four hazard categories related to the specific hazardous activity; the resulting hazard is indicated in brackets: H_P: Water Supply and Pumping (upconing or saltwater contamination); H_{CS}: Chemical Storage (chemical contamination); H_{SS}: Septic Systems (pathogen contamination); and H_{AP}: Agricultural Practices (chemical and pathogen contamination).

Each hazard threat from human activities was assessed according to its magnitude (quantity), the potential for release or occurrence, and the strength/longevity of the hazard, with a score assigned to each (Table 6.2). These scores were then multiplied to result in a value for each hazard. The magnitude of the hazard was based on the scale of the hazard, for example, the level of pumping or quantity of contaminants present. The potential for release or occurrence of the hazard was based on the storage or use of the chemical/pathogen so as to describe the potential of that hazard being released to the environment. The strength/longevity of a hazard was based on the

degree of damage to the FWL, duration of the expected damage or ability of the FWL to recover, and the persistence and mobility of the chemical/pathogen. This field accounts for temporal aspects of hazard impact, whereby some hazards are ranked lower due to expected recovery of the FWL after release/occurrence. For instance, the FWL may recover from pumping if high pumping is stopped, such that the pumping hazard threat is ranked as having a lower duration than chemical contamination, which may persist for many years after release/occurrence. The hazard fields were assessed based on a low (1), moderate (5), and high (10) score to provide a relative ranking amongst the hazards. The only exception was the magnitude/quantity field, which was assigned to reflect the range in magnitude of the potential hazard present. The scores for this field were assigned so that large magnitude/quantities were ranked relatively higher than smaller magnitudes within the hazard category (i.e. a large quantity of fuel ranked proportionally higher than a small quantity). The scoring scheme is described in detail below for each hazard category.

H_P - Water Supply and Pumping: This hazard describes activities related to the extraction of groundwater from the FWL, which may lead to upconing of the salt water from beneath the FWL. Individual properties were assigned a hazard score whenever a well is present on the property. The quantity field was assigned based on the expected amount of fresh water pumped from each well according to use. Private domestic wells were given a low score; wells used for commercial activities, such as small hotels and restaurants, were given a moderate score; and wells used for large industrial operations, such as a water bottling plant, were given a high score. The occurrence potential was assigned to all wells as moderate, as details of the well construction (i.e. depth of the well, where deeper wells are more likely to cause upconing) were unknown. The only exception was when reverse osmosis systems were used and the brine was reported to be disposed of at surface beside the well. These properties were assigned a high occurrence potential score because the disposal of brine at surface is likely to cause salt contamination of the aquifer. In addition, the use of reverse osmosis suggests that the wells may already be causing upconing as they are pumping brackish to salty water. The strength/longevity field was assigned a moderate score for all properties based on numerical modeling results, which showed that the FWL is largely able to recover from upconing when the hazard is removed (i.e. pumping ceases). The quality field was

assigned based on whether the water abstracted from the wells was brackish or fresh. When wells reported abstracting brackish water, they were assigned a lower score as they were assumed to be positioned outside of the FWL. All other wells were assigned a high quality score.

H_{CS} - Chemical Storage: This hazard describes the potential chemical contamination from activities related to the storage of chemicals. The quantity field was assigned based on the amount of chemical present, with larger quantities assigned a higher score. In order to capture the variability across different properties, the range of quantity scores was large. For example, from the survey, the amount of fuel on a given property was found to range from 1 gallon to over 100,000 gallons. The larger range of quantity values also reflects the higher threat posed from chemical contamination than other potential hazards. The release potential was assigned as low, moderate or high based on the typical storage and disposal of chemicals. When chemicals are not typically disposed of on the ground (e.g. engine oil is commonly reused to treat wood), the property was given a low release potential score. Chemicals, once used, may be disposed of on ground, or stored in containers that may leak unnoticed (e.g. single-wall underground fuel storage tanks). The properties with these chemicals were assigned a moderate likelihood of release score. Where there was a known release of chemicals (e.g. a fuel spill), the property was assigned a high likelihood of release score based on previous history. The strength/longevity field was assigned based on information related to the toxicity, persistence and mobility of each chemical present at the property (US Environmental Protection Agency (USEPA), 2004).

H_{SS} - Septic Systems: This hazard describes the potential pathogen contamination related to septic system usage. Due to the absence of municipal sewerage, the majority of properties on Andros Island use a septic system, although a small number of properties use composting toilets. The quantity field was assigned based on the number of septic system users per day, whereby the score assigned was equal to the number of users. All properties using septic systems were assigned a high release potential score due to the high water table, a lack of maintenance performed, and frequency of informal construction of septic tanks (e.g. unlined pits). Properties that employed composting toilets were assigned a zero for no release. The strength/longevity

field was assigned to all properties as moderate, based on the assumption that conditions within the septic system or vadose zone would remove some of the pathogens before they are transported in to the aquifer (Hagedorn et al., 1981). The one exception is the few properties that reported untreated disposal of sewer wastes at ground surface.

H_{AP} - Agricultural Practices: This hazard describes the potential pathogen and chemical contamination related to agricultural practices, such as fertilizer/pesticide application and livestock rearing. The quantity field was assigned based on the frequency of pesticide/fertilizer application, with higher frequency assigned a higher score. An additional field was added to capture potential hazards (e.g. pathogens or nitrogen loading) resulting from livestock rearing. This field was assigned a score based on the number of animals reported in the survey. A high release potential was assigned for all properties, because pesticides and fertilizers are known to be released to the surface. The strength/longevity field was assigned as low, moderate, or high based on the toxicity of each pesticide or fertilizer (USEPA, 2004). A low score was assigned to non-toxic compounds, a moderate score to low-nitrogen fertilizers, and a high score to all chemical pesticides.

The total hazard for an individual property was determined as the sum of each category value (i.e. $H_P + H_{CS} + H_{SS} + H_{AP}$). The total hazard value was then normalised on a 1-10 scale resulting in a **Hazard Threat from Human Activities (H_{HA})** indicator. The rankings are relative within each category, and each category is weighted equally to determine the final H_{HA} indicator. As a result, the hazard threat indicators represent the relative ranking of the cumulative hazard threat from each different hazard category. The score assignment for fields within each hazard category has a large impact on the final hazard threat indicator. Therefore, the scoring scheme was validated by checking that each property was appropriately ranked relative to the other properties. For example, a property with significant pesticide application ranked higher than a property with a small quantity of fuel storage or a moderate septic system. The relative ranking approach removes some of the uncertainty in the score assignment, and determination of total hazard threat.

The location of each property and its associated hazard threat indicator were compiled in the GIS. Large properties, such as farms, were represented as polygons outlining the extent of the property. All other properties were represented as points, buffered with a 30 m radius to represent the potential source zone. Although only a sample of residences was surveyed, a background hazard threat indicator was assigned for all settled areas based on the average for the surveyed residential properties. Properties that did not have survey results (e.g. informal landfills) were ranked based on assumptions and observations regarding land-use practices.

The two-dimensional mapping approach assumes that the contaminant will travel vertically downward to intersect the FWL. The hazard map does not consider the movement of the contaminant once it reaches the FWL. This would require a groundwater flow and transport model specific to each contaminant. The groundwater velocities computed from the numerical modeling are on the order of 2 m/day and, at an island scale, the groundwater flow generally is directed toward the coast. Thus, lateral movement of conservative contaminants (such as chloride) would be on the order of a few hundred metres per year.

Climate Change

Hazard threat indicators for climate change were assigned within a similar assessment framework as used for hazards related to human activities. The principal difference is that hazards related to climate change are not related to individual properties or specific geospatial extents; therefore, the hazard threat is represented as equally present across the island (i.e. climate change impacts the entire island).

The hazard threats from climate change include: H_{SLR}: Sea Level Rise (sea water intrusion and land inundation); and H_{SS}: Storm Surge (seawater overwash and surface inundation). The impact of reduced recharge due to climate change was not considered a hazard in this study; rather it was assessed in terms of how reduced recharge impacts the susceptibility of the FWL (as described earlier).

A score was assigned to each field: magnitude (quantity), the occurrence potential, and the strength/longevity of the hazard (Table 6.2). The scores were then

multiplied to result in a value for each climate change hazard. The quantity field relates to the degree of inundation expected, or amount of saltwater contamination that may occur. The occurrence potential field describes the potential for these hazards to occur. The strength/longevity of the hazard reflects the temporal variability in terms of the reversibility of impacts resulting from occurrence of the hazard. Similar to the assessment used for hazards related to human activities, the hazard fields were assessed based on a low (1), moderate (5), and high (10) score to provide a relative ranking. The scoring scheme is discussed in detail below for each climate change hazard category.

H_{SLR} - Sea Level Rise: This hazard relates to the occurrence of sea level rise and associated land surface inundation. The quantity field is assigned a high score because complete inundation is expected for any affected area. The occurrence potential is assigned a moderate score because, although sea level rise is likely to occur, the timing and extent of this change are uncertain. The strength/longevity field is assigned a high score because the inundating water represents a high hazard to FWL quality and the impact of sea level rise is generally irreversible (unless mitigative action is taken, such as dyking). This hazard threat category represents temporal variability as the spatial assignment of the hazard threat reflects a future scenario for the year 2100 (using the maximum sea level rise projections).

H_{SS} - Storm Surge: This hazard relates to the occurrence of a storm surge whereby high waves may cause inland flooding with salt water. The quantity field is assigned a high score because complete inundation is expected for any affected area. The occurrence potential is assigned a moderate score because, although storm surge may occur, the location of occurrence and extent of impact (i.e. size of the storm) are unknown. The strength/longevity field is assigned a moderate score based on numerical modeling results, which indicate that the impact is likely temporary as the FWL will usually recover from a storm surge event. Therefore, overall, the storm surge hazard threat was assigned a slightly lower score than the sea level rise hazard threat based on the shorter longevity (or duration) of the anticipated impact. This reflects the temporal aspects of a storm surge hazard that applies for all future scenarios.

The total climate change hazard was determined as the sum of each category value (i.e. H_{SLR} + H_{SS}). The total hazard value was then normalised on a 1-10 scale resulting in a **Hazard Threat from Climate Change (H_{CC})** indicator. These climate change related hazard threats are not shown on a map because the hazard threat is constant across the entire island and does not vary spatially. However, the threats posed from these hazards are included in the vulnerability assessment calculations as discussed below.

Table 6.2. Hazard threat indicator scoring scheme

ID	Category	Breakdown Field	Score	Basis of Score	Description
H_W	Water Supply and Pumping	Quantity (Use)	10	High pumping	High pumping represents wells used for public water supply or industrial activities; Moderate pumping represents wells used for commercial activities; Low pumping represents single private wells.
			5	Moderate pumping	
			1	Low pumping	
		Occurrence Potential	10	High	A high score is assigned when reverse osmosis brine is disposed of at surface alongside the pumping well, which may lead to saltwater contamination. Most wells were assigned a moderate score due to insufficient details regarding well construction.
			5	Moderate	
		Strength / Longevity	5	Moderate	The upconing water is fully saline and would pose a significant hazard to the FWL; however, the FWL would be expected to recover (based on modeling) so a moderate score is assigned.
		Quality	10	High (fresh)	Wells located within the FWL and abstracting fresh water pose a higher hazard than wells located outside of the FWL and abstracting brackish (or saline) water.
			5	Moderate (brackish)	

ID	Category	Breakdown Field	Score	Basis of Score	Description
H_{CS}	Chemical Storage	Quantity	500	100,000+	A higher hazard threat score is assigned to larger quantities of a contaminant; a score of zero is applied when no chemicals are present.
			100	10,000-99,999	
			50	1,000-9,999	
			10	100-999	
			8	50-100	
			4	20-50	
			2	5-20	
			1	< 5 gallons	
		Release Potential	10	High	High score where there is a known release of chemicals; Moderate score for all other chemicals that may leak from storage containers or be disposed of on ground; Low score for chemicals not typically disposed of on ground or in septic systems.
			5	Moderate	
			1	Low	
		Strength / Longevity	10	High	Based on US Environmental Protection Agency designations and information related to toxicity and environmental fate (i.e. persistence and mobility) of each chemical.
			5	Moderate	
			1	Low	
H_{SS}	Septic Systems	Quantity	0 – 500	Input specific number of users	Number of users per day per septic system.
		Release Potential	10	High	High release is assumed for all standard septic systems due to the high water table and lack of maintenance performed; No release is associated with composting toilets.
			0	No release	
		Strength / Longevity	10	High	High score is assigned where waste is untreated and disposed of at surface; Most properties were assigned a moderate score.
			5	Moderate	

ID	Category	Breakdown Field	Score	Basis of Score	Description
H_{AP}	Agricultural Practices	Quantity	10	Daily	Frequency of application of fertilizers/pesticides.
			8	Weekly	
			6	Bi-weekly	
			4	Monthly	
			2	Semi-annually	
			1	Annually	
		Release Potential	10	High	Fertilizers/pesticides applied directly to ground surface.
		Strength / Longevity	10	High (pesticides)	Based on the US Environmental Protection Agency designations for each fertilizer/pesticide identified in the survey. High score refers to chemical pesticides; Moderate score refers to fertilizers with low nitrogen mixes; Low score refers to non-toxic compounds.
			5	Moderate (fertilizers)	
			1	Low (non-toxic)	
		Livestock	5	80-100+ animals	The presence of large numbers of animals and manure spreading represent a nitrogen load and potential high pathogen load, thereby increasing the agricultural hazard.
			4	60-80 animals	
			3	40-60 animals	
			2	20-40 animals	
			1	0-20 animals	
H_{SLR}	Sea Level Rise	Quantity	10	High	Complete inundation expected.
		Occurrence Potential	5	Moderate	Sea level rise is likely to continue to occur; however, the timing and extent of sea level rise is uncertain.
		Strength / Longevity	10	High	The inundating water is fully saline, and therefore represents a high hazard to FWL. The impact is generally irreversible.
H_{SS}	Storm Surge	Quantity	10	High	Complete inundation expected.
		Occurrence Potential	5	Moderate	Storm surge is likely to occur on Andros Island but the location of occurrence and extent of surge is unknown.
		Strength / Longevity	5	Moderate	The inundating water is fully saline, and would pose a significant hazard to FWL; however, the FWL is likely to recover from the hazard.

6.3.3. Vulnerability

The vulnerability indicator for human activities **(V_{HA})** was determined based on multiplying the Total Susceptibility indicator by the Hazard Threat from Human Activities indicator according to.

$$V_{HA} = S_{Total} \times H_{HA} \quad (6.3)$$

As mentioned previously, the climate change hazards are constant across the whole island because they lack spatial variability. It is the geospatial distribution of the susceptibility which provides the topographical and geospatial constraints on the hazard threats from climate change. Therefore, the vulnerability from climate change hazards **(V_{CC})** was determined separately, and then added to the vulnerability resulting from human activities according to:

$$V_{Total} = V_{HA} + V_{CC} \quad (6.4)$$

The total vulnerability score map was normalised on a 1-10 scale to determine the **Total Vulnerability (V_{Total})** indicator (Figure 6.6c).

6.3.4. Loss

Loss describes the consequences of hazards occurring, resulting in an undesirable condition. There are many possible definitions of loss depending on the perspective of the stakeholders. Therefore, this component of the assessment framework may be modified to accommodate different perspectives on risk or updated to capture changing socio-economic and environmental scenarios (Adger, 2006).

In this study, loss was defined in terms of access to fresh water. The **Loss (L_W)** indicator reflects the relative impact to the water supply. The developed areas of Andros Island were assigned a high loss score as there is current reliance on the FWL for water supply. Areas within the forested parts of Andros Island were assigned a moderate loss score because there is a potential for future development, which could increase demand for water. In addition, the forests rely on the FWL, which in turn support other industries

related to tourism and forestry. Areas of the island where development is unlikely to occur due to an uninhabitable environment (e.g. wetlands) were assigned a low loss score because a demand for future water supply is unlikely. Although the FWL is generally not present in these areas, a low loss score was assigned, as the FWL may have an indirect impact on the ecosystem if there is a loss of freshwater discharge along the coastline. The scoring scheme is outlined in Table 6.3.

Table 6.3. Loss scoring scheme

ID	Category	Score	Basis of Decision	Description / Justification
L_W	Loss of water supply.	10	Settlements present with current water supply and demand for water.	Populated areas and places where development (wellfields, etc.) is present.
		5	No settlements; however, a potential for future settlement. Ecosystem (pine forests) reliant on freshwater lens.	Forested, unpopulated areas.
		1	No settlements present; no demand for water supply. Future settlement unlikely; potential reliance on fresh water by ecosystem.	Unpopulated areas, coastal areas with salty wetlands. A value of 1 is used to represent potential impact on ecosystem.

6.3.5. Risk

The risk to water security was determined by multiplying the Total Vulnerability indicator with the Loss indicator according to:

$$\text{Risk} = V_{Total} \times L_W \quad (6.5)$$

The results were then normalised on a 1-10 scale to produce the **Risk to Water Security (R_{WS})** indicator map.

6.4. Results

Figure 6.5 shows the mapped scores for the various susceptibility categories. The intrinsic susceptibility of the aquifer is lowest for the thicker lens in the north and central regions of Andros Island (Figure 6.5a). The smaller, thinner lenses in the southern region correspond to a large area of moderate susceptibility, where the FWL may only provide a small-scale water supply but is likely to be impacted by reductions in recharge. Areas of high intrinsic susceptibility are located along the periphery of the FWL, where the lens is anticipated to be less robust to reductions in recharge based on modeling results. These areas are defined based on projections of climate change up to the year 2100, and therefore, reflect the potential changing conditions of the FWL for a future scenario within this timeframe. Susceptibility related to preferential pathways tends to be limited to small areas surrounding wells within the settled areas and/or near seasonal ponds, which are distributed throughout the island (Figure 6.5b). High susceptibility related to coastal topography is mapped along the southwestern and northern coastlines, reflecting the greater likelihood of inundation occurring because they have low relief (Figure 6.5c). However, high susceptibility related to overall topography (i.e. susceptibility to storm surge) is mapped across much of the island, with only small high topographic areas having low susceptibility along the east coast due to the high elevation of the ridge.

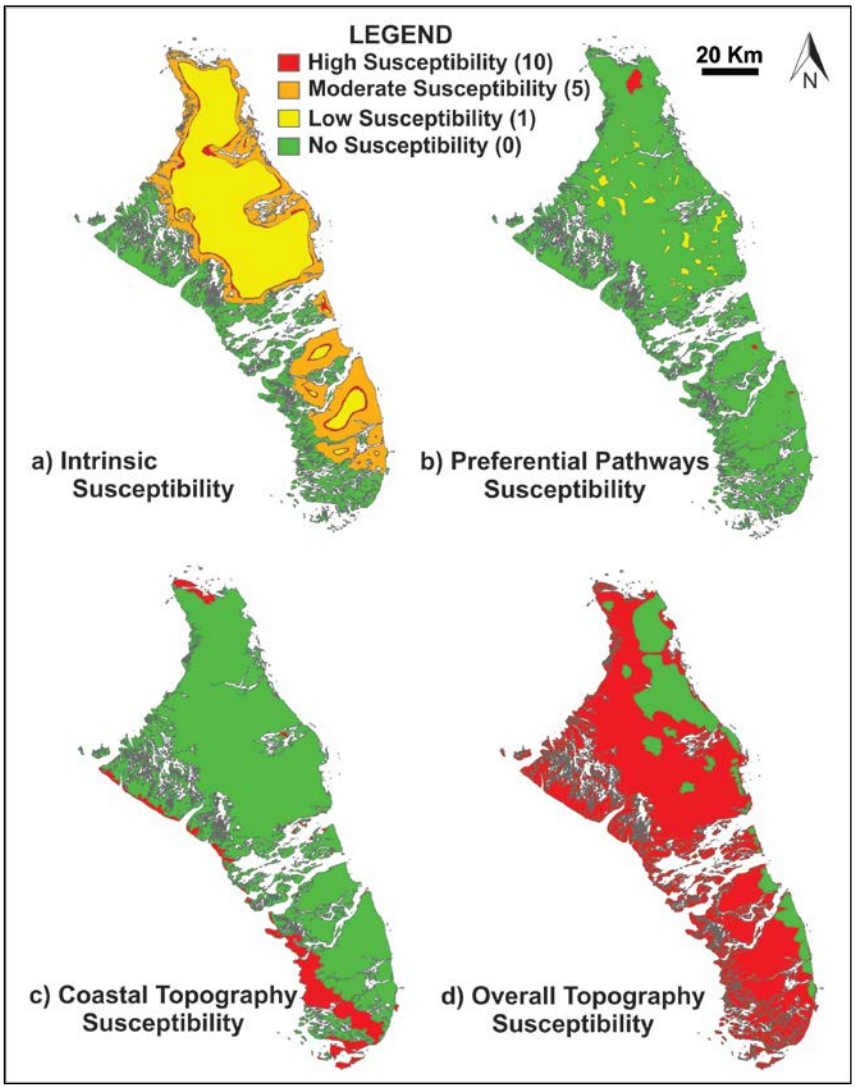

Figure 6.5. Mapped categories of Susceptibility: a) intrinsic; b) preferential pathways; c) coastal topography; and d) overall topography

The four susceptibility category maps combine to produce a Total Susceptibility **(S_{Total})** map (Figure 6.6a). In general, areas of low total susceptibility are present along the eastern coastline. These low susceptibility areas are representative of where low susceptibilities for each of the components coincide, particularly where the intrinsic susceptibility is low due to the presence of a thick FWL, and where susceptibility due to coastal and overall topography are low (i.e. high ground elevation).

Figure 6.6b shows the Hazard Threat from Human Activities **(H_{HA})** indicator map. Due to the large size of the island and dispersed nature of the settlements, inset maps at

a smaller scale are included to show the detail. The highest hazards are those related to chemical storage (particularly fuel), farming and waste disposal (e.g. landfills). However, the occurrence of these hazards is limited to relatively small properties within or near settlements. Hazards related to climate change, such as sea level rise and storm surge, represent a moderate hazard threat relative to that from human activities. The hazard threat indicators represent a relative valuation of the different hazard threat categories, where the hazard threat score is weighted equally in determining the total hazard threat indicator. This approach removes some of the uncertainty in score assignment, as the scores are only assigned on a relative low, moderate and high scale. The assessment framework then provides the relative ranking of the cumulative score for each hazard category.

At an island scale, the total vulnerability (Figure 6.6c) is largely influenced by the susceptibility, which (as mentioned earlier) is generally low in developed areas where hazards threat is high. Therefore, the vulnerability related to human activities is relatively low when viewed at the island scale, but at the local scale near settlements there are areas of high vulnerability related to human activities (not visible on the vulnerability map due to the small-scale of the properties). Although the settlements cover a relatively small proportion of the island, water wells are concentrated in these developed areas. The result is that water supply systems are often in close proximity to areas of high human hazard threat, represented by the small pockets of high vulnerability within the developed areas. Areas of high vulnerability are also focused along the northern and western coastlines, where the island is low-lying, and thus has a high susceptibility to inundation.

The loss **(L_W)** indicator is presented on Figure 6.6d. The spatial distribution of loss is related to the presence of developed areas and the potential for future settlement. Loss is concentrated in currently developed areas where the impact of hazard occurrence would be greatest. The potential for future development is included in the loss indicator, whereby moderate loss represents areas that may support future settlements.

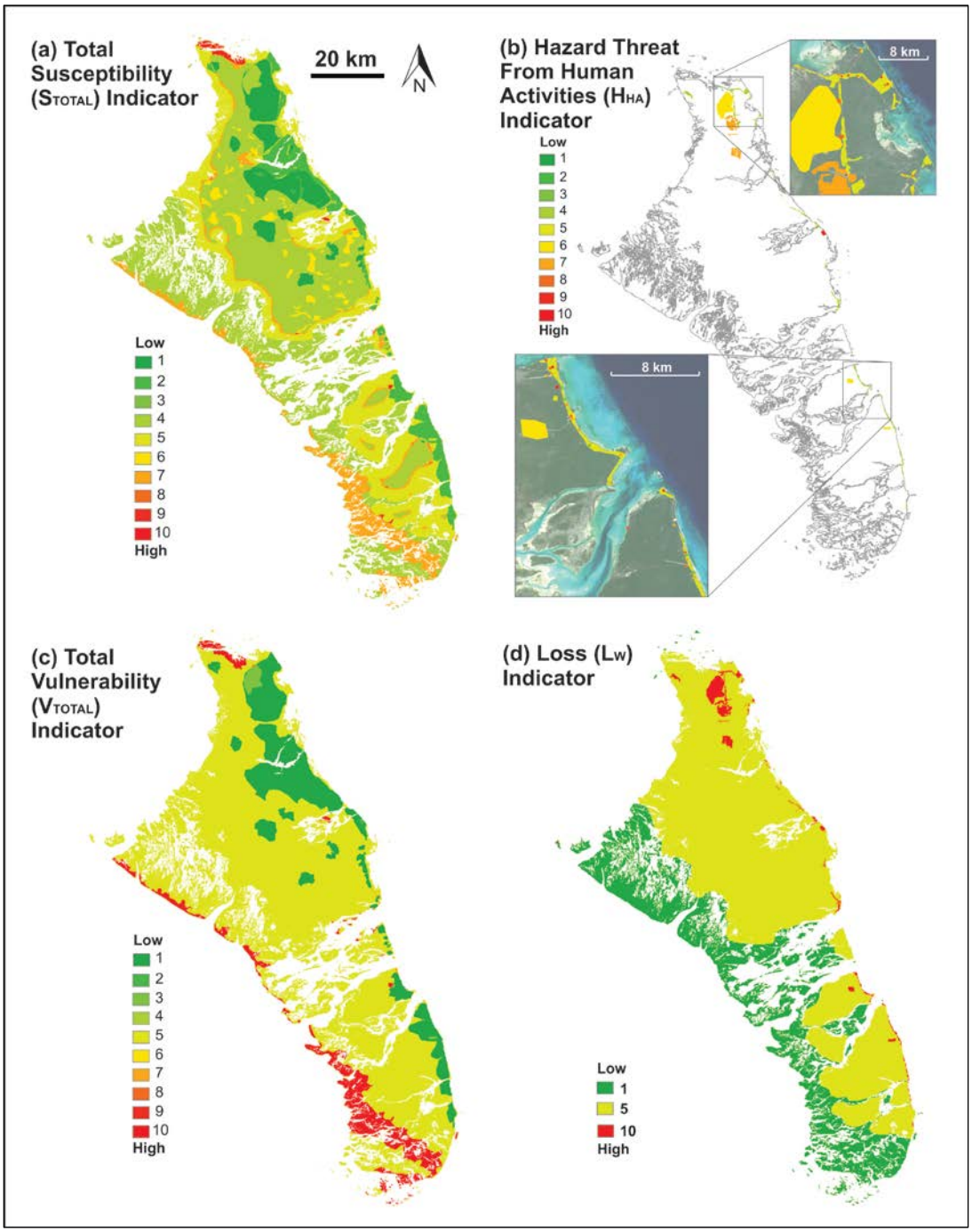

Figure 6.6. **a) Total Susceptibility (S_{Total}) Indicator; b) Hazard Threat from Human Activities (H_{HA}) Indicator; c) Total Vulnerability (V_{Total}) Indicator; d) Loss (L_W) Indicator**

Risk is generally low across the island, partly because loss is concentrated around the settlements and reflects the low population density (Figure 6.7). Although overall risk appears low at an island-scale, there is significant risk within the developed areas, largely related to human activities. In addition, areas of moderate risk, generally related to climate change, are focussed along the coastline near settlements.

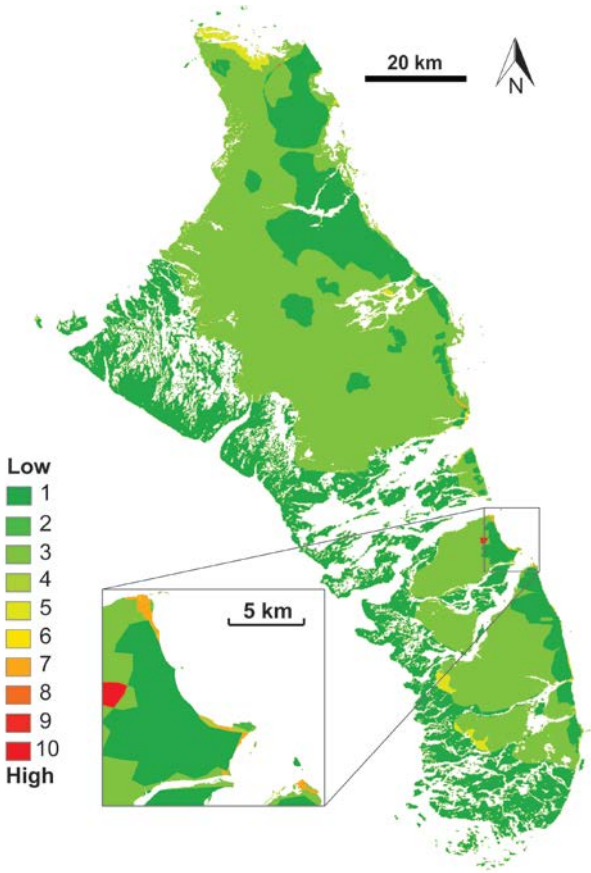

Figure 6.7. Risk Indicator for Andros Island. Most of Andros has low risk to water security. Within the small developed areas (inset map) the risk is significantly higher largely due to human activities

6.5. Discussion

This assessment was performed at an island-scale; however, variability at the local scale is crucial to adequately capture risk to water security for Andros Island because much of the risk is concentrated in developed areas. Water and land use management should consider risk within individual settlements in order to identify

potential source zones or high risk areas of concern. Areas of risk along the coastline near settlements also pose a significant threat to water security. Changing demographic patterns and tourism pressure drives more infrastructure development along the coasts, rather than at the traditional inland locations, on many small islands (Ranjan et al., 2009; Cashman et al., 2010). This concentrates hazards and loss in areas that have high susceptibility, increasing risk to water security. Therefore, risk within developed coastal areas should also be considered at a local scale, and included in future development planning.

The assessment framework is intended to be a generalised tool that can be applied to evaluate water security when datasets are limited, which is often the case for small islands (Cashman et al., 2010; Robins, 2013). Data limitations for this study included a lack of current FWL morphology data and cadastral property maps that delineate property boundaries. These limitations were addressed by using numerical groundwater modeling based on historical FWL morphology data and by estimating property boundaries from aerial photographs alongside the hazard survey data. When applying this assessment framework to other small islands, it is likely that similar data limitations will be encountered. There are several data that are critical in order to effectively utilise this framework, and these data would need to be compiled from existing sources or estimated through modeling. These data include: 1) an estimate of the current FWL morphology (thickness and extent); 2) future climate change and development scenarios for the region; 3) an estimate of FWL response to projected changes in the climate; and 4) a geospatial survey of potentially hazardous land-use activities. If it is not feasible to conduct a dedicated study evaluating the FWL response to changes, it may be possible to estimate the robustness of the lens based on current FWL morphology and expert knowledge. For example, the periphery and thin areas of the FWL are likely to be less robust than the central, thicker areas because there is less freshwater volume present so that even small changes in recharge may result in loss of FWL areal extent. In addition, although this study relied on a hazard survey for each property, it would not be necessary to conduct a survey if the assessment framework is applied to another island. An alternative method would be to obtain the cadastral data, which would provide the geospatial distribution of different property types. With this information (or an estimate of property location and type obtained from another method),

a reasonable estimate of the hazard threat for each property can be assigned based on common land-use practices for each property type. This approach has been successfully employed in other water security risk assessments where it was not reasonable to conduct a door-to-door hazard survey (Simpson et al., 2013).

The determination of the scores and geospatial extent of each area contain elements of uncertainty in the assessment framework. Much of the uncertainty is based on data limitations, the uncertainty associated with the modeling results, and the uncertainty in future events. Within the assessment framework, uncertainty in the data was addressed by using a relative scale. Each indicator was normalised on a 1-10 scale so that the values retain their relative position (i.e. greater or less risk), although the score assigned to a specific area may not be accurate. Modeling uncertainty was addressed by calibrating the model to observed field data to establish a reasonable representation of the hydrogeological system. The model results were also compared to other studies and anticipated response of the FWL to ensure the results were probable and realistic. Uncertainty in future events was addressed by using climate change projections based on an ensemble of 15 different global climate change models (McSweeney et al., 2010). A more comprehensive risk assessment would consider the uncertainty of different potential future scenarios, perhaps using a range of GCMs and emissions scenarios and incorporating probability into the assessment. However, this was outside the scope of this study due to the computational demand involved.

Despite these uncertainties, the resulting risk assessment significantly improves previous understanding of risk to water resources on Andros Island. Climate change contributes substantial uncertainty to risk assessment; however, it is imperative adaptation planning is not neglected, but instead that potential impacts are managed within the limitations imposed by uncertainty (Hallegatte, 2009; IPCC, 2014). An appropriate initial step towards addressing uncertain risk is to undertake “low-regret” or “no-regret” measures, which can provide positive results regardless of the impacts of climate change (Hallegatte, 2009). Some examples include risk communication and education between policy-makers and local citizens, and informed restrictive land-use planning to safeguard resources (Hallegatte, 2009; IPCC, 2012). Identifying risk to water

security allows policy-makers to make informed plans for the future and mitigate potential impacts.

The results of this work were provided to several Bahamian government departments and non-governmental organizations to promote risk communication and education. The Bahamas Ministry of Environment is using the risk assessment results to assist with the management of Andros Island's water resources, as well as in decision-making regarding future development plans for the island which may impact the FWL. The hazard threat assessment was used to tailor educational seminars on Andros Island, conducted by The Nature Conservancy, aimed at raising awareness about water conservation and environmental protection technologies, such as alternative wastewater treatment systems. The Nature Conservancy also presented the results of this work at public events in The Bahamas. The risk assessment for Andros Island is also being used by the Bahamas Environment, Science and Technology Commission to guide scientific research, permitting a focus on studies impacting high risk areas and activities. Lastly, the results of the work are integrated into ongoing projects conducted by the Bahamas National Trust, a non-governmental conservation organisation, which include education activities aimed at promoting better land-use practices around areas of potential risk that may negatively impact the national parks on Andros Island. The impacts of risk identification and communication provided by this study are ongoing and have yet to be determined; however, it is a positive first step towards understanding the risks to water security on Andros Island.

6.6. Conclusions

Freshwater resources on small islands are particularly vulnerable to climate change and human impacts. Therefore, water security assessments that are tailored to the unique aspects of island hydrogeology are critical in order to effectively manage island water resources. The assessment framework outlined in this paper provides a method of incorporating the results from numerical modeling and land-use/hazard surveys into an accessible map format. The maps have provided useful tools for water managers and policy-makers in The Bahamas by identifying high risk areas for near-term action and informing long-term planning. The maps also provide a platform to

engage local residents and raise awareness about the relationship between hazardous land-use activities and the resulting impact on water security. The assessment framework is an adaptive tool that can be refined when additional data become available.

Chapter 7.

Conclusions

This research improves the understanding of the response of small island freshwater lenses (FWLs) to common stressors such as changes in recharge, sea level rise, overwash events, and increases in pumping. It also provides a comprehensive assessment of risk to water security within a small island hydrogeological setting that informs water management and policy development so that it may adapt to future changes. The following sections highlight the major conclusions of this research.

7.1. FWL Response to Climate Change Stressors

The impacts of climate change stressors occur primarily at the periphery of the lens. Here, the FWL is less resilient to stressors because the FWL is thinner. On Andros Island, scenarios of reduced recharge, projected under future climate change due to warmer temperatures and lower precipitation, result in greater loss of freshwater resources (up to 19% volume loss) relative to scenarios of sea level rise (up to 5% volume loss). Recharge is the main driver of lens formation and maintenance, and therefore, has a significant effect on the FWL response to stressors. In addition, Andros Island is a recharge-limited system, such that the FWL is able to rise in the subsurface in response to sea level rise. Other island systems may have larger impacts to the FWL volume if they are topographically-limited, which restricts the upward lens movement in response to sea level rise. Although sea level rise may not have a significant impact on the FWL on Andros Island, it may increase the severity of other events, such as extreme tides and overwash, due to a higher baseline sea level. The response time of the FWL was also found to increase as the magnitude of the stressors increase, resulting in a longer period of adjustment to the new state.

7.2. Human Stressors

Pumping simulations conducted as part of this study showed that when well pumping rates are steadily increased (up to ten times current rates), upconing of the underlying salt water is observed. However, when pumping is stopped, the FWL is generally able to recover with limited residual upconing remaining. Under conditions of reduced recharge and sea level rise, scenarios of increasing pumping result in greater upconing, and larger residual upconing after pumping is stopped. This is in accordance with the previously presented results of simulations of reduced recharge, which indicate that lower recharge environments delay FWL response and recovery to stressors.

7.3. Remedial Action and FWL Recovery from Overwash

Many small islands use shallow, open-trench water supply systems in order to limit upconing that may result from pumping deeper wells. However, trench-based wellfields provide a direct pathway for large saltwater plumes to enter the aquifer following an overwash event. Notwithstanding, wellfields also allow for remedial actions, such as draining the trenches, which can help speed up recovery by removing some of the salt water from the top of the FWL. The recovery of a fresh water source is of critical importance to the local population in a post-storm environment.

The simulations conducted in this study suggest that the trenches should be drained as soon as possible following inundation. There is a limited time frame in which to perform remedial action to remove the salt water before it is transported deeper into the aquifer. When draining was simulated within one day of inundation, recovery time was reduced by up to 30 days. This resulted in the restoration of potable water to the trenches one month sooner than if draining had not been conducted. After a period of delay (4 days on Andros Island), there is little improvement in recovery times of the FWL. While remedial action should be undertaken as soon as possible following an overwash event, draining should only be conducted for a short duration. Longer draining duration (i.e. multiple days) results in delays to recovery because draining of the trenches removes the recharging fresh water, along with the salt water.

7.4. Overwash Impact Factors

On a global scale, the impact of overwash on a small island FWL is based on several factors that affect the response and recovery of the FWL to overwash events. These factors depend on the hydrogeological setting of the island, and include the recharge rate, vadose zone thickness, hydraulic properties, and geologic heterogeneities. The dominant factors affecting the FWL response (i.e. degree of saltwater contamination resulting from an overwash event) are the presence of geological heterogeneities and the thickness of the vadose zone. Horizontally-oriented zones with relatively lower hydraulic conductivity than the principal aquifer may impede saltwater migration from reaching the underlying freshwater. In addition, horizontally-oriented zones with high hydraulic conductivity may channel infiltrating saltwater out of the aquifer quickly, thus limiting saltwater contamination of the FWL. However, vertically-oriented zones with higher relative hydraulic conductivity may transport the saltwater deep into the aquifer. The presence of a thick vadose zone results in a large amount of salt water collected during inundation, which must eventually be flushed out of the subsurface. However, the amount of saltwater entering the subsurface is limited if the vadose zone has a low hydraulic conductivity.

The dominant factor affecting recovery of the FWL (i.e. return to pre-overwash morphology) is the recharge rate. Recharge is the main driver of FWL recovery as it is the mechanism by which the saltwater plume is flushed from the system. Thus, low recharge environments can result in significant delays to FWL recovery. Other important factors affecting the return of potable water are the hydraulic properties of the subsurface and positioning of the water supply infrastructure (i.e. depth of the wells or trenches) relative to geological heterogeneities. When the water supply infrastructure is positioned within a high hydraulic conductivity material, it is likely to recover potable water faster than if it were positioned within a lower hydraulic conductivity material. Therefore, islands with low recharge may still obtain a water supply before the lens has fully recovered. In contrast, if the water supply infrastructure is positioned below a geological heterogeneity that limits recharge from flushing out the saltwater plume (e.g. a low hydraulic conductivity zone), and then return of potable water is likely to be delayed.

7.5. Risk to Water Security

The results of the modeling were integrated into a risk assessment framework resulting in geospatial maps that characterise the susceptibility and hazard threat (vulnerability) and loss (or consequence), leading to a final risk to water security map for Andros Island. Low susceptibility areas were identified where a thick FWL is present and susceptibility to sea level rise and overwash events is low due to topography. These areas also coincide with the location of the majority of settlements on the island, and therefore, the existing communities are well situated to take advantage of natural low susceptibility. However, hazard threat is concentrated within the developed areas, particularly near properties engaged in high hazard activities such as fuel storage, farming, and waste disposal. Additional hazard threat is also identified along the coastlines related to sea level rise and storm surge. Loss, evaluated in terms of access to potable water, is concentrated in the developed areas, with low loss areas along the uninhabitable areas of the island, such as the marshes and wetlands. Although there is low risk to large areas of the island, there are local-scale areas of high risk concentrated within the developed areas that may result in significant impact to water supply. Therefore, risk assessment should be considered at a local-scale to effectively capture potential areas of concern. The water security risk assessment framework developed in this research reflects the unique aspects of island hydrogeology and provides a useful tool to address climate change and human impacts to the freshwater resources of small islands. The results were shared with local partners working in The Bahamas, and formed a platform to inform water management and engage local residents to raise awareness about factors impacting water security.

7.6. Contributions

The main contributions of this research include the following:

1. A risk assessment framework that addresses the unique aspects of island vulnerability and provides quantified risk results at the local level. No water security assessment framework (regardless of whether it addresses risk or not) has been previously developed to address the unique aspects of island vulnerability where

hazards are present along the land surface, as well as along the coastlines and underlying the FWL. Therefore, there was no assessment method to address water security for the small island setting. In addition, the majority of existing water security assessments focus only on the current conditions and do not account for risk to water security for potential consequences under future scenarios. This is an important aspect of policy-planning and effective water governance so that adaptation and management approaches may be designed appropriately for long-term effectiveness (Dunn et al., 2012). Although there is significant uncertainty related to the potential future outcomes of water security, it is critical to engage in adaptation planning, such as risk communication (IPCC, 2014). Communication of risk at the local level equips communities to address water security issues, regardless of the eventual climate change outcomes (Hallegatte, 2009).

2. Insight into the response timeframes of FWL systems to long-acting and short-acting climate stressors. Previous studies have investigated many aspects of major stressors to FWL (e.g. sea level rise, saltwater intrusion, pumping); however, few studies have specifically evaluated the temporal response of the FWL system. Some of the results of this research corroborate previous observations in terms of the critical role of recharge; however, this research also provides new insight into the response timeframes of the FWL as it adjusts or recovers to different climate stressors. For long-acting climate stressors (such as sea level rise or changes in recharge), the response time of the FWL increases as the magnitude of stressors increases so that it takes longer for the FWL to adjust over time. For short-acting climate stressors, the response time of the FWL is affected by the presence of trenches that provide direct access to the FWL. However, the recovery time may be decreased (i.e. faster recovery) through remedial actions, although there is a narrow time period in which these must occur to affect the overall lens recovery.

3. Simulation of overwash using HGS and comparison of the FWL response and recovery for multiple hydrogeological settings. Previous studies have identified some of the critical factors that affect the impact of overwash events on small islands, such as recharge rate, vadose zone thickness, and hydraulic parameters of the aquifer (Illangesekare, 2006; Anderson and Lauer, 2008; Sivakumar and

Elango, 2009; Terry and Falkland, 2010; Chui and Terry, 2012; Terry and Chui, 2012). However, these studies did not compare the effect of the combination of these factors for multiple hydrogeologic settings, as is conducted in this study. As overwash has the potential to seriously damage the freshwater resources of many small islands, assessing the susceptibility to these events is a valuable, though large, undertaking (Walsh et al., 2011). This research provides generalised observations of the FWL response and recovery to overwash for different island settings so that the susceptibility of any given island may be determined based on the results for the corresponding island type. In addition, this research identifies the key role that geological heterogeneities play in influencing the baseline FWL morphology, the degree of contamination (or FWL response) and the recovery of the lens.

7.7. Recommendations for Future Research

Although this research provides important contributions to this field of study, recommendations for further research that may improve or refine this work include the following:

- Improvement of recharge estimates, as recharge is a critical factor affecting FWL response and recovery. The recharge modeling used in this study may overestimate recharge by not accounting for high intensity rainfall events. As intense rainfall events are common in the Tropics, a study that looks at how recharge is affected by these events would be beneficial to assessing the reliability of this recharge modeling approach for tropical areas. Additionally, as extreme rainfall events may increase in the future with climate change, this would contribute to an understanding of the impacts to freshwater resources overall.
- Use of downscaled climate change projections for the local scale. The results of the ensemble of GCMs used in this study were available as raw data, mapped on a smaller grid size. This approach is based on the coarse spatial resolution of the GCMs and is likely to neglect local-scale variability. Therefore, using downscaled data from the GCMs would provide climate change projections more specific, and potentially more accurate, to Andros Island.

- Evaluation of the impact of overwash for complex island types that combine multiple hydrogeological settings. Some islands combine multiple hydrogeologic settings (such as low-lying limestone surrounding old volcanic) which may affect the FWL response and recovery to overwash events. Simulations that include combination island types could identify how these settings might affect overwash impact.
- Combining the generalised analysis of overwash impacts based on island type with an analysis of climatic variations worldwide to provide a global risk to overwash assessment. The observations from this study assist in the assessment of island susceptibility. Using data that characterises the current tidal variations and overlaying projections for sea level rise and extreme tide events would result in a hazard characterisation for overwash. Loss areas could be mapped out based on populated areas. In this way, a generalised assessment of risk to overwash for small islands may be developed, which would be particularly helpful in areas that lack field data to conduct island-specific assessments.
- Application of the risk to water security assessment framework to other small islands to test the transferability of the framework. The intention of developing this assessment framework was to provide a tool that could be applied to other islands. However, as the framework is specific to Andros Island, adjustments and assumptions would need to be made to apply it to other islands. The feasibility of applying the framework to other islands could be tested on several different island types to assess any limitations of the framework scoring and setup to capturing water security issues on other islands.

References

Adger, W.N. (2006), Vulnerability, Global Environmental Change, 16, 268-281.

Adger, W.N., K. Brown, D.R. Nelson, F. Berkes, H. Eakin, C. Folke, K. Galvin, L. Gunderson, M. Goulden, K. O'Brien, J. Ruitenbeek, and E. Tompkins (2011), Resilience implications of policy responses to climate change, WIREs Climate Change, 2, 757-766.

Allen, D.M., A.J. Cannon., M.W. Toews and J. Scibek (2010), Variability in simulated recharge using different GCMs, Water Resources Research, 46, W00F03.

Aller, L.T., T. Bennet, J.H. Lehr, R.J. Petty and G. Hackett (1987), DRASTIC. A Standardized System for Evaluating Ground Water Pollution Potential Using Hydrogeologic Settings, U.S. Environmental Protection Agency / 600/2-87/035. Washington, D.C. p 455.

Anderson, W.P. Jr. (2002), Aquifer salinization from storm overwash, Journal of Coastal Research., 18 (3), 413-420.

Anderson, M.P. and W.W.Woessner (1992), Applied groundwater modeling: simulation of flow and advective transport, Academic Press, San Diego, California, USA.

Angeles, M. E., J.E. Gonzalez, D.J. Erickson III and J.L. Hernandez (2007), Predictions of future climate change in the Caribbean region using global general circulation models, Int. J. Climatol., 27 (5), 555-569.

Aquanty (2013), HydroGeoSphere User Manual, Release 1.0, Aquanty Inc., Waterloo, Canada.

Ayers, J.F., and H.L. Vacher (1986), Hydrogeology of an atoll island: A conceptual model from detailed study of a Micronesian example, Ground Water, 24, 185-198.

Bakker, K. (2012), Water security: Research challenges and opportunities. Science, 337(6097), 914-915.

Banerjee, P., and V.S. Singh (2011), Optimization of pumping rate and recharge through numerical modeling with special reference to small coral island aquifer, Physics and Chemistry of the Earth, 36 (16), 1363-1372.

Barlow, P.M. (2003) Ground Water in Freshwater-Saltwater Environments of the Atlantic Coast, U.S. Department of the Interior, U.S. Geological Survey, Circular 1262, Reston, Virginia, USA.

Barnett, J., S. Lambert, and I. Fry (2008), The hazards of indicators: insights from the environmental vulnerability index, Annals of the Association of American Geographers, 98, 102-119.

Bates, B.C., Z.W. Kundzewicz, S. Wu, and J.P. Palutikof (Eds.) (2008), Climate Change and Water. Technical Paper of the Intergovernmental Panel on Climate Change, IPCC Secretariat, Geneva, 210 pp.

Beach, D.K., and R.N. Ginsburg (1980), Facies succession of Pliocene-Pleistocene carbonates, northwestern Great Bahama Bank, AAPG Bull. -Am. Assoc. Petr. Geol., 64(10), 1634-1642.

Bear, J., A.H.D. Cheng, S. Sorek, I. Herrera and D. Ouazar (Eds.) (1999), Seawater Intrusion in Coastal Aquifers, Kluwer Academic Publishers, Dordrecht, The Netherlands.

Ataie-Ashtiani, B., A.D. Werner, C.T. Simmons, L.K. Morgan and C. Lu (2013), How important is the impact of land-surface inundation on seawater intrusion caused by sea-level rise?, Hydrogeology Journal, 21, 1673-1677.

Biasutti, M., A.H. Sobel, S.J. Camargo, and T.T. Creyts, (2012). Projected changes in the physical climate of the gulf coast and caribbean. Climatic Change, 112(3-4), 819-845.

Birkmann, J. (2006), Measuring vulnerability to promote disaster resilient societies: Conceptual frameworks and definitions. In: Birkmann, J. (ed.) Measuring vulnerability to natural hazards: towards disaster resilient societies. United Nations University Press, Tokyo, pp 9–54.

Boardman, M.R., and C. Carney (1997), Influence of sea level on the origin and diagenesis of the shallow aquifer of Andros Island, Bahamas, in Carew, J.L., (Ed.), Proceedings of the Eighth Symposium on the Geology of the Bahamas, Bahamian Field Station, San Salvador, Bahamas, 13-32.

Bobba, A.G. (2002), Numerical modeling of salt-water intrusion due to human activities and sea-level change in the Godavari Delta, India, Hydrological Sciences Journal, 47, 67-80.

Bowleg, J. and D.M. Allen (2011). Effects of storm surges on groundwater resources, North Andros Island, Bahamas. In: Treidgel H, Martin-Bordes JL and Gurdak JJ (Eds.). Climate Change Effects on Groundwater Resources: A Global Synthesis of Findings and Recommendations. IAH International Contributions to Hydrogeology, CRC Press.

Bricker, S.H. (2007), Impacts of climate change on small island hydrogeology - a literature review. British Geological Survey Internal Report, OR/09/025. 28 pp.

Bukowski, J.M., C. Carney, R.W. Jr. Ritzi and M.R. Boardman (1999) Modeling the fresh-salt water interface in the Pleistocene aquifer on Andros Island, Bahamas, in Curran, H.A., and J.E. Mylroie (Eds.), Proceedings of the Ninth Symposium on the Geology of the Bahamas, Bahamian Field Station, San Salvador, Bahamas, 1-13.

Cant, R.V. and P.S. Weech (1986) A review of the factors affecting the development of Ghyben-Herzberg lenses in the Bahamas, Journal of Hydrology, 84, 333-343.

Carreira, P.M., J.M., Marques, D. Nunes, F.A. Monteiro Santos, R. Gonçalves, A.Pina, and A.M. Gomes (2013), Isotopic and geochemical tracers in the evaluation of groundwater residence time and salinization problems at Santiago Island, Cape Verde, Procedia Earth and Planetary Science, 7, 113-117.

Cashman, A., L. Nurse, and J. Charlery (2010), Climate change in the Caribbean: the water management implications, The Journal of Environment and Development 19(1), 42-67.

Christensen, J.H., Hewitson, B., Busuioc, A., Chen, A., Gao, X., Held, I., Jones, R., Koli, R.K., Kwon, W.T., Laprise, R., Rueda, V.M., Mearns, L., Menéndez, C.G., Räisänen, J., Rinke, A., Sarr, A. and Whetton, P. (2007). Regional climate projections. Climate Change 2007: The Physical Science Basis. In: Solomon, S., Qin, D., Manning, M., Chen, Z., Marquis, M., Averyt, K.B., Tignor, M. and Miller, H.L. (Eds.). Contribution of Working Group I to the Fourth Assessment Report of the Intergovernmental Panel on Climate Change, Cambridge University Press, Cambridge, p. 847-940.

Chui, T. F. M., and J.P. Terry (2012) Modeling fresh water lens damage and recovery on atolls after storm-wave washover. Ground Water, 50(3), 412-420

Chui, T.F. and J.P. Terry (2013), Influence of sea-level rise on freshwater lenses of different atoll island sizes and lens resilience to storm-induced salinization, Journal of Hydrology, 502, 18-26.

Civita, M. and M. De Maio (1997), SINTACS - A parametric system for the assessment and cartography of the assessment of groundwater vulnerability to pollution, Metodologia e automazione, Pitagora Ed., Bologna.

Contractor, D.N. and J.W. Jenson (2000), Simulated effect of vadose infiltration on water levels in the Northern Guam Lens Aquifer, Journal of Hydrology, 229, 232-254.

Cook, C. and K. Bakker (2012), Water security: Debating an emerging paradigm, Global Environmental Change-Human and Policy Dimensions 22(1), 94-102.

DHI-WASY GmbH, (2010), FEFLOW 6.0, Finite element subsurface flow and transport simulation system.

Doerfliger, N. and F. Zwahlen (1997), EPIK: new method for outlining of protection areas in karstic environments. EC International Symposium, Karst Water and Environment Impacts, Antalaya, Turkey, Balkema, Rotterdam, The Netherlands, pp 117–123.

Döll, P. (2009), Vulnerability to the impact of climate change on renewable groundwater resources: A global-scale assessment, Environmental Research Letters, 4(3).

Dunn, G. and K. Bakker (2011), Fresh water-related indicators in Canada: an inventory and analysis, Canadian Water Resources Journal, 36 (2), 135-148.

Dunn, G., C. Cook, K. Bakker and D. Allen (2012), Water Security Guidance Document: Part 1, Section 1: Defining and Assessing Water Security http://watergovernance.ca

Environ (2010), Water conservation strategy and assessment of technologies for Andros Island, The Bahamas. Report Prepared by: ENVIRON International Corporation, Washington, DC, Project 0125334A.

Environ (2013), Water management plan, Andros Island, The Bahamas. Report Prepared by: ENVIRON International Corporation, Boca Raton, Florida, USA, Project 01-31058A.

Falkenmark, M. (1999), Forward to the future: A conceptual framework for water dependence, Ambio, 28(4), 356-361.

Falkenmark, M., A. Berntell, A. Jägerskog, J. Lundqvist, M. Matz, and H. Tropp (2007), On the verge of a new water scarcity: a call for good governance and human ingenuity, Stockholm International Water Institute Policy Brief.

Falkland, A. (Ed.) (1991), Hydrology and water resources of small island: a practical guide, United Nations Educational, Scientific, and Cultural Organization (UNESCO), Paris.

Foster, S.S.D. and R.C.A. Hirata (1988), Groundwater pollution risk evaluation: the methodology using available data, WHO-PAHO/HPE-CEPIS Technical Manual, Lima, Peru p 78.

Franklin, J., R. Pasch, L. Avila, J. Beven, M. Lawrence, S. Stewart, and E. Blake (2006). Atlantic hurricane season of 2004. Monthly Weather Review, 134(3): 981-1025.

Freeze, R.A., and J.A. Cherry (1977), Groundwater, Prentice-Hall, Upper Saddle River, NJ, USA.

Gamble, D.W. and R.D. Jordan (2006). Spatial variability of precipitation on San Salvador, Bahamas 2001-2003. In: Davis, R.L. and Gamble, D.W. (Eds.). Proceedings of the Twelfth Symposium on the Geology of the Bahamas and Other Carbonate Regions, Gerace Research Center, San Salvador, Bahamas, p.52-60.

Ghassemi, F., J. Molson, A. Falkland and K. Alam (1999), Three-dimensional simulation of the home island freshwater lens: preliminary results, Environmental Modeling and Software, 14 (2-3), 181-190.

Global Water Partnership (GWP) 2000. Towards Water Security: A Framework for Action. GWP, Stockholm.

Goderniaux, P., S. Brouyere, H.J. Fowler, S. Blenkinsop, R. Therrien, P. Orban, and A. Dassargues (2009), Large scale surface-subsurface hydrological model to assess climate change impacts on groundwater reserves. Journal of Hydrology, 373(1-2), 122-138.

Goderniaux, P., Brouyere, S., Blenkinsop, S., Burton, A., Fowler, H. J., Orban, P., et al. (2011), Modeling climate change impacts on groundwater resources using transient stochastic climatic scenarios, Water Resources Research, 47, W12516.

Greaver, T.L. and L.S.L. Sternberg (2010), Decreased precipitation exacerbates the effects of sea level on coastal dune ecosystems in open ocean islands, Global Change Biology, 16(6), 1860-1869.

Green, T. R., M. Taniguchi, H. Kooi, J.J. Gurdak, D.M. Allen, K.M. Hiscock, and A. Aureli (2011), Beneath the surface of global change: Impacts of climate change on groundwater, Journal of Hydrology, 405(3-4): 532-560.

Grey, D. and C.W. Sadoff (2007), Sink or swim? Water security for growth and development, The World Bank, Water Policy 9, 545-571.

Guo, W. and C.D. Langevin (2002), User's guide to SEAWAT: A computer program for simulation of three-dimensional variable-density ground-water flow, U.S. Geological Survey Techniques and Methods Book 6, Chapter A7, Florida, USA.

Hagedorn, C., E.L. McCoy, and T.M. Rahe (1981), The potential for groundwater contamination from septic effluents, Journal of Environmental Quality, 10, 1-8.

Hallegate, S. (2009), Strategies to adapt to an uncertain climate change, Global Environmental Change 19, 240-247.

Holding, S.T., and D.M. Allen (2014), Responses to Climate Change and Development Stressors on Small Oceanic Islands, 23rd Salt Water intrusion Meeting, Conference Proceedings, June 16-20, 2014, Husum, Germany.

Holman, I. P. (2006), Climate change impacts on groundwater recharge-uncertainty, shortcomings, and the way forward? Hydrogeology Journal, 14(5): 637-647.

Holman, I. P., D.M. Allen, M.O. Cuthbert, and P. Goderniaux (2012), Towards best practice for assessing the impacts of climate change on groundwater. Hydrogeology Journal, 20(1), 1-4.

Illangasekare, T., et al. (2006), Impacts of the 2004 tsunami on groundwater resources in Sri Lanka, Water Resources Research, 42, W05201.

IPCC (Inter-Governmental Panel on Climate Change) (1990). First Assessment Report (FAR).

IPCC (1995) Second Assessment Report (SAR).

IPCC (2001) Third Assessment Report (TAR).

IPCC (2007), Climate Change 2007: The Physical Science Basis. S. Solomon, D. Qun, M. Manning, Z. Chen, M. Marquis, K.B. Averyt, M. Tignor and H.L. Miller (Eds.). Contribution of Working Group I to the Fourth Assessment Report of the Intergovernmental Panel on Climate Change, Cambridge University Press, Cambridge, UK

IPCC (2012). Managing the Risks of Extreme Events and Disasters to Advance Climate Change Adaptation. A Special Report of Working Groups I and II of the Intergovernmental Panel on Climate Change [Field, C.B., V. Barros, T.F. Stocker, D. Qin, D.J. Dokken, K.L. Ebi, M.D. Mastrandrea, K.J. Mach, G.-K. Plattner, S.K. Allen, M. Tignor, and P.M. Midgley (eds.)]. Cambridge University Press, Cambridge, UK, and New York, NY, USA, 582 pp.

IPCC (2013). Climate Change 2013: The Physical Science Basis. Contribution of Working Group I to the Fifth Assessment Report of the Intergovernmental Panel on Climate Change [Stocker, T.F., D. Qin, G.-K. Plattner, M. Tignor, S.K. Allen, J. Boschung, A. Nauels, Y. Xia, V. Bex and P.M. Midgley (eds.)]. Cambridge University Press, Cambridge, United Kingdom and New York, NY, USA.

IPCC (2014). Climate Change 2014: Impacts, Adaptation, and Vulnerability. Part B: Regional Aspects. Contribution of Working Group II to the Fifth Assessment Report of the Intergovernmental Panel on Climate Change [Barros, V.R., C.B. Field, D.J. Dokken, M.D. Mastrandrea, K.J. Mach, T.E. Bilir, M. Chatterjee, K.L. Ebi, Y.O. Estrada, R.C. Genova, B. Girma, E.S. Kissel, A.N. Levy, S. MacCracken, P.R. Mastrandrea, and L.L. White (eds.)]. Cambridge University Press, Cambridge, United Kingdom and New York, NY, USA.

Irish, J. L., D.T. Resio, and J.J. Ratcliff (2008). The influence of storm size on hurricane surge, Journal of Physical Oceanography, v.38(9), p.2003-2013.

IWCAM (2011), Andros Land and Sea Use Plan, Integrating Watershed and Coastal Areas Management, Andros Island, The Bahamas.

Jakovovic, D., A.D. Werner and C.T. Simmons (2011), Numerical modeling of saltwater up-coning: Comparison with experimental laboratory observations, Journal of Hydrology,402, 261-273.

Jelesnianski, C.P., J. Chen, W.A. Shaffer, and A.J. Gilad (1984), SLOSH – A hurricane storm surge forecast model, Oceans1984, 314-317.

Jyrkama, M.I., and J.F. Sykes (2007), The impact of climate change on spatially varying groundwater recharge in the grand river watershed (Ontario), Journal of Hydrology, 338, 237-250.

Knutson, T.R., J.L. McBride, J. Chan, K. Emanuel, G. Holland, C. Landsea, I. Held, J.P. Kossin, A.K. Srivastava and M. Sugi (2010), Tropical cyclones and climate change, Nature Geoscience 3, 157-163.

Kohout, F. (1960), Cyclic flow of salt water in the biscayne aquifer of southeastern florida, Journal of Geophysical Research, 65(7), 2133-2141.

Konikow, L. F. (2011), The secret to successful solute-transport modeling, Ground Water, 49 (2), 144-159.

Langevin, C.D., D.T. Thorne Jr., A.M. Dausman, M.C. Sukop, and W. Guo (2007), SEAWAT Version 4: A Computer Program for Simulation of Multi-Species Solute and Heat Transport: U.S. Geological Survey Techniques and Methods Book 6, Chapter A22, 39 p.

Langevin, C.D. and M. Zygnerski (2013), Effect of sea-level rise on salt water intrusion near coastal well field in southeastern Florida, Ground Water, 51(5), 781-803.

Lautze, J. and H. Manthrithilake (2012), Water Security: Old concepts, new package, what value? Natural Resources Forum 36, 76-87.

Liggett, J.E., and D.M. Allen (2010), Comparing approaches for modeling spatially distributed direct recharge in a semi-arid region (Okanagan Basin, Canada), Hydrogeology Journal, 18, 339-357.

Liggett, J.E., A.D. Werner, and C.T. Simmons (2012), Influence of the first-order exchange coefficient on simulation of coupled surface-subsurface flow, Journal of Hydrology, 414-415, 503-515.

Little, B.G., D.K. Buckley, A. Jefferiss, J. Stark and R.N. Young (1973), Land resources of the commonwealth of the Bahamas, Volume 4 Andros Island, Land Resources Division, Tolworth Tower, Surrey, UK.

Lugo, A.E. (2000). Effects and outcomes of Caribbean hurricanes in a climate change scenario. The Science of the Total Environment, 262: 243-251.

Masterson, J.P. and S.P. Garabedian (2007), Effects of sea-level rise on ground water flow in a coastal aquifer system, Ground Water, 45(2), 209-217.

McCarthy, J.J., O. Canziani, N.A. Leary, D.J. Dokken, and K.S. White (Eds.) (2001), Climate Change 2001: Impacts, Adaptation and Vulnerability, IPCC Working Group II, Cambridge University Press, Cambridge.

MCK Environmental Ltd. (2013), Blue Water Project Community Surveys, The Nature Conservancy Northern Caribbean Office Report, June 2013, 320 pp.

McSweeney, C., M. New, G. Lizcano and X. Lu (2010). The UNDP Climate Change Country Profiles, Bull. Am. Met. Soc., 91, 157-166.

Meyssignac, B., D. Salas y Melia, M. Becker, W. Llovel, and A. Cazenave (2012), Tropical Pacific spatial trend patterns in observed sea level: internal variability and/or antropogenic signature? Climate of the Past, 8, 787-802.

Michael, H.A., C.J. Russoniello and L.A. Byron (2013), Global assessment of vulnerability to sea-level rise in topography-limited and recharge-limited coastal groundwater systems, Water Resources Research, 49 (4), 2228-2240.

Mollema, P.N., and M. Antonellini (2013), Seasonal variation in natural recharge of coastal aquifers, Hydrogeology Journal, 21, 787-797.

Momi, K., J. Shoji and K. Nakagawa (2005), Observations and modeling of seawater intrusion for a small limestone island aquifer, Hydrological Processes, 19, 3897-3909.

NOAA (2014a). http://www.nhc.noaa.gov/ [accessed on June 10, 2014]

NOAA (2014b). http://www.nws.noaa.gov/om/hurricane/resources/surge_intro.pdf [accessed on June 10, 2014]

Norman, E., G. Dunn, K. Bakker, D. Allen and dA. Cavalcanti (2013), Water security assessment: Integrating governance and freshwater indicators, Water Resources Management 27(2), 535-551.

Nunn, P.D. (2009), Responding to the challenges of climate change in the Pacific Islands: management and technological imperatives, Climate Research 40, 211-231.

Obeysekera J., J. Park, M. Irizarry-Ortiz, J. Barnes and P. Trimble (2013), Probabilistic projection of mean sea level and coastal extremes, Journal of Waterway, Port, Coastal, and Ocean Engineering 139 (2), 135-141.

Oude Essink, G.H.P. (2001), Improving fresh groundwater supply – problems and solutions, Ocean and Coastal Management, 44, 429-449.

Palanisamy, H., M. Becker, B. Meyssignac, O. Henry, and A. Cazenave (2012), Regional sea level change and variability in the Caribbean sea since 1950. Journal of Geodetic Science. 2(2), 125–133.

Rahmstorf, S. (2007), A semi-empirical approach to projecting future sea-level rise, Science, 315, 368-370.

Ranjan, P., S. Kazama, M. Sawamoto and A. Sana (2009), Global scale evaluation of coastal fresh groundwater resources, Ocean and Coastal Management, 52, 197-206.

Rasmussen, P, T.O. Sonnenborg, G. Goncear and K. Hinsby (2013), Assessing impacts of climate change, sea level rise, and drainage canals on saltwater intrusion to coastal aquifer, Hydrology and Earth System Sciences, 17, 421-443.

Richardson, C.W., and D.A. Wright (1984), WGEN: a model for generating daily weather variables, ARS-8, Agricultural Research Service, USDA, 83 pp.

Ritzi, R., J. Bukowski, C. Carney and M. Boardman (2001), Explaining the thinness of the fresh water lens in the Pleistocene carbonate aquifer on Andros Island, Bahamas, Ground Water, 39 (5), 713-720.

Robins, N., and A. Lawrence (2000), Some hydrogeological problems peculiar to various types of small islands, Water and Environment Journal, 14 (5), 341-346.

Robins, N.S. (2013), A review of small island hydrogeology: progress (and setbacks) during the recent past, Quarterly Journal of Engineering Geology and Hydrogeology 46,157-165.

Rockström, J., M. Lannerstad, and M. Falkenmark (2007), Assessing the water challenge of a new green revolution in developing countries, Proceedings of the National Academy of Sciences of the USA, 104(15), 6253-6260.

Rolle, A. (1990), A Storm Surge Atlas for the Northern and Central Bahamas, National Weather Service of the Bahamas and Storm Surge Group, National Hurricane Center, NOAA, Florida.

Scanlon, B.R., R.W. Healy and P.G. Cook (2002), Choosing appropriate techniques for quantifying groundwater recharge, Hydrogeology Journal, 10 (2), 18-39.

Schaap, M.G., F.J. Leij, M.T. van Genuchten (2001), ROSETTA: a computer program for estimating soil hydraulic parameters with hierarchical pedotransfer function, Journal of Hydrology, 251, 163-176.

Schneider, J., and S. Kruse (2003), A comparison of controls on freshwater lens morphology of small carbonate and siliciclastic islands: Examples from barrier islands in Florida, USA, Journal of Hydrology, 284 (1-4), 253-269.

Schneider, J., and S. Kruse (2005), Assessing selected natural and anthropogenic impacts on freshwater lens morphology on small barrier islands: Dog Island and St. George Island, Florida, USA, Hydrogeology Journal, 14 (1-2), 131-145.

Schroeder, P.R., T.S. Dozier, P.A. Zappi, B.M. McEnroe, J.W. Sjostrom and R.L. Peyton (1994), The Hydrologic Evaluation of Landfill Performance (HELP) model: Engineering documentation for Version 3, Rep. EPA/600/R-94/168b, U.S. Environmental Protection Agency, Washington, D.C., USA.

Scibek, J., and D.M. Allen (2006), Modeled impacts of predicted climate change on recharge and groundwater levels, Water Resources Research, 42 (11), W11405.

Simpson, M.W.M., D.M. Allen, and M.M. Journeay (2013), Assessing risk to groundwater quality using an integrated risk framework, Environmental Earth Science.

Singh, B. (1997). Climate changes in the greater and southern Caribbean. International Journal of Climatology, 17, 1093-1114.

Singh, V., and C. Gupta (1999), Feasibility of groundwater withdrawal in a coral island, Hydrological Sciences Journal-Journal Des Sciences Hydrologiques, 44(2), 173-182.

Sivakumar, C., and L. Elango (2010), Application of solute transport modeling to study tsunami induced aquifer salinity in India. Journal of Environmental Informatics, 15(1), 33-41.

Stoeckl, L., and G. Houben (2012), Flow dynamics and age stratification of freshwater lenses: Experiments and modeling, Journal of Hydrology, 458, 9-15.

Sullivan, C., J. Meigh, A. Giacomello, T. Fediw, P. Lawrence, M. Samad, M., et al. (2003), The water poverty index: Development and application at the community scale, Natural Resources Forum, 27(3), 189-199.

Sulzbacher, H., H. Wiederhold, B. Siemon, M. Grinat, J. Igel, T. Burschil, T. Günther and K. Hinsby (2012), Numerical modeling of climate change impacts on freshwater lenses on the North Sea Island of Borkum using hydrological and geophysical methods, Hydrology and Earth System Science, 16 (10), 3621-3643.

Tarbox, K.L. (1987), Occurrence and development of water resources in The Bahamas, in H.A. Curran (Ed.), Proceedings of the Third Symposium on the Geology of the Bahamas, Bahamian Field Station, San Salvador, Bahamas, 139-144.

Taylor R.G., B. Scanlon, P. Döll, M. Rodell, R. van Beek, Y. Wada et al. (2013), Ground water and climate change, Nature Climate Change 3, 322 – 329.

Terry, J.P., and Falkland, A.C. (2010) Responses of atoll freshwater lenses to storm-surge overwash in the Northern Cook Islands, Hydrogeology Journal, 18, 749-759.

Terry, J. P., and Chui, T. F. M. (2012), Evaluating the fate of freshwater lenses on atoll islands after eustatic sea-level rise and cyclone-driven inundation: A modeling approach, Global and Planetary Change, 88-89, 76-84.

Therrien, R., R. McLaren, E. Sudicky, and S. Panday (2010), HydroGeoSphere – A three-dimensional numerical model describing fully-integrated subsurface and surface flow and solute transport, University of Waterloo and Université Laval, Canada.

TNC (The Nature Conservancy) (2011). Andros Land and Sea Use Plan. Global Environment Facility (GEF) funded IWCAM (Integrated Watershed and Coastal Areas Management) project for Caribbean Small Island Developing States.

Toews, M.W., and D.M. Allen (2009), Evaluating different GCMs for predicting spatial recharge in an irrigated arid region, Journal of Hydrology, 374, 265-281.

UNDP (United Nations Development Programme) (2010), Climate Change Country Profiles, The Bahamas.

UNESCO GRAPHIC (Groundwater Resources Assessment under the Pressures of Humanity and Climate Change) (2008) Concept Note: Understanding Climate Change and Linked Human Impacts on Groundwater Resources of the Caribbean Region: Collaborative GRAPHIC Case Study in Bahamas.

UNESCO-IHP (2012), Final Report. 20th Session of the Intergovernmental Council. Paris, 4-7 June, 2012. Paris, France: UNESCO.

USEPA - US Environmental Protection Agency (2004), Potential sources of drinking water contamination index. http://water.epa.gov/drink/contaminants/. Accessed May 2013.

Vacher, H.L. (1988), Dupuit-Ghyben-Herzberg analysis of strip-island lenses, Bulletin of the Geological Society of America, 100, 580-591, doi: 10.1130/0016-7606.

Vacher, L.H., and T.M. Quinn (Eds.), (1997), Geology and hydrogeology of carbonate island, Developments in Sedimentology Vol. 54, Elsevier, Tampa Bay, Florida, USA.

van Genuchten, M.T. (1980), A closed-form equation for predicting the hydraulic conductivity of unsaturated soils, Soil Science Society of America Journal, 44(5), 892-898.

van Leeuwen, C.J., J. Frijns, A. van Wezel, and F.H.M. van de Ven (2012), City Blueprints: 24 indicators to assess the sustainability of the urban water cycle, Water Resources Management 26, 2177 – 2197.

van Stempvoort D., D. Ewert and L. Wassenaar (1992), AVI: A Method for Groundwater Protection Mapping in the Prairie Provinces of Canada. PPWD pilot project, Sept. 1991 - March 1992. Groundwater and Contaminants Project, Environmental Sciences Division, National Hydrology Research Institute, Saskatoon.

Voss, C.I. and A.M. Provost (2008), SUTRA, a model for saturated-unsaturated variable density ground-water flow with solute or energy transport, U.S. Geological Survey Water-Resources Investigations Report 02-4231, Virginia, 270 pp.

Wallis, T.N., H.L. Vacher and M.T. Stewart (1991), Hydrogeology of freshwater lens beneath a Holocene strandplain, Great Exuma, Bahamas, Journal of Hydrology, 125, 93-109.

Walsh, K.J.E., K.L. McInnes, and J.L. McBride (2012), Climate change impacts on tropical cyclones and extreme sea levels in the South Pacific — A regional assessment, Global and Planetary Change*,* 80–81, 149-164.

Werner, A.D., and C.T. Simmons (2009), Impact of sea-level rise on sea water intrusion in coastal aquifers, Ground Water, 47, 197-204.

Werner, A.D., D. Jakovovic and C.T. Simmons (2009), Experimental observations of saltwater up-coning, Journal of Hydrology, 373, 230-241.

Whitaker, F., and P. Smart (1997). Climatic control of hydraulic conductivity of Bahamian limestones. Ground Water, 35(5), 859-868.

White, N.J., J.A. Church and J.M. Gregory (2005), Coastal and global averaged sea level rise for 1950 to 2000, Geophysical Research Letters, 32, L01601.

White, I. and A. Falkland (2010), Management of freshwater lenses on small Pacific islands, Journal of Hydrogeology 18,227-246.

Wolfe, P.J., A.L. Adams and C.K. Carney (2001), A resistivity study of the freshwater lens profile across North Andros Island, The Bahamas, in Greenstein, B.J., and C.K. Carney (Eds.), Proceedings of the Tenth Symposium on the Geology of the Bahamas and Other Carbonate Regions, Gerace Research Center, San Salvador, Bahamas, 31-40.

WHO (World Health Organisation) (2011), Guidelines for drinking-water quality, 4th Edition.

Yang, J., T. Graf, M. Herold, and T. Ptak (2013), modeling the effects of tides and storm surges on coastal aquifers using a coupled surface-subsurface approach, Journal of Contaminant Hydrology, 149, 61-75.

Younger, P.L. (1993), Simple generalised methods for estimating aquifer storage parameters, Quarterly Journal of Engineering Geology and Hydrogeology, 26, 127-135.

Zwahlen, F. (2004), Vulnerability and Risk Mapping for the Protection of Carbonate (Karstic) Aquifers, Final report COST action 620. European Commission Directorate - General for Research, Brussels, Luxemburg.

Appendix A.

Background Data

The following tables (A1 to A3) present pre-existing data for Andros Island used in this research. Table A1 presents borehole data; Table A2 presents the hazard survey form; and Table A3 presents the hazard survey results.

Table A1. Baseline borehole data

Borehole ID#	Depth to Salt (DTS) (mbgs)	DTS After Settling (mbgs)	Depth to Water (mbgs)	Depth of Well (mbgs)	Month/Year Drilled
1	17.0	12.3	1.7	17.0	May 1971
2	18.5	9.3	1.7	20.0	May 1971
3	17.0	7.7	0.4	17.0	May 1971
4	13.9	3.1	0.6	14.5	Oct 1971
5	7.7+	17.0	0.9	30.8	May 1971
6	15.4	9.3	1.8	15.4	Jun 1971
7	15.4	9.3	1.5	14.5	Jun 1971
8	13.9	12.3	4.3	13.9	Jun 1971
9	13.9	7.7	0.7	13.9	Jun 1971
10	15.4	12.3	0.6	15.4	Jun 1971
11	15.4	10.8	0.8	17.0	Jun 1971
12	13.9	6.2	0.7	13.9	Jun 1971
13	13.9	9.3	2.5	13.9	Jun 1971
14	13.9	0.0	0.3	13.9	Jan 1972
15	17.0	13.9	1.4	17.0	Jun 1971
16	12.3	6.2	0.5	12.3	July 1971
17	15.4	10.8	1.0	15.4	Jun 1971
18	17.0	10.8	0.9	17.0	Jun 1971
19	15.4	13.9	0.7	15.4	Jun 1971
20	15.4	9.3	1.8	15.4	Jun 1971
21	13.9	0.0	0.4	15.4	Jun 1971
22	0.0	9.3	0.9	13.9	Jun 1971
23	17.0	12.3	1.0	17.0	July 1971
24	13.9	10.8	0.5	13.9	Jun 1971
25	15.4	12.3	1.2	18.5	July 1971
26	18.5	12.3	0.6	18.5	Jun 1971
27	15.4	12.3	2.5	15.4	Oct 1971

Borehole ID#	Depth to Salt (DTS) (mbgs)	DTS After Settling (mbgs)	Depth to Water (mbgs)	Depth of Well (mbgs)	Month/Year Drilled
28	12.3	0.0	0.3	12.3	Jun 1971
29	15.4	12.3	0.9	15.4	Jun 1971
30	12.3	9.3	0.8	12.3	Jun 1971
31	17.0	17.0	0.9	17.0	July 1971
32	23.1	17.0	0.6	23.1	Jun 1971
33	15.4	15.4	2.2	15.4	Jun 1971
34	12.3	9.3	0.5	13.9	July 1971
35	9.3	0.0	0.3	10.8	Jan 1972
36	13.9	7.7	0.3	13.9	July 1971
37	12.3+	12.3	0.6	18.8	Oct 1971
38	10.8	9.3	0.3	12.3	July 1971
39	20.0	13.9	0.6	20.0	July 1971
40	21.6	15.4+	0.5	21.6	July 1971
41	12.3	0.0	0.3	12.3	July 1971
42	15.4	13.9	0.9	16.7	July 1971
43	17.0	10.8+	0.9	17.0	Aug 1971
44	21.6	10.8+	0.4	21.6	Aug 1971
45	23.1	9.3+	0.3	23.1	Aug 1971
46	18.5	10.8+	0.0	37.0	Nov 1971
47	17.0	12.3	0.7	18.5	Jan 1972
48	21.6	17.0	0.9	23.1	Dec 1971
49	27.8	30.8	0.6	29.3	Jan 1972
50	35.5	29.3	0.6	35.5	Nov 1971
51	23.1	0.0	0.3	24.7	Aug 1971
52	35.5	33.9	0.3	35.5	Dec 1971
53	18.5	9.3	0.3	21.6	Jan 1972
54	21.6	10.8	0.9	23.1	Jan 1972
55	29.3	29.3	0.5	30.2	Dec 1971
56	20.0	9.3	0.3	20.0	Dec 1971
57	38.6	32.4	0.3	38.6	Sep 1971
58	35.5	30.8	0.3	35.5	Dec 1971
59	18.5	13.9	0.2	18.5	Nov 1971
60	18.5	3.1	0.5	18.5	Jan 1972
61	21.6	18.5	0.0	21.6	Oct 1971
62	20.0	20.0	0.2	20.0	Oct 1971

Borehole ID#	Depth to Salt (DTS) (mbgs)	DTS After Settling (mbgs)	Depth to Water (mbgs)	Depth of Well (mbgs)	Month/Year Drilled
63	33.9	21.6	0.5	33.9	Dec 1971
64	20.0	13.9	0.3	20.0	Oct 1971
65	20.0	10.8	0.9	20.0	Oct 1971
66	0.0	27.8	0.2	46.3	Nov 1971
67	13.9	0.0	0.6	15.4	Jan 1972
68	15.4	12.3	1.2	15.4	Oct 1971
69	12.3	12.3	2.2	12.3	Nov 1971
70	6.2	0.0	0.9	6.2	Nov 1971
71	3.1	0.0	1.2	4.6	Nov 1971
72	4.6	0.0	2.5	4.6	Nov 1971
73	13.9	6.2	1.5	13.9	Nov 1971
74	15.4	10.8	1.5	15.4	Nov 1971
75	17.0	12.3	0.5	17.0	Jan 1972
76	20.0	17.0	1.5	20.0	Jan 1972
77	20.0	13.9	0.6	20.0	Nov 1971
78	17.0	12.3	0.9	17.0	Jun 1972
79	17.0	10.8	0.3	17.0	Jan 1972
80	12.3	12.3	0.5	12.3	Jan 1972
81	18.5	15.4	1.4	18.5	Dec 1971
82	13.9	12.3	0.5	15.4	Dec 1971
83	15.4	9.3	0.6	15.4	Dec 1971
84	15.4	15.4	0.6	15.4	Dec 1971
85	10.8	4.6	0.5	12.3	Dec 1971
86	15.4	4.6	1.2	15.4	Dec 1971
87	9.3	7.7	1.2	9.3	Jan 1972
88	4.6	0.0	1.5	4.6	Dec 1971
89	15.4	12.3	1.2	15.4	Nov 1971
90	15.4	13.9	0.5	17.0	Jan 1972
91	17.0	9.3	0.7	17.0	Jan 1972
92	15.4	13.9	0.2	15.4	Jan 1972
93	12.3	12.3	1.2	12.3	Dec 1971
94	12.3	10.8	1.1	12.6	Dec 1971
95	20.0	17.0	0.3	20.0	Oct 1971
96	13.9+	12.3	1.5	13.9	Dec 1971
97	15.4	12.3	1.5	15.4	Jan 1972

Borehole ID#	Depth to Salt (DTS) (mbgs)	DTS After Settling (mbgs)	Depth to Water (mbgs)	Depth of Well (mbgs)	Month/Year Drilled
98	7.7	7.7	1.5	7.7	Jan 1972
100	18.5	17.0	1.5	18.5	Jan 1972
101	20.0	15.4	0.3	20.0	Jan 1972
102	21.6	13.9	1.9	21.6	Jan 1972
103	21.6	20.0	0.6	21.6	Jan 1972
104	24.7	23.1	0.5	26.2	Jan 1972
105	26.2	20.0	0.8	26.2	Jan 1972
106	20.0	12.3	2.0	20.0	Jan 1972
107	15.4	0.0	2.5	15.4	Jan 1972
108	24.7	20.0	4.9	24.7	Jan 1972
109	20.0	12.3	1.9	20.0	Jan 1972
110	17.0	4.6	1.5	17.0	Jan 1972
111	17.0	9.3	1.2	17.0	Jan 1972
112	17.0	3.1	0.9	17.0	Jan 1972
113	21.6	17.0	0.8	21.6	Jan 1972
114	24.7	21.6	0.8	24.7	Feb 1972
115	18.5	12.3	1.5	20.0	Feb 1972
116	12.3	6.2	1.5	12.3	Jan 1972
117	20.0	15.4	2.2	21.6	Jan 1972
118	10.8	4.6	2.8	18.5	Jan 1972
119	15.4	0.0	3.7	20.0	Jan 1972
120	12.3	6.2	2.2	12.3	Jan 1972
121	0.0	0.0	1.7	4.0	Nov 1971
122	0.0	0.0	0.6	6.2	Nov 1971
123	0.0	9.3+	1.1	9.3	-
124	0.0	7.7+	1.8	8.0	-
125	0.0	3.1	2.7	11.4	-
126	0.0	0.0	0.6	3.4	-
127	6.2	4.6	2.1	6.2	-
128	0.0	0.0	2.5	6.2	-
129	7.7	0.0	1.5	9.3	-
130	0.0	0.0	1.5	3.1	-
131	9.3	0.0	0.0	9.3	-

Note: All depths are reported in metres below ground surface (mbgs); + indicates depth to salt was greater than this depth, as measurements to this depth were fresh and no deeper measurements provided; depth to salt is characterised based on salinity greater than 400 mg/L. Data obtained from Little et al. (1973).

Table A2. Hazard survey form

Blue Water Project Community Survey				
Property ID:	**Property or Owner Name:**			
□ **Residential**	□**Commercial**	□**Industrial**	□**Agricultural**	□**Other**_____
Description of Property:				
GPS Coordinates:		Settlement Name:		
Water Supply				
Private Well on Property? Y / N	Approx. Depth of Well:	Well Drilled or Excavated/Dug?		
Water Use? Domestic/ Commercial/ Industrial/ Other_____		Approx. year of well construction:		
Is there a cap/cover on the well? Y / N	Was a surface seal installed during construction? (show diagram + explain) Y / N			
What well maintenance do you perform?				
Do you treat your well water for bacteria? Y / N	If so, with what?	How often?		
Is your water ever salty? Always / Sometimes / Rarely / Never	When does this occur?			
Use Reverse Osmosis? Y / N	How do you dispose of the brine from RO system?			
Wastewater Disposal				
What type of wastewater disposal do you use? (septic tank/ field, treatment system)				
Do you perform regular maintenance? Y / N	What maintenance?			
How often do you perform maintenance?	How many residents/visitors/workers per day use the system?			
Have you ever heard of or used composting toilets? Y / N	If so, where?			
Solid Waste Disposal				
Where do you dispose of your solid waste?				
Do you separate / recycle any of your garbage? Y / N	If so what?			
Where is that separated/recycled material disposed of?				
Chemical Storage / Disposal				
Do you store any fuel on the property? Y / N	Petrol / Diesel (circle one)	How much fuel is stored?		
What kind of storage? (tank above/below ground, jerry can)				
Do you store/use any engine oil? Y / N	How much?	How is it stored?		
Do you store/use any solvents? Y /N	How much?	What kind?	How is it stored?	
Do you store/use any paints? Y / N	How much?	What kind? (marine or building)	How is it stored?	
Do you store/use any other chemical products? Y / N	How much?	What Kind?	How is stored?	
Where do you dispose of used chemicals (i.e. waste oil, paint, solvents, household cleaners)?				
Any other observations/comments				

Table A2. Hazard survey form (cont'd)

Additional Information for Specific Properties			
Agriculture/ Farms			
Do you use irrigation? Y / N	What is the source of water for irrigation?		
What method of application for irrigation? (drip/ spray)	How often do you irrigate?	What rate?	
Do you use pesticides? Y / N	What kind?		
How often do you apply?	Approx. how much is used per application?		
Do you use fertilizers? Y / N	What kind?		
How often do you apply?	Approx. how much is used per application?		
Do you keep livestock? Y / N	What kind of animals?	Approx. how many?	
What do you do with the manure? (collect in cesspool, spread on ground, etc.)			
Androsia Textile Plant			
Where does the discharge water from washing go?	How much water is used on average?		
What are the dyes made of?	What kind of detergent is used in washing?		
Are there any other chemicals involved in process?			
Quarrying/ Mining Operations			
Approx. how deep are the excavations?			
Do you pump water to de-water the pits? Y / N	Approx. how much water is pumped?		
Large Hotels			
Where is your laundry done?	How many loads per day?		
Landfills			
What separate classifications are there for waste?			
Is there a liner in landfill? Y / N	What material is it made of?		
How is waste managed? (covered/buried/mixed/other)			
How long has the landfill been operating?			
Healthcare Community Clinics			
Form of burial: (ground, cremation)	How many years has cemetery been used?		
Are any chemicals used in burial preparation? Y / N	What chemicals?	How much stored?	
Where is biomedical waste disposed?			
Is any laundry/disinfection performed on site? Y/N	What disinfectants used?	How much stored?	
Are prescription medicines stored? Y/N	What kind? (antidepressants, birth control)		
How are these disposed of when they expire?			
Any other potential hazards?			

Table A3. Hazard survey results

Survey Question	Percentage of Respondents Answering Yes or No (%)	
	Yes	No
Have private well	25	75
If yes:		
Perform maintenance on well	22	78
Water ever salty	15	85
Well used for irrigation	13	87
Use reverse osmosis desalination system	7	93
Use septic tank system	100	0
Perform septic tank maintenance	30	70
Solid waste disposal in unlined landfill	100	0
Recycling or separation of waste	12	88
Have chemicals on-site in greater than household quantities (e.g. fuel, engine oil, cleaning products)	92	8
Used chemicals disposed of on ground or in septic tanks	98	2
If agricultural, use pesticides or fertilizers	46	54

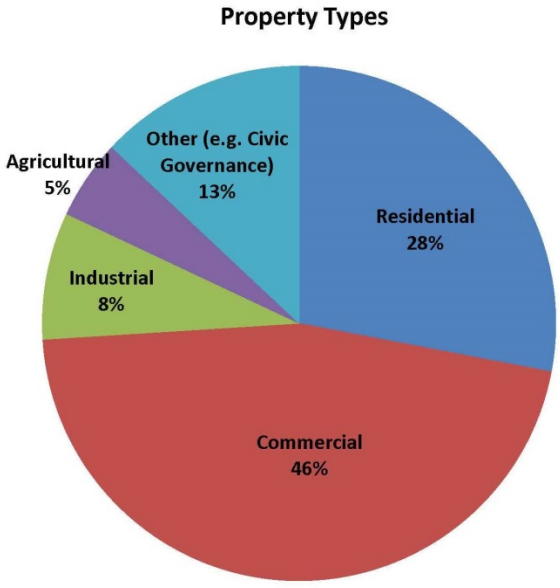

Figure A1. Property types for surveyed properties

Appendix B.

Grok Input File Examples for HGS Models

The following text forms the input files (groks) for the three phases of overwash modeling in HydroGeoSphere. These files are presented as examples of the model inputs used.

Phase 1 – Development of the Freshwater Lens

```
!-------------------------  Problem description
Running Phase 1 freshwater lens development to steady state
end title

!-------------------------  Grid generation
generate uniform rectangles
   2400.0 2400
   1.0  1

   generate layers interactive

      base elevation
         elevation constant
         0.0
      end ! base elevation

      ! layer between 0-20m: 1m thick
      new layer
         layer name
         layer_1
         elevation constant
         20.0
         uniform sublayering
         20
      end ! new layer

      ! layer between 20-40m: 0.5m thick
      new layer
         layer name
         layer_2
         elevation constant
         40.0
         uniform sublayering
         40
      end
```

```
      ! layer between 40-43.5m(ground surface): 0.35m thick
      new layer
         layer name
         layer_3
         elevation from xz pairs
            0.0  43.5
            1199.0 43.5
            1200.0 41.5
            1201.0 41.5
            1202.0 43.5
            2400.0 43.5
         end
         uniform sublayering
         10
      end
   end ! generate layer interactive

end ! grid generation

!--------------------------  General simulation parameters
units: kilogram-metre-day
transient flow
do transport
unsaturated
finite difference mode
dual nodes for surface flow

!--------------------------  Porous media properties
use domain type
porous media
properties file
v1pm.mprops
clear chosen elements
choose elements all
new zone
1
clear chosen elements
choose elements block
0 2400
0 1
25 26
choose elements block
0 2400
0 1
30 31
new zone
2
clear chosen zones
choose zone number
```

```
1
read properties
Lucayan
clear chosen zones
choose zone number
2
read properties
Paleosol

!--------------------------  Overland properties
use domain type
surface
properties file
v1olf.oprops
clear chosen faces
choose faces top
new zone
1
clear chosen zones
choose zone number
1
read properties
surface

!--------------------------  Initial Conditions for flow
use domain type
porous media
! Set initial head in subsurface
clear chosen nodes
choose nodes all
function z initial head
0.0   41.036
40.0  40.0

! Set initial water depth in surface domain
use domain type
surface

clear chosen nodes
choose nodes all
initial water depth
1.0e-6 1.0d0
!--------------------------  Boundary Conditions for flow
use domain type
surface

clear chosen nodes
choose nodes top
create face set
```

```
top_face
!specified flux boundary of 877 mmperyear in mperday
boundary condition
   type
   rain
   face set
   top_face
   time value table
   0.0 2.4e-3
   end
end

clear chosen nodes
choose nodes block
-0.1 0.1
0 1
43.4 43.6
create segment set
west_surface
boundary condition
   type
   critical depth
   segment set
   west_surface
end

clear chosen nodes
choose nodes block
2399.9 2400.1
0 1
43.4 43.6
create segment set
east_surface
boundary condition
   type
   critical depth
   segment set
   east_surface
   end

use domain type
porous media
clear chosen nodes
choose nodes block
-0.001 0.001
0 1
0  40
create node set
west
```

```
!specified head for left side
boundary condition
   type
   head equals initial
   node set
   west
end

clear chosen nodes
choose nodes block
2399.9 2400.1
0 1
0  40
create node set
east
!specified head for right side
boundary condition
   type
   head equals initial
   node set
   east
end

!---------------------------- tracer
solute
name
salt
affects fluid properties
free-solution diffusion coefficient
8.7e-10
relative concentration
1.0    cmax
1025.9 rhomax
end solute

reference fluid density
1000.0
constant viscosity
picard convergence criteria
0.01
0.1
5
relaxation for density-dependent picard iteration
0.5
transport time weighting
1
control volume
upstream weighting of velocities
1.0 1.0 1.0
```

```
!------------------------------ initial conditions for transport
use domain type
porous media
clear chosen nodes
choose nodes all
initial concentration
1.0

use domain type
surface
clear chosen nodes
choose nodes all
initial concentration
0.0 1.0

!------------------------------ boundary conditions for transport
use domain type
porous media
!constant concentration along sides of model
clear chosen nodes
choose nodes block
-0.001 0.001
0 1
0 40
choose nodes block
2399.9 2400.1
0 1
0 40
specified concentration
1
0.0 1.0e20 1

!------------------------------ concentration output
make observation point
trench
1200 0 41.7
make observation point
aquifunder
1200 0 40.5

!--------------------------  Timestep controls
Newton maximum iterations
15
Jacobian epsilon
1.0d-6
Newton absolute convergence criteria
1.0d-3
Newton residual convergence criteria
```

```
1.0d-3
head control
0.5
maximum timestep
1.0
initial timestep
1.0e-5
maximum timestep multiplier
1.2
minimum timestep multiplier
0.5

output times
365
730
1095
1460
1825…
end
```

Phase 2 – Inundation

```
!--------------------------  Problem description
Running Phase 2 inundation
end title

!--------------------------  Grid generation
generate uniform rectangles
   2400.0 2400
   1.0  1

   generate layers interactive

      base elevation
         elevation constant
         0.0
      end ! base elevation

      ! layer between 0-20m: 1m thick
      new layer
         layer name
         layer_1
         elevation constant
         20.0
         uniform sublayering
         20
      end ! new layer

      ! layer between 20-40m: 0.5m thick
```

```
      new layer
        layer name
        layer_2
        elevation constant
        40.0
        uniform sublayering
        40
      end

      ! layer between 40-43.5m(ground surface): 0.35m thick
      new layer
        layer name
        layer_3
        elevation from xz pairs
          0.0  43.5
          1199.0 43.5
          1200.0 41.5
          1201.0 41.5
          1202.0 43.5
          2400.0 43.5
        end
        uniform sublayering
        10
      end
    end ! generate layer interactive

end ! grid generation

!--------------------------  General simulation parameters
units: kilogram-metre-day
transient flow
do transport
unsaturated
finite difference mode
dual nodes for surface flow

!--------------------------  Porous media properties
use domain type
porous media
properties file
v1pm.mprops
clear chosen elements
choose elements all
new zone
1
clear chosen elements
choose elements block
0 2400
0 1
```

```
25 26
choose elements block
0 2400
0 1
30 31
new zone
2
clear chosen zones
choose zone number
1
read properties
Lucayan
clear chosen zones
choose zone number
2
read properties
Paleosol

!-------------------------- Overland properties
use domain type
surface
properties file
v1olf.oprops
clear chosen faces
choose faces top
new zone
1
clear chosen zones
choose zone number
1
read properties
surface

!-------------------------- Initial Conditions for flow
use domain type
porous media
! Set initial head in pm domain
clear chosen nodes
choose nodes all
restart file for heads
v1steady.hen

! Set initial water depth in olf domain
use domain type
surface
clear chosen nodes
choose nodes all
restart file for heads
v1steady.hen
```

```
!-------------------------  Boundary Conditions for flow
use domain type
surface
clear chosen nodes
choose nodes top
create face set
top_face
!specified flux boundary of 877 mmperyear in mperday
boundary condition
   type
   rain
   face set
   top_face

   time value table
   0.0 2.4e-3
   end
end

clear chosen nodes
choose nodes block
-0.1 0.1
0 1
43.4 43.6
create segment set
west_surface
boundary condition
   type
   critical depth
   segment set
   west_surface
end

clear chosen nodes
choose nodes block
2399.9 2400.1
0 1
43.4 43.6
create segment set
east_surface
boundary condition
   type
   critical depth
   segment set
   east_surface
   end

clear chosen nodes
```

```
choose nodes top
create node set
top_node
boundary condition
   type
   head
   node set
   top_node
   time value table
   0.0     43.5
   0.0069  43.6
   0.0139  43.7
   0.0208  43.8
   0.0278  43.9
   0.0347  44.0
   0.0416  44.1
   0.0486  44.2
   0.0555  44.3
   0.0625  44.4
   0.0694  44.5
   end
end

use domain type
porous media
clear chosen nodes
choose nodes block
-0.001 0.001
0 1
0  40
create node set
west
!specified head for western coast
boundary condition
   type
   head equals initial
   node set
   west
end

clear chosen nodes
choose nodes block
2399.9 2400.1
0 1
0  40
create node set
east
!specified head for eastern coast
boundary condition
```

```
   type
   head equals initial
   node set
   east
end

!---------------------------- tracer
solute
name
salt
affects fluid properties
free-solution diffusion coefficient
8.7e-10
relative concentration
1.0    cmax
1025.9 rhomax
end solute

reference fluid density
1000.0
constant viscosity
picard convergence criteria
0.01
0.1
5
relaxation for density-dependent picard iteration
0.5
transport time weighting
1
control volume
upstream weighting of velocities
1.0 1.0 1.0

!------------------------------ initial conditions for transport
use domain type
porous media
clear chosen nodes
choose nodes all
restart file for concentrations
v1steady.cen

use domain type
surface
clear chosen nodes
choose nodes all
restart file for concentrations
v1steady.cen

!------------------------------ boundary conditions for transport
```

```
use domain type
porous media
!constant concentration along sides of model
clear chosen nodes
choose nodes block
-0.001 0.001
0 1
0 40
choose nodes block
2399.9 2400.1
0 1
0 40
specified concentration
1
0.0 1.0e20 1

use domain type
surface
clear chosen nodes
choose nodes top
specified concentration
1
0.0  0.1458   1

!------------------------------ concentration output
make observation point
trench
1200 0 41.7
make observation point
aquifunder
1200 0 40.5

!--------------------------  Timestep controls
Newton maximum iterations
15
Jacobian epsilon
1.0d-6
Newton absolute convergence criteria
1.0d-3
Newton residual convergence criteria
1.0d-3
head control
0.5
maximum timestep
1.0
initial timestep
1.0e-5
maximum timestep multiplier
1.2
```

```
minimum timestep multiplier
0.5

output times
0.00694
0.0139
0.0208
0.0278
0.0347
0.0416
0.0486
0.0555
0.0625
0.0694
0.1458
end
```

Phase 3 – Freshwater lens recovery

```
!----------------------------  Problem description
Running Phase 3 baseline freshwater lens recovery
end title

!----------------------------  Grid generation
generate uniform rectangles
   2400.0 2400
   1.0  1

   generate layers interactive

      base elevation
         elevation constant
         0.0
      end ! base elevation

      ! layer between 0-20m: 1m thick
      new layer
         layer name
         layer_1
         elevation constant
         20.0
         uniform sublayering
         20
      end ! new layer

      ! layer between 20-40m: 0.5m thick
      new layer
         layer name
         layer_2
```

```
      elevation constant
      40.0
      uniform sublayering
      40
    end

    ! layer between 40-43.5m(ground surface): 0.35m thick
    new layer
      layer name
      layer_3
      elevation from xz pairs
        0.0  43.5
        1199.0 43.5
        1200.0 41.5
        1201.0 41.5
        1202.0 43.5
        2400.0 43.5
      end
      uniform sublayering
      10
    end
  end ! generate layer interactive

end ! grid generation

!--------------------------  General simulation parameters
units: kilogram-metre-day
transient flow
do transport
unsaturated
finite difference mode
dual nodes for surface flow

!--------------------------  Porous media properties
use domain type
porous media
properties file
v1pm.mprops
clear chosen elements
choose elements all
new zone
1
clear chosen elements
choose elements block
0 2400
0 1
25 26
choose elements block
0 2400
```

```
0 1
30 31
new zone
2
clear chosen zones
choose zone number
1
read properties
Lucayan
clear chosen zones
choose zone number
2
read properties
Paleosol

!--------------------------  Overland properties
use domain type
surface
properties file
v1olf.oprops
clear chosen faces
choose faces top
new zone
1
clear chosen zones
choose zone number
1
read properties
surface

!--------------------------  Initial Conditions for flow
use domain type
porous media
! Set initial head in pm domain
clear chosen nodes
choose nodes all
restart file for heads
v2rise.hen

! Set initial water depth in olf domain
use domain type
surface
clear chosen nodes
choose nodes all
restart file for heads
v2rise.hen

!--------------------------  Boundary Conditions for flow
use domain type
```

```
surface
clear chosen nodes
choose nodes top
create face set
top_face
!specified flux boundary of 877 mmperyear in mperday
boundary condition
   type
   rain
   face set
   top_face
   time value table
   0.0 2.4e-3
   end
end

clear chosen nodes
choose nodes block
-0.1 0.1
0 1
43.4 43.6
create segment set
west_surface
boundary condition
   type
   critical depth
   segment set
   west_surface
end

clear chosen nodes
choose nodes block
2399.9 2400.1
0 1
43.4 43.6
create segment set
east_surface
boundary condition
   type
   critical depth
   segment set
   east_surface
   end

use domain type
porous media
clear chosen nodes
choose nodes block
-0.001 0.001
```

```
0 1
0  40
create node set
west
!specified head for western coast
boundary condition
   type
   head equals initial
   node set
   west
end

clear chosen nodes
choose nodes block
2399.9 2400.1
0 1
0  40
create node set
east
!specified head for eastern coast
boundary condition
   type
   head equals initial
   node set
   east
end

!---------------------------- tracer
solute
name
salt
affects fluid properties
free-solution diffusion coefficient
8.7e-10
relative concentration
1.0    cmax
1025.9 rhomax
end solute

reference fluid density
1000.0
constant viscosity
picard convergence criteria
0.01
0.1
5
relaxation for density-dependent picard iteration
0.5
transport time weighting
```

```
1
control volume
upstream weighting of velocities
1.0 1.0 1.0

!------------------------------ initial conditions for transport
use domain type
porous media
clear chosen nodes
choose nodes all
restart file for concentrations
v2rise.cen

use domain type
surface
clear chosen nodes
choose nodes all

restart file for concentrations
v2rise.cen

!------------------------------ boundary conditions for transport
use domain type
porous media
!constant concentration along sides of model
clear chosen nodes
choose nodes block
-0.001 0.001
0 1
0 40
choose nodes block
2399.9 2400.1
0 1
0 40
specified concentration
1
0.0 1.0e20 1

!------------------------------ concentration output
make observation point
trench
1200 0 41.7
make observation point
aquifunder
1200 0 40.5

!--------------------------  Timestep controls
Newton maximum iterations
15
```

Jacobian epsilon
1.0d-6
Newton absolute convergence criteria
1.0d-3
Newton residual convergence criteria
1.0d-3
head control
0.5
maximum timestep
5
initial timestep
1.0e-3
maximum timestep multiplier
5
minimum timestep multiplier
0.5
output times
0.0833
0.1666
0.2499
0.3332
0.4165
0.4998
0.5831
0.6664
0.7497
0.833
0.9163
0.9996
2
3
4
5
6
7
14
21
28
…
365
…
3650
end